Signalling Functions of Polyubiquitin Chains and Ubiquitin-binding Domains

Shengkai Zhao

University College London

and

Cancer Research UK London Research Institute

PhD Supervisor: Dr. Helle D Ulrich

A thesis submitted for the degree of

Doctor of Philosophy

University College London

September 2010

Declaration

I, Shengkai Zhao, confirm that the work presented in this thesis is my own. Where information has been derived from other sources, I confirm that this has been indicated in the thesis.

Abstract

The ubiquitin signalling system has been shown to regulate many important biological events, ranging from DNA repair to the immune response. Different polyubiquitin chains linked by various linkages have been identified *in vivo*, and can be recognised by proteins containing ubiquitin-binding domains that act as downstream effectors. However, functions for many of them are not well understood. I have studied the function of K63-linked and linear polyubiquitin chains on a common substrate. The other branch of my study was to investigate the role of ubiquitin binding for a novel ubiquitin-interacting protein, SPC25.

K63-linked and linear polyubiquitin chains have a similar topology, but whether they convey a similar signal *in vivo* remains unclear. I have used the eukaryotic replication clamp PCNA, a natural substrate of K63-linked polyubiquitylation, as a model substrate to directly compare the consequences of modification by different types of polyubiquitin chains. I have shown that K63-polyubiquitylated PCNA is not subject to proteasomal degradation. In contrast, linear, non-cleavable ubiquitin chains do not promote DNA damage tolerance, but function as general degradation signals. I found that a linear tetraubiquitin chain is sufficient to afford proteasomal targeting through the Cdc48-Npl4-Ufd1 complex without further modification.

In the second part of my thesis, I describe the identification of SPC25, a subunit of the Ndc80 complex, as a novel ubiquitin-binding protein, using tetra-ubiquitin chains as baits in a genome-wide two-hybrid screen. I have shown that the C-terminal region of SPC25 interacts with ubiquitin *in vivo* and *in vitro*. This region does not exhibit significant similarity with any known ubiquitin-binding domains. Further genetic evidence suggests that this ubiquitin-binding domain contributes to the stability of the kinetochore complex.

Acknowledgement

First and foremost I would like to thank my supervisor Helle Ulrich. It has been a great experience for being her student. She taught me the way science should be. She guided me all the way through my projects, from the big questions to the little technical details. I appreciate her continuous support on my projects and allowing me to pursue many interesting ideas. She was always available for answering my questions and giving countless brilliant suggestions. She was also very patient with my unprofessional English, carefully correcting my reports, meeting abstracts, posters and the PhD thesis, thanks, Helle.

I also would like to thank my thesis committee Jesper Svejstrup and Simon Boulton for their constructive suggestions, generous support with lab reagents and continuous encouragement during the progress of the projects.

Thanks give to all current and past Ulrich lab members for creating a friendly and organised working environment. Without all of you, I would not have such enjoyable lab experience in the past four years. Special thanks go to Irene, Jo and Addie for teaching me many techniques and sharing their valuable scientific experiences; Thank you Nicola for your constructive ideas and helpful discussions; Thank you Yasu for the good time while we were waiting for 84. Thank you Andrea, Diana, Oliver, Olivier, Laure, Liz, Magda and other people who have worked in D36.

I can not forget my friends in Clare Hall, specially Ling, Feng, Namita and Ozan, the admin office, mass spectrometry and other Cancer Research UK-LRI services for their kind help during my PhD. Special thanks go to Sally and Erin for organising various student events and making the life of an international student much easier. Of course, I want to thank Cancer Research UK for funding the research and providing generous studentship.

Last but not least, I would like to thank my mother Xiaomin Wang and my father Jianying Zhao for their endless love and continuous encouragement on my study since I was a child. Sorry for being far away from both of you in the past few years. I want to thank my girl friend Luo, for her love, being with me, giving me support on daily life, bringing me a lot of laugh during the time of thesis writing and telling me that life is more than just science.

Table of Contents

Table of figures

List of tables

Abbreviations

AD	activation domain
AMP	adenosine monophosphate
APC/C	anaphase promoting complex
ARK5	AMPK-related kinase 5
ARS	autonomous replication sequence
ATP	adenosine triphosphate
BD	DNA binding domain
BRCA1	breast and ovarian cancer susceptibility protein 1
BRCT	Brca1 C-terminal
CH domain	calponin homology domain
Co-IP	co-immunoprecipitation
COMA	Ctf19, Okp1, Mcm21 and Ame1
CP	core particle
dCTP	deoxycytidine triphosphate
CUE	coupling of ubiquitin conjugation to ER
DNA	deoxyribonucleic acid
DSB	double-strand break
DTT	dithiothreitol

DUB	deubiquitylating enzyme
EBI	european bioinformatics institute
ER	endoplasmic reticulum
ERAD	ER-associate degradation
ESCRT	endosomal sorting complex required for transport
FACS	fluorescent activated cell sorting
GST	glutathione sulfur transferase
HECT	homologous to E6-AP carboxy terminus
IAP	inhibitor of apoptosis
ICL	interstrand cross links
IDCL	interdomain connector loop
IκB	inhibitor of NF-κB
IKK	IκB kinase
IP	immunoprecipitation
IPTG	isopropyl β-D-1-thiogalactopyranoside
KMN	Knl-1, Mtw1 complex and Ndc80 complex
LB	Luria broth
LUBAC	linear ubiquitin chain assembly complex
MIND	Mtw1, Nsl1, Nnf1 and Dsn1

MIU	motif interacting with ubiquitin
MMS	methyl methanesulfonate
NEMO	NF-κB essential modulator
NF-κB	nuclear factor kappa-light-chain-enhancer of activated B cells
NMR	nuclear magnetic resonance
ORF	open reading frame
PBS	phosphate buffered saline
PCR	polymerase chain reaction
PCNA	proliferating cell nuclear antigen
PDB	protein data bank
PGK	phosphoglycerate kinase
PH fold	pleckstrin homology fold
PML-NBs	PML-nuclear bodies
PRU domain	PH receptor for ubiquitin domain
RING	really interesting new gene
RNA	ribonucleic acid
RP	regulatory particle
SCF	Skp1-Cullin-F-box protein
SC medium	synthetic complete medium

SDS-PAGE	sodium dodecyl sulfate polyacrylamide gel electrophoresis
SPR	surface plasmon resonance
SUMO	small ubiquitin like modifier
TAP	tandem affinity purification
TCA	trichloroacetic acid
TLS	translesion synthesis
TNF	tumour necrosis factor
TNFR	tumour necrosis factor receptor
TRADD	TNFR1-associated death domain protein
Ts mutant	temperature-sensitive mutant
UBA domain	ubiquitin-associated domain
UBAN domain	ubiquitin binding in ABIN and NEMO domain
UBC domain	ubiquitin-conjugating enzyme-like domain
UBD	ubiquitin-binding domain
UBL domain	ubiquitin-like (UBL) domain
UBM	ubiquitin binding motif
UBZ	ubiquitin binding Zn finger
UFD	ubiquitin fusion degradation
UPS	ubiquitin proteasome system

UV	ultraviolet
YPD	yeast peptone glucose medium
ZnF	zinc-finger

Chapter 1. Introduction

1.1 Ubiquitylation

Cellular proteins are constantly exposed to changes in their environments, and as part of the natural response many proteins are posttranslationally modified. Posttranslational modifications therefore greatly extend the functional diversity of a protein. Ubiquitylation is among the most common and important forms of posttranslational modification in the cell. This section will introduce ubiquitin, the biochemical pathway of ubiquitylation and the enzymes involved in this process.

1.1.1 Ubiquitin

Ubiquitin is a 76-amino acid protein conserved in all eukaryotes. It is a member of a family of structurally related proteins, which includes many other ubiquitin like proteins such as SUMO (small ubiquitin like modifier), Nedd8 (neural precursor cell expressed developmentally down-regulated 8). In the early 1980s, it was found as a posttranslational protein modifier, which can be covalently conjugated onto substrate proteins (Hershko and Ciechanover, 1998). The structure of ubiquitin consists of a 5-stranded β-sheet, a short 3_{10} helix and a 3.5-turn α-helix. The most important functionally relevant features are a surface hydrophobic patch formed by L8-I44-V70 and a solvent-exposed carboxyl-terminal tail (Figure 1.1A). The hydrophobic patch is important for interacting with many ubiquitin-binding proteins, and the carboxyl-terminal tail is involved in ubiquitin conjugation and deconjugation reactions. There are seven lysine residues on the surface of ubiquitin, and all lysines together with the N-terminal methionine can be used in the formation of polyubiquitin chains (Figure 1.1A).

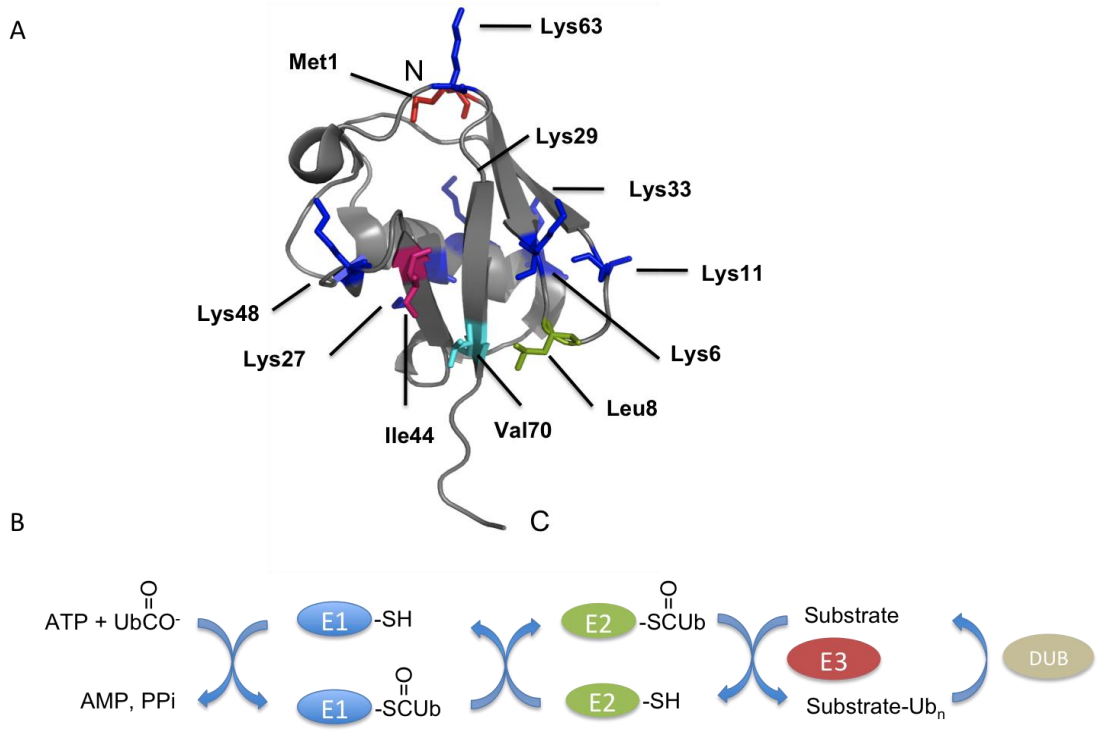

Figure 1.1 The structure of ubiquitin and the enzymatic pathway of ubiquitylation (A) A ribbon representation of a ubiquitin monomer, protein data bank (PDB) code: 1D3Z. Seven solvent-exposed lysine residues (blue) as well as the amino terminus (red) are available for chain assembly. Hydrophobic amino acids L8, I44, V70, which are important for interacting with many ubiquitin-binding domains, are labelled in green, pink and cyan respectively. This image was generated by PyMol. (B) The enzymatic pathway of ubiquitin conjugation and deconjugation. The process requires E1 (blue oval), E2 (green oval) and E3 (red oval) with the consumption of ATP to conjugate ubiquitin onto substrate proteins. DUB (brown oval) can remove ubiquitin from the substrate. This figure was adapted from (Pickart, 2001).

1.1.2 Biochemistry of Ubiquitylation

The biochemical process of protein ubiquitylation requires a cascade of enzymatic reactions involving a series of enzymes named ubiquitin-activating enzyme (E1), ubiquitin-conjugating enzyme (E2) and ubiquitin ligase (E3). A glycine residue at the C-terminus of ubiquitin is activated by the E1 in an ATP-dependent manner to form an intermediate ubiquitin adenylate while releasing PPi. Ubiquitin is then linked to a cysteine residue via a thiolester bond with the release of AMP. The activated ubiquitin is then transferred to the cysteine residue within the active site of E2. Finally, E3 catalyses the formation of an amide isopeptide bond between the C-terminus of

ubiquitin and a ε-amino group of a lysine residue on the substrate protein (Hershko and Ciechanover, 1998) (Figure 1.1B). In some special cases, ubiquitin can also be conjugated on the N-terminus of the substrate protein independent of lysine residues, where a peptide bond is formed between the C-terminus of ubiquitin and the N-terminal α-amino group of a substrate protein (Aviel et al., 2000, Breitschopf et al., 1998). The enzymatic reaction can continue to put a second ubiquitin onto either a lysine residue of the first ubiquitin, which after several rounds of reaction leads to a polyubiquitin chain, or another site on the substrate protein, which in turn gives a multiply monoubiquitylated substrate.

1.1.3 Ubiquitin Conjugation Enzymes

E1 is the enzyme on the top of the ubiquitylation cascade. In yeast, there is only one E1 enzyme that is responsible for activating ubiquitin for the entire ubiquitylation system. Each fully loaded E1 molecule carries two activated ubiquitin molecules: one as an ubiquitin adenylate and the other as a thiolester. The E1 is a very efficient enzyme, which has an ATP-AMP turn over number of 1-2 S^{-1} (Haas et al., 1982), 10-100 fold faster than the catalytic rate of protein ubiquitylation. This allows efficient production of activated ubiquitin.

E2 functions between E1 and E3 to transfer the ubiquitin from E1 to an active cysteine residue in E2 in the form of a thiolester. There are significant but limited number of E2s in the cell (11 E2s in *S. cerevisiae* and more in higher eukaryotes). All of them share a conserved domain and each of them works with several E3s to reach their functional specificity. For example, Ubc2/Rad6 can work with E3 Ubr1 and functions in N-end rule proteolysis (Dohmen et al., 1991); alternatively, it can cooperate with E3 Rad18 to ubiquitylate PCNA in the DNA damage tolerance pathway (Bailly et al., 1994, Hoege et al., 2002).

The function of E3 involves substrate recognition and ligation. Ubiquitylation does not always have a common target sequence, which makes the identification of ubiquitylation targets by bioinformatic approaches very difficult. In fact, ubiquitylation can occur in a so-called destruction box (D box) sequence, RXALGXIXN, which has been found in many anaphase promoting complex (APC/C) substrates (Koepp et al., 1999). In other cases, E3 mediated ubiquitylation events are not really site selective, such as the multiubiquitylation of c-Jun (Treier et al., 1994). E3s can be classified into three main groups based on the structural feature of their ligase domain. The first class of the E3 contains a homologous to E6-AP carboxyl terminus (HECT) domain, which is a conserved ~350-residue domain first identified in E6-associated protein (E6-AP) (Huibregtse et al., 1995). This type of E3 binds E2s, but not through the HECT domain itself, and forms a thiolester with the activated ubiquitin that is transferred from the E2. It then catalyses the isopeptide bond formation between ubiquitin and the substrate (Pickart, 2001). Other examples of HECT E3 include Rsp5, Ufd4, etc. The second class of E3 contains the Really Interesting New Gene (RING) finger, which has a series of cysteine and histidine residues in coordination with two zinc ions. The RING family E3s function as a scaffold to bring E2s and substrates together, and transfer the activated ubiquitin from E2 directly onto the substrate (Petroski and Deshaies, 2005). Some of the RING family E3s have a single subunit, this type includes Ubr1 (N-end rule pathway), Rad18 and Rad5 (*RAD6* pathway), etc. In some other cases, RING finger proteins form part of multi-subunit E3 complexes. APC/C, SCF (Skp1-Cullin-F-box protein) are typical examples and extra subunits play roles in aspects such as substrate recognition. There is a third type of E3, containing a U-box domain, also known as E4 enzyme. The first example of such enzyme was yeast Ufd2, in which a conserved C-terminal domain (~70 amino acids) was identified as a U-box domain. Ufd2 binds to mono- or oligoubiquitylated model substrates and drives polyubiquitin chain assembly in the presence of E1, E2 and E3 (Koegl et al., 1999). *In vivo*, mammalian Ufd2a-mediated multiubiquitylation of ataxin-3 requires extra E3 activity to initiate ubiquitylation, suggesting the enzyme is different from E3s in a physiological context (Matsumoto et al., 2004). However, the U-box domain is structurally related to the RING finger motif found in RING type E3s (Aravind and Koonin, 2000), and it can interact with its cognate E2 Ubc4 to facilitate ubiquitin transfer to relevant substrates

(Tu et al., 2007). In many instances U-box proteins are therefore better classified as E3s, and E4 function may just be a special case.

1.1.4 Ubiquitin Deconjugation Enzymes

The ubiquitylation reaction can also be reversed by a process called deubiquitylation, which is catalysed by a class of enzymes named deubiquitylating enzymes, DUBs. A proteolytic reaction is catalysed by DUBs to cleave the isopeptide linkage between a lysine residue and G76 or even a peptide bond between M1 and G76 in linear polyubiquitin chains (Figure 1.1B). In cells, head-to-tail arranged linear polyubiquitin are produced from ubiquitin genes as a precursor. DUB is required to process precursors into ubiquitin monomers (Reyes-Turcu et al., 2009). The activity of DUB relies on the C-terminal amino acid sequence of distal ubiquitin, in which R74 and G75 are crucial for ubiquitin recognition (Drag et al., 2008). Usually a DUB binds to a substrate ubiquitin chain in a special conformation to ensure that the C-terminus of the distal ubiquitin sits in the catalytic centre of the DUB (Komander et al., 2009a).

1.2 Ubiquitin Signals

As one of the major protein modifiers, ubiquitin appears as a number of different forms on substrate proteins to conduct their signalling functions. Proteins can be modified by monoubiquitin, multiple monoubiquitin, and polyubiquitin chains with various linkages (Figure 1.2). Various forms of ubiquitin signals usually convey different messages. Especially, polyubiquitin chains with different linkages exhibit distinct conformations. So far, structures of K48-, K63-, K11-linked and linear ubiquitin chains have been solved. In addition to that, even same type of ubiquitin signal can signal for different functions in different contexts. This section will describe different forms of ubiquitin signals, their characteristics and their reported functions.

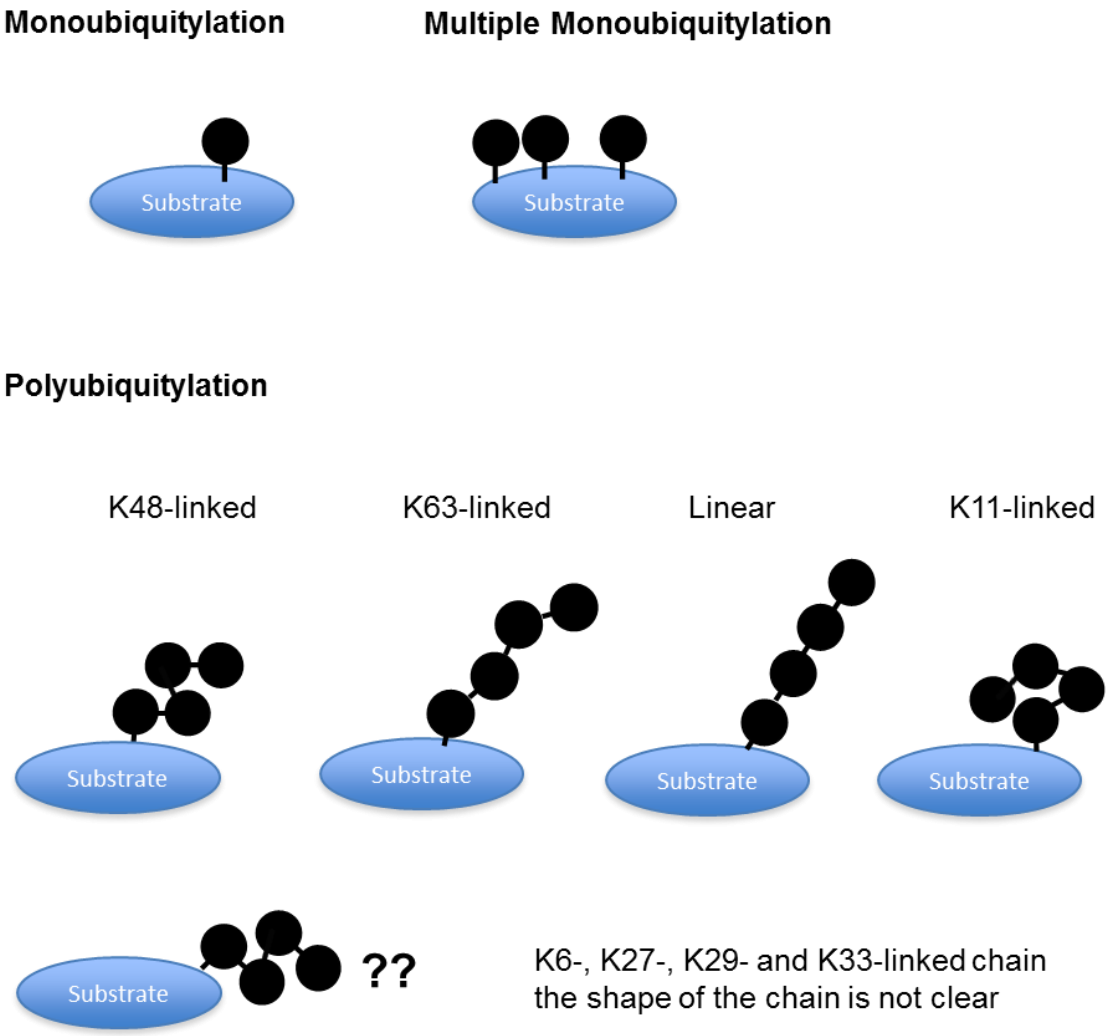

Figure 1.2 Forms of ubiquitin signals
Ubiquitin (black filled circle) can modify a substrate (blue oval) as monoubiquitin, multiple monoubiquitin or polyubiquitin chains. Polyubiquitin chains exhibit distinct structures and seven lysine residues as well as the N-terminus of ubiquitin can all be used for chain formation. K48-linked chains adopt a closed conformation whereas K63-linked chains have an open conformation almost identical to linear ubiquitin chains. K11-linked chains also exhibit a compact structure, but with its hydrophobic patches exposed, different from K48-linked chains. The structure of K6-, K27-, K29- and K33-linked chains are still unknown.

1.2.1 Monoubiquitylation

Proteins can be monoubiquitylated on a single lysine residue or even on multiple lysine residues (Figure 1.2). Monoubiquitylation usually regulates the localisation and activity of many cellular proteins. Histone H2A was found to be modified by monoubiquitin as

the first known substrate of ubiquitylation (Goldknopf and Busch, 1977). Monoubiquitin at histone C-terminal tail is important for meiosis (Robzyk et al., 2000) and also plays roles in DNA damage response and transcription regulation (Vissers et al., 2008). Monoubiquitylation also regulates other factors such as FANCD2, PCNA and plays important roles in the DNA damage response (section 1.5.3 and 3.1.2)(Ulrich and Walden). Multiple monoubiquitylation of many proteins localised on the plasma membrane causes their internalisation into primary endocytic vesicles and eventually degradation by the lysosome (Hicke, 2001). Some elegant studies showed further that ubiquitin fused in frame to a lysine-less receptor protein, or even to a heterologous protein that is not normally internalised can also stimulate internalisation (Shih et al., 2000, Roth and Davis, 2000). This trafficking process is mainly mediated by the endosomal sorting complex required for transport (ESCRT) machinery (Williams and Urbe, 2007).

1.2.2 K48-linked Polyubiquitin Chains

Cellular proteins are also modified by polyubiquitin chains with various linkages. Peng and coworkers confirmed by mass spectrometry the presence of different types of polyubiquitin chains in vivo, which are linked via seven available lysine residues on the surface of ubiquitin (Peng et al., 2003). Among those, approximately 29% of total polyubiquitin chains are K48-linked, which is the most abundant form (Peng et al., 2003, Xu et al., 2009). An early biochemical study of the N-end rule substrate β-galactosidase revealed that a polyubiquitin chain linked via K48 linkage is sufficient to target a model substrate to the 26S proteasome for degradation (Chau et al., 1989). Soon after this, Finley and coworkers found that yeast cells expressing K48R mutant as the only source of ubiquitin do not survive and that the degradation of proteins containing amino acid analogues is severely inhibited in cells, where the K48R mutant gradually replaces the wild type ubiquitin, suggesting that the K48-linked chain is the principal degradation signal for the proteasome *in vivo* (Finley et al., 1994). Further *in vitro* work has demonstrated that four ubiquitin moieties is the minimal length of K48-linked chain required for efficient proteasome targeting (Thrower et al., 2000). However,

proteasome-independent functions of K48-linked polyubiquitin chain have also been reported. Transcription factor Met4 is polyubiquitylated by SCF^{Met30} at K163. The ubiquitin chain is linked via K48-linkage, however, inhibition of such chain formation does not stabilise Met4 (Flick et al., 2004). The crystal structure of K48-linked tetraubiquitin shows a closed, compact chain structure, in which the hydrophobic patch L8-I44-V70 of all four ubiquitin moieties is buried within the structure and mediates an intra-chain interaction between ubiquitin units (Figure 1.3A)(Eddins et al., 2007). However, the ubiquitin–ubiquitin interaction is weak so that the hydrophobic surfaces are still accessible for other recognition factors (Pickart and Fushman, 2004).

1.2.3 K63-linked Polyubiquitin Chains

The second well-studied type of polyubiquitin chain is the K63-linkd polyubiquitin chain, which accounts for 16.3 % of total cellular ubiquitin conjugates in budding yeast (Xu et al., 2009). An early genetic study revealed that the ubiquitin K63R mutant is defective in DNA repair, but has normal proteolytic function (Spence et al., 1995). It was first introduced as a new type of ubiquitin chain in the report that identified Mms2-Ubc13 as a heterodimeric E2 complex catalysing the formation of K63-linked chains in the context of DNA damage bypass (Hofmann and Pickart, 1999). Later, K63-linked polyubiquitin chains were found to modify the proliferating cell nuclear antigen (PCNA) at K164 and this modification initiates an error-free DNA damage bypass process (Hoege et al., 2002), whose molecular mechanism is still not clear (see section 3.1 for more details). K63-linked chains have also been identified as essential signals in the NF-κB (nuclear factor kappa-light-chain-enhancer of activated B cells) signalling pathway, formed by RING E3 ligase TRAF6 and E2 complex Ubc13-Uev1A. This type of chain was found to play a proteasome-independent role in activating IκB kinase (IKK) (Deng et al., 2000). It has now become clear that K63-linked ubiquitin chains function as scaffolds for the assembly of signalling complex in the NF-κB pathway (section 1.5 for more details) (Skaug et al., 2009). This non-degradative function of K63-linked chains is consistent with a recent report showing that cellular K63-linked ubiquitin conjugates do not accumulate upon the inhibition of proteasome activity,

whereas all other six types of lysine-linked chains increase (Xu et al., 2009). However, there are individual cases where a K63-linked chain functions as a degradation signal. An *in vitro* assembled K63-linked ubiquitin chain is sufficient to target a model substrate to the proteasome in a degradation assay and can bind the proteasome with an affinity similar to the K48-linked chain (Hofmann and Pickart, 2001). Recently, Saeki et al have shown that Rsp5-assembled K63-linked chains on Mga2 can lead to proteasomal degradation of Mga2, suggesting that a proteolytic role is also possible *in vivo* (Saeki et al., 2009). Structural work shows that the K63-linked tetraubiquitin chain has an extended conformation with no direct contact between the hydrophobic surfaces on each ubiquitin moiety (Figure 1.3B)(Datta et al., 2009).

1.2.4 K11-linked Ubiquitin Chains

Among all the non-canonical polyubiquitin chains, the K11 linkage has caught a lot of attention recently. Despite there being few examples of functionally relevant K11 linkages *in vivo*, surprisingly the K11-linked chain is the second most abundant ubiquitin chain in budding yeast, accounting for about 28% of total ubiquitin conjugates, similar to K48-linked chains (Peng et al., 2003, Xu et al., 2009). In human cells, the APC/C works together with E2s UbcH10/UBE2C and UBE2s to catalyse the formation of K11-linked chains on various substrates including cyclin A and securin (Jin et al., 2008, Garnett et al., 2009, Williamson et al., 2009). In addition to that, K11-linked chains have also been reported in the ERAD pathway (Alexandru et al., 2008). The conjugation reaction requires a cluster of residues around K11 on ubiquitin, named TEK-box, homologous of which has also been found in many APC/C substrates to facilitate chain nucleation. K11-polyubiquitylated substrates are degraded by the proteasome (Jin et al., 2008). In yeast, APC/C does not assemble K11-linked polyubiquitin chains on its substrates, and substrates modified by a K11-linked chain remain to be identified to explain the high abundance of this type of chain *in vivo*. Recently, the structure of a K11-linked diubiquitin was solved (Bremm et al., 2010). This type of chain adopts a compact conformation with K29 and K33 of the proximal ubiquitin facing the interface of the two ubiquitin moieties. An interesting feature is that

the hydrophobic patch is not involved in intra-chain interaction but rather exposed to solvent (Figure 1.3C) (Bremm et al., 2010).

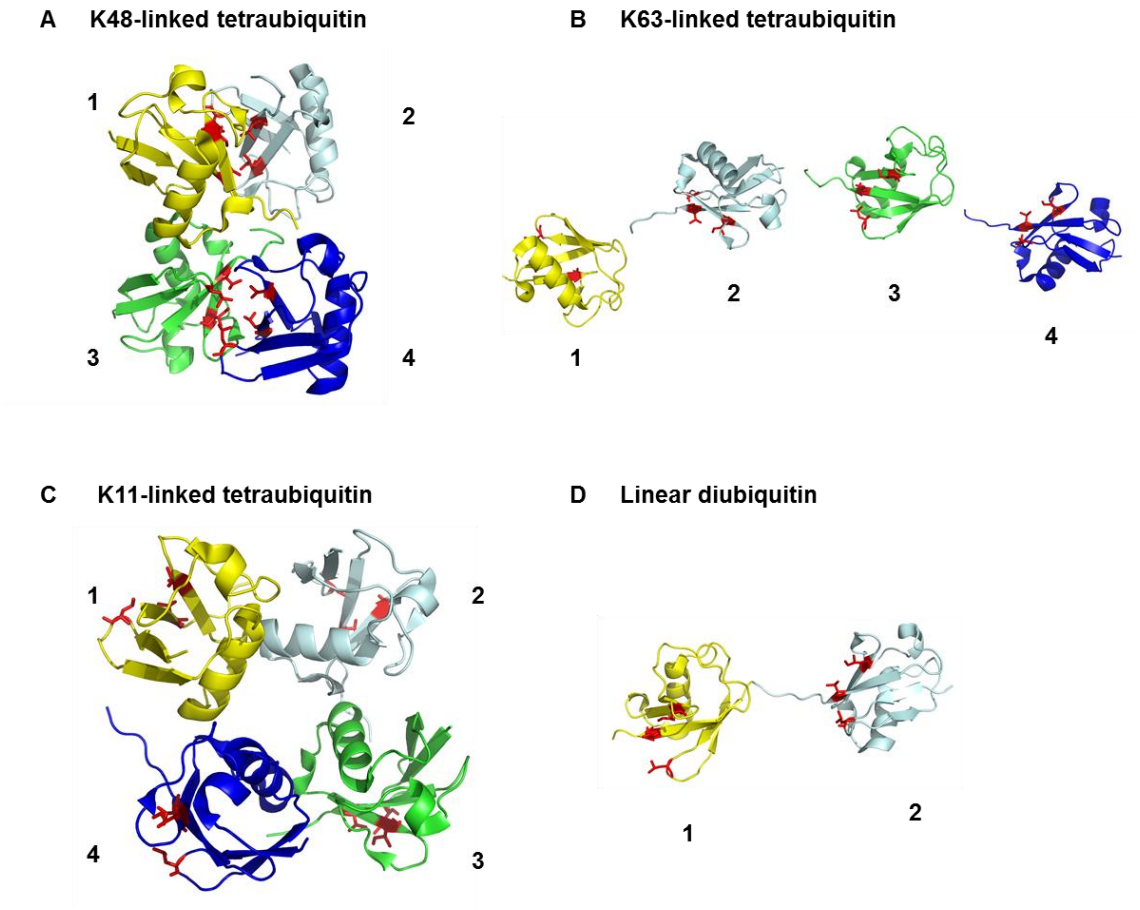

Figure 1.3 Crystal structures of K48-, K63-, K11-linked and linear ubiquitin chains

(A) Crystal structure of K48-linked tetraubiquitin, PDB code: 2O6V. The colouring of ubiquitin moieties from proximal ubiquitin (ubiquitin moiety close to the substrate) to distal ubiquitin (ubiquitin moiety far away from the substrate) is: yellow-cyan-green-blue (1-2-3-4) and there are intra-chain contact between ubiquitin units. The L8-I44-V70 (red) hydrophobic patches of each ubiquitin are buried inside of the chain structure. The colouring scheme for ubiquitin moieties and hydrophobic patches are the same for all structures. (B) Structure of K63-linked tetraubiquitin, PDB code: 3HM3. The chain exhibits an open conformation and there is no contact between ubiquitin units. (C) Structure of K11-linked tetraubiquitin, PDB code: 2XEW. The K11-linked tetraubiquitin also exhibits a compact conformation, but unlike the K48-linked chain, the hydrophobic patches are exposed. (D) Crystal structure of linear diubiquitin, PDB code: 2W9N. The linear diubiquitin adopts a linear shape quite similar to the K63-linked chain. This figure was generated by PyMol.

1.2.5 Other Lysine-linked Ubiquitin Chains

K6-, K27-, K29- and K33-linked ubiquitin chains have also been detected *in vivo* in budding yeast (Peng et al., 2003) and higher eukaryotes (Nishikawa et al., 2004, Al-Hakim et al., 2008), although they only represent relatively small proportions of total cellular ubiquitin conjugates: 10.9% (K6), 9% (K27), 3.2% (K29) and 3.5% (K33) in yeast. Breast and ovarian cancer susceptibility protein 1 (BRCA1) can work together with BARD1 to assemble K6-linked polyubiquitin chains on itself (Wu-Baer et al., 2003) and the K6-polyubiquitylated BRCA1 is recognised by the proteasome. However, it is processed differently from a regular proteasome substrate, as it is deubiquitinated rather than degraded *in vitro* (Nishikawa et al., 2004). K29-linked chains were first described in the initial ubiquitylation step of the UFD (ubiquitin fusion degradation) pathway (see section 1.4.2 for more details), where the K29-linked chains are initially assembled by Ufd4 on the model substrate (Johnson et al., 1995). More recently, K29-linked chains have been reported to function in lysosomal degradation of proteins *in vivo* (Chastagner et al., 2006). Furthermore, AMPK-related kinase 5 (ARK5) and MARK4 kinases are polyubiquitylated *in vivo* through K29/K33-linked chains, whose function is to block the kinase activation by interfering with phosphorylation of the activation-loop residues (Al-Hakim et al., 2008).

1.2.6 Linear Ubiquitin Chains

The scope of ubiquitin signals is broader than expected. Apart from seven lysine residues on the surface of ubiquitin, the discovery of linear ubiquitin chains has demonstrated that the N-terminal methionine can also be used to form a peptide bond with G76. In yeast, linear ubiquitin chains, synthesised as polyproteins by expression of a tetraubiquitin gene, *UBI4*, were initially considered as a source of cellular ubiquitin that is produced under stress conditions and quickly processed into ubiquitin monomers shortly after its production (Ozkaynak et al., 1984, Pickart and Fushman, 2004). Now LUBAC (linear ubiquitin chain assembly complex), a specific ligase complex composed of two E3s HOIL-1 and HOIP, has been identified to actively assemble linear ubiquitin chains linked via M1-G76 peptide bond in higher eukaryotes (Kirisako et al.,

2006). It has been reported in the same study that overexpression of LUBAC promotes the degradation of model substrates, suggesting a potential role of linear ubiquitin chains in the proteasomal degradation pathway. More recently, NEMO (NF-κB essential modulator), the regulatory component of IκB kinase (IKK) complex, was shown to be the first physiological substrate of linear ubiquitin chains. LUBAC specifically assembles linear ubiquitin chains at K285 and K309 of NEMO (Tokunaga et al., 2009), and a UBAN (ubiquitin binding in ABIN and NEMO) domain of NEMO can interact specifically with this linear ubiquitin chain (Rahighi et al., 2009). Linear ubiquitylation of NEMO and the interaction between linear chains and UBAN domain are both required for the activation of the NF-κB signalling pathway. This is supported by experimental evidences from *HOIL-1L* knock out mice and cell lines expressing the mutant form of UBAN domain (Tokunaga et al., 2009, Rahighi et al., 2009). Finally, another interesting feature of linear ubiquitin chains is that they adopt a conformation very similar to K63-linked ubiquitin chains because M1 of ubiquitin is only 6.3 Å away from K63. Komander and coworkers have solved the crystal structure of linear diubiquitin (Figure 1.3D), which shows a structure almost identical to the K63-linked chain (Komander et al., 2009b). However, whether linear ubiquitin chains are functionally equivalent to K63-linked chains *in vivo* remains to be investigated.

1.3 Ubiquitin-binding Domains

The versatile ubiquitin signals need to be translated in cells, and ubiquitin-binding domains (UBDs) are protein modules that recognise different forms of ubiquitin signals. To date, more than twenty different types of UBDs have been identified. According to the structure they fold into they can be classified into several groups including α-helical structures, zinc-fingers (ZnFs), ubiquitin-conjugating enzyme-like (UBC) domains and pleckstrin homology (PH) folds (Dikic et al., 2009). Recent advancement of structural biology to crystallise UBDs in complex with ubiquitin has greatly improved our understanding on UBD-ubiquitin interactions. This section will focus on the recognition of monoubiquitin and different polyubiquitin chains by various UBDs.

1.3.1 Ubiquitin Recognition by Different Types of UBDs

α-helical structures, the biggest family of UBDs, are commonly binding the hydrophobic patch in the β-sheet of ubiquitin centred around L8-I44-V70. The ubiquitin-associated domain (UBA) shows a perfect example where two discontinuous α-helices of the UBA domain interact with the I44 patch on ubiquitin (Figure 1.4A). ZnFs are the second largest family of UBDs and they can recognise three different surfaces of ubiquitin, therefore offering more diversity in ubiquitin recognition and binding affinity. For example, the A20 ZnF predominantly binds the polar patch on the ubiquitin centred on D58, the ZnF in NPL4 interacts with the surface around I44, and the ZnF of isopeptidase T binds to ubiquitin's C-terminus (Figure 1.4B). It also suggests even a same class of UBD can have multiple ways to recognise ubiquitin and experimental approaches remain to be the most reliable way to determine the binding surface on both ubiquitin and ubiquitin-binding proteins. The third group of UBD are UBC-related domains and most of the time they are found in E2s. They usually recognise a surface on ubiquitin containing the hydrophobic patch around I44 (Figure 1.4C). Last but not least, PH fold is a less represented group of UBD. The most well-known example in this group is the PRU (PH receptor for ubiquitin) domain of Rpn13, which binds ubiquitin with very strong affinity (Husnjak et al., 2008). In this case, three loops in the PRU domain of Rpn13 can form hydrogen bonds with H68, which significantly contributes to the interaction with ubiquitin in addition to the canonical I44-centred binding surface (Figure 1.4D).

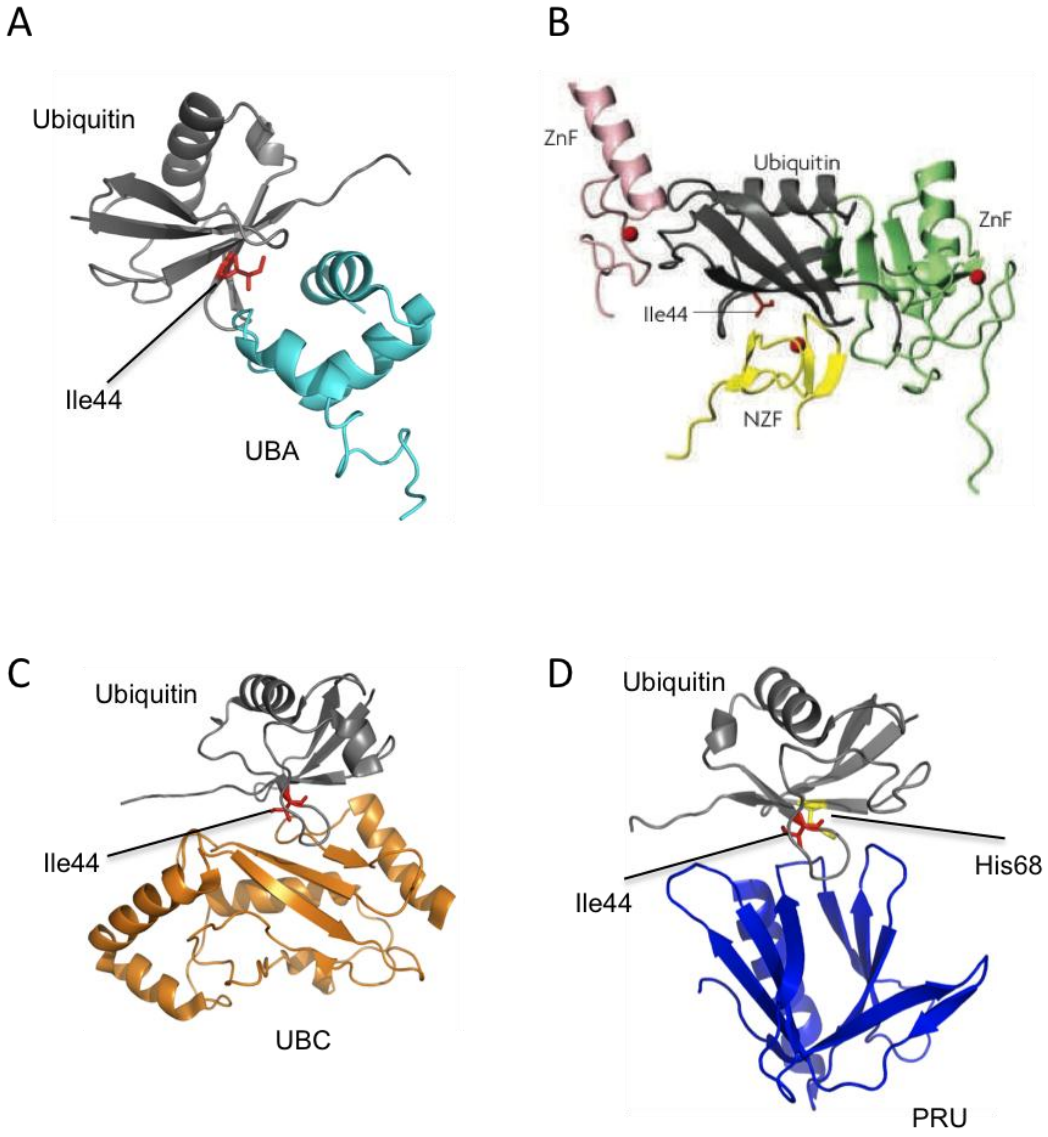

Figure 1.4 Structures of different ubiquitin-UBD complexes
Co-crystal structures show several different structural domains binding to ubiquitin. Ubiquitin is shown in grey and I44 is labelled in red in all panels (A) Structure of ubiquitin in complex with the UBA domain (shown in cyan) of PLIC1 (protein linking IAP with cytoskeleton 1), PDB code: 2JY6. The UBA domain recognises hydrophobic patch centred around I44. (B) Structure of three different ZnFs in complex with ubiquitin: ZnF (also called NZF) of NPL4 (shown in yellow, PDB code: 1Q5W) binds the hydrophobic patch around I44 of ubiquitin; ZnF of RABEX5 (shown in light green, PDB code: 2FIF) binds the D58-centred polar surface on ubiquitin; ZnF of isopeptidaase T (shown in pink, PDB code: 2G45) interacts with the C-terminus of ubiquitin. This picture was taken from (Dikic et al., 2009). (C) Structure of ubiquitin in complex with UBC domain of UBCH5C (shown in orange, PDB code: 2FUH). (D) Structure of ubiquitin in complex with the PRU domain of RPN13 (shown in dark blue, PDB code: 2Z59). Both I44 (red) and H68 (yellow) on ubiquitin contribute to the interaction with the PRU domain. Figure A, C and D were generated by PyMol.

1.3.2 Linkage-Specific Recognition of Polyubiquitin Chains by UBDs

Many UBDs can bind polyubiquitin chains to mediate specific cellular signalling events. As we know, ubiquitin chains exhibit diverse conformations depending on which lysine residue is used as linkage, for example K48-, K63-, K11-linked and linear ubiquitin chains all have distinct structures. Special UBDs of downstream effector proteins can act as signal receptors and transducers to bind ubiquitin chains with specific linkage. K48-linked chains exhibit a compact conformation as shown in Figure 1.3A, with the I44-centred patch of each ubiquitin moiety buried within the chain. The UBA domain has been shown to bind the K48-linked chain specifically due to its ability to insert into the space between otherwise tightly folded diubiquitin and interact with the I44-centred patches of both ubiquitin molecules (Figure 1.5A)(Varadan et al., 2005). A K63-linked ubiquitin chain has an extended structure with the I44-centred hydrophobic patches exposed. The K63-specific deubiquitylating enzyme AMSH-LP in complex with a K63-linked diubiquitin illustrates that the enzyme not only recognises K63 but also neighbouring residues such as Q62 and E64 on the proximal ubiquitin to achieve its specificity (Figure 1.5B). This type of interaction also ensures that only K63-linked chains with correct orientation can bind to the enzyme. The I44-centred hydrophobic patch on the distal ubiquitin forms an additional interaction surface for AMSH-LP (Sato et al., 2008). More interestingly, some UBDs, such as UBAN domain, are even able to distinguish linear chains from K63-linked chains, two highly similar forms of ubiquitin signals. The UBAN domain of NEMO, a coiled-coil dimer, forms a heterotetrameric complex with two linear diubiquitin molecules (Rahighi et al., 2009, Ivins et al., 2009). Linkage specificity is achieved by a continuous surface along the coiled-coil that interacts with the I44-centred patch and the C-terminal tail (R72-G76) of the distal ubiquitin plus a unique interaction surface of the proximal ubiquitin (Rahighi et al., 2009) (Figure 1.5C).

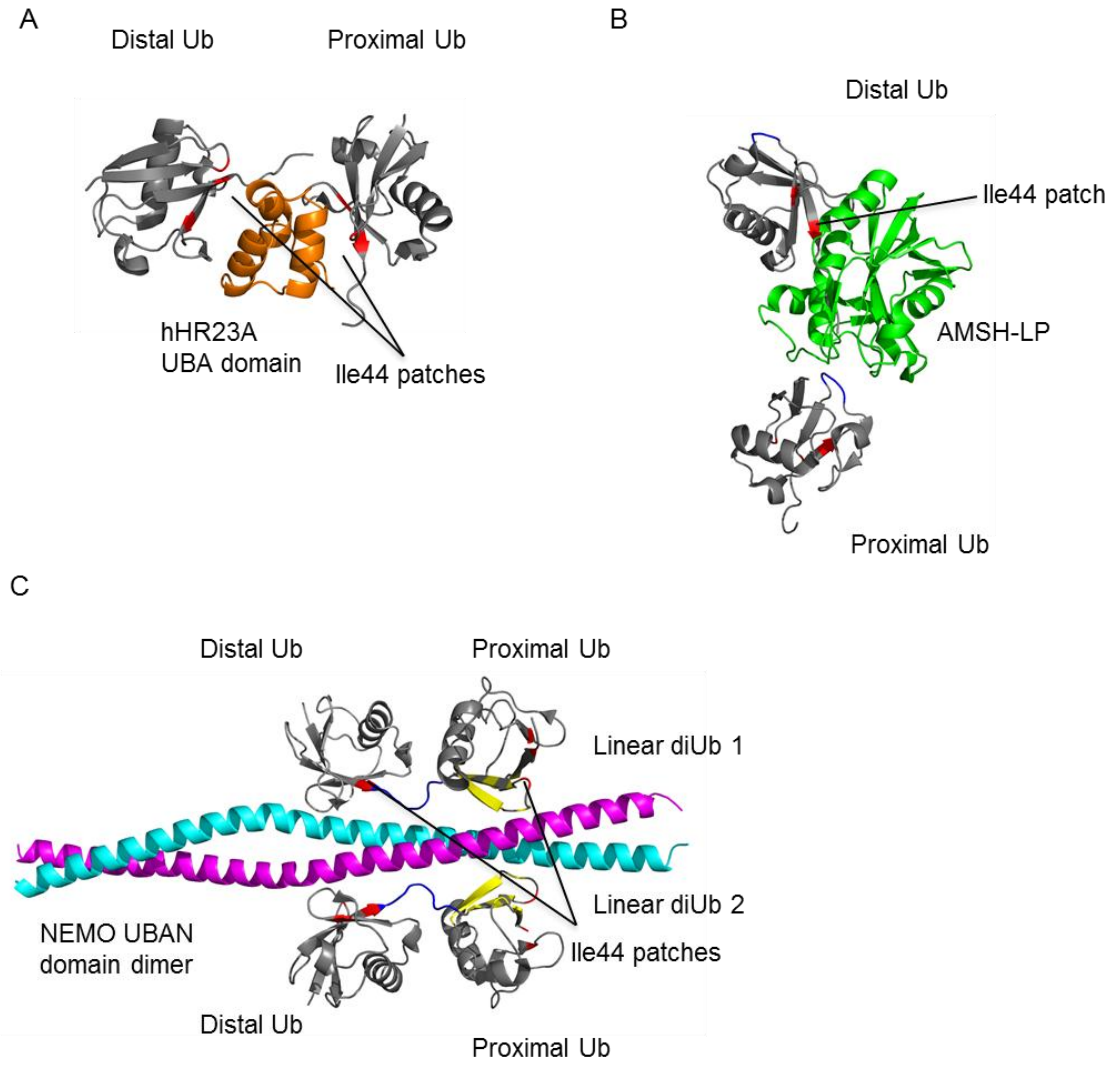

Figure 1.5 The structure of different ubiquitin chains bound to proteins
(A) Structure of K48-linked diubiquitin (grey) in complex with UBA2 domain from hHR23A (orange), PDB code: 1ZO6. The UBA2 domain inserts into the compact K48-linked diubiquitin to interact with both I44-centred hydrophobic patches (red) (B) Structure of K63-linked diubiquitin (grey) in complex with AMSH-LP (green), PDB code: 2ZNV. The interaction surfaces on K63-linked diubiquitin include a surface formed by Q62-K63-E64 (shown in blue) on the proximal ubiquitin and I44-centred hydrophobic patch (red) on the distal ubiquitin. (C) Structure of two linear diubiquitin (grey) in complex with the NEMO UBAN domain dimer (cyan/megenta), PDB code: 2ZVN. The contact surface covers the I44-centred patch (red) and the C-terminal tail (R72-G76, shown in blue) of the distal ubiquitin plus a unique interaction surface of the proximal ubiquitin (Q2, F4, K6, G10, T12, I13, T14, E16, E64 and T66; shown in yellow). All figures were generated from indicated PBD files with PyMol.

However, the same type of UBD does not always show the same linkage specificity. For instance, UBA domains are present in many ubiquitin-interacting proteins, but a systematic study shows that UBA domains have subgroups specifically binding to K48- or K63-linked chains, respectively. Some of the UBA domains do not show any preference for polyubiquitin chains (Raasi et al., 2005). Overall, the interaction between the ubiquitin monomer and UBDs is quite weak, in the range of 10-500 μM (Ikeda and Dikic, 2008), with the highest affinity observed so far (around 300 nM) for the PRU domain of Rpn13 (Husnjak et al., 2008). While the interaction between polyubiquitin chains and UBDs are stronger than the case of monoubiquitin. The interaction between ubiquitin and UBD is usually compensated by additional interactions between the ubiquitin-binding effector proteins and the ubiquitylated proteins. It is therefore more important to analyse the role of UBDs in a specific interaction between a ubiquitylated protein and a ubiquitin-binding protein. Examples of UBDs in ubiquitin mediated signalling will be described in Section 1.5.

1.4 The Proteasome-dependent Degradation Pathway

Ubiquitin is best known for its function to tag a protein and signal for proteasomal degradation. This section will introduce the major cellular degradation machinery, the 26S proteasome, and pathways that ubiquitylate and target substrate proteins to the proteasome.

1.4.1 The 26S Proteasome

The ubiquitin proteasome system (UPS) is the major system for protein degradation in eukaryotes. Degradation of polyubiquitylated proteins occurs in the 26S proteasome, which is a giant protein complex with an overall size over 2.5 MDa (Finley, 2009). The proteasome contains two major parts, the core particle (CP) and the regulatory particle (RP), which sit on one or both ends of the cylinder-shaped core particle. The proteasome's proteolytic activity lies within the large internal chamber of the CP, where β-type subunits form a heptameric ring structure hosting the proteolytic active sites

(Finley, 2009). Substrate access to the CP catalytic chamber is blocked through a topological mechanism, as substrates have to be unfolded and then pass through the narrow translocation channel in the RP in order to reach the CP. The RP has 19 subunits and has been subdivided into base and lid, which are proximal and distal to the CP, respectively. The basic function of RP is to recognise and process ubiquitin conjugates. The base of RP has subunits with ATPase activity, required for protein unfolding, translocation and proteolysis, and other subunits like Rpn10 and Rpn13 serve as receptors for ubiquitin conjugates. The lid of the RP harbours subunit Rpn11 with deubiquitylation activity, which positively contributes to the proteasome activity (Verma et al., 2002, Yao and Cohen, 2002). Overall, a polyubiquitylated substrate is first recognised and bound to the ubiquitin receptors in the base of the proteasome. Polyubiquitin chains are disassembled by the DUB activity of the lid and the substrate is unfolded and passed through the translocation channel to reach the CP for degradation. The second step, the unfolding, is mediated by ATPases in the base of the proteasome (Finley, 2009). Interestingly, the proteasome does not selectively degrade ubiquitin conjugates linkage-specifically. Proteasomal ubiquitin receptors include Rpn10, Rpn13, Ddi1, Rad23 and Dsk2, which do not show preference for ubiquitin chains of a specific linkage (Raasi et al., 2005), and many different types of ubiquitin chains can target substrates for proteasomal degradation *in vitro* (Hofmann and Pickart, 2001, Zhao and Ulrich, 2010). More recently, mass-spectrometry has detected an increase of six types of lysine-specific chains (K6, K11, K27, K29, K33 and K48) in cells treated with proteasome inhibitor, suggesting that the proteasome usually processes each of these types of chains (Xu et al., 2009).

1.4.2 The N-end Rule and the UFD Pathway

Generally, a substrate protein is recognised and ubiquitylated by specific E3 enzymes and the modified substrate is taken to the 26S proteasome for destruction. Therefore, the proteasomal degradation pathway can be divided into a substrate ubiquitylation step and a proteasome targeting step. Our understanding about ubiquitin-mediated substrate degradation stems largely from studying model substrates. Varshavsky and co-workers

found that expressing an ubiquitin-β-galactosidase fusion protein in yeast leads to cleavage of the ubiquitin and results in a deubiquitylated β-galactosidase exposing its N-terminal residue (Bachmair et al., 1986). Depending on the identity of the exposed N-terminal residue, β-galactosidase exhibits a half-life from 3 minutes to more than 20 hours. The relation between the metabolic stability of a protein and the identity of its N-terminal residue is called the N-end rule, and the process in which cells recognise potential substrates by means of their N-termini and target them for degradation is called the N-end rule pathway (Varshavsky, 1996). Later, it became clear that an E3 enzyme, Ubr1, specifically recognises N-end rule substrates and assembles K48-linked polyubiquitin chains on the substrate protein to trigger its degradation (Bachmair and Varshavsky, 1989, Chau et al., 1989, Bartel et al., 1990) (Figure 1.6A). The N-end rule pathway has been successfully used to develop the degron system, which can deplete a target protein in a regulatable manner (Turner and Varshavsky, 2000).

Model substrates have also contributed to the identification of several factors downstream of substrate ubiquitylation, which are required for proteasome-dependent degradation. Varshavsky and co-workers used a short-lived, but non-cleavable version of ubiquitin-β-galactosidase to search for factors involved in its degradation (Johnson et al., 1995). Factors found in that screen were named as ubiquitin fusion degradation 1 (Ufd1), Ufd2, Ufd3 (Doa1), Ufd4 and Ufd5 (Rpn4). Further studies have extended the UFD pathway and shown that relevant model substrates or physiological ERAD (ER-associate degradation) substrates are initially mono- or di-ubiquitylated and bound by the Cdc48-Npl4-Ufd1 complex, where the Cdc48-bound factor Ufd2 further elongates the ubiquitin chain on the substrate to a length optimal for proteasome targeting. Then cellular ubiquitin shuttling factors like Rad23 and Dsk2 bind to the polyubiquitylated substrate and deliver it to the proteasome (Richly et al., 2005) (Figure 1.6B).

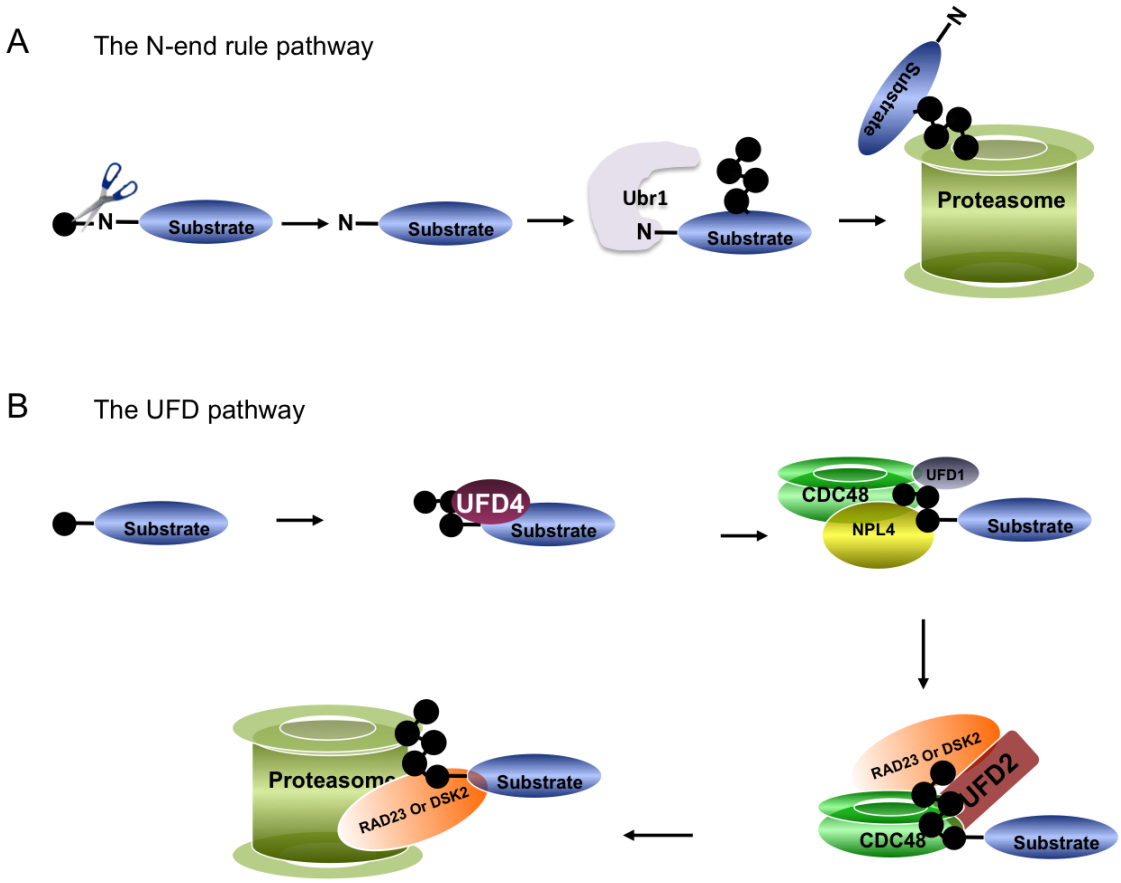

Figure 1.6 The N-end rule pathway and the UFD pathway
(A) A schematic illustration of the N-end rule pathway. The ubiquitin moiety (black filled circle) of an ubiquitin-β-galactosidase fusion protein is cleaved off to generate a deubiquitylated β-galactosidase (blue oval) with an exposed N-terminal residue. E3 Ubr1 (pink) recognises the N-terminal residue and assembles K48-linked polyubiquitin chains on β-galactosidase. The polyubiquitylated β-galactosidase is targeted to the proteasome (green cylinder shape) for degradation. (B) A schematic illustration of the UFD pathway. A non-cleavable ubiquitin-β-galactosidase fusion protein is first mono- or di-ubiquitylated by an E3 Ufd4 (purple oval) through K29-linkage. The oligoubiquitylated substrate is bound to the Cdc48-Npl4-Ufd1 complex (green-yellow-grey) and the Cdc48-associated factor Ufd2 (red) further elongates the short ubiquitin chain on the substrate via K48-linkage. Rad23 and Dsk2 (orange oval) are recruited to the Cdc48 complex via Ufd2. They bind to the polyubiquitylated substrate and deliver it to the proteasome (green cylinder shape) for degradation.

Within the UFD pathway, many factors participated in the process of substrate ubiquitylation and the proteasome targeting. In the case of UFD model substrates such as the non-cleavable ubiquitin-β-galactosidase, the E3 Ufd4 initially assembles a short K29-linked chain on the substrate (Johnson et al., 1995). Cdc48 forms a complex with

its cofactor Npl4 and Ufd1, which are important for substrate recruiting (Rape et al., 2001, Meyer et al., 2000, Hitchcock et al., 2001). Ufd2 was described as an E4 enzyme and a Cdc48-associated factor (Koegl et al., 1999). It has two distinct functions in the UFD pathway: firstly, its U-box domain catalyses the elongation reaction of short ubiquitin chains on Cdc48-bound substrate proteins; secondly, it binds to Cdc48 and mediates the association of Rad23/Dsk2 with the Cdc48 complex (Richly et al., 2005). Rad23 and Dsk2 are ubiquitin shuttling factors. They each contain a UBA domain, which allows ubiquitin binding, and an ubiquitin-like (UBL) domain, which in turn can dock on-to the proteasome. Such elegant arrangement allows both factors to provide a connection between ubiquitylated substrates and the proteasome. The functions of Rad23 and Dsk2 *in vivo* are partially overlapping. Together with three additional ubiquitin receptor proteins, Ddi1, Rpn10 and Rpn13, they provide extra layers of substrate selectivity for the proteasome (Verma et al., 2004, Husnjak et al., 2008).

1.5 Proteolysis-Independent Functions of Ubiquitin Signalling

The proteolysis-independent functions of ubiquitin signalling are as important as its function as a degradation signal. The non-proteolytic functions of ubiquitin have been reported in the immune response, apoptosis and the DNA damage response. In those cases, mono- or poly-ubiquitin can function as a mediator for protein-protein interactions, where it provides extra binding sites for downstream UBD-containing effector proteins. Alternatively, the conjugation of ubiquitin can have allosteric effects on substrate proteins to effect subtle changes to protein structure or enzymatic activity. There are many examples of different non-proteolytic functions of ubiquitin. However, in this section I will describe only a few selected ones that are illustrative of the mechanism of ubiquitin signalling.

1.5.1 NF-κB Pathway

The NF-κB pathway is part of the cellular response to different stimuli including bacterial and viral antigens, free radicals, cytokines and stress. It has important roles in regulating the immune response to infection. The pathway functions to activate a transcription factor, NF-κB, which presents as a dimer of p50/p65 and controls a group of genes involved in immunity, inflammation and cell survival. However, inhibitor of NF-κB (IκB) binds to NF-κB and inhibits its activity by retaining the dimer in the cytoplasm under basal conditions. Ubiquitin-mediated signalling has been nicely illustrated in the NF-κB pathway, where K63-linked and linear ubiquitin chains fulfil non-proteolytic roles in the activation of the NF-κB, and deubiquitylating enzymes also negatively regulate this process. In the tumour necrosis factor (TNF) pathway, a sub-branch of the NF-κB pathway, TNFα binding to the TNF receptor (TNFR) results in the rapid formation of a receptor-associated complex, which includes TNFR1-associated death domain protein (TRADD), TRAF2, cIAP1, cIAP2 and the receptor interacting protein kinase (RIP1) (Skaug et al., 2009). The TRAF2 and cIAPs assemble K63-linked polyubiquitin chains on RIP1 to recruit and activate TAK1 and IKK complexes (Ea et al., 2006). The K63-linked polyubiquitin chain acts as a platform for the assembly of the downstream signalling complex. TAB2 and NEMO, which are the regulatory subunits of TAK1 and IKK complexes, respectively, contain UBDs selective for K63-linked chains to mediate this recruitment (Ea et al., 2006, Wu et al., 2006, Kanayama et al., 2004). Finally, the activated TAK1 phosphorylates and activates the IKK complex, which subsequently leads to the phosphorylation, ubiquitylation and proteasomal degradation of IκB and activates NF-κB (Figure 1.7). During this process, the ubiquitylation and ubiquitin-binding of NEMO positively regulates the activation process. NEMO is the regulatory subunit of the IKK complex. It is modified with linear ubiquitin chains via the newly identified LUBAC complex at K285/K309 and this modification is important for the activation of NF-κB (Tokunaga et al., 2009). NEMO also has a UBAN domain, which has been shown to bind linear ubiquitin chains as well as K63-linked chains, and that is also crucial for NF-κB activation (Rahighi et al., 2009, Wu et al., 2006). A structural study shows that the UBAN domain of NEMO, a coiled-coil dimer, forms a heterotetrameric complex with two linear diubiquitin molecules (section 1.3.2 and Figure 1.5C). Although it has been proposed that linear ubiquitin

chain binding of IKK complex mediates its multimerisation, the exact mechanism of NF-κB activation by linear chains remains unclear (Iwai and Tokunaga, 2009). Last but not least, several deubiquitylating enzymes like CYLD and A20 also contribute to the downregulation of NF-κB by disassembling those functional important polyubiquitin chains, reflecting a dynamic regulation process mediated by ubiquitin signalling (Skaug et al., 2009).

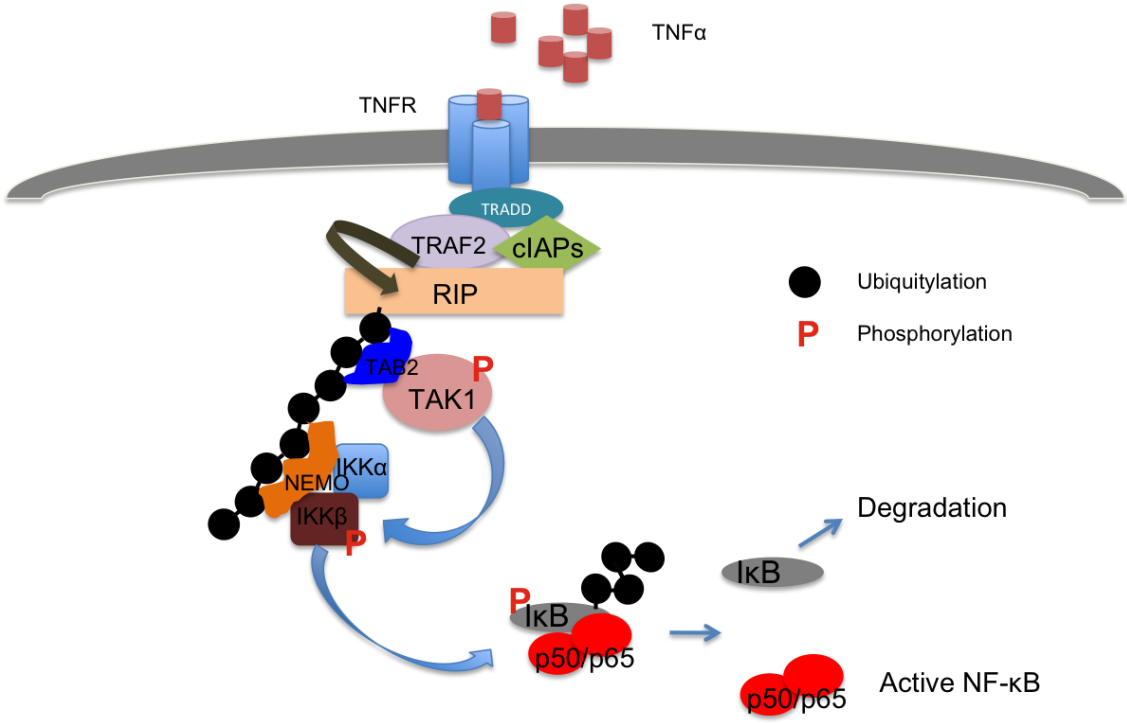

Figure 1.7 Role of ubiquitin in the TNF pathway
Binding of TNFα (ruby) to the TNF receptor (blue) triggers the formation of a receptor-associated complex, which consists of TRADD (dark green), RIP1 (light orange), cIAPs (green) and TRAF2 (purple). TRAF2 and cIAPs quickly assemble K63-linked polyubiquitin chains on RIP1, which recruits the TAK1 complex (TAB2/TAK1, shown in dark blue/pink) and the IKK complex (NEMO/IKKα/IKKβ, shown in orange/blue/dark red). TAK1 is activated via auto-phosphorylation, and it then phosphorylates IKKβ to activate the IKK. IκB (grey) is phosphorylated by the IKK and further modified by K48-linked polyubiquitin chains, which target IκB for proteasomal degradation. Finally, the free NF-κB dimer (p50/p65) (red) enters the nucleus to activate gene transcription.

1.5.2 Apoptosis

In apoptosis, ubiquitin signalling has also played a number of regulatory roles at various stages of this important process (Broemer and Meier, 2009). Caspase activation and regulation is crucial for apoptosis. The inhibitor of apoptosis (IAP) proteins function as E3 ligases to negatively regulate the function of caspases. The mammalian X-linked IAP (XIAP) can catalyse the formation of polyubiquitin chains on caspase 3 (Suzuki et al., 2001, Morizane et al., 2005). Similarly, DIAP (*Drosophila* IAP) assembles K63-linked polyubiquitin chains onto effector caspase drICE (homologue of caspase-3 and caspase-7). This modification does not affect protein levels of drICE or reduce its proteolytic activity directly. However, the K63-linked polyubiquitin chain sterically interferes with substrate entry to the catalytic site and may even cause a conformational change, which reduces the catalytic processivity of the enzyme (Ditzel et al., 2008). Moreover, cIAP1 and cIAP2 can also have negative effects on apoptosis via facilitating TNF-receptor-induced signalling to NF-κB, which in turn promotes the expression of many pro-survival genes. A UBA domain has been identified in many IAPs, and the presence of this UBD is required for constitutive activation of the NF-κB pathway, possibly by directly interacting with K63-polyubiqutylated NEMO (Gyrd-Hansen et al., 2008).

1.5.3 Genome Stability

A third field, where proteasome-independent ubiquitin signalling plays many important roles, is maintaining genome stability. Genome stability is well maintained in the cell by various DNA damage responses and repair processes. In the double-strand break (DSB) repair, the recruitment and assembly of a signalling complex including the key DSB repair factor BRCA1 are mediated by a series of ubiquitylation events. E3 proteins including RNF8, RNF168 are sequentially involved in this process and UBDs (such as MIU domain of RNF168) contribute to the localisation of their host proteins to the DSB site. The ubiquitin conjugates generated by a series of ubiquitylation events at the DSB site are believed to be K63-linked chains (Stewart et al., 2009, Doil et al., 2009, Sobhian et al., 2007) and this polyubiquitin signal functions as a scaffold to facilitate the assembly of a complex including RAP80, abraxas, BRCC45, NBA1 and BRCC36

for a subsequent recruitment of BRCA1 (Kim et al., 2007, Liu et al., 2007, Sobhian et al., 2007, Wang et al., 2007). Any interruption on ubiquitylation or ubiquitin–binding domain within this signalling cascade leads to defects in the recruitment of the entire complex and key factors such as BRCA1, suggesting an crucial role of ubiquitin signalling in DSB repair. Intracellular interstrand cross-links (ICL) are mainly repaired by the Fanconi anaemia pathway. In this case, Fanconi core complex FANCA, FANCB, FANCE, FANCG, FAAP100 and the catalytic subunit FANCL form a multisubunit E3 complex. The core complex monoubiquitylates FANCD2-FANCI and leads to the complex localised onto the chromatin (Garcia-Higuera et al., 2001, Smogorzewska et al., 2007). The monoubiquitylation event is absolutely required for the repair of ICLs. Deubiquitylation of the FANCD2-FANCI complex is also required by the Fanconi anaemia pathway. Interestingly, monoubiquitin fused to a non-ubiquitylable FANCD2 mutant only partially rescues cellular ICLs repair defects (Matsushita et al., 2005, Ishiai et al., 2008) and it became clear later that USP1 mediated deubiquitylation of FANCD2 is required for ICL repair (Oestergaard et al., 2007, Nijman et al., 2005).

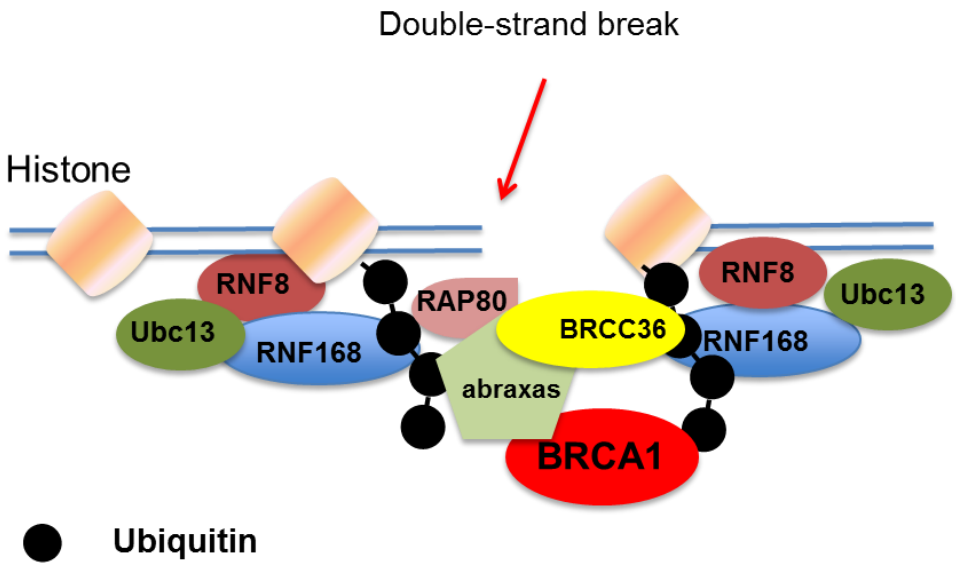

Figure 1.8 Ubiquitin signalling at double-strand breaks
A cascade of ubiquitylation events and ubiquitin-binding events occurs in reponses to double-strand breaks. E3 enzyme RNF8 (ruby) and RNF168 (blue) act sequentially to assemble K63-linked ubiquitin chains (black), which then leads to the recruitment of RAP80 (purple), BRCC36 (yellow), abraxas (light green) and BRCA1(red) eventually.

Because ubiquitin plays so many important roles in processes such as the immune response, apoptosis and DNA repair, it is not surprising that the ubiquitin signalling system has become a very attractive target for the development of anti-cancer drugs. Treatment of proteasome inhibitors leads to severe defective consequences in degradation of cellular proteins and recycling of the free ubiquitin, therefore affecting multiple cellular pathways. Now the first approved proteasome inhibitor bortezomib has been successfully used in clinics to treat multiple myeloma. Some studies have suggested that large basal level of ER stress associated with high levels of immunoglobulin production makes myeloma especially sensitive to proteasome inhibitors (Meister et al., 2007). The success of the first proteasome inhibitor-based drug has proved that studying the function of ubiquitin signalling has great clinical values.

1.6 The Aims of the Thesis

I have just given a very general introduction to the ubiquitin system, from the enzymatic reactions, the signalling diversity to its biological functions in different contexts. This study mainly focuses on two parts: polyubiquitin signals and UBDs. The first project was to address the question whether linear and K63-linked ubiquitin chains are functional interchangeable. Towards this end, PCNA was used as a model substrate to evaluate the function of two highly similar ubiquitin signals on a common substrate. The functions of linear and K63-linked chains on PCNA were studied separately. The second project aimed at identifying factors that specifically interact with K63-polyubiquitylated PCNA and meanwhile search for novel ubiquitin-binding proteins. The focus of this project quickly shifted towards a characterisation of Spc25, a potential ubiquitin-binding protein identified in the screen. This thesis describes further studies of the ubiquitin-binding properties of Spc25, the identification of mutants that abolish ubiquitin binding in Spc25 and an investigation of the biological functions of ubiquitin binding in Spc25. Further efforts were undertaken to investigate the ubiquitylation of kinetochore proteins, especially those that interact with Spc25, and to identify the identity of modification targets.

Chapter 2. Materials and Methods

2.1 Strains

2.1.1 Yeast Strains

Please see Appendix 1 for a list of yeast strains used in this thesis.

2.1.2 *E.coli* strains

Please see Appendix 2 for a list of *E.coli* strains used in this thesis.

2.2 Plasmids

2.2.1 List of Plasmids

Please see Appendix 3 for a list of Plasmids used in this thesis.

2.2.2 Construction of Linear Fusions of Ubiquitin to PCNA

Constructs of Ub^*_n-$PCNA^*$ were created based on Ub^*-$PCNA^*$, which was described previously (Parker et al., 2007). The open reading frame of ubiquitin with K29/48/63R and G76R mutations was sequentially inserted once or multiple times in frame at the N-terminus of *pol30 (K127/164R)* as a *Bam*HI/*Bgl*II fragment, resulting $Ub^*_{2\text{-}4}$(L)-$PCNA^*$ constructs. The linker sequence VQIQ between each ubiquitin moiety was generated as a ligation product of the *Bam*HI/*Bgl*II sites. The linkerless version of Ub^*_4-$PCNA^*$ was generated by insertion of a four-ubiquitin (Ub^*_4) module at the N-terminus of *pol30 (K127/164R).* The Ub^*_4 module was assembled by blunt ligation of a *Stu*I/*Msc*I fragment bearing the ubiquitin (K29/48/63R, G76V) open reading frames. A ligation reaction was set up in the presence of *Stu*I and *Msc*I in order to eliminate ligation products with incorrect orientations (tail-to-tail or head-to-head). The reaction mix was incubated at 37℃ overnight, where the ligase activity was reduced but restriction enzyme activity was optimal. $PCNA^*$-Ub^*_4 was generated by replacing the Ub^* of $PCNA^*$-Ub^* (Parker et al., 2007) with the Ub^*_4 module as a PCR product digested with *Kpn*I and *Pst*I. The C-terminal ubiquitin was truncated after amino acid 74 (referred as ΔGG) to prevent conjugation reactions. Ub^{K63*}-$PCNA^*$ was generated by replacing the Ub^* unit of Ub^*-$PCNA^*$ with an Ub^{K63*} (K29/48R, G76V). All constructs were individually cloned into a YIplac128 derivative, where the expression was under control

of the *POL30* promoter. For protein production, Ub^{*}_{4}-PCNA* was cloned into pET28a as a *Hind*III/*Eco*RI fragment.

2.2.3 Construction of Linear Fusions of Ubiquitin to βGal

The Ub-βGal construct was obtained from E. Johnson (Johnson et al., 1995). The episomal plasmid was originally called Ub^{V76}-V-$e^{\Delta K}$-βGal and expression of the protein is under control of the *GAL10* promoter. In order to create Ub^{*}_{4}-βGal, the single Wt ubiquitin moiety was replaced by the Ub^{*}_{4} module which was described above. The Ub^{V76}-V-$e^{\Delta K}$-βGal was first digested with *Sph*I and followed by a blunt end reaction to the linearised plasmid. The Ub^{*}_{4} module PCR amplified from pGAD-Ub^{*}_{4} was digested with *Bgl*II and followed by a blunt end reaction. The vector was then ligated with the Ub^{*}_{4} module to have a Ub^{*}_{5}-βGal. The product was digested with *BamH*I to remove the Wt Ub moiety originated from the parent vector, and a blunt end reaction and a ligation reaction were performed subsequently to have Ub^{*}_{4}-βGal. The control βGal construct was generated by deletion of the ubiquitin moiety as *Sph*I/*BamH*I fragment and performing a blunt end reaction to the vector following by a religating reaction. To create Ub^{*}_{8}-βGal, a second Ub^{*}_{4} module was inserted into as *BamH*I/*Bgl*II fragment into the *BamH*I site of Ub^{*}_{5}-βGal cloning intermediate, which was described above. Then the Wt Ub moiety was removed from the resulting Ub^{*}_{9}-βGal as a *Sph*I/*BamH*I fragment. Ub^{*}-βGal was generated by inserting the Ub^{*} module into a *BamH*I site directly upstream of the βGal moiety of Ub-βGal and subsequent removal of the remaining Ub sequence (*Sph*I/*BamH*I) followed by religation. Plasmids were propagated in yeast on uracil-free medium.

2.3 DNA Oligonucleotides

Please see Appendix 4 for a list of oligonucleotides used in this thesis.

2.4 Buffers and Reagents

2.4.1 Common Medium Solutions

LB: Luria Broth (0.5% bacto-tryptone, 0.25% bacto-yeast extract, 170 mM NaCl, pH 7.0 with NaOH) for bacterial growth was prepared by the Cancer Research UK London Research Institute Medium Service. Antibiotics were added into LB medium before use and medium with antibiotics was stored at 4℃. Ampicilin was dissolved in water to make a 100 mg/mL working stock, and a final concentration of 100 μg/mL was used in LB+Amp medium. Kanamycin was dissolved in water to make a 50 mg/mL working stock, and a final concentration of 50 μg/mL was used in LB+Kan medium.

YPD: Yeast peptone glucose medium (1% yeast extract, 2% peptone, 2% glucose) and YPD agar were prepared by the Cancer Research UK London Research Institute Medium Service.

Dropout Powder Stock: This was prepared by overnight mixing of 2 g p-aminobenzoic acid and 20 g of each of the following compounds: alanine, arginine, asparagine, aspartic acid, cysteine, glutamine, glutamic acid, glycine, inositol, isoleucine, lysine, methionine, phenylalanine, proline, serine, threonine, tyrosine and valine.

Synthetic Complete (SC) Powder Stocks: These were prepared by overnight mixing of 36.7 g dropout powder, 4 g leucine, 2 g histidine, 2 g tryptophane, 2 g uracil and 0.5 g adenine. One or more amino acids were omitted to make specific stocks of SC medium.

Synthetic Complete (SC) Medium 2.5x Stock: This was prepared by mixing 5 g synthetic complete (SC) powder stock, 4.25 g Difco yeast nitrogen base (without amino acids and ammonium sulfate) and 12.5 g ammonium sulfate. The mix was dissolved in 1 L H_2O and autoclaved.

Synthetic Complete Medium: 200 mL of 2.5x SC medium stock was mixed with 50 mL of 20% glucose (w/v) and 250 mL of sterile H_2O to obtain 1x SC medium with 2% glucose. For promoter shut-off experiments, 2% lactate was used to replace 2% glucose as carbon source, and 2% galactose was used later to induce protein expression from the

GAL promoter. To prepare SC complete (SC) medium agar plates, appropriate 2.5x stock solution (250 mL) was mixed with 200 mL of melted 4% (w/v) bacto agar and 50 mL of 20% glucose (w/v). The mix was poured into Petri dishes and allowed to solidify before use.

20% Glucose/Lactate/Galactose: 20% glucose stock solution was prepared by the Cancer Research UK London Research Institute Medium Service. 20% lactate was prepared by dissolving 20 g of lactate in 100 mL sterile H_2O and adjusting the pH to 6.0. 20% galactose was prepared by dissolving 20 g of galactose in 100 mL H_2O. All final solutions were autoclaved before use.

2.4.2 Buffers and Solutions

2.4.2.1 Buffers for Yeast Manipulation and Experiments

LIT buffer: 100 mM LiOAc and 10 mM Tris-HCl, pH 7.4. The solution needs to be autoclaved before use.

LIT/PEG buffer: 100 g PEG (3350) was dissolved in 100 mL of LIT buffer. The solution needs to be autoclaved before use.

Large scale transformation pre-mix: 1.08 mL 1 M LiOAc, 300 µL 10 mg/mL ssDNA, 7.2 mL 50% PEG and 2.22 mL H_2O

HU buffer: 8 M urea, 5% (w/v) SDS, 200 mM Tris-HCl pH 6.8, 1 mM EDTA, 0.1% (w/v) bromophenol blue and 1.5% (w/v) DTT (added fresh)

Sporulation medium: 1% KOAc, autoclaved

Z 0.5 Solution: 37 µL STE buffer (1.2 M sorbitol, 25 mM Tris-HCl pH 8.0, 25 mM EDTA, pH 8.0) +2 µL of 1 M DTT + 1µL zymolase 20T (20 mg/mL)

2.4.2.2 Buffers for E.coli Manipulation

Tfb I buffer: 30 mM KOAc, 100 mM RbCl, 10 mM $CaCl_2$, 50 mM $MgCl_2$ and 15% v/v glycerol, pH 5.8

Tfb II buffer: 10 mM MOPS, 75 mM $CaCl_2$, 10 mM RbCl and 15% v/v glycerol, pH 6.5

2.4.2.3 Buffers for DNA Manipulation

TAE buffer: 40 mM Tris base, 40 mM glacial acetic acid and 1 mM EDTA.

6x DNA Loading buffer: 50% (w/v) sucrose and 0.1% (w/v) bromophenol blue dissolved in TE and filtered through a 0.45 μm filter (Milipore).

2.4.2.4 Buffers for RNA Manipulation

Glyoxal reaction mix: 60% v/v DMSO, 20% v/v deionised glyoxal, 1.2x BPTE electrophoresis buffer and 5% glycerol

RNA loading dye: 95% deionised formamide, 0.025% w/v bromophenol blue, 0.025% w/v xylene cyanol FF, 5 mM EDTA pH 8.0 and 0.025% w/v SDS

BPTE electrophoresis buffer: 100 mM PIPES, 300 mM Bis-Tris and 10 mM EDTA

10x SSC buffer: 1.5 M NaCl and 150 mM $Na_3C_6H_5O_7$ pH 7.0

2.4.2.5 Buffers for Protein Manipulation and Analysis

Coomassie de-staining solution: 45% methanol v/v, 10% glacial acetic acid v/v

Gel-drying solution: 3% glycerol, 20% methanol and H_2O

5x Laemmli Sample buffer: 250 mM Tris-HCl pH 6.8, 500 mM DTT, 10% (w/v) SDS, 0.1% (w/v) bromophenol blue and 10% (v/v) glycerol

5x Laemmli Running buffer: 125 mM Tris base, 1.25 M Glycine and 0.5% (w/v) SDS

PBS (Phosphate Buffered Saline) buffer: NaCl 137 mM, KCl 2.7 mM, Na_2HPO4 10 mM, KH_2PO4 1.76 mM, pH 7.4. The solution was prepared by Cancer Research UK London Research Institute Medium Service

PBST buffer: 1xPBS and 0.05% Tween20

Ponceau Staining Solution: 0.1% (w/v) ponceau S in 5% (v/v) acetic acid

Western blot transfer buffer I: 300 mM Tris-HCl, pH 10.4 and 15% methanol v/v

Western blot transfer buffer II: 30 mM Tris-HCl, pH 10.4 and 15% methanol v/v

Western blot transfer buffer III: 25 mM Tris-HCl, pH 9.4, 40 mM 6-aminocaproic acid and 15% methanol v/v

5% milk PBST solution: 5% milk w/v, PBS+ 0.05% Tween20 w/v

Western blot stripping buffer: 100 mM Tris-HCl pH 7.5, 10 mM EDTA, 0.5% SDS and β-mercaptoethanol 7 μL/mL v/v

Lysis buffer for GST-tagged protein: 1xPBS, 0.1% NP-40

Elution buffer for GST-tagged protein: 50 mM Tris-HCl, 10 mM reduced glutathione, pH 8.0

Benzamidine column binding buffer: 500 mM NaCl and 50 mM Tris-HCl, pH 7.4

Lysis buffer for His-tagged protein: 100 mM NaCl, 50 mM NaH_2PO_4, 10 mM Imidazole, 0.1% NP-40, pH 8.0

Washing buffer for His-tagged protein: 100 mM NaCl, 50 mM NaH_2PO_4, 20 mM imidazole, pH 8.0

Elution buffer for His-tagged protein: 100 mM NaCl, 50 mM NaH_2PO_4, 250 mM imidazole, pH 8.0

$^{His}Ub^{*}_{4}$-PCNA* buffer: 200 mM NaCl, 50 mM Tris-HCl pH 7.5 and 10% glycerol

Gel filtration buffer: 150 mM NaCl, 50 mM Tris-HCl, pH 7.5, and 10% glycerol

Buffer P: 50 mM Tris-HCl, pH 7.5, 100 mM NaCl and 10% glycerol

Pull-down buffer I: 1x PBS, 20% glycerol, 0.1% Triton X-100, 1 mg/mL BSA and 5 mM DTT

Pull-down buffer II: 1x PBS, 20% glycerol, 0.1% Triton X-100, 1 mg/mL BSA

HBS running buffer: 10 mM HEPES pH 7.4, 150 mM NaCl, 3 mM EDTA and 0.0005% P20 surfactant

QIAGEN buffer A solution: 6 M guanidine HCl, 100 mM Na_2HPO_4/NaH_2PO_4, pH 8.0 and 10 mM Tris-HCl, pH 8.0.

QIAGEN buffer C/0.05% Tween20: 8 M Urea, 100 mM Na_2HPO_4/NaH_2PO_4 , pH 6.3 and 10 mM Tris-HCl, pH6.3

2.4.3 Antibodies

Please see Appendix 5 for a list of antibodies used in this thesis.

2.5 Methods for Yeast Manipulation and Experiments

2.5.1 Yeast Cultivation

Yeast cells were grown in YPD medium at 30 ℃ as a standard condition. Cells harbouring episomal plasmids were grown in synthetic complete (SC) drop-out medium lacking specific amino acids according to the relevant auxotrophic markers. 2% glucose was used as a primary carbon source in most of cases. For inducing protein expression under the control of a *GAL* promoter, galactose was used after an overnight incubation in medium containing lactate as a sole carbon source. Temperature-sensitive mutants were allowed to grow normally at their permissive temperature, and the experiments usually took place at a restrictive temperature.

2.5.2 Yeast Transformation

Yeast cultures were grown to logarithmic phase (OD_{600} 1-2) in YPD or in selective SC medium at 30 ℃ (or permissive temperature for temperature-sensitive strains). Cells were harvested by centrifugation at approximately 2000xg at room temperature for 3 min. The pellet was then re-suspended in LIT buffer at a ratio of 5 OD_{600}/ 100 µL. For each transformation, 100 µL of the LIT cell mix were transferred into an Eppendorf tube with 500 µL of LIT/PEG buffer. 10 µL of 10 µg/µL ssDNA and 1-2 µg of DNA (circular or linearised plasmids) were added into the tube. Cells and DNA were mixed in the tube by vortexing and continuously incubating on a rotating wheel for 20-30 min at room temperature. 50 µL of DMSO were added to each tube of transformation and cells were heat-shocked for 15 min (3-5 min for temperature-sensitive mutants) at 42 ℃. Finally, cells were spun down at 800xg for 30 s and the supernatant was carefully removed. Cells were finally re-suspended in YPD medium and plated on relevant selective plates, which were incubated for 2-3 days at 30 ℃ (or permissive temperature).

2.5.3 Yeast Colony PCR

Single isolated colonies were picked and re-suspended in 25 µL of H_2O, of which 1 µL was used in a 10-µL standard PCR reaction mix as a source of DNA template. A 15 min

prolonged step at 95℃ was applied at the beginning of the PCR reaction to break the cells and 40 amplification cycles were usually required.

PCR programme:

1. 95℃ for 15 min

2. 95 ℃ for 45 seconds

3. 56℃ for 1 minute

4. 72 ℃ for 1-2 min (depending on the length of PCR product)

5. Step 2-4, 40 cycles

6. 72 ℃ for 5 min

7. 4 ℃ forever

2.5.4 Yeast Gene Disruption and Gene Epitope Tagging

For gene disruption, a pair of specific primers was designed as a 50-nucleotide long 5' overhang region, which is complementary to either upstream or downstream of targeted ORF, combined with a 3' end region that anneals to the knock-out cassette (Longtine et al., 1998), which encodes a selectable marker with its own promoter/terminator. A PCR reaction was performed to amplify a sufficient amount of knock-out cassette DNA, followed by ethanol precipitation. The concentrated cassette DNA was transformed into yeast strains, and the transformants were selected on plates selecting for specific auxotrophic markers. The positive transformants were usually confirmed by colony PCR and phenotypes if available.

For gene epitope tagging, a pair of specific primers was designed as a 50-nucleotide long 5' overhang region, which is complementary to the sequence either immediately upstream or immediately downstream of the stop codon in the targeted ORF, combined with a 3'end that anneals to an appropriate epitope tagging cassette (Knop et al., 1999), which consists a desired epitope tag and a selectable marker. A PCR reaction was performed and the product was transformed into targeted strains as described above. The positive transformants were confirmed by colony PCR and western blot with antibody against that specific epitop tag.

2.5.5 Isolation of Yeast Genomic DNA

2 OD_{600} of yeast cells were harvested and subject to protocols described in the TAKARA Gentle^{TM} kit for isolating genomic DNA. Genomic DNA was finally dissolved in sterile H_2O and stored at 4 ℃. Yeast genomic DNA was commonly used as a DNA template in PCR reaction to amplify specific yeast genes.

2.5.6 Preparation of Total Cell Extracts from Yeast Cells

Around 1 OD_{600} of cells was harvested from a growing yeast culture and pelleted in an Eppendorf tube. Each sample pellet was re-suspended in 500 µL of ice-cold sterile H_2O with 75 µL of NaOH/ β-mercaptoethanol solution. The sample was mixed by vortexing and incubated on ice for 20 min. Subsequently, 75 µL of 55% TCA (w/v) solution was added and the sample was mixed by vortexing followed by incubation on ice for another 20 min. During this time, proteins in the cells were precipitated. A 10 min centrifugation at 16000xg at 4 ℃ was applied to recover precipitated proteins. After removing the majority of the supernatant, another short spin was applied to collect all remaining liquid and remove it by pipetting. Finally, the pellet was re-suspended in 20-30 µL of HU buffer and incubated at 65°C for 15 min. If needed, the pH of the samples was adjusted by addition of 1-2 µL of Tris-HCl buffer, pH 10.4.

2.5.7 Mating and Tetrad Dissection

From a saturated overnight culture, 5 μL of a *MAT α* strain and 5 μL of a *MAT a* strain were mixed and spotted on a YPD plate. Cells were incubated at 30 ℃ for 3-4 h allowing them to mate. 1-2 drops of H_2O were applied to the cell spot, and the diluted cells were spread out on the YPD plate. A micromanipulator (Singer) was used to isolate 8-10 zygotes and deposit them onto a different area of the plate. After 2-3 days of incubation at 30 ℃, the colonies derived from the zygotes were inoculated in 2 mL sporulation medium and incubated in 30 ℃ for 2-3 days. Cells were analysed under the microscope for tetrad formation. After successful sporulation, 5 μL of the culture were mixed with 5 μL Z 0.5 solution to digest the ascus wall. The digested mixture was spotted onto a fresh YPD plate, and tetrads were separated by a micromanipulator. Plates were incubated at 30 ℃ for 2-3 days and all the spores were tested for the mating types and the distribution of specific genetic markers.

2.5.8 Spot Assays

The relevant yeast strains were grown to logarithmic phase in YPD medium and the OD_{600} for each culture was measured. Cells were then diluted with YPD medium to reach a final OD_{600} of 1, which contained approximately $2x10^7$ cells/mL. A series of 10-fold dilutions was made, and 3.5 μL of each dilution were spotted on plates with specific drug concentration. The plates were kept in the incubator for 2-3 days, and images of the plates were recorded by scanning every day to monitor the growth of sample strains at different drug concentrations. In the case of temperature sensitivity assay, similar dilutions of yeast cultures were spotted on YPD plates. Plates were kept in incubators at a range of temperatures from 25 ℃ to 37 ℃.

Plates containing the DNA-damage agent MMS were prepared as following: 100% MMS (liquid) was diluted to 1% with DMSO to generate a working stock. Typically, 25 mL of melted YPD agar were enough for a Petri dish plate. The calculated volume of MMS stock was added into a 50 mL falcon tube containing melted YPD agar, the drug

was well mixed with the YPD agar in the tube before the mix was poured into the Petri dish to solidify.

In the case of benomyl, high concentrations of the drug are known to be difficult to dissolve in YPD medium. Therefore, a 10 mg/mL working stock of benomyl was added into the medium drop by drop to the desired concentration in order to avoid precipitation.

2.5.9 UV Survival Assay

The relevant yeast strains were grown to logarithmic phase in YPD medium and the OD_{600} for each culture was measured. Dilutions were made to obtain appropriate cell densities, and 50 μL of culture were usually plated on YPD plates. Plates were left to dry and irradiated with the desired UV dose at 254 nm in a UV crosslinker (Stratalinker 2400, Stratagene). Plates were then incubated in the dark for 2-3 days at 30℃ before counting colonies. Culture dilutions were set up depending on the UV dose and the anticipated sensitivity of the strain to achieve a final number of ca. 200 cells per plate for convenient counting. Error bars were generated from triplicate experiments.

2.5.10 Plasmid Loss Assay

Wt or relevant mutant strains were transformed with plasmids pHU669 pHK110 and pHU794 pHT4467Δ. The transformants were selected on SC-URA plates. Isolated colonies from the transformation plates were grown in SC-URA liquid medium to saturation, and cultures were diluted to a cell density OD_{600} 0.01 in YPD medium. Cells were allowed to grow for another 10 generations, aiming for a final cell density of ca. 10 OD_{600}. Cultures were diluted to a concentration of 10 cells / μL and, 30 μL of the diluted cultures were plated on YPD and SC-URA plates. The proportion of cells that maintained the plasmids was calculated as (Number of colonies on SC-URA/ Number of colonies on YPD). Three separate colonies were assayed for each strain to have

triplicate experiments, from where error bars were derived. Due to the fact that pHU669 pHK110 has a short version of ARS, this plasmid was more difficult to maintain, and an elevated plasmid loss rate was generally seen in strains with this plasmid compared to that of strains harbouring pHU794 pHT4467Δ strain.

2.5.11 Growth Rate Assay

The relevant yeast strains were grown overnight and diluted to a cell density of ca. 0.2 OD_{600} in the morning. Cultures were incubated again at 30 ℃, and the cell density of each sample strain was recorded spectrophotometrically as OD_{600} every 15 min. A growth curve, in which cell density was plotted against growth time, was used to compare the growth rate between different strains.

2.5.12 Cell Synchronisation

Yeast cells were grown to logarithmic phase in YPD medium, and α-factor was added to a final concentration of 5 μg/mL. Cells were incubated for another 2 h, and samples were analysed under the microscope for G1 cells. When most of cells had reached the G1 phase, cells were spun down and washed twice with fresh YPD medium. Finally, cells were released into fresh YPD medium, and cell cycle progression was monitored by Fluorescent Activated Cell Sorting (FACS) analysis. Nocodazole (15 μg/mL) was added to cultures to test if cells were able to arrest at G2/M phase in some experiments.

2.5.13 Fluorescent Activated Cell Sorting (FACS)

1 mL of cells (OD_{600} 1-2) was harvested for each sample. The cell pellet was washed in H_2O and re-suspended in 70% ethanol for fixation. Cells can be kept at this stage at 4 ℃ before further processing. Cell pellets were washed with 50 mM Sodium Citrate buffer twice (pH 7.0) and re-suspended in 1 mL of the same buffer. 25 μL RNAase (10 mg/mL) were added to each sample to degrade RNA. Samples were mixed by vortexing and incubated at 50°C in a water bath for 60 min. 15 μL of proteinase K (Fluka82456

20,000U/mL) were added to each sample, followed by a 60 min incubation at 50 ℃. 3-5 s sonication was then applied to each sample to break up cell clumps and separate mother and daughter cells. Finally, propidium iodide stock (160 μg/mL) was diluted to 20 μg/mL in sodium citrate buffer and 250 μL of cell samples were mixed with 1 mL of the diluted propidium iodide solution for FACS analysis. Fluorescence from intercalated propidium iodide was measured by FACS, and the result was illustrated as a histogram plotting counts on the Y-axis and propidium iodide signal on the X-axis.

2.6 Methods for *E.coli* Manipulation

2.6.1 *E. coil* Cultivation

E.coli strains were grown at 37 ℃ in Luria Broth (LB) medium as standard condition. Cells with plasmids were grown under selective pressure with appropriate antibiotic markers such as ampicilin, kanamycin, etc.

2.6.2 *E. coli* Transformation

E.coli strains Top10 and BL21 Condon^{2+}, which were used in this thesis, were prepared as chemically competent cells for transformation. 10 mL of an overnight culture were diluted into 1000 mL of medium, which was then incubated at 37 ℃ with aeration until an OD_{600} of ca. 0.5 was reached. Cells were chilled on ice for 15 min and were harvested by centrifugation at 5000xg for 5 min. Pellets were then re-suspended in 400 mL of Tfb I buffer and incubated on ice for 15 min. Cells were spun down again and the pellets were re-suspended in 40 mL of Tfb II buffer. Cells were incubated on ice for 15 min and aliquots of 100 μL were made to be frozen in liquid nitrogen, stored at -80 ℃.

Plasmid DNA was mixed with an aliquot of competent cells (100 μL) and chilled on ice for 10 min. The mixture was heat-shocked at 42 ℃ for 90 seconds. 1 mL of LB medium was added, and cells were incubated at 37 ℃ for 10-15 min before plating on a plate with selective antibiotic. For plasmid with kanamycin marker, a minimum of 30 min

incubation time was required after the heat shock to allow expression of the kanamycin-resistance gene.

2.7 Methods for DNA Manipulation

2.7.1 Isolation of Plasmid DNA

5 mL of an overnight *E.coli* culture harbouring the desired plasmid were centrifuged at 8000xg for 5 min. The supernatant was discarded, and cell pellets were treated according to protocols described in the manual of the QIAprep Spin miniprep kit. DNA was finally eluted from the spin column with sterile H_2O, and sample concentration was determined by measuring the absorbance at 260 nm. A Nanodrop ND-1000 spectrophotometer from Labtech Interactional was used for all measurements.

2.7.2 Agarose Gel Electrophoresis

Agarose gels with appropriate concentrations of agarose (0.8-2% w/v) in TAE buffer were used to analyse DNA samples of different sizes. DNA samples were mixed with 6x DNA loading buffer and separated by agarose gel electrophoresis in 1xTAE buffer in a horizontal gel electrophoresis apparatus from Jencons Scientific. 120 V were usually applied to the gel as a standard condition. 0.5 μg/mL of ethidium bromide or a 1:20,000 dilution of CYBR® Safe DNA gel stain (Invitrogen) were added into the agarose gel during preparation to visualise the DNA under a UV lamp (254 nm) or light at a wavelength of 473 nm, respectively. Lambda DNA digested with *Pst*I as well as commercially available 100 bp or 1 Kb DNA ladders were used as DNA size standards. Gel images were taken by the Fujifilm LAS-3000 system.

2.7.3 Polymerase Chain Reaction (PCR)

100 μL of PCR reaction contained 10 μL of thermo pol buffer (10x), 1-200 μg of DNA template, 1 μL of Taq DNA polymerase (Fisher Scientific), 2.5 μL of each DNA primer (10 μM), 1 μL of dNTP (25 mM each) and H_2O. For DNA amplification requiring high

fidelity, Phusion DNA polymerase (Finnzymes) was used in the PCR reaction. In such cases, 5x HF buffer or GC buffer was used in combination with the Phusion DNA polymerase.

PCR programme:

1. 95 ℃ for 5 min

2. 95 ℃ for 45 seconds

3. 56 ℃ for 1 minute

4. 72 ℃ for 1-2 min (depending on the length of PCR product)

5. Step 2-4, 30 cycles

6. 72 ℃ for 5 min

7. 4 ℃ forever

2.7.4 Site-Directed Mutagenesis

To introduce mutations within the ORF of *SPC25*, two internal primers with mutated nucleotide sequences at the desired sites were designed. The first round of PCR reactions were performed as such external primer 1/internal primer 2 and external primer 2/ internal primer 1 to have two separate but overlapping PCR products covering the entire ORF (Figure 2.1). 12.5 µL of each PCR reaction product was mixed to have a total amount 25 µL. After addition of 25 µL of 0.2 M NaOH, the mix was incubated at room temperature for 5 min. 50 µL of H_2O, 100 µL of 3 M NaOAc pH 5.2 and 200 µL of isopropanol were added into the mix followed by 30 min incubation on ice. The sample was spun at 2,000xg for 20 min and the pellet was washed with 70% ethanol. Finally, the sample was spun at 2,000xg again for 20 min and the pellet was re-suspended in PCR mix. The second round of PCR was performed without external primers as following program:

1. 95 ℃ 5 min

2. 95 ℃ 30 s

3. 50 ℃ 30 s

4. 72 ℃ 30 s

5. Step 2-5, 5 cycles

6. 95 ℃ forever

The second round PCR served to extend the two overlapping PCR products from the first round PCR reactions to the end of the *SPC25* ORF. The sample tube was chilled on ice for 3 min and external primers were added into the mix. A final round of PCR reaction was performed to amplify the mutagenised ORF.

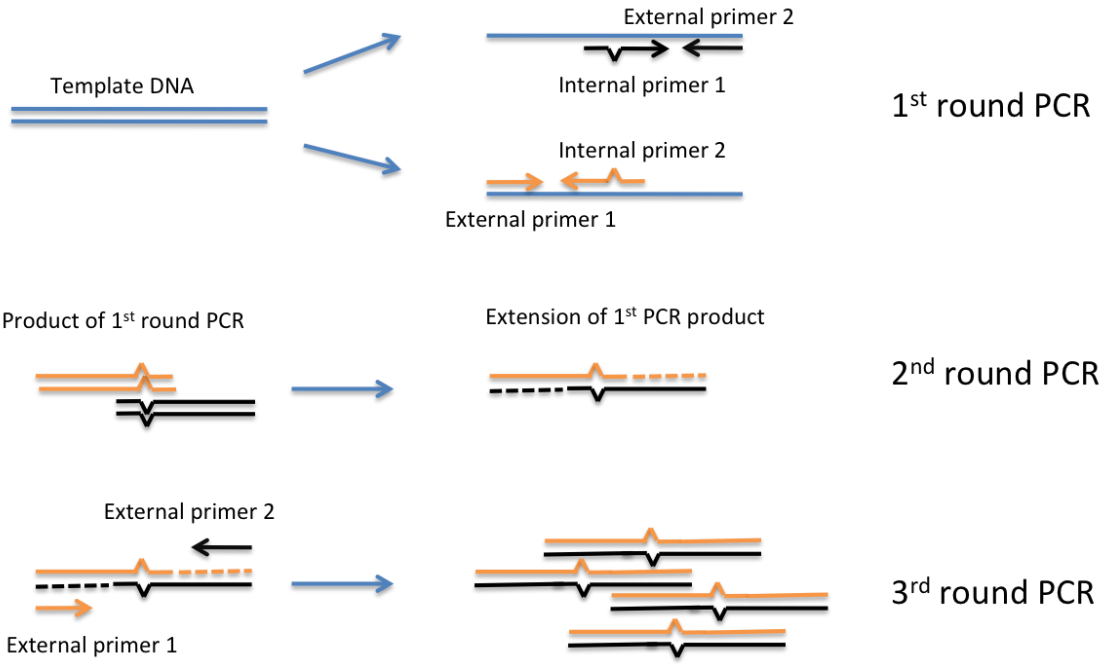

Figure 2.1 PCR-based site-directed mutagenesis
A schematic illustration of PCR-based site directed mutagenesis. In the first round of PCR, two overlapping PCR products were generated with primer pairs: external primer 2/ internal primer 1 (black primer pair) and external primer 1/ internal primer 2 (orange primer pair). In the second round of PCR reaction, the overlapping products from the first PCR were extended. The third round PCR served to amplify the full-length product with the desired mutation.

2.8 Methods for RNA Manipulation

2.8.1 Isolation of Total RNA from Yeast Cells

Up to 5 OD_{600} yeast cells were harvested from cultures grown in logarithmic phase, and cells were lysed by mechanical disruption using the Fastprep®-24 system (MP Biomedicals). Total RNA was isolated from yeast lysate by following the protocol described in the QIAGEN RNeasy Mini Kit.

2.8.2 Preparation of the Probes for Northern Blot Analysis

Radiolabelled PCR products were used as probes in northern blot analysis. PCR reactions (50 µL) were performed using oligos oHU 412/79 to amplify a C-terminal 408 bp fragment of *POL30* gene and using oligos oHU 640/641 to amplify a 464 bp fragment of *LacZ* gene. PCR products of *POL30* and *LacZ* gene fragments were labelled with dCTP P^{32}, using Ready-To-Go DNA labelling beads (GE Healthcare) and following the manufacturer's protocol to generate specific probes for northern blot analysis. The labelled PCR products were purified from excessive dCTP P^{32} using ProbeQuant G-50 microcolumns (GE Health). A final concentration for radiolabelled probe is 10 ng/mL in the hybridisation solution.

2.8.3 Northern Blot Analysis

Total RNA samples were first separated by agarose gel electrophoresis. 2 µL of RNA solution (5 µg) were mixed with glyoxal reaction mix and incubated at 55 ℃ for 1 h. The sample was then chilled on ice immediately for 10 min. A short centrifugation was applied to the sample tube to collect all the liquid, and 2 µL of RNA loading dye were added. RNA samples were then analysed on a 1.5% agarose gel in BPTE electrophoresis buffer, 50 V for 5 h. After electrophoresis, the gel was washed successively in sterile H_2O (10 min), 75 mM NaOH (30 min), 0.5M Tris, pH 7.2 (twice, 10 min each) and 1.5 M NaCl (twice, 10 min each).

RNA samples were transferred from the agarose gel to a nylon membrane in 10x SSC buffer overnight by capillary transfer and the membrane was dried and baked for 30 min at 80℃ prior to UV cross-linking. Hybridisation was performed with radiolabelled probes in ExpressHyb solution (Clontech) at 68°C for 1 h following manufacture's protocol. Membranes were exposed to Amersham hyperfilm ECL (GE Health) for different times, and the films were developed with an automatic X-Ray film processor (Model JP-33, Jungwon Precision Industry). Alternatively, membranes were exposed to Amersham Bioscience phosphor screens, which were analysed on a Typhoon Trio variable mode imager (GE Health) using ImageQuant Software.

2.9 Methods for Protein Manipulation and Analysis

2.9.1 Determination of Protein Concentration

Protein concentration was primarily determined by measuring absorbance at 280 nm. Protein samples were analysed using the Nanodrop ND-1000 Spectrophotometer, (Labtech International) for absorbance at 280 nm. The extinction coefficient (ε) was calculated for each protein by the formula shown below:

ε (cm^{-1} M^{-1}) = 5500 x (the number of Tryptophan residues) + 1490 x (the number of Tyrosine residues)

and the protein concentration was calculated by Beer-Lambert Law:

Protein concentration = A (absorbance at 280 nm)/ε (extinct coefficient) x l cm

Alternatively, the Bradford method based Bio-Rad Protein Assay was used according to manufacture's instruction to determined protein concentration. The absorbance at 595 nm was measured by a Biophotometer (Eppendorf), and the protein concentration was estimated by comparing the absorbance with a known BSA standard curve.

2.9.2 SDS-PAGE

Tris-glycine SDS-polyacrylamide gels were prepared according to Laemmli (Laemmli, 1970) in a Bio-Rad mini protein gel system to analyse most of the protein samples. Tris-glycine SDS-polyacrylamide resolving gels were used at a concentration range of 6 to 15% polyacrylamide, and the stacking gel had 5% polyacrylamide. Gel solutions and running buffers were prepared according to described protocols (Sambrook, 1989). Protein samples were mixed with sample loading buffer and then incubated at 95 ℃ for 5 min. Gels were applied to a constant 150 V for approximately 1 h in 1x Laemmli running buffer.

Alternatively, NuPAGE pre-cast gradient gels (4-12%) were purchased from Invitrogen to analyse protein samples requiring better resolution. Protein samples were mixed with reducing agent and loading buffer according to the manufacturer's instructions and incubated for 10 min at 70 ℃. Gels were run at constant voltage (165 V) for approximately 90 min.

2.9.3 Coomassie or Instant Blue Staining

After SDS-PAGE, polyacrylamide gels were soaked in Coomassie Blue staining solution up to 1 h. Stained gels were de-stained in de-staining solution a few times as required. Gels were rinsed with H_2O and incubated with gel-drying solution for 30 min. Gels were dried on a 3MM Whatman paper in a GelAir Dryer (Bio-Rad).

Alternatively, Instant blue (Expedeon) was used to stain total proteins in the gels after SDS-PAGE. Protein bands were visualised on the gel after 10-20 min of staining by the Instant Blue solution at room temperature.

2.9.4 Western Blots

After SDS-PAGE, protein samples were transferred to a PVDF membrane (Millipore), which was activated by methanol in advance. A gradient transfer system consisting of three buffers (refer to section 2.4 buffers and reagents for details) was applied. 6 layers

of Whatman gel blotting paper were prepared at the size of the gel. Two layers of paper were soaked in western blot transfer buffer I, one layer of paper was soaked in western blot transfer buffer II and three layers of paper were soaked in western blot transfer buffer III. The transfer gradient was set up such that two layers of buffer I soaked paper were overlaid by one layer of buffer II soaked paper. On top of that, the activated PVDF membrane and gel were laid following by three layers of buffer III soaked paper. This stack was placed onto the anode plate of a semi-dry gel blotter apparatus (Roche). A constant current of 40 mA per gel was applied to the transfer device for 60-90 min. After transferring, the membrane was incubated with 5% milk PBST solution for 30 min at room temperature. The membrane was then incubated with primary antibody (appropriate dilution in 5% milk PBST solution) for 2 h at room temperature or overnight at 4℃. After three washes of 10 min each in PBST buffer, the membrane was incubated with secondary antibody (appropriate dilution in 5% milk PBST solution) for 1 h at room temperature. Finally, another three washing steps with PBST were carried out, and Western Lightning^{TM} chemiluminescence reagent plus (Perkin Elmer) was applied to the membrane according to the manufacturer's instruction. The membrane was exposed to Amersham hyperfilm (GE Healthcare) for various times and the films were developed in an automatic X-Ray film processor (model JP-33; Jungwon Precision Industry). In the case of re-blotting with another antibody, membranes were incubated with western blot stripping buffer at 50℃ for 30 min. After this incubation, membranes were washed with PBST three times, 10 min each, following by another blocking step as described before. Primary and secondary antibodies incubations were applied subsequently.

2.9.5 Protein Purifications

Most of the proteins produced in this thesis were expressed with either a GST tag or a 6-His tag. The purification methods for both types of proteins were as follows.

2.9.5.1 Purification of GST Fusion Proteins

$^{GST}Ub^{*}_{4}$, $^{GST}Ub^{*}_{4}$(L), ^{GST}Ub, $^{GST}UBAN$ and $^{GST}Spc25$ (107-221) [co-purified with $^{His}Spc24$ (154-213)] were all expressed as GST-tagged proteins and purified by

glutathione affinity chromatography. $^{GST}Ub^{*}_{4}$ was expressed from an *E.coli* BL21 Codon^{2+} strain using a pGEX-4T-1 vector (Amersham/GE Healthcare). Cells carrying the expression construct were grown overnight at 37 ℃ and diluted 100-fold to have a final cell density of approximately 0.05 OD_{600} in fresh LB medium. Cells were grown at 37 ℃ up to an OD_{600} of 0.5-0.8, and at that time 0.1 mM IPTG was added to the culture to induce protein production. The culture was shifted to 30 ℃ for 6 h. At the end of the incubation, cells were harvested by centrifugation at 7700xg for 10 min at 4 ℃. Cell pellets were then washed with lysis buffer for GST-tagged protein and re-suspended in the same lysis buffer with Complete® protease inhibitor Roche. Cells were passed through a homoginiser (Model TC5-612W-332) at 70 MPa at 4 ℃ and lysed further by sonication (Branson sonifier) with a programme giving 5 short bursts of 10 seconds at 40% of output and 1 minute incubation on ice between each pulse. The lysate was then rotated in 50 mL falcon tubes in the cold room for 30 min to enhance protein solubility. The soluble fraction was then separated from the cell debris by a centrifugation step at 40,000xg for 20 min. A glutathione affinity column was self-packed with Glutathione Sepharose Fast Flow 4 (GE Healthcare) and equilibrated with the lysis buffer (without protease inhibitor). The soluble lysate was passed through the column, and the column was washed extensively with the same lysis buffer to get rid of all non-specifically bound materials. $^{GST}Ub^{*}_{4}$ was then eluted from the column with elution buffer for GST-tagged protein. The eluted protein was dialysed against PBS buffer and the final protein concentration was determined spectrophotometrically as described in section 2.8.1. In order to remove the GST tag, 300 µL of $^{GST}Ub^{*}_{4}$ (1 mg/mL) were incubated with 5 µL of 1.4 unit/µL thrombin (Novagen) at room temperature overnight on a rotating wheel. The cleaved GST moiety was removed from the protein sample by incubation with glutathione beads at room temperature for 2 h. The sample was then passed through a benzamidine column, which was equilibrated with benzamidine column binding buffer, at a flow rate 1 mL/ min on an ÄKTA protein purification system (Model UPC-900, GE Healthcare) to remove the thrombin.

^{GST}Spc25 (107-221)/^{His}Spc24 (154-213) were expressed separately from pGEX-4T-1 (GE Healthcare) and pET15b (Novagen) in separate strains. Both cultures were induced

with 0.2 mM IPTG and were incubated at 18 ℃ overnight to allow a slow protein expression under conditions of slow growth. The cell lysates were prepared as described above and were combined to allow an association between the expressed subunits. Then a single step of affinity purification on glutathione Sepharose was applied to the mixed lysate (same as described protocol above), and ^{His}Spc24 (154-213) was co-purified with ^{GST}Spc25 (107-221). The eluted protein sample was dialysed against PBS buffer with 10% glycerol and 1 mM DTT. Other GST fusion proteins [^{GST}Ub$^{*}_{4}$(L), ^{GST}Ub, ^{GST}UBAN] were purified by the standard protocol as described above.

2.9.5.2 Purification of His-Tagged Proteins

^{His}Ub$^{*}_{4}$-PCNA*, ^{His}Spc24 (154-213) and ^{His}Spc25 (107-221) were all expressed from pET series of vectors (Novagen) and purified by Ni-NTA affinity chromatography.

^{His}Ub$^{*}_{4}$-PCNA*

^{His}Ub$^{*}_{4}$-PCNA* was expressed from *E.coli* BL21 Codon^{2+} strains using a pET28a vector (Novagen). Cells harbouring the expression construct were grown overnight at 37 ℃ and diluted 100-fold in fresh LB medium to a final OD_{600} of approximately 0.05 the next morning. Cells were grown at 37 ℃ up to an OD_{600} of 0.5-0.8, and at that time 0.1 mM IPTG was added into the culture to induce protein production. The culture was shifted to 18 ℃ for an overnight incubation. At the end of the incubation, cells were harvested by centrifugation at 7700xg for 10 min at 4 ℃. Cell pellets were then washed with lysis buffer for His-tagged protein and re-suspended in the same lysis buffer but with Complete® protease inhibitor tablet from Roche. Cell lysate was prepared as described in section 2.8.5.1. An ultracentrifugation was also performed at 100,000xg at 4 ℃ for 30 min (Beckman Ultracentrifuge) to separate all the membranes from the soluble fraction. In the end, the soluble fraction was incubated with Ni-NTA resin (QIAGEN) pre-equilibrated with the lysis buffer for 1 h at 4 ℃ to allow His-tagged protein binding to the resin. The mixture was applied to an empty column to capture the resin and release the flow-through. The column was washed with washing buffer for His-tagged protein extensively to reduce non-specific binding. Finally, bound proteins were eluted from the column with elution buffer for His-tagged protein. The eluted

sample $^{His}Ub^{*}_{4}$-PCNA* was applied to a Superdex 200 10/300GL gel filtration column (GE Healthcare) on an ÄKTA protein purification system (GE Healthcare). The peak fractions representing $^{His}Ub^{*}_{4}$-PCNA* were collected and the purified $^{His}Ub^{*}_{4}$-PCNA* after gel filtration column was in $^{His}Ub^{*}_{4}$-PCNA* buffer.

^{His}Spc25 (107-221)/^{His}Spc24 (154-213)

The ^{His}Spc25 (107-221)/ ^{His}Spc24 (154-213) complex was co-expressed in a BL21 Codon^{2+} *E.coli* strain from pET15b and pET28a respectively. Cells were grown in LB medium with 100 μg/mL ampicilin and 50 μg/mL kanamycin at 37°C and both proteins were purified using Ni-NTA affinity chromatography as described above. The eluted protein sample was immediately applied to a Superdex 200 10/300GL gel filtration column (GE Healthcare) on an ÄKTA protein purification system (GE Healthcare), which was equilibrated with gel filtration buffer. The peak fractions representing a heterodimer of Spc25(C)/Spc24(G) were collected and analysed on SDS-PAGE for Coomassie staining and anti-His western blot. The sample was further concentrated by a Vivaspin protein concentrator with a 5 kDa cut-off and the final protein concentration was determined by the Nanodrop analysis. A maximum concentration of 5 mg/mL protein for each subunit, which is equivalent to approximately 400 μM, can be obtained by this method.

2.9.6 Assays for Protein Stability

2.9.6.1 Cycloheximide Chase Analysis

An appropriate yeast culture was grown to logarithmic phase (OD_{600} 1-2) in YPD or selective SC medium at 30℃ (or permissive temperature for temperature-sensitive strains). Cells were treated with 100 μg/mL cycloheximide to inhibit global protein synthesis and further incubated at the appropriate temperature. To observe an effect in temperature-sensitive mutants such as *pre1-1* and *npl4-1*, cells were shifted to their restrictive temperature (30℃) after addition of cycloheximide. Aliquots of equal volume were withdrawn from the culture at appropriate time points and frozen in dry

ice. Protein of interests with in the total cell extract were analysed by SDS-PAGE followed by western blot with specific antibody.

2.9.6.2 Promoter Shut-Off Assay

Wt as well as different mutant yeast strains were transformed with episomal plasmids that express a series of βGal fusion proteins under control of a *GAL10* promoter. Cells were grown in SC-URA medium with 2% glucose as carbon source at 25 ℃, followed by an overnight period in SC-URA medium with 2% lactate as carbon source. The following day, protein production was induced by addition of 2% galactose and incubation in this medium for 2 h. Then cells were shifted back to SC-URA +2% glucose medium in the presence of 100 μg/mL cycloheximide to terminate protein production. At this stage, temperature-sensitive mutants were shifted to 30 ℃. Aliquots of equal volume were withdrawn for further analysis by western blot against βGal.

2.9.6.3 In Vitro Degradation Assay

Degradation assays were performed at 37 ℃ in a reaction mix containing 5 nM human 26S proteasome (Enzo life science), 200 nM PCNA* (provided by Jo Parker in the lab) or Ubi$_4^{*}$-PCNA*, Buffer P, 2 mM ATP, 5 mM $MgCl_2$, and 1 mM DTT. The reaction mix was pre-incubated for 5 min at 37 ℃, and the reaction was initiated by adding proteasome. 1 volume of sample was withdrawn at each time point, and SDS loading buffer was added to stop the reaction. Samples were finally analysed on SDS-PAGE/Western blot using anti-PCNA antibody. This protocol was adapted from (Saeki, 2005) and further modified by myself.

2.9.7 Assays for Protein-Protein Interaction

2.9.7.1 Yeast Two-hybrid Analysis

For genome-wide yeast two-hybrid screening, Ub$^{*}_{(3\text{-}4)}$ (L)-PCNA* and Ub$^{*}_4$ -PCNA* were cloned into the vector pGBT9 in frame with the DNA-binding domain derived

from the transcription factor Gal4. These constructs served as baits in the screens. $Ub^*_{(3-4)}$(L) and Ub^*_4 were also cloned into the vector pGBT9 in the same way to serve as controls. The yeast genomic library used in the screen was described in (James et al., 1996). It was made from putting fragmented yeast genomic DNA sequences into a pGAD424 series vectors in frame with a transcription-activation domain from Gal4 transcription factor in all three open reading frames (James et al., 1996). A large-scale yeast transformation was performed to reach highest efficiency and obtain as many colonies as possible to represent the entire yeast genome. The genomic library comes in all three frames due to single nucleotide differences upstream of the insertion sites. For each library, a 150 mL yeast culture was grown up to ca. 1.0 OD_{600} and cells were harvested by a 5-minute 3000xg centrifugation step. Pellets were re-suspended in 3 mL 100 mM LiOAc and incubated at 30 ℃ for 15 min. The cells were spun down and the supernatant was discarded. The pellet was then re-suspended in 10.8 mL of large scale transformation pre-mix. 30 μL of genomic library DNA was added to the mix. After 30 min incubation at 30 ℃, cells were subjected to a 40 min heat shock at 42 ℃. During the course of the heat shock, cells were inverted to mix for 15 s every 5 min. Cells were then spun down and re-suspended in 30 mL YPD for another 1 h incubation at 30 ℃. Finally, cells were harvested and re-suspended in 20 mL YPD. 500 μL of cells were plated on each 50 mL square plate using a total of 40 plates. After 3 days of incubation at 30 ℃, the resulting colonies were washed off the plates with YPD. Over 2 million transformants were collected per library in the end. Cells were frozen down by placing them directly into a -80 ℃ freezer, which allows a slow freezing process and gives optimal recovery later on. The resulting transformants together with the bait constructs were sent to a company for the actual screen as described in (Albers et al., 2005), where a Y187 strain with an opposite mating type and suitable reporter construct was transformed with the bait plasmids, and the resulting transformants were mated with the genomic library transformants. A physical interaction between the bait protein and an unknown factor X expressed from the genomic library would activate transcription at the reporter genes. The company performed automated screens and quantitatively analysed signals from reporter genes to reveal positive hits. Colonies representing positive interactions were then amplified to determine the identity of the inserts via sequencing.

For direct yeast two-hybrid analysis, genes of interests were cloned into both pGBT9 and pGAD424. Plasmids with gene A in pGBT9 and gene B in pGAD424, or the reverse combination, were transformed into yeast two-hybrid reporter strain PJ69-4A. As a control, empty plasmid vectors were usually included in the experiment to rule out false positive interactions caused by auto-activation. 0.5 μg of plasmid DNA for each construct was used in every transformation. Positive transformants were selected on –LW plates. Five positive colonies were picked from each plate, combined and suspended in 500 μL of sterile H_2O. 3.5 μL of this suspension were finally spotted on selective plates, which monitor the transcription of specific reporter genes. Positive interactions were monitored by a *HIS3* reporter gene, which selects relatively weak interactions, and an *ADE2* reporter gene, which was used to identify strong interactions. Plates -HLW (SC medium lack histidine, leucine and tryptophan) and –AHLW (SC medium lack adenine, histidine, leucine and tryptophan) were used for selection. For some cases, 5-fold dilutions of the original cell samples were also spotted on selection plates for a clearer result. Plates were incubated at 30 ℃ for 2-3 days, and growth was monitored by scanning images from day 2 onwards.

2.9.7.2 In Vitro Pull-down Assay

^{GST}UBAN and Ub$^{*}_{4}$ pull-down

To detect an interaction between ^{GST}NEMO-UBAN and Ub$^{*}_{4}$, GST (3 μg) and ^{GST}NEMO-UBAN (4 μg) were immobilised on 20 μL glutathione Sepharose 4 Fast Flow (GE Healthcare) for 2 h at room temperature in 500 μL pull-down buffer I. The beads were subsequently washed twice with the same buffer and were incubated with 1 μg Ub$_4^{*}$ in 500 μL pull-down buffer for another 2 h. The beads were washed five times with pull-down buffer, mixed with 20 μL of 2x loading buffer, and incubated at 95 ℃ for 3 min. The bound material was analysed on SDS-PAGE/western blot with an anti-ubiquitin antibody.

Ubiquitin Sepharose and ^{GST}Spc25(C)/^{His}Spc24(G) pull-down

For pull-down experiment with ubiquitin Sepharose, GST (60 μg) and ^{GST}Spc25(C)/^{His}Spc24(G) (180 μg) were incubated with ubiquitin Sepharose or control resin (protein G Sepharose) in 300 μL pull-down buffer II for 2 h. The beads were washed three times with the binding buffer and the bound materials were analysed by SDS-PAGE/western blot with an anti-GST antibody.

$^{GST}Ub^{*}_{(n)}$ and $^{His}Spc25(C)/^{His}Spc24(G)$ pull-down

To study the interaction between Spc25/Spc24 and ubiquitin, GST and GST fusion proteins were immobilised on glutathione Sepharose 4 Fast Flow (GE Healthcare). GST (2 μg), ^{GST}Ub (2.7 μg) and $^{GST}Ub^{*}_{4}$(L) (4.7 μg) were incubated with 20 μL of glutathione Sepharose for 2 h in 500 μL of pull-down buffer II. The charged beads were washed twice with binding buffer and incubated with 180 μg ^{His}Spc25(C)/^{His}Spc24(G) in 500 μL of binding buffer for 1 h at 4 ℃. The beads were then washed five times with the binding buffer before incubation in protein loading dye at 95 ℃. The bound material was analysed on SDS- PAGE/western blot with an anti-His antibody.

2.9.7.3 BIACORE Analysis

Surface plasmon resonance measurements were performed using a BIACORE 3000 instrument (GE Healthcare). All the experiments were performed at 25 ℃ using a constant flow rate 5 μL/min in manufacturer supplied HBS running buffer. The analysed ligands were ^{GST}Ub, which was immobilised on the surface of the chip, and ^{His}Spc25(C)/^{His}Spc24(G), which was flowing over the chip surface. A CM5 sensor chip, which was developed for standard amine-coupling, was first equilibrated in HBS running buffer for 30 min to prevent condensation. The chip surface was activated by injecting 30 μL of NHS/EDC mix (1:1 ration) at a flow rate of 5 μL/min. After activation, 35 μL of anti-GST antibody, diluted to 30 μg/mL in coupling solution supplied by the manufacturer, was injected. The chip surface was then deactivated with 35 μL ethanolamine. Approximately 5,000 RU of GST antibody were captured by this method, and the resulting chip was used to capture GST fusion proteins. The chip was divided into two parallel flow cells in the experiments to capture GST and ^{GST}Ub separately. Around 500 RU of GST and 673 RU of ^{GST}Ub, which corresponds to

approximately stoichiometric amounts, were captured on the chip by injection of appropriate volumes. A series of samples of ^{His}Spc25(C)/^{His}Spc24(G) at a concentration range of 1-40 μM in HBS buffer were passed over the chip surface, and changes in RU were monitored. Signals generated from the GST control flow cell were subtracted from those of the ^{GST}Ub flow cell, and sensorgrams were analysed using the BIAevaluation software. The RUs at equilibrium state of each ligand concentration were plotted against ligand concentrations, and the dissociation constant was calculated from the graph.

2.9.8 Assays for Identifying Ubiquitylation in Vivo

2.9.8.1 Detection of Ubiquitylated PCNA

Yeast strains bearing the ^{His}*POL30* allele were prepared for efficient isolation of PCNA under denaturing condition. The strain yHU 1097 (^{His}*POL30*) carries a deletion of endogenous *POL30* and is rescued by integration of ^{His}*POL30* into the *LEU2* (Papouli et al., 2005). The *PDR5* gene was deleted in the ^{His}*POL30* strain to allow an efficient uptake of proteasome inhibitor MG132. The *UMP1* gene was deleted in ^{His}*POL30* to generate yHU 2336 ^{His}*POL30 ump1*. pHU 732 (YIp128-P30-His-PCNA) (Davies et al., 2008)was integrated into *PRE1* and *pre1-1* to generate yHU 2338 (^{His}*POL30 PRE1*) and yHU 2339 (^{His}*POL30 pre1-1*).

Appropriate yeast strains were grown overnight and a diluted culture (OD_{600} 0.5) of 50 mL was set up for each strain. Cultures were incubated for another 2 h and then treated with 0.02% MMS for 60-90 min to introduce DNA damage. For the inhibition of proteasome activity, ^{His}*POL30 pdr5* cells were treated with 50 μM MG132 for 2 h prior to MMS treatment. Cells were then harvested and re-suspended in 5 mL ice-cold H_2O. 0.75 mL 2M NaOH and 75 μL β-mercaptoethanol were added to each sample. Samples were mixed properly and incubated on ice for 20 min. After that, 0.8 mL of 55% w/v TCA were added to every sample, followed by mixing and a 20-min incubation on ice. Samples were then centrifuged at 16,000xg at 4℃ for 20 min. The supernatant was

removed and the pellet was re-suspended in 1.5 mL QIAGEN buffer A solution. Samples were rotated for 60 min at room temperature until the entire pellet was dissolved. A 10,000xg centrifugation was applied for 15 min at room temperature to remove all the insoluble material. The supernatant was used for the subsequent Ni-NTA pull-down experiment. 40 µL of equilibrated Ni-NTA agarose beads (QIAGEN) were incubated together with the supernatant, 22.5 µL of 1M imidazole and 22.5 µL of 10% Tween20. After an overnight incubation at room temperature on a rotating wheel, beads were recovered by a short spin and washed twice with 1 ml each of buffer A/0.05% Tween20 and three times with QIAGEN buffer C/0.05% Tween20. Finally, the beads were incubated with 40 µL loading buffer at 95 °C for 3 min. The bound material was analysed by SDS-PAGE/western blot with anti-PCNA and anti-ubiquitin antibodies.

2.9.8.2 Detection of Ubiquitylated Kinetochore Proteins

Yeast strains expressing C-terminally TAP-tagged genes of interest were obtained from the West Lab (Originally Open Biosystems) and transformed with plasmids pHU 308 (YEplac181) and pHU 821 (YEp181-CUP1-His-Ub). Positive transformants were grown in SC-LEU medium in the presence of 0.1 mM $CuSO_4$ to induce the expression of ^{His}Ub. Total cellular ubiquitin conjugates were isolated by Ni-NTA pull-down as described in section 2.8.8.1 and bound material was analysed by western blot with anti-TAP antibody to detect the protein of interest. To confirm the ubiquitylation events under conditions where ubiquitin levels are close to the endogenous situation, cells were grown in medium without $CuSO_4$. Basal expression of ^{His}Ub from the *CUP1* copper inducible promoter was enough for Ni-NTA pull-down analysis without significantly altering cellular ubiquitin level.

Chapter 3. Results I: Distinct Consequences of Posttranslational Modification by Linear versus K63-Linked Polyubiquitin Chains

3.1 Introduction

3.1.1 Background

Polyubiquitin chains linked via different lysine residues adopt different geometries (Ikeda and Dikic, 2008). Downstream effector proteins that specifically recognise one type of chain are believed to mediate the signal transduction after the modification. Although there are seven lysine residues on the surface of ubiquitin available for chain formation, only a few types are well studied for their biological functions.

K48-linked polyubiquitin chains function as signals for proteasomal degradation. Solution structure has demonstrated that K48-linked chains exhibit a compact and "closed" conformation (Varadan et al., 2002). Similarly, K29-linked polyubiquitin chains also have a proteolytic role as shown in the UFD pathway (Johnson et al., 1995)(section 1.4.2 for more details). K63-linked polyubiquitin chains assembled by the heterodimeric E2 complex of Ubc13 and the E2-like Uev1 (or yeast homologue, Mms2) have been reported to function in the NF-κB signalling pathway as well as the DNA damage tolerance pathway (Deng et al., 2000, Hofmann and Pickart, 1999, Ulrich, 2009). Their role in NF-κB activation is unrelated to proteolysis; instead they appear to act as scaffolds for the assembly of a signalling complex. The role of K63-linked polyubiquitin chains in the DNA damage tolerance pathway remains unclear. A proteolytic role of K63-linked polyubiquitin chains in this case has not been fully excluded. In fact, K63-linked chains are able to target model substrates for degradation *in vitro* and recent evidence has suggested they may also function as degradation signals *in vivo* (Saeki et al., 2009, Hofmann and Pickart, 2001). The solution structure of K63-

linked chains indicates they adopt an extended and open conformation, which is quite different from K48-linked polyubiquitin chains (Varadan et al., 2004). And indeed, many ubiquitin-binding domains have a strong preference for one type of chain over the other (Ikeda and Dikic, 2008).

The picture of ubiquitin chain linkage is further complicated by the recent discovery of linear ubiquitin chains, where ubiquitin moieties are linked through N-terminal methionine and C-terminal glycine (Kirisako et al., 2006). As M1 is very close to K63 in space (only 6.3 Å away), linear chains adopt a conformation almost identical to that of the K63-linked polyubiquitin chains (Komander et al., 2009b). The E3 complex LUBAC, which catalyses the formation of linear ubiquitin chains in higher eukaryotes, was found to be important for NF-κB activation (Tokunaga et al., 2009). But the function of linear ubiquitin chains does not overlap with K63-linked chains in this case; this is consistent with the observation that a UBAN domain in NEMO has a strong preference on linear chains over K63-linked chains (Rahighi et al., 2009). Furthermore, LUBAC has been proposed to play a role in promoting model substrate degradation when it was originally identified, suggesting linear ubiquitin chains may be involved in proteasome targeting (Kirisako et al., 2006).

Because of their distinct conformations, it is not difficult to understand that K48-linked chains are able to convey messages different from K63-linked chains. However, it may not be the case for linear and K63-linked chains, and current observations have raised some interesting questions. First of all, the high degree of similarity in structural conformation between these two types of chains has challenged the ability of cellular machineries to make a successful distinction. Secondly, both linear and K63-linked chains have been reported for their non-proteolytic functions as well as their potential proteolytic function in several separate events. It is relatively difficult to predict the outcome of each modification on a specific substrate. Therefore, it is interesting to answer a general question as to what extent linear and K63-linked polyubiquitin chains are interchangeable in their functions, and whether or not they act as degradation

signals. To address these questions, I directly compared the consequences of modifications by linear and K63-linked polyubiquitin chains on a common substrate PCNA. I would like to first introduce the DNA damage tolerance pathway, which I used as readout in my study to monitor the function of differently modified PCNA.

3.1.2 The DNA Damage Tolerance Pathway

DNA damage that has not been removed by the global DNA repair processes before the onset of the replication can create problems with the progression of the replication fork and the completion of the cell cycle. The mechanism that cells rely on to deal with those replication-blocking lesions is known as the DNA damage tolerance pathway. The process is targeting lesions that cannot be used as a template by the high fidelity replicative polymerase either in an error-prone manner or in an error-free manner.

3.1.2.1 The RAD6 pathway

In *S. cerevisiae*, the group of genes that are involved in DNA damage tolerance is named the *RAD6* pathway. Through genetic analysis, the *RAD6* pathway genes can be further classified into two subgroups: error-prone genes, which mediate damage-induced mutagenesis, and error-free genes, which promote error-free bypass of the damage, respectively (Lawrence, 1994). The *RAD18* and *RAD6* genes are required for both branches of the damage tolerance. *REV1*, *REV3*, *REV7* and *RAD30* are only involved in the error-prone branch whereas *RAD5*, *MMS2* and *UBC13* are involved primarily in the error-free branch. Later it became clear that *REV1*, *REV3*, *REV7* and *RAD30* encode translesion DNA polymerases: REV1, polymerase ζ (Polζ) and polymerase η (Polη) respectively (Ohmori et al., 2001). *RAD18* and *RAD5* encode E3 ubiquitin ligases, while *RAD6* and *MMS2-UBC13* encode E2 ubiquitin conjugating enzymes (Hofmann and Pickart, 1999, Jentsch et al., 1987, Ulrich and Jentsch, 2000).

3.1.2.2 The ubiquitylation of PCNA in damage tolerance

The substrate of the *RAD6* pathway was identified to be PCNA (Hoege et al., 2002), which forms a homotrimeric ring encircling the DNA to function as a processivity factor for replicative DNA polymerases. PCNA is monoubiquitylated by E3 Rad18 in cooperation with Rad6 at K164. Rad5 cooperating with the E2 complex Mms2-Ubc13 can further modify PCNA on the same lysine residue with K63-linked polyubiquitin chains (Hoege et al., 2002)(Figure 3.1). The polyubiquitylation of PCNA is a sequential reaction that is initiated by the monoubiquitylation and followed by stepwise elongation (Parker and Ulrich, 2009). Initial genetic analysis has shown that mono-, but not polyubiquitylated PCNA is required for translesion DNA synthesis and damage-induced mutagenesis (Stelter and Ulrich, 2003). *In vitro* experiments further confirmed that monoubiquitylated PCNA could stimulate Polη and Rev1 activity to bypass the abasic sites (Garg and Burgers, 2005). Monoubiquitylation can directly enhance the affinity between PCNA and TLS polymerases Polη and Rev1 (Bienko et al., 2005); therefore promoting the switch between replicative polymerase and TLS polymerase at the stalled replication fork (Guo et al., 2006, Parker et al., 2007). PCNA polyubiquitylation is instead required for the error-free damage bypass, which may involve a template switch process to use the genetic information from the newly synthesised and undamaged sister chromatid (Zhang and Lawrence, 2005, Hoege et al., 2002). However, the molecular mechanism remains unclear and the possibility that K63-linked chains on PCNA may signal for proteasomal degradation has also not been experimentally addressed.

Ubiquitylation of PCNA is a highly conserved event. Monoubiquitylation of PCNA has been successfully observed in various model organisms from budding yeast to frog, chicken and humans (Ulrich, 2009). The polyubiquitylation of PCNA has been difficult to observe in higher eukaryotes, but identification of the mammalian Rad5 homologue SHPRH and HLTF provides support for the existence of the error-free pathway in higher eukaryotes (Unk et al., 2006, Unk et al., 2008, Motegi et al., 2006, Motegi et al., 2008).

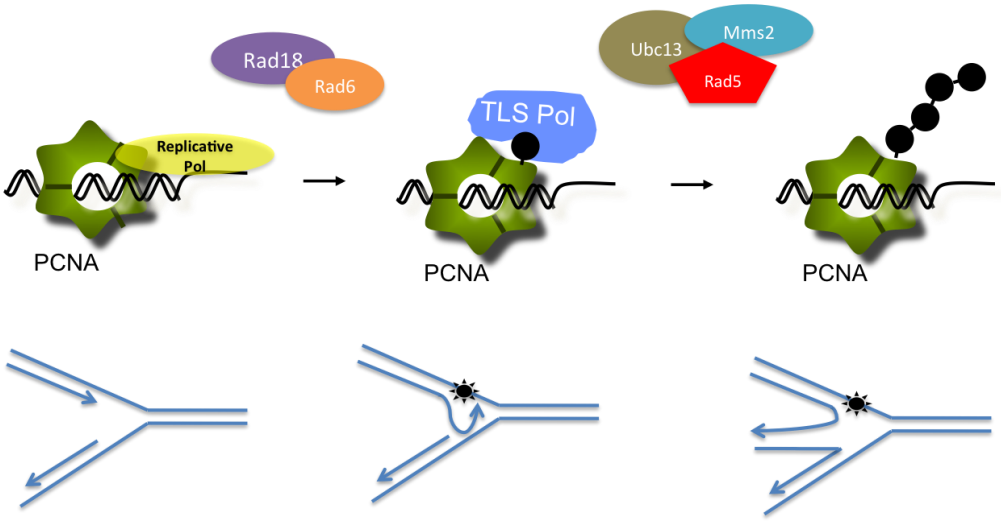

Figure 3.1 Mechanism of DNA damage tolerance pathway
During normal replication, the replicative polymerase (yellow oval) is associated with PCNA (green) for accurate DNA replication; when the replicative polymerase encounters a lesion (black star) on the template strain, PCNA is monoubiquitylated by the E2/E3 complex Rad6/Rad18 (orange oval and purple oval respectively) and recruits TLS polymerase (blue) to bypass the lesion in an error-prone manner. PCNA can also be polyubiquitylated after its monoubiquitylation with the help of the E2/E3 pair Mms2-Ubc13/Rad5 (brown-green ovals and red pentagon). The pathway triggered by polyubiquitylated PCNA uses genetic information from the undamaged newly synthesised sister chromatid to facilitate an error-free mode of bypass, whose molecular mechanism remains unclear. Whether the indicated "chicken-foot" structure is physiologically relevant remains to be determined. But recent publication suggests such a structure is unlikely to be relevant in yeast (Daigaku et al., 2010, Karras and Jentsch, 2010).

3.1.2.3 Monoubiquitylated PCNA and TLS polymerases

Normal replicative polymerase cannot process DNA lesions such as abasic sites due to its high fidelity catalytic site. There is a group of alternative DNA polymerases with active sites that are able to cope with those lesions, named TLS polymerases. In yeast TLS polymerases include Y-family polymerases Rev1, Polη and B-family polymerase Polζ (Prakash et al., 2005). Humans have two additional Y-family TLS polymerases, Polι and Polκ (Prakash et al., 2005). These TLS polymerases are less processive and more error-prone compared with the replicative polymerases Polδ and Polε, and they interact with the interdomain connector loop (IDCL) of PCNA, usually independently of ubiquitylation. The monoubiquitylation of PCNA functions as a molecular switch for

the replication machinery to change polymerases (Kannouche et al., 2004, Watanabe et al., 2004). The identification of UBM (ubiquitin binding motif) and UBZ (ubiquitin binding Zn finger) domains in TLS polymerases gives an explanation for the polymerase switch mechanism (Bienko et al., 2005). A yeast two-hybrid screen aiming to identify unconventional I44-independent ubiquitin interactors revealed human Polι as an interactor and later bioinformatic analysis identified two UBM domains within the protein. A similar domain structure was identified in another Y-family polymerase, Rev1, as well (Bienko et al., 2005). Another kind of ubiquitin-binding domain, the UBZ domain was identified in Polη (Rad30 in yeast) and Polκ (Figure 3.2)(Bienko et al., 2005, Plosky et al., 2006). Hence, the most attractive hypothesis was that the ubiquitin-binding domain in TLS polymerases might enhance the affinity between monoubiquitylated PCNA and TLS polymerases. This was experimentally addressed and confirmed by a number of studies (Guo et al., 2006, Parker et al., 2007, Guo et al., 2008). Most interestingly, a monoubiquitin fused to the N-or C-terminus of a non-ubiquitylable PCNA can partially rescue the UV sensitivity of *rad18* cells in a TLS-dependent manner (Parker et al., 2007). In a physical interaction study, the monoubiquitin-PCNA fusion preferentially interacted with Rev1 (Guo et al., 2006). These observations suggested that monoubiquitin-PCNA is a functional mimic of physiological K164-monoubiquitylated PCNA. Moreover, the monoubiquitin-PCNA fusion has proved to be a useful tool *in vitro* to study the regulation of the mechanisms of polymerase switching and PCNA polyubiquitylation (Zhuang et al., 2008, Parker and Ulrich, 2009). More recently, a split version of PCNA, which consists of one polypeptide covering a region from the N-terminus to residue 163 and a second polypeptide consisting of ubiquitin fused to residue 165 of the C-terminal portion of PCNA, can self-assemble and support both cell survival and TLS. The crystal structure of this "monoubiquitylated" PCNA has been solved (Freudenthal et al., 2010). In higher eukaryotes, the monoubiquitylation of PCNA can be reversed by USP1, and this process might contribute to the later stages of the polymerase switch, where the TLS polymerase is replaced by the processive replicative polymerase once the lesion is bypassed (Huang et al., 2006). Some TLS polymerases are ubiquitylated themselves, and the ubiquitin attached to the polymerase can compete with that on PCNA for UBDs

via an intramolecular interaction to promote the removal of TLS polymerase from the PCNA (Bienko et al., 2005).

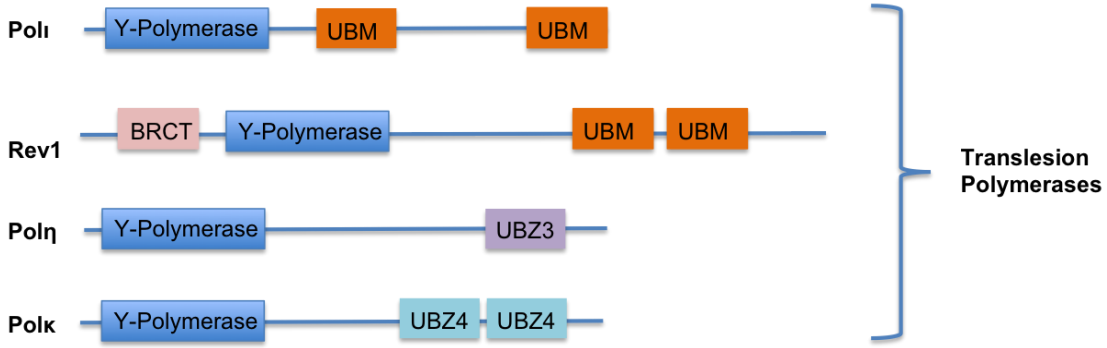

Figure 3.2 Domain structure of translesion synthesis polymerases
It shows the presence of ubiquitin-binding domains in Y-family TLS polymerases. The UBM domain is shown as an orange box; the UBZ domain is shown as a purple/green box. BRCT domain (Brca1 C-terminal domain) is shown as a pink box. This figure was adapted from (Hofmann, 2009).

3.1.2.4 Polyubiquitylated PCNA

PCNA is polyubiquitylated at K164 and the ubiquitin chain is K63-linked (Hoege et al., 2002). Genetic analysis has shown that PCNA polyubiquitylation is required for error-free damage bypass and further suggests a template switch mechanism that might use genetic information from the undamaged newly synthesised sister chromatid (Hoege et al., 2002, Zhang and Lawrence, 2005). However, the molecular details downstream of PCNA polyubiquitylation are not known. The K63-linked polyubiquitin is well-known for its non-proteolytic function, and an early genetic study showed a 10-fold lower UV-sensitivity in a *pre1 pre2 rev3* strain compared with a *ubc13 rev3* strain. If the main function of the K63-linked chain is to target PCNA for proteasomal degradation, mutations in proteasome active sites would show a similar effect to blocking ubiquitin chain assembly, therefore *pre1 pre2 rev3* and *ubc13 rev3* would have a similar UV sensitivity. In contrast, the observation did not fit with the hypothesis that the K63-linked polyubiquitin chains signal for degradation (Hofmann and Pickart, 2001). However, another genetic study has proposed a potential link between the proteasome and the *RAD6* pathway by showing an epistatic relationship between proteasome maturation factor *UMP1* and *RAD6* pathway genes (Podlaska et al., 2003). This

discrepancy, derived from indirect genetic data, necessitates a direct experimental approach to test the hypothesis if a K63-linked polyubiquitin chain targets PCNA for degradation. Furthermore, factors specifically recognising K63-polyubiquitylated PCNA remain to be identified in order to fully understand the molecular process downstream of PCNA polyubiquitylation.

In this chapter of work, PCNA has been used as a model substrate to directly compare the consequences of modifications by linear and K63-linked polyubiquitin chains. My results indicate that the DNA damage tolerance pathway is able to differentiate between linear and K63-linked polyubiquitin chains. K63-polyubiquitylated PCNA is not a target for proteasomal degradation. In contrast, linear, non-cleavable ubiquitin chains do not promote DNA damage tolerance, but instead function as general degradation signals.

3.2 Linear Ubiquitin Chains Do Not Promote DNA Damage Tolerance

In order to directly compare the consequences of modifications by linear and K63-linked polyubiquitin chains, I decided to start my study with a model substrate on which both modifications can occur. There were two options: find a physiological substrate of K63-linked polyubiquitylation and replace the modification with linear ubiquitin chains or vice versa. PCNA is physiologically polyubiquitylated by K63-linked chains upon DNA damage and this modification event is highly conserved from yeast to human. It therefore provided me with a unique model substrate to analyse the exact outcomes of linear versus K63-linked polyubiquitylation. It is possible to create linear polyubiquitin chains as tandem repeats of ubiquitin units by molecular cloning. I can also take advantage of yeast genetics to determine the molecular details downstream of these modifications by manipulating readout strains. The other option involves putting K63-linked polyubiquitin chains on a substrate of linear polyubiquitylation. The only such substrate reported up to date was NEMO and the far more complicated experimental

setting in a mammalian cell line system compared with a similar but more simple approach in a yeast system prevented me from pursuing this option. In the case if linear chains are able to substitute K63-linked chains to function in DNA damage bypass, I could then use it to make mimics of real polyubiquitylated PCNA in order to investigate its biological functions. If linear chains do not function the same as K63-linked chains, I would still be able to investigate the functional differences between these two types of chains in the context of the DNA damage tolerance pathway.

Based on these stated reasons, I wanted to analyse linear polyubiquitylated PCNA and K63-polyubiquitylated PCNA for their functions in the DNA damage tolerance pathway. Firstly, I need to create a linear polyubiquitylated form of PCNA. Previous observations from our lab showed that a single, non-extendable ubiquitin (K29R, K48R, K63R) fused to either N- or C-terminus of PCNA successfully complements a defect in monoubiquitylation at K164 (Parker et al., 2007). These data suggest that the position of ubiquitin on PCNA is not critical, at least for function in TLS. In addition to that, *in vitro* the PCNA polyubiquitylation machinery is able to assemble chains on a fusion construct with WT ubiquitin fused to either N- or C-terminus of PCNA* (K127R, K164R), whose major ubiquitylation and SUMOylation sites are mutated (Parker and Ulrich, 2009). It suggests that the polyubiquitylation machinery for PCNA is not selective for modification sites on PCNA at least *in vitro* and polyubiquitin chains attached to the N-terminus of PCNA may still function. Therefore, I further extended this system to generate a linear ubiquitin chain modified form of PCNA. I designed linear fusions of polyubiquitin arrays to the N- or C-terminus of PCNA (Figure 3.3). In order to allow for some conformational flexibility, I designed a series of constructs containing two to four ubiquitin repeats separated by a short linker (Ub^{*}_{n}(L)-PCNA*), and two constructs in which four ubiquitin moieties were joined precisely in a head-to-tail manner (Ub^{*}_{4}-PCNA* and PCNA*-Ub^{*}_{4}). In addition to ubiquitylation, PCNA is SUMOylated at K164 primarily as well as K127 (Hoege et al., 2002). The SUMOylated PCNA recruits Srs2 helicase to inhibit homologous recombination (Papouli et al., 2005, Pfander et al., 2005). In order to prevent further modification on my fusion constructs, the major ubiquitylation or SUMOylation sites on PCNA (K164 and K127) and on

ubiquitin (K29, K48 and K63) were mutated to arginine (indicated by an asterisk in our notation). A glycine to valine mutation at the C-terminus of ubiquitin was introduced to prevent isopeptidase cleavage. The last ubiquitin moiety at the C-terminus of PCNA*-Ub*$_4$ had a two-amino acid truncation (G75 and G76) represented as ΔGG to prevent further conjugation. Finally, in order to verify if K63-linked polyubiquitin chains can indeed support DNA damage tolerance even at the N-terminus of PCNA, I generated a construct named Ub^{K63*}-PCNA*, similar to the previously described non extendable Ub*-PCNA* fusion but with K63 available for further modification. The *in vitro* data for such a construct (Parker and Ulrich, 2009) would predict activity in both error-prone and error-free branches of damage tolerance.

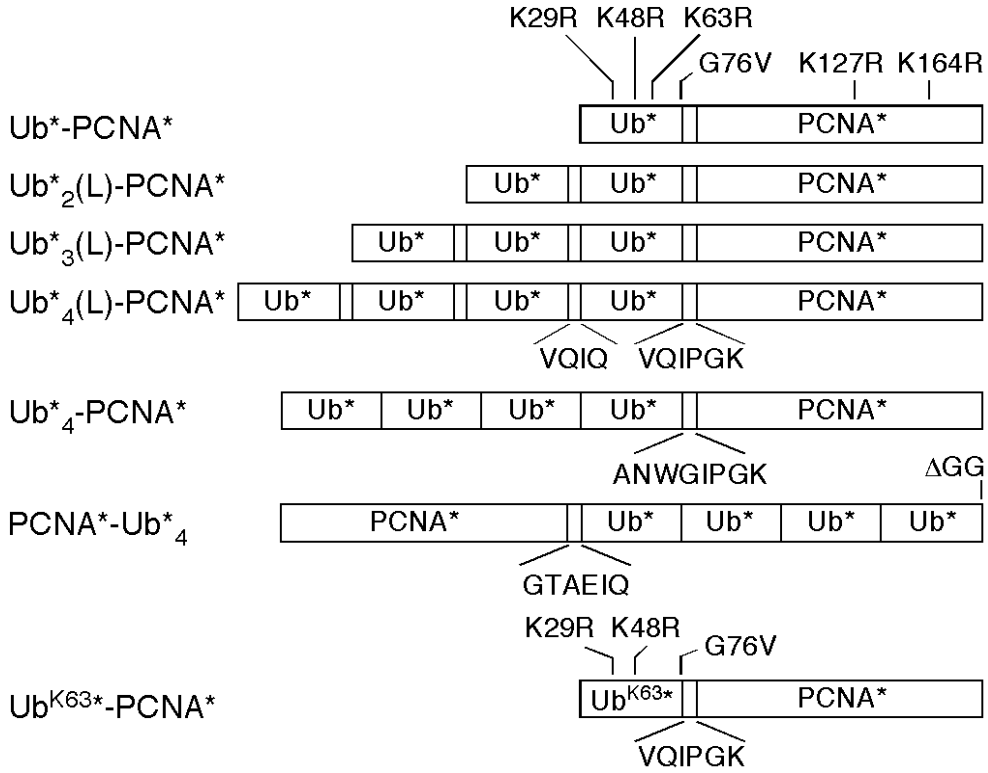

Figure 3.3 Linear ubiquitin-PCNA fusion constructs
Schematic view of the linear ubiquitin-PCNA fusion constructs used in this study. Mutations in the open reading frames of ubiquitin (K29/48/63R, G76V) and PCNA (K127/164R) are indicated only once per panel; the mutant versions are presented as Ub* and PCNA*, respectively. Amino acid sequences of linker peptides are shown below the constructs. The last ubiquitin moiety at the C-terminus of PCNA*-Ub*$_4$ has a two-amino acid truncation (G75 and G76) represented as ΔGG.

The constructs were expressed under control of the *POL30* promoter in a *rad18* strain, which is not able to ubiquitylate endogenous PCNA. In that case, the linear ubiquitin-PCNA fusion proteins were the only source of modified PCNA and their abilities in supporting damage tolerance would be reflected as sensitivities of host strains to the DNA damage agents methyl methanesulfonate (MMS) or ultraviolet (UV) irradiation. In the *rad18* strain, I observed that Ub^{K63*}-$PCNA^{*}$ was able to suppress the damage sensitivity in MMS drug spot assay even at a concentration of 0.002% MMS, almost 10-fold higher than the level of resistance observed in Ub^{*}-$PCNA^{*}$ (Figure 3.4). The suppression effect of Ub^{*}-$PCNA^{*}$ was mainly mediated by TLS as cell survival was abolished in the *ΔTLS* background, where all three TLS polymerases in budding yeast were defective due to *rev1 rev3 rad30* mutations. However, the suppression effect of Ub^{K63*}-$PCNA^{*}$ was largely independent of TLS as the cell survival was only partially reduced in *ΔTLS* background (Figure 3.4). This result beautifully illustrated that Ub^{K63*}-$PCNA^{*}$ can rescue damage sensitivity of *rad18* cells independent of TLS-mediated error-prone damage bypass, most likely by activating the error-free branch of the DNA damage tolerance pathway. This result is also consistent with previously reported *in vitro* observations, where polyubiquitin chains can be formed on Ub-$PCNA^{*}$ by the PCNA polyubiquitylation machinery (Parker and Ulrich, 2009), and it suggests that K63-linked polyubiquitin chains are indeed functional even at the N-terminus of PCNA. From this observation, I ruled out the possibility that changing the modification site from K164 to the N-terminus of the protein might have influence on the biological outcomes of polyubiquitylation on PCNA, therefore I was able to make a fair comparison for linear and K63-linked polyubiquitin chains on the same modification site of a common substrate.

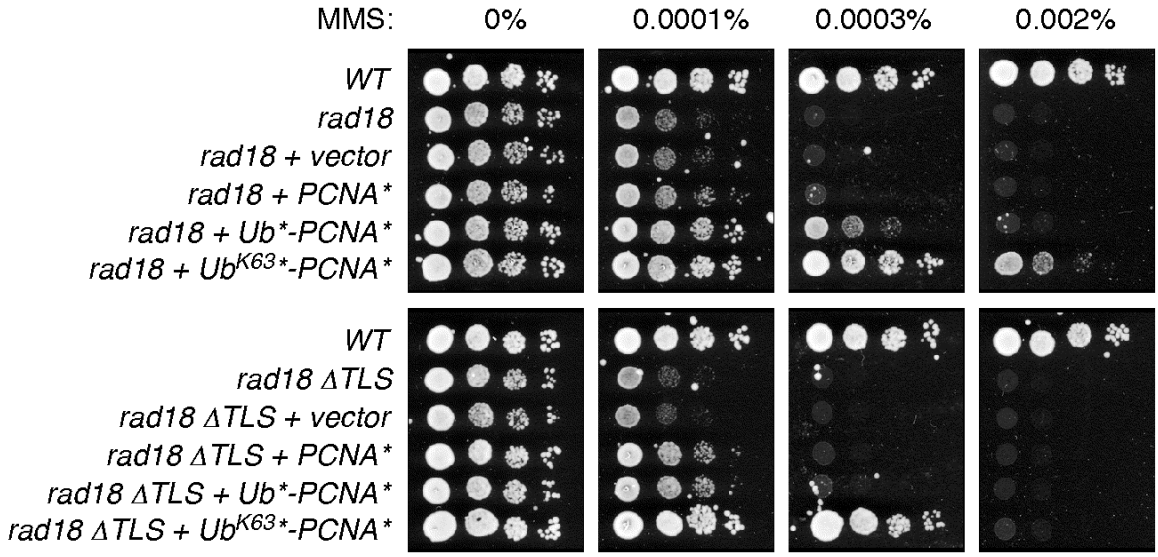

Figure 3.4 K63-linked polyubiquitin chains support damage tolerance even at the N-terminus of PCNA
Sensitivities of the indicated strains to MMS were determined by spot assays. Ub^{K63*}-$PCNA^{*}$ permits formation of a K63-linked chain on the N-terminus of PCNA, suppresses the damage sensitivity of *rad18* in a TLS-independent manner, indicating that the attachment site of the ubiquitin chain on PCNA is irrelevant for function in damage bypass. The *rad18 ΔTLS* strain (*rad18 rev1 rev3 rad30*) is defective in all three budding yeast TLS polymerases (Bottom).

For linear fusion constructs, Ub^{*}_{4}(L)-$PCNA^{*}$ suppressed the damage sensitivity of *rad18* cells to some degree (Figure 3.5A). In contrast, the linkerless versions, Ub_4^{*}-$PCNA^{*}$ and $PCNA^{*}$-Ub_4^{*} did not show much rescue beyond the effect of $PCNA^{*}$ alone (Figure 3.5B). In addition to that, all of the linker-bearing constructs Ub^{*}_{2}(L)-$PCNA^{*}$, Ub^{*}_{3}(L)-$PCNA^{*}$ and Ub^{*}_{4}(L)-$PCNA^{*}$ showed a rescue effect same as that of the construct equivalent to monoubiquitylated PCNA (Figure 3.5A). Most importantly, the rescue effect observed in cells with all these constructs required the presence of TLS polymerases, as the viability dropped back to the level of $PCNA^{*}$ alone when similar experiments were performed in a *rad18ΔTLS* strain (Figure 3.5A). This result was further confirmed by UV survival assay with the same strains used in MMS drug spot assay (Figure 3.6).

These data indicate that Ub^*_n(L)-PCNA* only support TLS, but not the error-free branch of damage bypass and increasing the length of the linear ubiquitin chain does not seem to help with TLS efficiency. The linkerless construct was even unsuccessful in TLS, suggesting that damage tolerant polymerases may require specific interaction sites on PCNA and proximal ubiquitin moiety, which could be masked by the head-to-tail linkage. Taking into account the fact that K63-linked polyubiquitin chains are functional at the N-terminus of PCNA, but none of the linear fusion constructs are able to support polyubiquitylation-dependent damage bypass, it indicates that in the context of the DNA damage tolerance pathway linear and K63-linked polyubiquitin chains are functionally distinct.

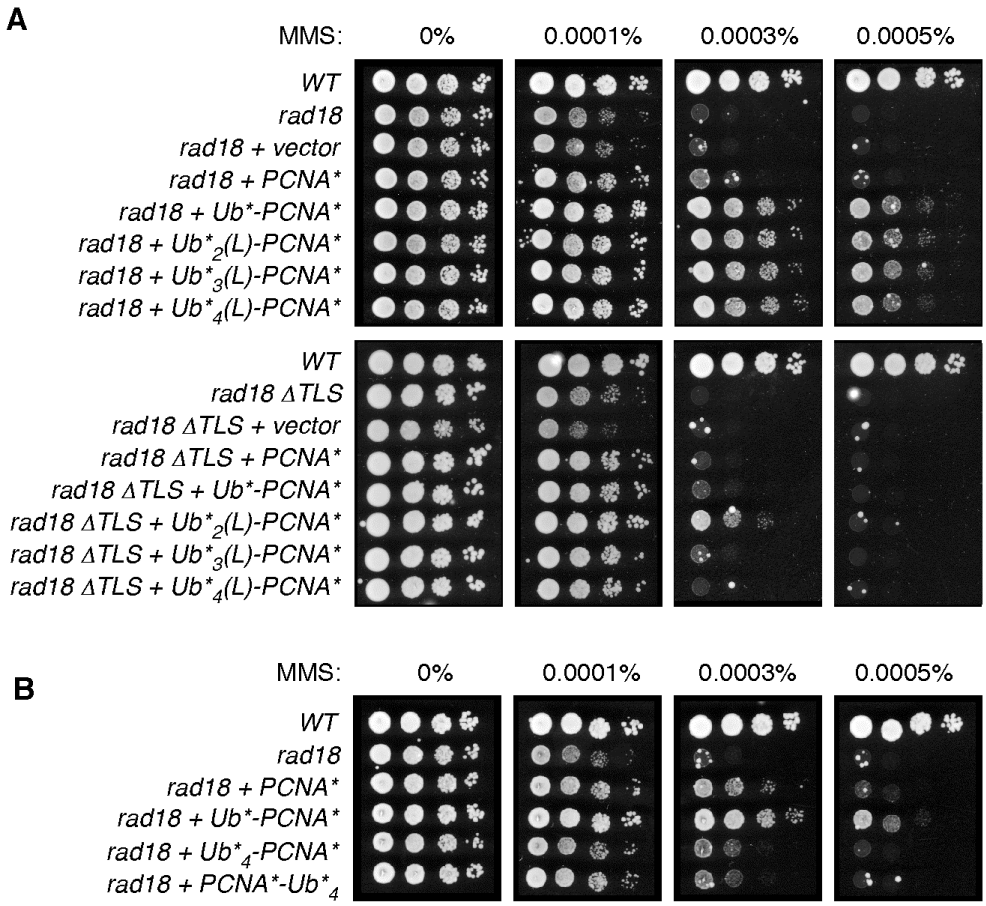

Figure 3.5 Linear non-cleavable polyubiquitin chains on PCNA cannot substitute for the K63-linked modification in DNA damage bypass
Sensitivities of the indicated strains to MMS were determined by spot assays. (A) Linker-bearing ubiquitin-PCNA fusions [Ub^*_n(L)-PCNA*] support only TLS, irrespective of the number of ubiquitin moieties. (B) Linkerless fusions of tetraubiquitin to PCNA (Ub^*_4-PCNA* and PCNA*-Ub^*_4) do not promote damage bypass.

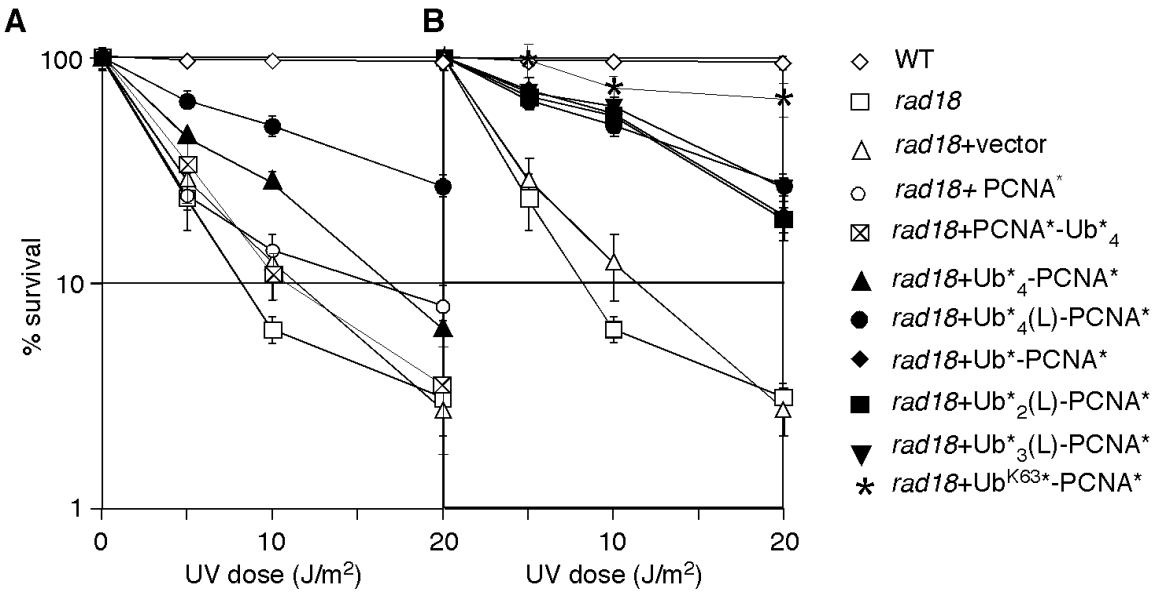

Figure 3.6 Linear ubiquitin fusions to PCNA rescue the UV sensitivity of *rad18* cells to different extents

(A) Linear tetraubiquitin fusions to PCNA rescue the UV sensitivity of *rad18* cells to different extents. UV sensitivities were determined for *rad18* cells bearing the indicated constructs. (B) The number of ubiquitin units fused to PCNA* does not affect the extent of rescue. UV survival assays were carried out as in (A). Diamond shape: WT; square shape: *rad18*; triangle shape: *rad18*+vector; circle shape: *rad18*+PCNA*; square with an "x"inside: *rad18*+PCNA*-Ub*4; solid black triangle: *rad18*+Ub*-PCNA*; solid black circle: *rad18*+Ub*4 (L)-PCNA*; solid black diamond: *rad18*+Ub*-PCNA*; solid black square: *rad18*+Ub*2 (L)-PCNA*; upside down solid black triangle: *rad18*+Ub*3(L)-PCNA*; *: *rad18*+Ub^{K63*}-PCNA*.

3.3 Linear Polyubiquitin Chains Target PCNA for Proteasomal Degradation

The fact that the DNA damage tolerance pathway is able to distinguish linear and K63-linked polyubiquitin chains led me to investigate the exact function of each type of chain in this specific context. The first clue comes from analysing the protein levels of different linear fusions used in DNA damage sensitivity studies described in Figure 3.5. I noticed a dramatic reduction in the abundance of all fusion proteins with tetraubiquitin chains compared with the shorter versions or endogenous PCNA in *rad18* strains (Figure 3.7). The potential effects caused by different levels of fusion proteins on their function in damage bypass will be discussed in detail in section 3.8.1. Similar patterns were observed when I expressed all fusion constructs in a WT strain (Figure 3.8A). It

has been shown that the minimum length for K48-linked polyubiquitin chains to be effectively recognised by the 26S proteasome is four ubiquitin moieties (Thrower et al., 2000). I hypothesised that linear ubiquitin chains may also function as proteasomal degradation signals.

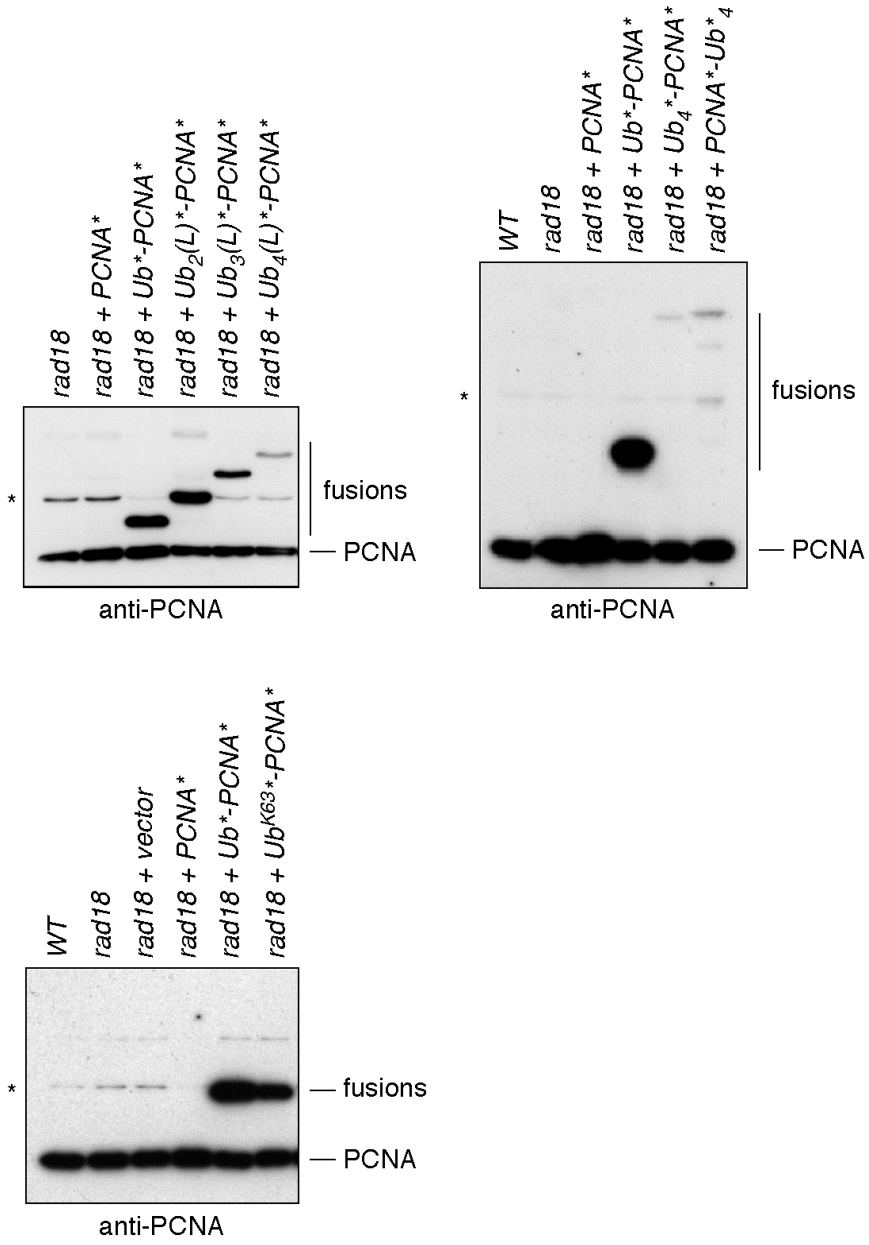

Figure 3.7 Expression and abundance of ubiquitin-PCNA fusion proteins in *rad18* cells

Protein levels of the PCNA fusions used in MMS spot assay and UV sensitivity assay (Figure 3.4, 3.5 and 3.6) in total extracts of *rad18* cells, detected by Western blots analysis. The asterisks indicate cross-reactive bands, possibly SUMOylated endogenous PCNA.

I first tested if proteasome mutants were able to stabilise fusion proteins with tetraubiquitin chains. By expressing fusion proteins in a proteasome mutant *pre1-1* strain, which has impaired catalytic activity, and its isogenic WT, I observed increased steady-state levels of full-length fusion proteins in the proteasome mutant strain whereas the endogenous PCNA level remains equal in all lanes serving as loading control (Figure 3.8B). There were species reactive with PCNA-antibody migrating at the size between full-length fusion proteins and endogenous PCNA. It is likely that they are partially processed fusion proteins and their appearance in *pre1-1* cells could be due to the remaining proteasomal activity in this mutant.

This effect could be a result of up-regulation of protein production or protein stabilisation in proteasome mutant cells. To distinguish these two possibilities, I performed Northern blot experiments to directly assess the levels of transcripts of Ub_4^*-$PCNA^*$ in both WT and proteasome mutant cells. Total RNA was isolated from both strains and a *POL30* gene specific probe was used to detect Ub_4^*-$PCNA^*$ transcripts and endogenous PCNA transcripts. I did not see any obvious changes in the amount of transcripts between WT and *pre1-1* cells in this experiment, suggesting that increased protein levels of fusion constructs in proteasome mutant were not due to changes in the amount of specific transcripts in *pre1-1* cells (Figure 3.8C). Therefore, stabilisation of fusion proteins in *pre1-1* cells is most likely to be the reason.

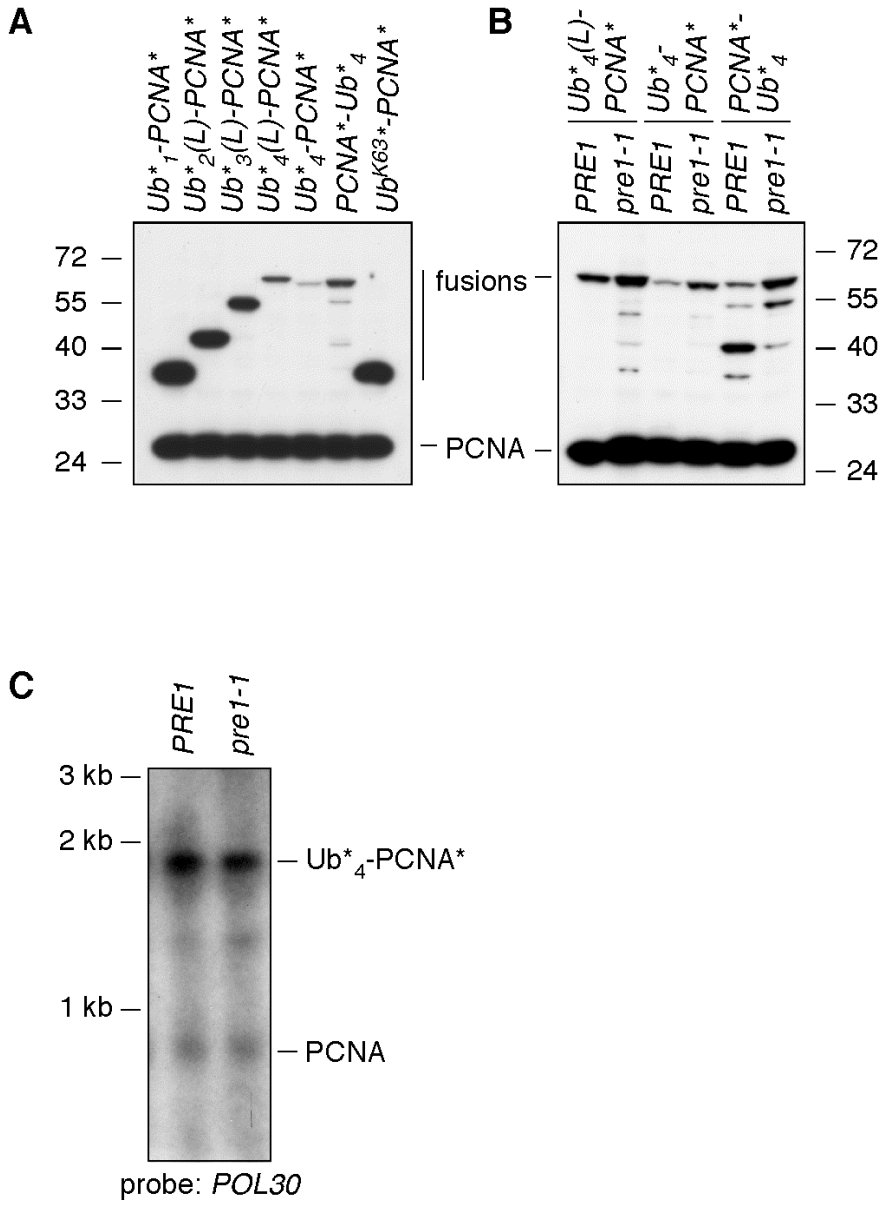

Figure 3.8 Protein levels of linear tetraubiquitin-PCNA fusions increase in a proteasome mutant

(A) Protein levels of the ubiquitin-PCNA fusion constructs and endogenous PCNA were compared by Western blots with an anti-PCNA antibody. Linear tetraubiquitin chains destabilise the respective fusion proteins. (B) Steady-state protein levels of tetraubiquitin fusions to PCNA are increased in a proteasome mutant. The observed PCNA antibody-reactive species between full-length fusion proteins and endogenous PCNA are likely to be processed intermediates of the fusion proteins. (C) Northern blots, probed with a *POL30*-specific probe and showing mRNA levels of Ub^{*}_{4}-$PCNA^{*}$ and PCNA in the indicated strains.

To directly test this possibility, I decided to analyse the stability of tetraubiquitin-PCNA fusions *in vivo*. I treated *PRE1* and *pre1-1* cells with cycloheximide, a translation inhibitor, to block de novo protein synthesis and performed chasing experiments to analyse fusion protein levels from culture samples taken at different time points. Indeed, all tetraubiquitin-PCNA fusion proteins were degraded in WT cells and were stabilised in proteasome mutant cells (Figure 3.9). But the half-lives varied considerably from 60 minutes to a few hours between the different fusion constructs. $PCNA^{*}$-Ub^{*}_{4} had the shortest half-life and it was almost completely degraded in 60-80 minutes. In contrast, Ub_4^{*}-$PCNA^{*}$ needed more than 15 hours to be degraded. It took even longer for Ub_4^{*}(L)-$PCNA^{*}$ to have an observable reduction in its protein level (Figure 3.9). It suggests that indeed tetraubiquitin-PCNA fusions are degraded *in vivo* in a proteasome-dependent manner. However, the observed turnover rate is at best moderate, not comparable with endogenous short-lived proteins or other model substrates whose degradation is mainly targeted by K48-linked polyubiquitin chains. The degradation rate of fusion proteins varies depending on the way ubiquitin moieties are connected in the linear chain or the attachment site on the substrate. Because the Ub_4^{*} construct most closely resembles the arrangement of a physiological linear ubiquitin chain and it functions as a better degradation signal, all subsequent studies were focused on this form of linear ubiquitin construct.

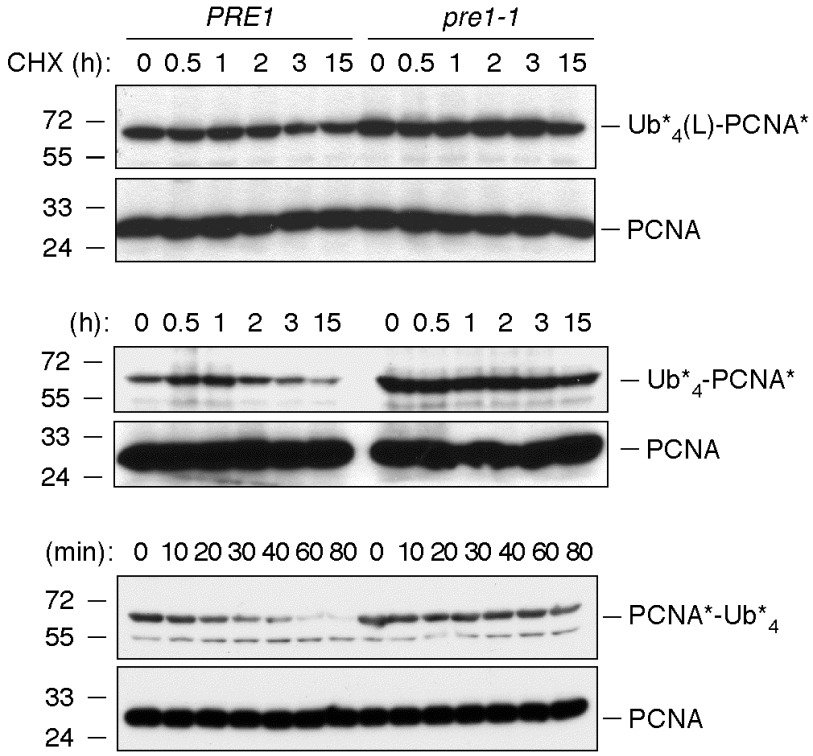

Figure 3.9 Linear non-cleavable tetraubiquitin chains target PCNA for degradation by the 26S proteasome *in vivo*
Cycloheximide chase experiments show the degradation of the tetraubiquitin fusion proteins in *PRE1* cells and their stabilisation in *pre1-1* cells. Exponential cultures were treated with 100 µg⁄mL cycloheximide to inhibit de novo protein synthesis, and samples corresponding to equal culture volumes were processed for Western blot analysis at the indicated time points.

In vivo, misfolded proteins are degraded via the 26S proteasome as part of the cellular quality control mechanism to eliminate defective proteins (Goldberg, 2003). In order to exclude the possibility that incorrect folding of the fusion protein causes proteasomal degradation, I decided to analyse if Ub_4^*-PCNA* can fold properly. PCNA forms homotrimer *in vivo* and a previous observation in our lab shows that Ub^*-PCNA* is able to trimerise and be loaded onto DNA (Parker et al., 2007). Therefore, I speculate that Ub_4^*-PCNA* should also be able to form trimers if the fusion protein can fold properly. I expressed $^{6His}Ub_4^*$-PCNA* as N-terminally 6His-tagged recombinant protein in *E.coli* and performed a Ni-NTA affinity purification. A gel filtration analysis was then performed to analyse the ability of Ub_4^*-PCNA* or PCNA* to form trimers. A mix of standard proteins was used to estimate the size of complexes presented in different

fractions. Recombinant PCNA alone was enriched in fractions #25-27 with a molecular weight around 90 kDa (Figure 3.10A). PCNA monomer has a size around 30 kDa, the observed enrichment at 90 kDa suggests PCNA* alone forms trimers *in vitro*. I found $^{6His}Ub^{*}_{4}$-PCNA* enriched in fractions #21-23 with a molecular weight around 210 kDa (Figure 3.10A, B). With its monomer about 70 kDa in size, the detected 210 kDa complex indicates that $^{6His}Ub^{*}_{4}$-PCNA* forms homotrimers as well *in vitro*. Therefore, Ub^{*}_{4}-PCNA* has a proper folding structure and protein misfolding is unlikely to be responsible for the degradation of this fusion protein.

Although three major ubiquitin acceptor sites (K29, K48 and K63) were mutated in my tetraubiquitin chains and there were no high molecular weight species on Western blots could indicate further modifications, I was interested to find out if a linear ubiquitin chain alone was sufficient for proteasomal targeting. I performed an *in vitro* degradation assay with purified 26S proteasome, which is commercially available. In my experiment, 5 nM 26S proteasome was supplied with 200 nM substrates protein. I observed that recombinant $^{6His}Ub^{*}_{4}$-PCNA* was degraded in a few hours, but recombinant PCNA was not degraded during the same time course (Figure 3.10C). This result suggests a linear ubiquitin chain alone is sufficient for proteasome targeting *in vitro*. Interestingly, the rate of substrate degradation was also quite slow in this case, which is not comparable with other short-lived proteasome substrates but correlates with my previous *in vivo* observation. Potential explanations for this phenomenon will be discussed in section 3.8.3.

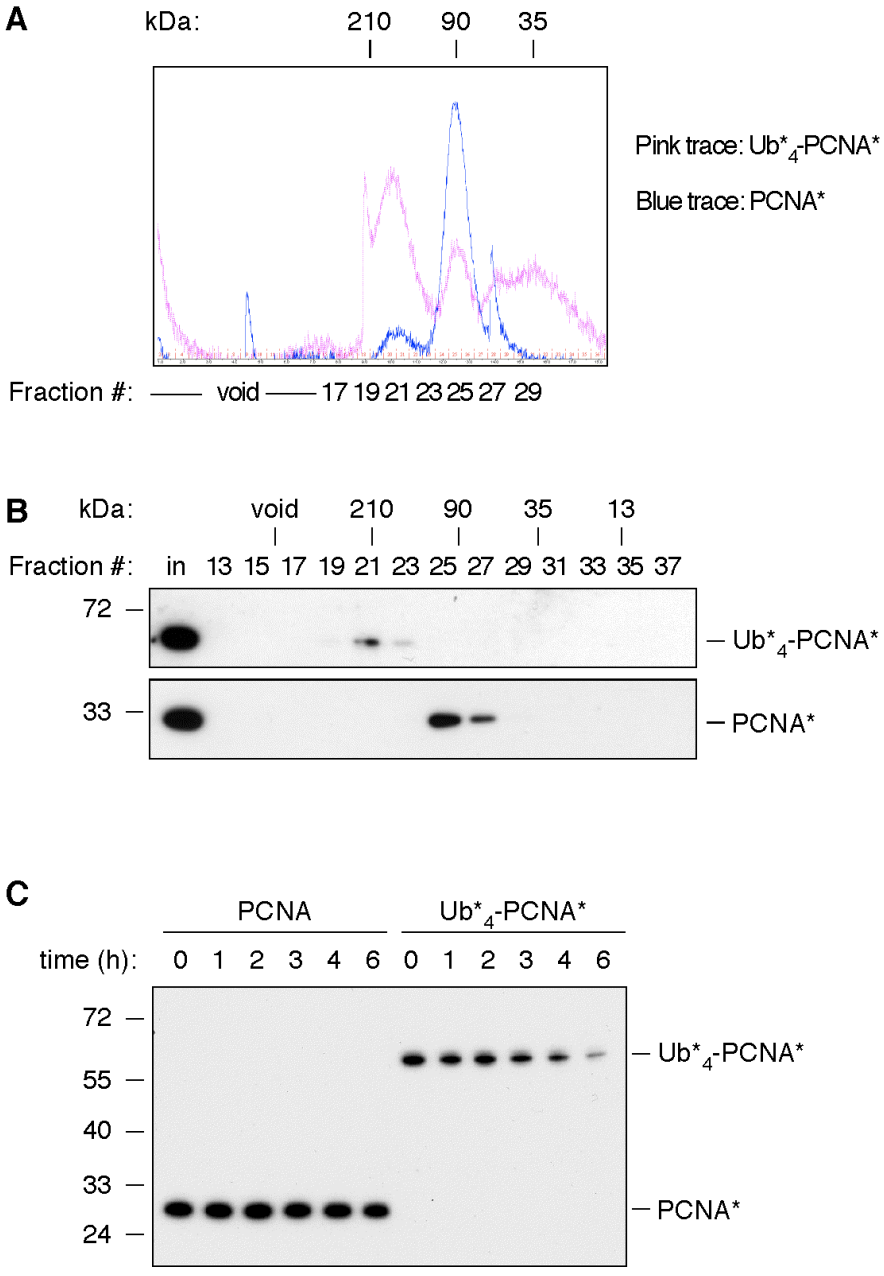

Figure 3.10 Recombinant Ub$^{*}_{4}$-PCNA* forms homotrimers and is degraded by the 26S proteasome *in vitro*

(A) and (B) Gel filtration analysis of PCNA* and Ub$^{*}_{4}$-PCNA*, followed by anti-PCNA Western blots, confirms the trimeric nature of the fusion protein. In (A), the pink trace represents Ub$^{*}_{4}$-PCNA* and the blue trace represents PCNA*. Fraction numbers are labelled below the trace and the molecular weight standards are above the trace. The second and third peak of the pink trace represent partially cleaved products of Ub$^{*}_{4}$-PCNA*. (B) Western blots of samples from gel filtration analysis; elution of molecular weight standards and the void volume are indicated above the fraction numbers. (C) *In vitro* degradation assays were set up with 200 nM purified recombinant PCNA* or Ub$^{*}_{4}$-PCNA* and 5 nM purified human 26S proteasome at 37 ℃. Samples were taken at the indicated time points and analysed by Western blot.

The linear ubiquitin chain constructs used in my study have extensive mutations on each ubiquitin moiety including: K29R, K48R, K63R and G76V. There are some evidences showing that lysine-less K0 ubiquitin has an altered surface charge and partial deficiency in its ability to interact with ubiquitin-binding domains (Komander, 2009). The fact that my linear ubiquitin chain was still able to target PCNA for degradation suggests this form of ubiquitin chain was at least functional, if not optimal, *in vivo*. To further strengthen this point, I decided to directly test its ability to interact with a UBAN domain, which is an ubiquitin-binding domain selective for linear ubiquitin chains (Komander et al., 2009b, Rahighi et al., 2009). I expressed $^{GST}Ub^{*}_{4}$ with an N-terminal GST-tag from *E.coli* and purified the fusion protein by glutathione sepharose based affinity chromatography. GST moiety was then cleaved by thrombin (Figure 3.11A) and protein samples were then passed through a glutathione column, followed by a benzamidine column to remove free GST and thrombin. The ^{GST}UBAN domain of NEMO was expressed and purified in a similar way. An *in vitro* pull-down experiment was performed and indeed ^{GST}UBAN is able to bind Ub^{*}_{4} (Figure 3.11B). This result suggests the linear ubiquitin chain used in this study is able to bind the UBAN domain despite a series of mutations on its surface.

In summary, these data suggest that linear polyubiquitin chains with sufficient length on PCNA act as proteasomal degradation signals *in vivo* and *in vitro* with a noticeably slower turnover rate compared to those of some short-lived endogenous proteins or model substrates (Johnson et al., 1995, Ciechanover et al., 2000).

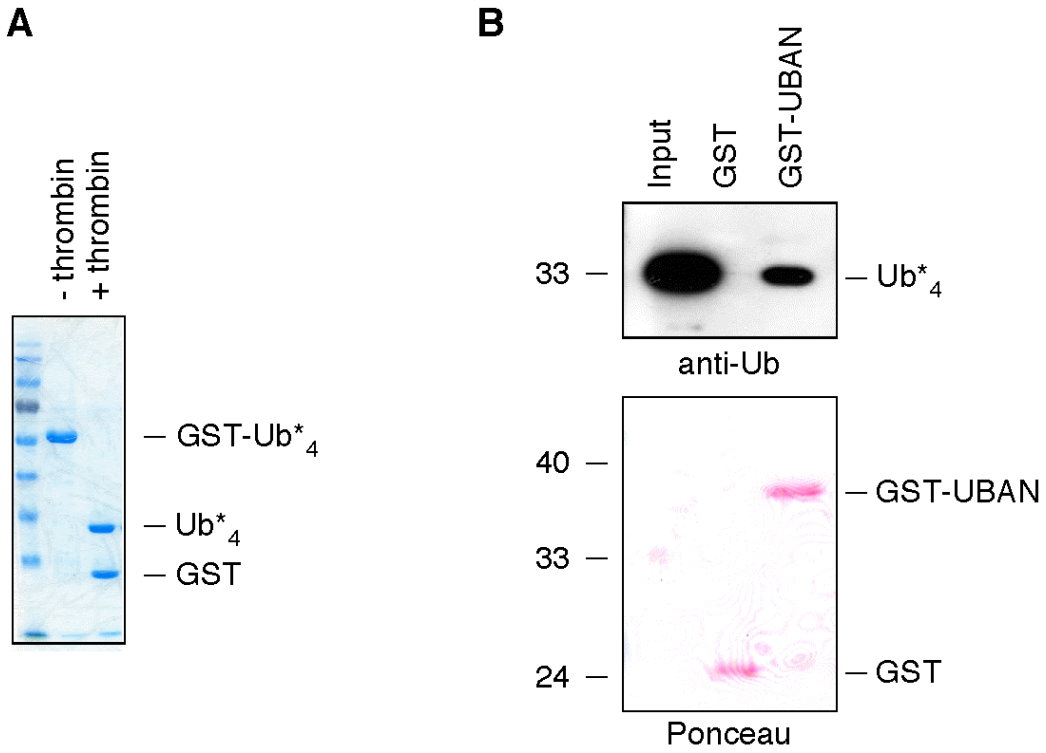

Figure 3.11 The linear non-cleavable Ub^*_4 array is bound by the UBAN domain of NEMO
(A) Coomassie staining of a gel shows purified $^{GST}Ub^*_4$ samples with or without thrombin treatment. $^{GST}Ub^*_4$ was expressed and purified from *E.coli* using glutathione affinity chromatography, the GST moiety was removed from the fusion protein by treating with thrombin overnight at room temperature and samples were applied to a glutathione column and a benzamidine column sequentially to remove free GST and thrombin. (B) GST pull-down experiments were performed with Ub^*_4 and a GST fusion of the NEMO UBAN domain. Proteins bound to the glutathione beads were detected by anti-ubiquitin Western blot and Ponceau staining of the membrane. 1.5% of the input and 12.5% of total bound material were loaded on this gel.

3.4 K63-Polyubiquitylation Does Not Target PCNA for Degradation

PCNA is polyubiquitylated by K63-linked chains under conditions of DNA damage. It remains unclear what is the function for K63-linked chains in this case. There is some indirect evidence suggesting two different possibilities. First of all, total cellular level of PCNA does not seem to drop after DNA damage-induced ubiquitylation, suggesting a non-proteolytic role of the modification (Hoege et al., 2002). However, as the fraction of polyubiquitylated PCNA is very little, lack of change at total PCNA level does not

necessarily indicate a non-degradative function. Further investigations are still required. The second possibility is based on genetic evidence that proteasome mutants exhibit DNA damage sensitivity and have an epistatic relationship with *RAD6* pathway genes (Podlaska et al., 2003). It suggests that the proteasome may be involved in DNA damage tolerance as a consequence of this modification. But, again there is evidence against this idea mainly from another genetic observation showing lack of synergism between *pre1-1 pre 2-2* and *rev3* mutants (Hofmann and Pickart, 2001). I was therefore interested to investigate the role of K63-linked polyubiquitylation on PCNA.

To address the possibility that K63-linked polyubiquitin chains may play a role as degradation signal on PCNA, I started to analyse the amount of polyubiquitylated PCNA in cells with normal or attenuated proteasome activity. As the first approach, I used a proteasome inhibitor to transiently block proteasome activity before introducing DNA damage. I treated yeast cells with proteasome inhibitor MG132 for 2 hours and then introduced DNA damage with MMS. A special yeast strain ^{His}*POL30 pdr5*, in which a multidrug transporter encoded by *PDR5* gene has been removed, was used to allow efficient uptake of proteasome inhibitor MG132. A 6His-tag was introduced into the *POL30* genomic locus to allow efficient isolation of PCNA. ^{His}PCNA was isolated from cell extracts under denaturing conditions to preserve polyubiquitylation. As a control for successful proteasome inhibition, I observed an accumulation of total cellular ubiquitin conjugates in the extracts from cells treated with proteasome inhibitor MG132 (Figure 3.12A). In contrast, the levels of damage-induced polyubiquitylated PCNA did not increase in those cells, instead, a small reduction was observed (Figure 3.12B).

In order to confirm this observation, I decided to analyse the damage-induced PCNA polyubiquitylation in proteasome mutants that have a persistent attenuation of proteasome activity compared with a transient inhibition with inhibitor MG132 treatment. I chose two mutants: *ump1,* a proteasome maturation factor mutant, *UMP1* has been reported to be epistatic with *RAD6* pathway genes (Podlaska et al., 2003);

pre1-1, a catalytic mutant of the proteasome. In these proteasome mutants, a similar result was observed. Total cellular ubiquitin conjugates were accumulated in mutant strains and the levels of polyubiquitylated PCNA again showed a subtle reduction (Figure 3.13A, 3.13B). In Figure 3.13B, on the anti-ubiquitin Western blot, there was a noticeable increase in high-molecular weight signals specifically from proteasome mutant samples, that could be due to elevated pull-down background from proteasome mutant strains since none of them are damage specific or PCNA reactive. Therefore, it is unlikely the modified species have converted to longer chains in this case. To summarize, all these data clearly indicate that damage-induced K63-linked PCNA polyubiquitylation normally does not lead to proteasomal degradation. When proteasome activity is attenuated, the reduction in the amount of polyubiquitylated PCNA is likely due to the depletion of free ubiquitin that results from a lack of recycling.

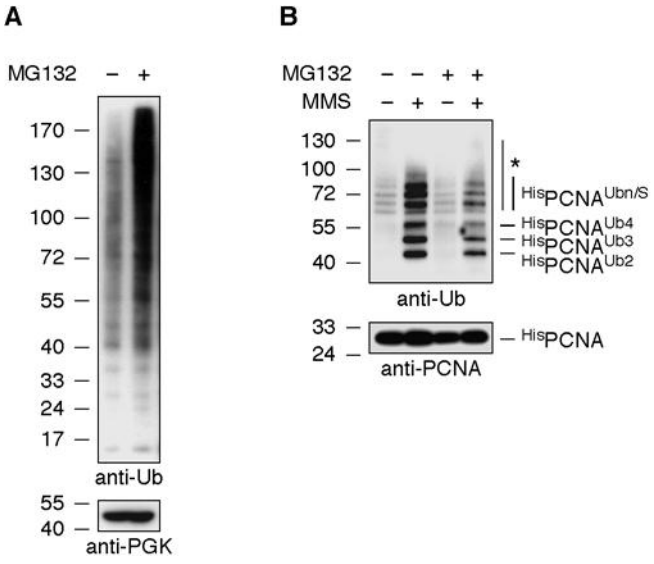

Figure 3.12 K63-polyubiquitylated PCNA does not increase in cells treated with proteasome inhibitor MG132
(A) Inhibition of the proteasome by the chemical inhibitor MG132 causes an accumulation of total ubiquitin conjugates. Exponential cultures of ^{His}*POL30 pdr5* cells were treated with 50 μM MG132 for 2 h where indicated, and ubiquitylated species were detected in total extracts by Western blots with an anti-ubiquitin antibody. Detection of phosphoglycerate kinase (PGK) served as loading control. (B) Damage-induced ubiquitylation of PCNA is reduced upon chemical inhibition of the proteasome. ^{His}PCNA was isolated by denaturing Ni-NTA pull-down from extracts of ^{His}*POL30 pdr5* cells treated with 50 μM MG132 for 2 h and 0.02% MMS for 90 min where indicated, and Western blots were developed with anti-PCNA and anti-ubiquitin antibodies.

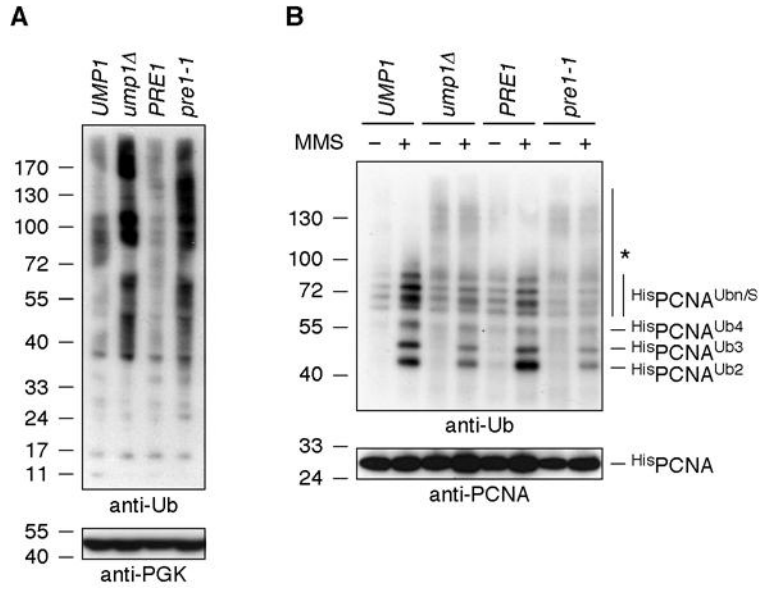

Figure 3.13 K63-polyubiquitylated PCNA does not increase in proteasome mutant cells
(A) Mutants with attenuated proteasome activity accumulate total ubiquitin conjugates. Extracts were prepared from the indicated strains and probed as in Figure 3.12A. (B) Damage-induced ubiquitylation of PCNA is reduced in mutants affecting proteasome activity. ^{His}PCNA and its ubiquitylated forms were isolated from the indicated strains and detected as in Figure 3.12B. The high-molecular weight signals in (B) marked with an asterisk are due to nonspecific isolation of ubiquitin conjugates; they are neither PCNA-reactive nor damage-dependent.

3.5 A Linear Ubiquitin Chain Acts as a General Degradation Signal

To generalise my observation that linear ubiquitin chains can act as degradation signals and to further investigate the slow turnover rate of substrates marked by linear ubiquitin chains, I decided to analyse the effect of linear chains on another model substrate β-galactosidase whose degradation pattern has been well studied (Bachmair et al., 1986). Based on the Ub-βGal construct originally described in the study of the UFD pathway (Johnson et al., 1992, Johnson et al., 1995), I generated a linear fusion of the head-to-tail tetraubiquitin chain to the N-terminus of β-galactosidase, named Ub^{*}_{4}-βGal (Figure 3.14). The Ub_4^{*}-βGal construct carrying mutations at three major modification sites K29, K48 and K63 as previously described and an expression construct for βGal alone were generated for protein stability assay along with Ub^{*}_{4}-βGal. All the constructs were expressed from episomal plasmids under control of the *GAL10* promoter. By comparing

the degradation rate of Ub^*_4-βGal with Ub-βGal, which is an extremely short-lived UFD pathway substrate, it should allow an estimation of the efficiency of linear ubiquitin chains acting as degradation signals.

I started with analysing the expression of all constructs by Northern blot. Total RNA was extracted from cells with or without galactose-induced fusion protein expression. Transcripts corresponding to the different constructs were detected with a radiolabelled probe specific for the *LacZ* gene. This experiment revealed that similar amounts of mRNA transcripts corresponding to each construct were made upon galactose induction (Figure 3.15A).

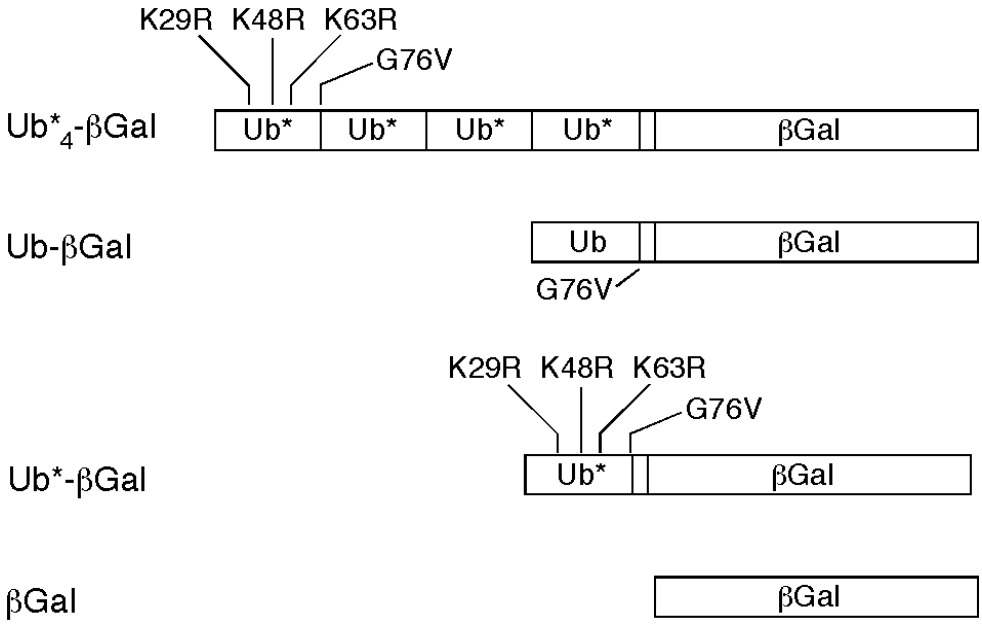

Figure 3.14 Schematic view of the βGal constructs used in this study
The asterisk denotes the ubiquitin mutant (K29/48/63R, G76V). Ub-βGal was originally described as Ub^{V76}-V-$e^{\Delta K}$-βgal. Ub^*_4-βgal was generated by replacing the Ub unit within the original construct Ub-βGal with a Ub^*_4 unit. Ub^*-βgal was constructed in a similar way using a Ub^* unit to replace the original Ub unit and βgal was generated by removing the Ub unit from the Ub-βGal construct.

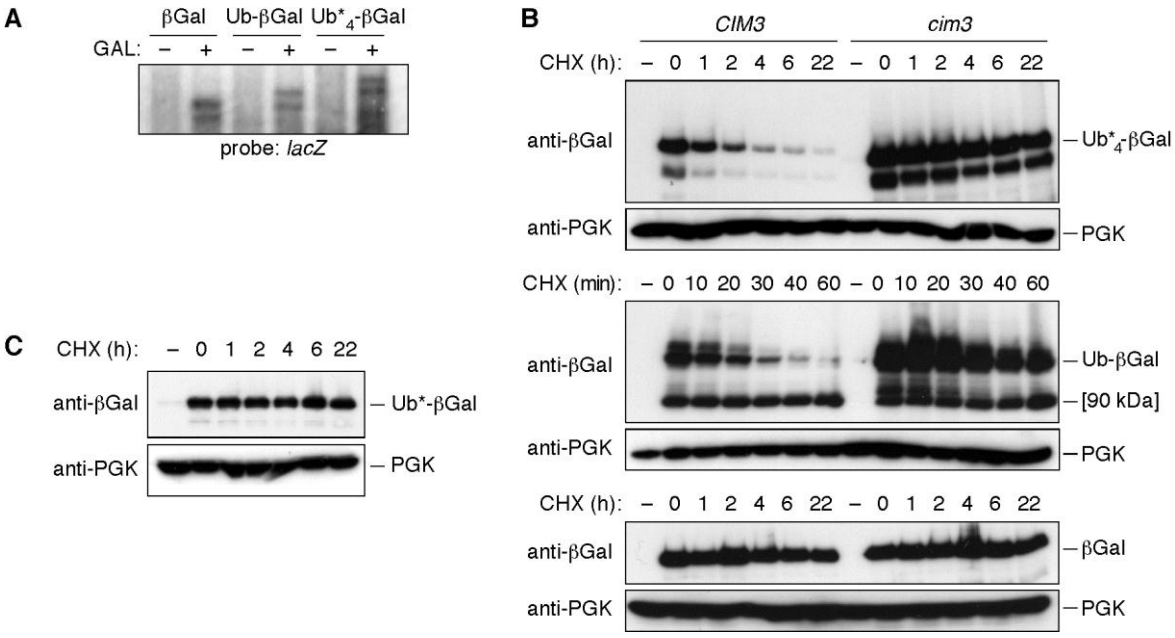

Figure 3.15 A linear non-cleavable tetraubiquitin chain acts as a general, but inefficient degradation signal
(A) Northern blot analysis indicates similar expression levels of all three βGal constructs upon induction with galactose (GAL). (B) Ub^{*}_{4}-βGal and Ub-βGal are degraded by the 26S proteasome with distinct kinetics. After growth in galactose medium for 2 h, a promoter shut-off (by shift to glucose) was combined with a cycloheximide chase (100 µg⁄mL) to inhibit de novo protein synthesis in the indicated strains, and samples were processed as in Figure 3.9. The βGal construct served as a stable control protein. Lanes labelled "-" represent samples from cultures grown in glucose medium. Note that degradation of Ub-βGal produces a stable fragment of ca. 90 kDa (Bachmair et al., 1986). (C) A promoter shut-off/cycloheximide chase, performed as described in (B), demonstrates complete stability of Ub^{*}-βGal in WT cells over the course of the experiment. Mutation of K29, K48, and K63 of the UFD substrate Ub-βGal is sufficient to completely stabilise the fusion protein.

Then I checked fusion protein stability by an experiment combining promoter shut–off and cycloheximide chasing. After 2 hours of protein expression in galactose medium, cells were shifted back to glucose medium in the presence of cycloheximide to terminate protein synthesis. The result showed Ub^{*}_{4}-βGal was indeed degraded suggesting linear ubiquitin chains can also target βGal for degradation (Figure 3.15B). This degradation was mediated by the proteasome as well because the fusion protein was completely stabilised in a proteasomal mutant *cim3,* which has defects in the 19S regulatory particle of the proteasome. Moreover, I noticed a remarkable difference in the turnover rate of Ub^{*}_{4}-βGal and Ub-βGal. Ub^{*}_{4}-βGal was degraded within a few

hours whereas Ub-βGal was degraded within minutes (Figure 3.15B). The observed kinetics were consistent with the degradation rate of Ub^{*}_{4}-PCNA*. As control, βGal remained stable during the course of the entire experiment (Figure 3.15B). In addition to that, I mutated K29/K48/K63 on the Ub-βGal construct and named the new construct Ub^{*}-βGal. This fusion construct was also stable during the entire experiment (Figure 3.15C). Overall, these data show that a linear non-cleavable tetraubiquitin chain serves as a general, but relatively inefficient proteasomal degradation signal.

3.6 Substrates Marked by Linear Polyubiquitin Chains Are Targeted to the Proteasome by Components of the UFD Pathway

As my results demonstrated that a linear non-cleavable ubiquitin chain could target substrates for degradation, it is very interesting to know the downstream factors that mediate this process. Based on the fact that my Ub^{*}_{4}-βGal construct is very similar to the polyubiquitylated UFD pathway substrates, I hypothesised the degradation of Ub^{*}_{4}-βGal would require some factors of the UFD pathway. Taking advantage of yeast genetics, I have used different deletion mutants or temperature sensitive mutants to analyse the importance of UFD pathway factors in Ub^{*}_{4}-βGal degradation. UFD pathway factors can be classified into two groups: factors involved in ubiquitylation and factors involved in substrate binding and sorting. Ufd4 and Ufd2 belong to the first category and the Cdc48-Ufd1-Npl4 complex, Rad23 and Dsk2 belong to the second category. Based on my results that the linear ubiquitin chain targets substrates for proteasomal degradation, I speculated that the ubiquitylation factors may not be essential in this case but factors from the second class would be much more important for the degradation process.

To test this hypothesis, I performed protein stability assays similar to the one described in Figure 3.14B. In *ufd4* cells, the fusion protein was degraded with no difference in the

turnover kinetics compared with that in WT cells (Figure 3.16A). This result indicates that the UFD pathway specific E3 enzyme Ufd4 is dispensable for fusion protein degradation and it is consistent with the observation that there are no high-molecular weight modified forms of fusion protein in either WT or proteasome mutants (Figure 3.15B). Since a linear ubiquitin chain is already pre-attached to the substrate, no additional ubiquitylation step might be required. This notion would predict that Ufd2, the E4 enzyme required to convert short K29-linked chains on UFD substrates to longer K48-linked chains, would not be required for the degradation of Ub^{*}_{4}-βGal. Interestingly, I found the fusion protein was stabilized in *ufd2Δ* cells (Figure 3.16B). This result suggests Ufd2 is required for the degradation of linear chain marked substrates, which does not fit with my prediction. Richly and co-workers have demonstrated that Ufd2 can bridge the association between the Cdc48-Npl4-Ufd1 complex and Rad23/Dsk2 ubiquitin adaptors (Richly et al., 2005). So, the requirement of Ufd2 shown by this experiment could be a result of either its E4 enzymatic activity or its function as an interaction mediator, even a combination of both. It was therefore important to analyse different functions of Ufd2 separately. From two-hybrid based truncation analysis, the N-terminal region (amino acids 1-380) of Ufd2 is required for Rad23 interaction and the central part of the protein up to amino acid 856 is responsible for Cdc48 binding. Finally the U-box domain sits at the C-terminus of the protein with E4 enzymatic activity (Richly et al., 2005). Moreover, a structural based study later defined the C-terminal region (amino acids 884-947) as a U-box domain and the N-terminal region (amino acids 1-879) as a core domain (Figure 3.17). Amino acids Arg844 and Glu855 were further predicted to be the conserved residues important for Cdc48 binding (Tu et al., 2007).

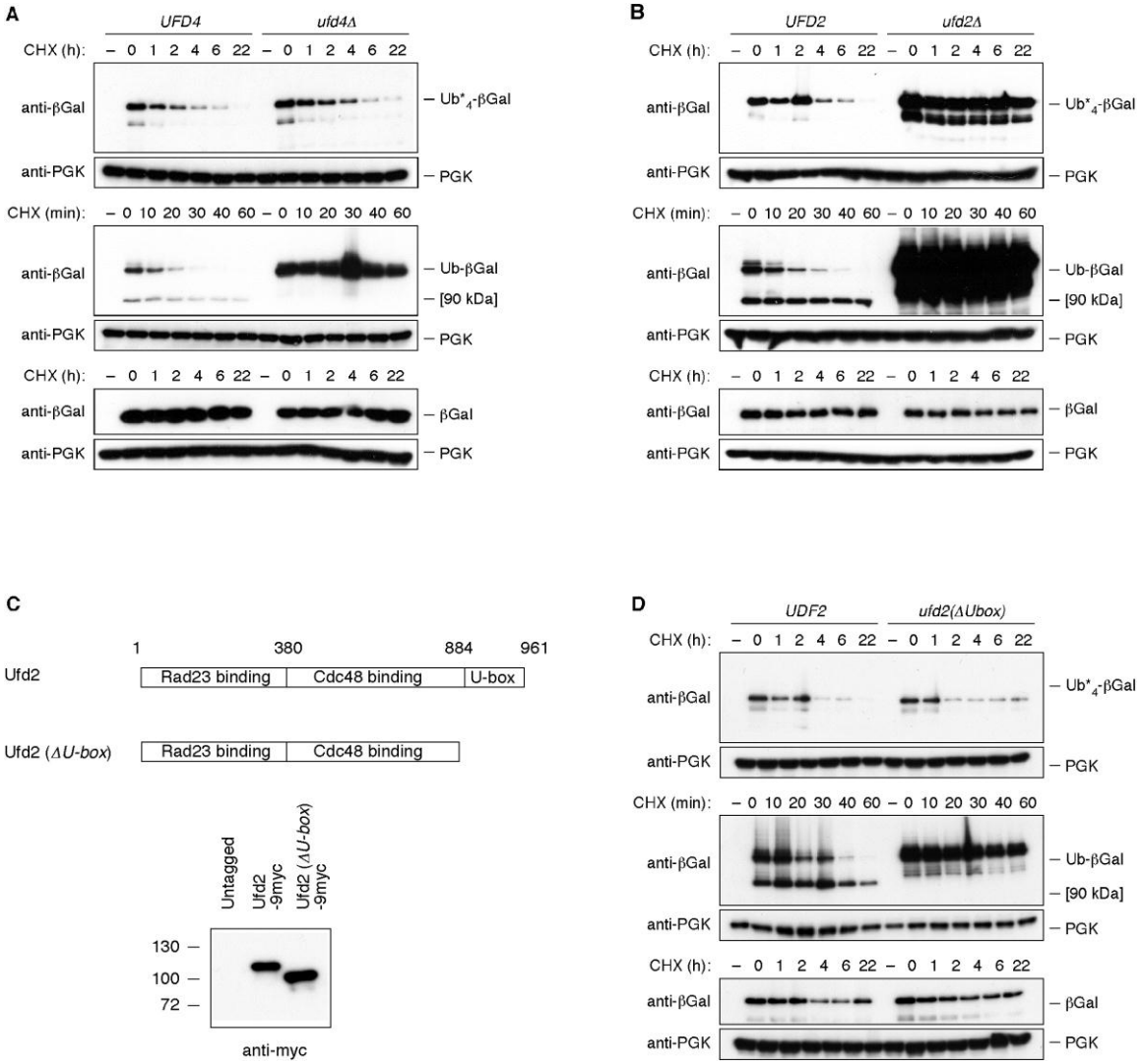

Figure 3.16 The ubiquitylation step of the UFD pathway is not required for the degradation of linear ubiquitin fusion proteins

(A), (B) and (D) Promoter shut-off/cycloheximide chase experiments were carried out with Ub^{*}_{4}-βGal, Ub-βGal, and βGal in the indicated UFD pathway mutants and their respective isogenic WT strains as described in Figure 3.15. (C) A schematic view of Ufd2 protein and the interaction information of each part/domain. The *ufd2 (ΔUbox)* carries a truncation of the *UFD2* open reading frame after amino acid 883. Protein levels of full-length Ufd2 and *Ufd2* (*ΔUbox*) are compared by Western blots with an anti-myc antibody.

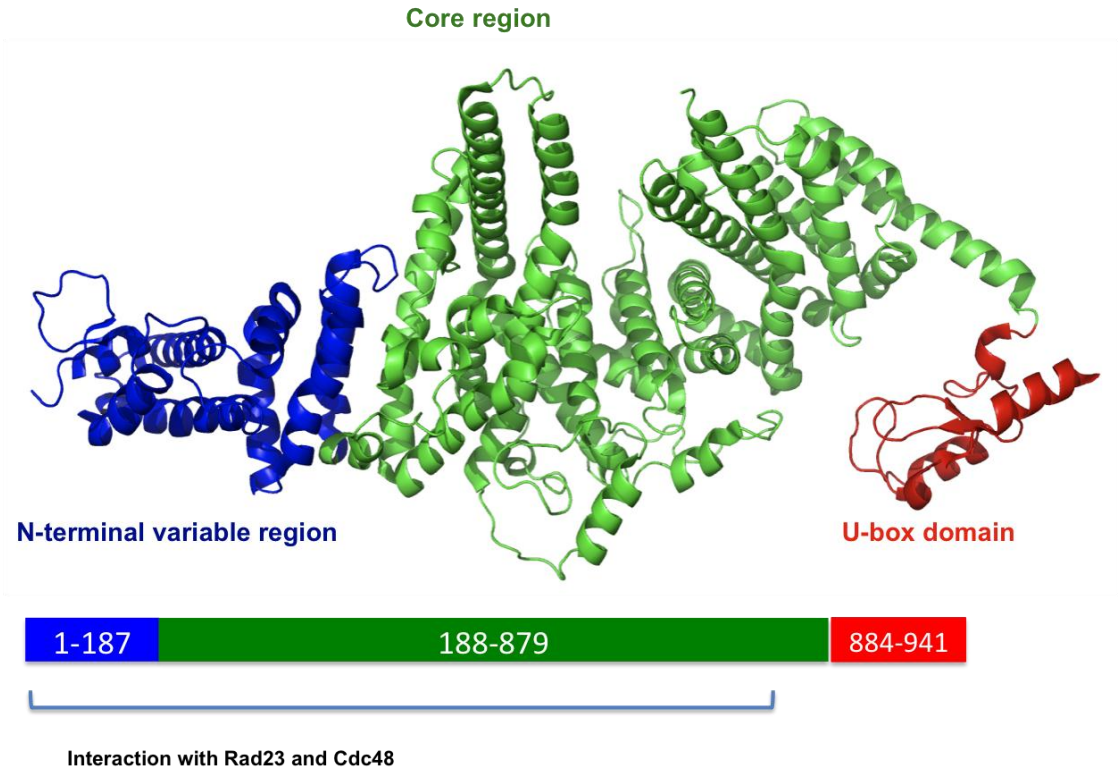

Figure 3.17 The crystal structure of Ufd2
Structure of Ufd2 (1-947), PDB code: 2QIZ. The N-terminal variable region (1-187) is coloured blue; the core region (188-879) is coloured green. The region (1-879) is important for Rad23 and Cdc48 interaction. The C-terminal U-box domain (884-947), coloured red, interacts with E2 Ubc4 and has ligase activity. This figure was generated by PyMol.

Based on these observations, I decided to make a C-terminal truncation form of Ufd2. An initial attempt of using 9myc tag to replace the C-terminal region (amino acids 856-961) has generated a truncation construct similar to the one previously described in two-hybrid analysis (Richly et al., 2005). However, this construct did not stabilise the fusion protein. Considering the key residues predicted for Cdc48 interaction Arg844 and Glu855 were adjacent to the site of truncation in my first construct and a C-terminal 9myc tag might directly interfere with Cdc48 binding in the cell, I decided to make another truncation mutant based on the structure of Ufd2, in order to delete the U-box domain while minimising the negative effect from the C-terminal tag. *Ufd2* (*ΔUbox*) mutant has the N-terminal region (amino acids 1-883), which has excluded the U-box domain completely and preserved the N-terminal core domain as much as possible to

maintain a stable Cdc48 association (Figure 3.16C). A strain expressing C-terminal 9myc-tagged full-length Ufd2 has also been created as a control. First of all, the expression levels of WT and mutant Ufd2 were compared on the western blot, and a similar amount of protein was observed suggesting the truncation did not destabilise Ufd2 (Figure 3.16C). Then I performed a protein stability assay again in this *Ufd2* (*ΔUbox*) mutant, the degradation was restored this time (Figure 3.16D). My results indicate the requirement for Ufd2 in this case is not due to its E4 enzymatic activity, but rather to its function of mediating protein-protein interactions.

The ubiquitylated UFD substrate needs to be recognised and transported to the proteasome for degradation. The Cdc48-Ufd1-Npl4 complex and Rad23/Dsk2 ubiquitin adaptor proteins play crucial roles in this process. I have also tested those non-ubiquitylation components of the UFD pathway. Because a *cdc48* null mutant is inviable, a temperature-sensitive allele, *cdc48-2*, was used to study the role of Cdc48 in model substrate degradation. At restrictive temperature, the fusion protein accumulated in *cdc48-2* mutant cells suggesting Cdc48 is required for the degradation targeted by linear ubiquitin chains (Figure 3.18A). The fusion protein was also stabilised in *npl4-1* mutant cells, suggesting Npl4 is also required for this degradation (Figure 3.18B). Rad23 and Dsk2 contain ubiquitin-binding domains to interact with ubiquitylated substrates and have ubiquitin-like domains to interact with the proteasome. Their functions are largely overlapped for some substrates *in vivo* and it is necessary to delete both genes in order to see a complete stabilisation of some model substrates (Funakoshi et al., 2002, Elsasser et al., 2004, Verma et al., 2004). I then analysed the degradation of the fusion protein in a *rad23 dsk2* double mutant and found the fusion protein was stabilised (Figure 3.18C). Further approaches to dissect the effect of Rad23 and Dsk2 separately showed that neither of them alone afforded to stabilise the fusion protein suggesting functional redundancy towards this particular substrate (Figure 3.18D). To exclude any βGal-specific effect in my study, I also performed a similar experiment with another model substrate Ub^{*}_{4}-PCNA*. Indeed, its degradation also depended on the UFD pathway component Npl4 (Figure 3.19).

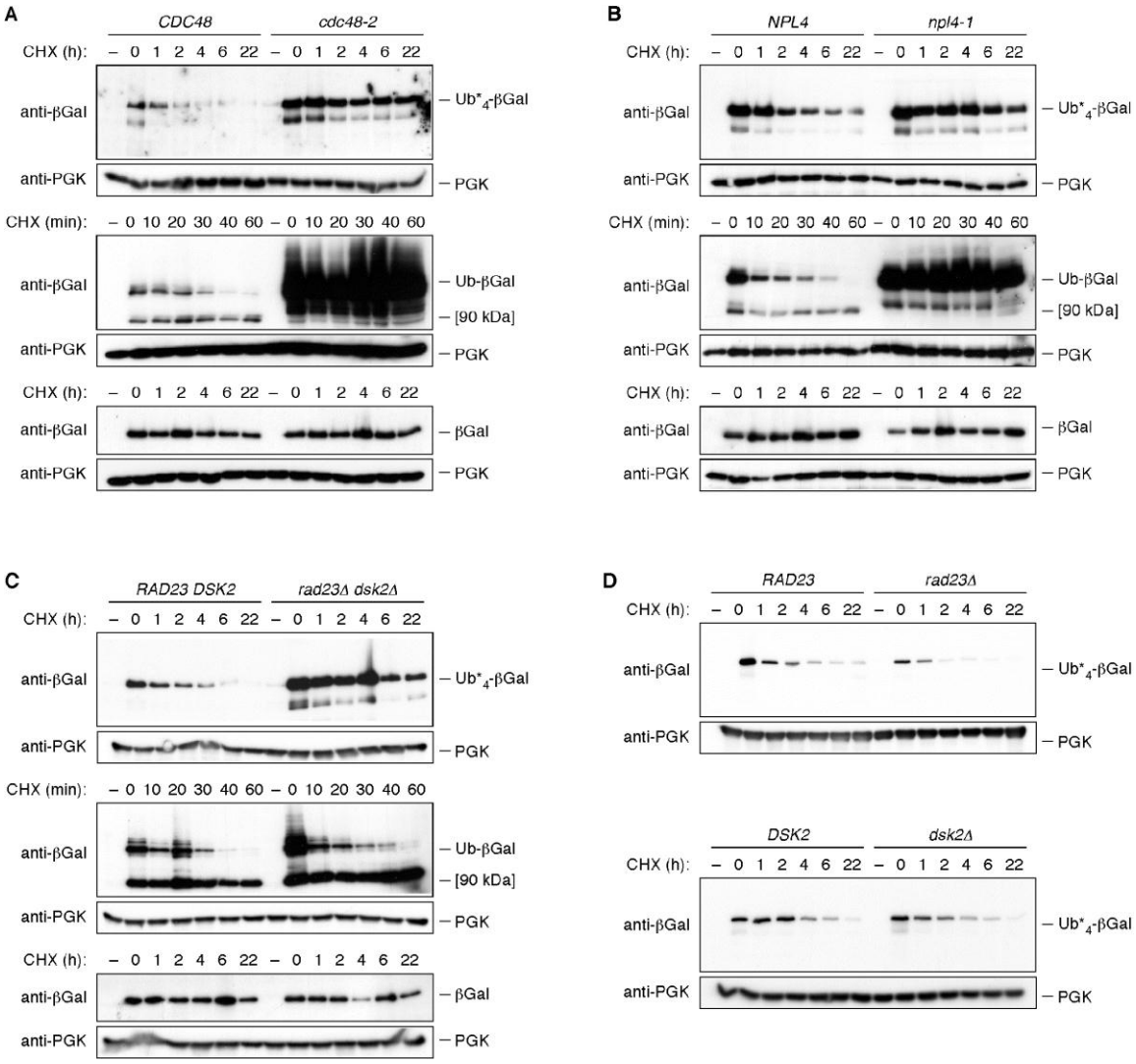

Figure 3.18 Degradation of linear ubiquitin fusion proteins depends on some components of the UFD pathway

(A)-(D) Promoter shut-off/cycloheximide chase experiments were carried out with Ub^*_4-βGal, Ub-βGal, and βGal in the indicated UFD pathway mutants and their respective isogenic WT strains as described in Figure 3.15. Experiments involving temperature-sensitive mutants were performed as follows: cells were pre-grown at permissive temperature (25 ℃) and shifted to galactose medium at 30 ℃ to induce protein production and inactivation of the respective factor. Subsequent steps of expression shut-off/cycloheximide chase were performed at 30 ℃ as well.

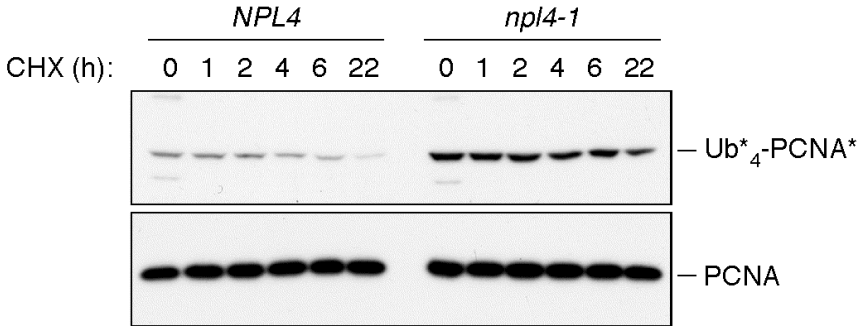

Figure 3.19 Ub*$_4$-PCNA* is targeted to the proteasome by the same mechanism as UFD pathway substrates
A cycloheximide chase experiment, performed as in Figure 3.9, shows stabilisation of the fusion protein in an *npl4-1* mutant.

In summary, it appears Ub*$_4$-βGal and UFD substrates share a common pathway for the targeting process to the proteasome with the noticeable exception of the initial stage of polyubiquitin chain assembly. UFD substrates require ubiquitylation factors Ufd4 and Ufd2 to assemble K48-linked polyubiquitin chains with sufficient length for proteasome recognition. Whereas linear ubiquitin chains fused with βGal do not require further modifications and therefore the enzymatic activity of Ufd4 and Ufd2 appear to be dispensable in this case. Similar to the UFD substrates, subsequent substrate recognition and proteasome targeting requires the Cdc48-Ufd1-Npl4 complex and Rad23/Dsk2 ubiquitin adaptor proteins.

3.7 Linear Ubiquitin Chain Length Is Not a Limiting Factor for Degradation

The relatively slow degradation of the fusion protein still needs an explanation. It is not substrate specific as similar degradation rates were observed from both PCNA and βGal based model substrates. Therefore, I hypothesised an inefficient recognition of linear tetraubiquitin chains by the proteasome may be responsible for this. Considering a K48-linked ubiquitin chain with four ubiquitin units was reported to be the minimal signal for efficient proteasome recognition (Thrower et al., 2000), I asked if an increase in the length of a linear ubiquitin chain would help to compensate the poor recognition and therefore accelerate the degradation.

For this purpose, I increased the length of the linear chain attached to the N-terminus of βGal from 4 to 8 ubiquitin units by simply duplicating the tetraubiquitin module. The resulting construct was named Ub^*_8-βGal as shown in Figure 3.20A. Similar promoter shut-off/cycloheximide chase experiments were performed to compare the kinetics of degradation between Ub^*_4-βGal and Ub^*_8-βGal. Unexpectedly, there was no clear difference in the degradation of both constructs, indicating that the chain length is not the rate-limiting factor in this particular case (Figure 3.20B).

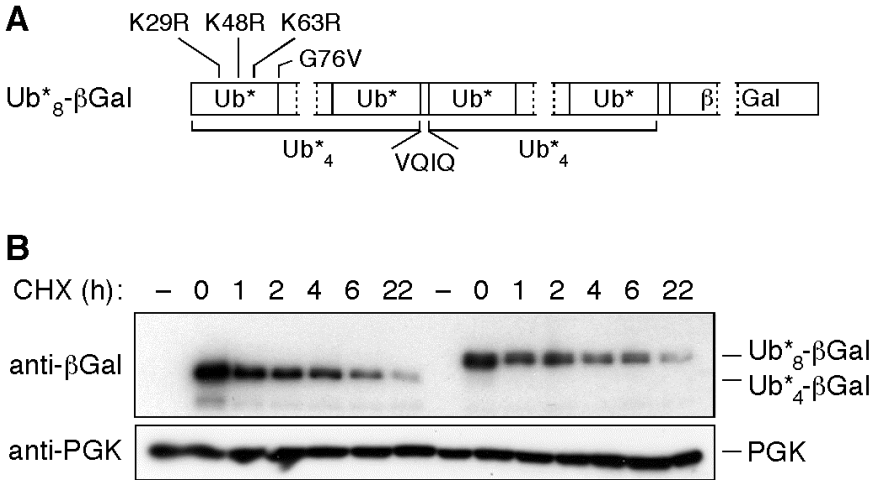

Figure 3.20 Ubiquitin chain length is not a rate-limiting factor in the degradation of linear ubiquitin fusions
(A) Schematic view of a Ub^*_8-βGal construct. Note that each of the Ub^*_4 modules used to create the octaubiquitin chain is identical to that used in Ub^*_4-βGal. (B) Ub^*_8-βGal is degraded at a rate comparable to that of Ub^*_4-βGal. Promoter shut-off / cycloheximide chase experiments were performed with the two constructs in a WT strain as described in Figure 3.15.

3.8 Discussion

The high structural similarity between linear and K63-linked polyubiquitin chains has challenged our understanding if cellular machinery can differentiate highly similar forms of ubiquitin signals. The outcomes of the modifications by these two types of polyubiquitin chains also vary when they are conjugated to different substrates based on a series of *in vivo* and *in vitro* studies. This work has addressed several important questions. First of all, I addressed the significance of chain linkage in the system of DNA damage tolerance, mediated by K63-linked polyubiquitylation of PCNA. My results showed that the DNA damage bypass pathway is able to differentiate between linear polyubiquitin chains and K63-linked polyubiquitin chains. Secondly, I asked if K63-linked ubiquitin chains act as degradation signals on PCNA. My results suggest it does not target PCNA for proteasomal degradation. Thirdly, I found that a linear non-cleavable ubiquitin chain is sufficient to target PCNA and another model substrate, β-galactosidase, for proteasomal degradation with a relative slow turnover rate. Substrates marked with linear ubiquitin chains bind to the Cdc48-Ufd1-Npl4 complex and subsequently get transferred to the proteasome via ubiquitin adaptor proteins Rad23 and Dsk2 (Figure 3.21). While answering these questions, my observations have also raised some more interesting questions.

3.8.1 Why Do Linear Chains Not Function in Damage Bypass

Structural studies have shown that a linear ubiquitin chain with a head-to-tail arrangement for each ubiquitin moiety adopts an extended conformation almost identical to that of a K63-linked chain, but quite different from the "closed" conformation of a K48-linked chain (Figure 1.3). Many ubiquitin-binding domains that differentiate between K48- and K63- linkages make no distinction between linear and K63-linked chains (Komander et al., 2009b). However, in my system linear ubiquitin chain fused to the N-terminus of PCNA does not support error-free DNA damage tolerance whereas a K63-linked chain on the same position does activate this pathway.

There are several possibilities for this observed difference in the damage tolerance pathway.

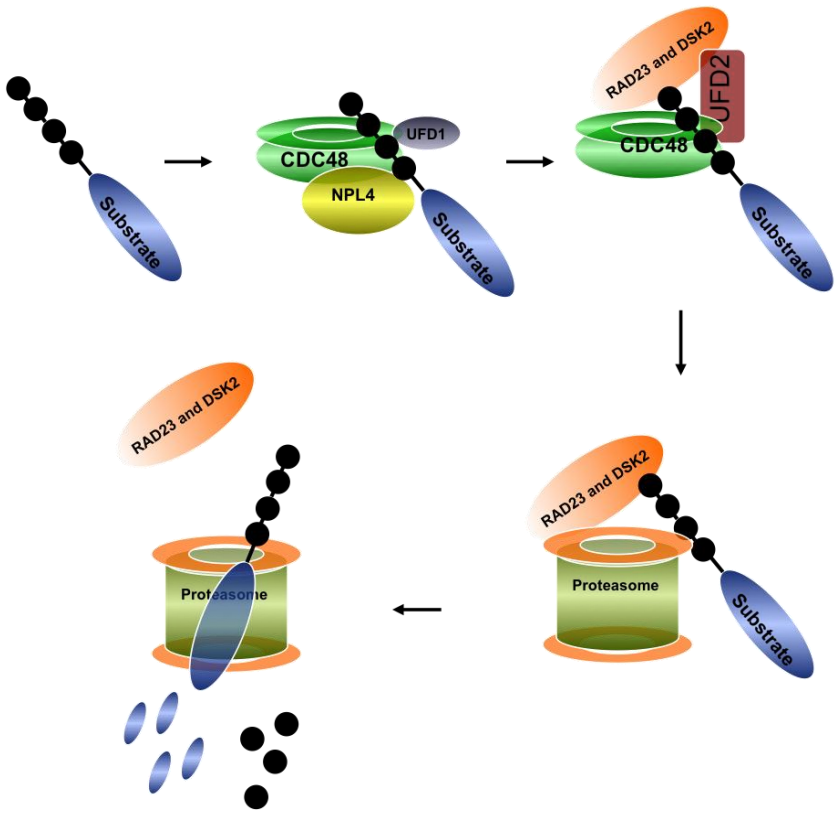

Figure 3.21 Model for the degradation of linear ubiquitin chain marked substrates
A model substrate (blue) marked with a linear ubiquitin chain (chain made of black filled circle) is recognised by the Cdc48-Ufd1-Npl4 complex (green, grey and yellow oval shapes) and the Cdc48-bound Ufd2 (brown rectangle) further recruits ubiquitin adaptor proteins Rad23/Dsk2 (orange oval). Finally, the substrates are taken to the proteasome and eventually broken down.

First of all, it is formally possible that the instability of the fusion protein prevents efficient error-free DNA damage bypass. I consider this unlikely because Ub^{*}_{4}(L)-$PCNA^{*}$ is active in TLS, but Ub^{*}_{4}-$PCNA^{*}$ or $PCNA^{*}$-Ub^{*}_{4} with protein levels similar to Ub^{*}_{4}(L)-$PCNA^{*}$ function poorly even in TLS. This observation suggests that the amount of fusion protein does not limit TLS function. Moreover, physiologically K63-polyubiquitylated PCNA only counts as a tiny portion of total PCNA and is able to activate the error-free pathway effectively. In addition to that, if protein instability was indeed responsible for the poor performance of the fusion constructs in activating error-

free damage bypass, I would expect to see a rescue effect beyond TLS from Ub^{*}_{4}-$PCNA^{*}$ in a proteasome mutant strain. In fact, an experiment analysing damage sensitivity of *rad18 pre1-1* strains expressing different fusion constructs was attempted and my preliminary observation did not find evidence for such increased rescue effect beyond TLS.

Secondly, I cannot exclude that the non-cleavable nature of the linear ubiquitin chain may interfere with its correct function in the error-free pathway. This is particularly important if the deubiquitylation step positively contributes to error-free damage bypass, although removal of the first ubiquitin is not required for activating TLS (Parker et al., 2007). In this case, a cleavable chain would not be helpful either, because it would be disassembled quickly and fusion proteins would be processed back to monoubiquitylated state or even unmodified state. One potential solution for this would be to create a linear ubiquitin chain that is partially accessible by DUBs. The substrate recognition of DUBs is partially mediated by the RLRGG motif at the C-terminal end of ubiquitin. Crystal structures of DUBs have revealed that G76 occupies a restricted tunnel in the centre of the active site; only glycine can fit into that position. However, at positions G75, R74 and L73, several other amino acids could substitute them and preserve partial activity of DUBs (Drag et al., 2008). An intermediate-level construct, which can only be processed by DUBs with reduced efficiency, would exhibit a rescue effect beyond that of the non-cleavable version if deubiquitylation were required for error-free damage bypass.

Finally, a K63-specific downstream ubiquitin-binding protein, which mediates error-free damage bypass, might not recognise the linear ubiquitin chain. Although a pull-down experiment with the UBAN domain showed a positive interaction (Figure 3.11), the mutations on ubiquitin moiety may interfere with efficient binding with a PCNA-specific ubiquitin receptor. Moreover, some ubiquitin-binding domains interact with K63-linked chains preferentially, such as the C-terminal NZF domain of TAB2. In this case, the NZF domain can bind to ubiquitin moieties in K63-linked chains in a two-side

manner due to the flexible joint of K63-linkage, whereas a linear chain could not satisfy this requirement (Kulathu et al., 2009). Such a domain may also exist for the damage tolerance pathway. At present, it is difficult to address this question since such downstream factors are still waiting to be identified.

3.8.2 Why Is K63-polyubiquitylated PCNA Not Degraded

Genetic data linking DNA damage bypass to proteasome activity have been indirect and rather controversial. A study from Hofmann and Pickart (Hofmann and Pickart, 2001) has analysed UV sensitivities of strains with *pre1-1 pre2-2 rev3* and *ubc13 rev3*. Based on their prediction, the former strain would show similar UV sensitivity to the latter one if the primary role of K63-linked chain on PCNA were to trigger degradation. The results showed *pre1-1 pre2-2 rev3* was 10-fold less UV-sensitive than the *ubc13 rev3* double mutant and there was no synergism between *pre1-1 pre2-2* and *rev3* mutants, suggesting a non-degradative function for K63-linked polyubiquitin chains. Others have proposed a role of the proteasome in limiting the mutagenic activity of TLS. This idea was supported by the fact that a proteasome mutant was epistatic with the TLS genes *RAD30* and *REV3*, and the spontaneous mutations in proteasome mutants were connected to the TLS activity (Podlaska et al., 2003, McIntyre et al., 2006).

I have for the first time directly assessed the response of PCNA polyubiquitylation to alterations in proteasome activity and I found no evidence for a degradation role for the K63-linked polyubiquitin chain on PCNA. Instead, my observation reflects the global behaviour of K63-linked ubiquitin chains, which is not a degradation signal. This is consistent with a published mass spectrometry study where the authors have analysed the abundance of ubiquitin chains with different linkage in response to proteasome inhibition. In that case K63-linked chains did not accumulate (Xu et al., 2009). Meanwhile, the accumulation of K48-linked and other alternatively linked ubiquitin chains and the resulting depletion of free ubiquitin (Xu et al., 2004) may in fact explain my observation that the level of K63-polyubquitylated PCNA drops in proteasome

mutants and in cells after a treatment of proteasome inhibitor MG132. To my knowledge, the recent report that K63-linked polyubiquitylation of transcription factor Mga2 by E3 enzyme Rsp5 leads to proteasome-dependent degradation remains to be the only isolated case of proteolysis mediated by K63-linked chains *in vivo* (Saeki et al., 2009). Even in that study, the contribution of K48-linked chains and chain editing by an Rsp5-associated deubiquitylation activity were not excluded.

In vitro, the proteasome is less selective towards its preferred K48-linked chains. It binds K63-linked chains with an affinity not much different from that of the K48-linked chains despite the significant conformational difference (Tenno et al., 2004, Varadan et al., 2004, Hofmann and Pickart, 2001). If linked to a model substrate, K63-linked chains indeed target protein degradation *in vitro* (Hofmann and Pickart, 2001). Moreover, even short, heterogeneous and multiply monoubiquitylated substrates are degraded *in vitro* (Kirkpatrick et al., 2006). Therefore, proteasomal recognition is not the reason for inefficient degradation of K63-linked chain modified substrate. Upstream ubiquitin adaptor proteins such as Rad23 and Dsk2 also showed no linkage preference based on affinity studies (Raasi et al., 2005). Hence, the most straightforward explanation for the inefficiency of K63-linked chain as a degradation signal *in vivo* is a limited chain length. The minimal length for K48-linked ubiquitin chains to be efficiently recognised by the proteasome is four ubiquitin moieties (Thrower et al., 2000). In fact *in vivo* polyubiquitylated PCNA exceeding the tetraubiquitylated state was very difficult to detect, and even the latter is less abundant than the mono- or di-ubiquitylated forms (Windecker and Ulrich, 2008). This stands in contrast with *in vitro* observations, in which long K63-linked chains could be assembled on PCNA by purified enzymes (Unk et al., 2008, Unk et al., 2006, Parker and Ulrich, 2009). It remains unclear how chain length is maintained *in vivo*, but the use of deubiquitylation enzymes such as mammalian Usp1 (Huang et al., 2006) may be an effective strategy. A recent study reported that proteasome-bound K63-linked polyubiquitin chains were rapidly deubiquitylated without efficient degradation of their substrate whereas the deubiquitylation of K48-linked chains was a lot slower (Jacobson et al., 2009). This

report provided evidences for another layer of regulation to limit the length of K63-linked chains from a proteasome perspective.

3.8.3 Linear Ubiquitin Chains as Degradation Signals

There has been some early evidence indirectly suggesting the possibility that linear ubiquitin chains could function as a degradation signal. *In vitro*, the proteasome is not particularly selective for certain linkages as discussed above. It processes K48-linked, K63-linked and other heterogeneous as well as multiple monoubiquitylated conjugates as substrates. It is therefore not surprising that linear ubiquitin chains can competitively inhibit degradation of K48-polyubiquitylated substrates (Thrower et al., 2000). There has been *in vitro* evidence showing that a linear non-cleavable ubiquitin chain fused to a model protein bearing a suitable unstructured N-terminal domain can trigger the degradation of its fusion partner *in cis* and a tightly associated protein *in trans* (Prakash et al., 2008). However, little is known about the suitability of linear chains as degradation signals *in vivo*. Non-cleavable tandem arrays of 2-8 ubiquitin units were shown to confer half-lives of less than 10 min to their fusion partner in reticulocyte lysates and cell culture (Stack et al., 2000, Prakash et al., 2008). When over-expressed in yeast, they effectively block the degradation of short-lived proteins. But extensive further ubiquitylation was observed in these cases, suggesting that the arrays of ubiquitin mainly function as efficient ubiquitin acceptors.

Since linear polyubiquitin chains are co-translationally processed into ubiquitin monomers (Turner and Varshavsky, 2000), the function *in vivo* was not well studied. Recent identification of the E3 complex LUBAC that catalyses the assembly of linear ubiquitin chain *in vivo* has recalled our attention to this type of chain and its biological function (Kirisako et al., 2006). Now I have shown that a linear tetraubiquitin chain, which cannot be further modified due to mutations on its major acceptor lysine residues, is able to target model substrates for degradation *in vivo*. In my linear ubiquitin chain constructs, there are still four lysine residues (K6, K11, K27 and K33) available for

further modification. But if any of these might have significant contributions to the degradation of fusion protein *in vivo*, it would have the same effect on all fusion constructs including the shorter ones. In fact, instability was only observed for those bearing at least four ubiquitin moieties and even within those a variable half-life were observed (Figure 3.8A, 3.9). Furthermore, there is evidence from previous reports showing chain extension of UFD substrates are via K29- or K48- linkage (Saeki et al., 2004b, Koegl et al., 1999, Johnson et al., 1995). Therefore, I consider further ubiquitylation on my constructs to be unlikely and linear non-cleavable ubiquitin chains to be sufficient for targeting degradation *in vivo*.

Overexpression of LUBAC promotes the degradation of ubiquitin-GFP fusion protein via the proteasome in mammalian cell culture (Kirisako et al., 2006). At the same time, LUBAC assembles linear ubiquitin chains at K285 and/or K309 of NEMO, but it does not promote degradation, suggesting that the position of the chain attached to the substrate may affect its ability to function as a degradation signal (Tokunaga et al., 2009). Similarly, in my system, linear ubiquitin chains attached to N- or C-terminus of PCNA revealed quite different degradation efficiency and Ub^{*}_{4}-βGal degradation was quite inefficient compared with its analogue UFD substrates. These observations initially suggested that poor recognition by the proteasome for a short linear ubiquitin chain might be responsible for the slow turnover rate. However, increasing the length of linear ubiquitin chains from 4 units to 8 units did not accelerate the degradation and a similar degradation pattern was also observed in my *in vitro* experiment, suggesting proteasome targeting is not the rate-limiting step in this case. This is supported by the fact that linear ubiquitin chains are associated with the proteasome *in vivo* although they are somehow less effective in competing for proteasome binding than K48-linked chains *in vitro* (Thrower et al., 2000, Saeki et al., 2004a). Taken together, these data rather suggest that proteasome processing will most likely be the reason for the observed slow turnover rate. This scenario is supported by the notion that proteasome-associated isopeptidase Rpn11 positively contributes to proteolysis, presumably by removing polyubiquitin chains from substrates as they enter the catalytic core particle of the proteasome (Yao and Cohen, 2002, Verma et al., 2002). In my system, the non-

cleavable nature of the linear chain has prevented chain disassembly such that the substrate protein was forced to be unfolded and degraded along with the long tetraubiquitin chain. Considering the tightly folded structure of ubiquitin, this may delay proteolysis especially since protein unfolding has been shown to affect degradation rate *in vitro* (Johnston et al., 1995, Thrower et al., 2000). Alternatively, some proteasome-associated ubiquitin binding factors such as Rpn10 and Rpn13 may persistently bind to the linear ubiquitin chain due to deficiency in chain disassembly. This prolonged association with the proteasome regulatory particle may eventually delay the entry of the substrate moiety into the catalytic core. In either case, variations in the linear ubiquitin chain attachment site on the substrate may change the way in which substrate is presented to the proteasome, therefore affecting the degradation rate.

Finally, linear ubiquitin chains have so far only been found in higher eukaryotes. Although a recent mass spectrometry study performed in yeast did not identify linear ubiquitin chains (Xu et al., 2009), the absence of evidence should never be interpreted as evidence of absence as pointed out by Kirkpatrick and colleagues (Kirkpatrick et al., 2005), because mass spectrometry is somewhat biased towards abundant species and the level of linear ubiquitin chains in yeast might be quite low. Nevertheless, in higher eukaryotes, if linear ubiquitin chains acting as degradation signals on any physiological substrates remain an open question. Proteasomal degradation might be a default pathway, however, in some cases, the suitable effector proteins would recognise the linear ubiquitin chains and then direct the substrate to non-degradative functions. In yeast, such effector proteins may not exist therefore exposing linear chains to the proteasomal degradation factors.

Chapter 4. Results II: Identification and Characterisation of Kinetochore Component SPC25 as a Novel Ubiquitin-binding Factor

4.1 Introduction

4.1.1 Background

Ubiquitylation is among the most well-conserved and widely used posttranslational modification mechanisms to regulate various cellular events. Its functional versatility is reflected by its appearance as different forms of ubiquitin signals such as monoubiquitin and various polyubiquitin chains with homotypic linkages as well as mixed linkages (Ikeda and Dikic, 2008). The outcomes of these types of modification are mediated by UBDs (ubiquitin-binding domains), which are able to recognise different ubiquitin signals specifically. There are more than 20 different types of known UBDs present in over 150 cellular proteins involved in many important cellular processes. For instance, in the proteasome-mediated degradation pathway, among ubiquitin receptor proteins the UBA domain of Rad23, Dsk2 and Ddi1, the UIM domain of Rpn10, and the PH domain of Rpn13 are all involved in recognising ubiquitylated substrates for proteasomal degradation (Dikic et al., 2009). Other examples have given extensive evidences for the contribution of UBDs to the regulation of apoptosis (Broemer and Meier, 2009), the DNA damage response (Hofmann, 2009), the endocytosis pathway (Williams and Urbe, 2007) and the immune response (Skaug et al., 2009). Considering the number of ubiquitylated proteins in the cells, these reported examples can only represent a small portion of functions that UBDs are actually involved in.

Our understanding of UBDs has been greatly expanded with the help of structural information, which nicely illustrates the way ubiquitin interacts with UBDs, and bioinformatic analysis, which in turn helps to identify potential candidate proteins

containing certain types of UBD. Based on the type of ubiquitin recognition structure they fold into, UBDs are classified into a few groups such as α-helical structures, zinc-fingers (ZnFs), ubiquitin-conjugating enzyme-like (UBC) domains and pleckstrin homology (PH) folds (Dikic et al., 2009). The α-helical structure is the most common type of UBD and it binds to a hydrophobic patch on the β-sheet of ubiquitin centred around I44. Members of this group include UIM, UBA, GAT or CUE domains. A few examples of different UBDs have been identified for other types of ubiquitin-binding structures respectively. Although most UBDs found so far recognise a common hydrophobic patch on ubiquitin centred around L8-I44-V70, in some cases, ubiquitin binding independent of this hydrophobic patch was reported such as for the UBM domain found in Rev1, a subunit of Y-family translesion synthesis polymerase ζ (Bienko et al., 2005). Biophysical methods have been applied to study the binding affinity of UBDs to various forms of ubiquitin signals. These have revealed that most of them interact with monoubiquitin quite weakly, in the range of 10-500 μM (Ikeda and Dikic, 2008) with the best affinity observed so far (around 300 nM) for the PRU domain of Rpn13 (Husnjak et al., 2008).

Taking advantage of the information from structural studies of known UBDs, bioinformatic analysis has been applied to search for other candidate proteins that may have this type of domain or other domains with similar secondary structure (Hofmann, 2009). This method has accelerated the identification of new ubiquitin-binding proteins and the characterisation of their functions in various biological pathways. However, bioinformatics has its limitations, since there is no evidence that the binding affinity for ubiquitin can be predicted on the basis of a UBD's structure. In contrast, even the same type of UBD within different proteins can show a dramatic difference in binding affinity towards ubiquitin (Raasi et al., 2005). Similarly, ubiquitin recognition can occur through different surfaces and structural elements of UBDs even when the same structural domain is used to bind the I44-centred hydrophobic patch (Dikic et al., 2009). These evidences illustrate the difficulties of using bioinformatics as a sole approach to study UBDs and ubiquitin-binding proteins and further emphasise that conventional experimental approaches are still crucial.

During the course of my PhD research, I was interested in the recognition of ubiquitin signals, particularly UBDs in the context of maintaining genome stability. Although a lot of UBDs and ubiquitin-binding proteins have been identified in the past decades, given the ubiquitous role of ubiquitin signalling, there must be many unidentified ubiquitin-binding factors or even novel UBDs that play important roles in previously undescribed fields of cell biology. In this part of my thesis work, I have performed a two-hybrid screen aiming to identify factors, which may recognise and bind to polyubiquitylated PCNA, as well as other novel ubiquitin-binding factors. Ub^{*}_{n}-$PCNA^{*}$ fusion and tetraubiquitin chains were used as bait constructs. Despite the failure in identifying factors that specifically interact with Ub^{*}_{n}-$PCNA^{*}$ fusion, I found two very interesting ubiquitin-binding factors, Spc25 and Etp1. I have focused on characterising the ubiquitin-binding of Spc25 *in vitro* and *in vivo,* and I have found phenotypes associated with the *spc25* ubiquitin-binding deficient mutant.

4.1.2 The Kinetochore Complex

The majority of the work presented in the chapter is about Spc25, a kinetochore component. It was identified as a potential ubiquitin-binding protein in my two-hybrid screen. Therefore, I would like to give an overview on the budding yeast kinetochore complex.

4.1.2.1 The Architecture of the Budding Yeast Kinetochore

Kinetochore is a multiprotein complex assembled on the centromeric region of DNA to connect the plus ends of the spindle microtubules to the chromosomes. In addition to its function as a bridge, the kinetochore complex also acts as a signalling module that monitors its own stability and the status of microtubule attachment (Westermann et al., 2007). The budding yeast centromere is characterised as a point centromere, which has a defined sequence of around 125 bp and is sufficient for kinetochore formation (Santaguida and Musacchio, 2009). Every point centromere only binds one microtubule

(Winey et al., 1995). In contrast, fission yeast and vertebrates have regional centromeres, which extend over quite large DNA regions. The kinetochore complex assembled on regional centromere bind multiple microtubules (Allshire and Karpen, 2008).

Due to its relatively simple structure, the most advanced biochemical description of kinetochores has been achieved in budding yeast. The budding yeast kinetochore is composed of over 60 different proteins, in which over 40 proteins are organised into subcomplexes, the CBF3, Ndc80, Mtw1 (MIND), Ctf19 (COMA and 12 additional proteins), Spc105, Dam1 and Ipl1 complexes (McAinsh et al., 2003, Westermann et al., 2007)(Figure 4.1). Based on their relative position on the chromosome-microtubule axis, kinetochore proteins can be classified into three categories: inner kinetochore proteins, which directly interact with DNA and form platforms for the assembly of other kinetochore complexes; the microtubule-binding proteins, which associate with microtubules and the kinetochore; and the central kinetochore proteins, which link the inner kinetochore to the outer kinetochore-microtubule interface (Cheeseman et al., 2002). Based on proteomic analysis that describes tightly interacting kinetochore subcomplexes and depletion experiments that analyse the effect of depleting one particular kinetochore protein on the localisation of other kinetochore proteins, the architecture of the kinetochore complex has been elucidated (Figure 4.1). The CBF3 complex (Cep3, Ctf13, Ndc10 and Skp1) binds to the CDEIII element of the budding yeast point centromere, and its association with DNA is required for the recruitment of all other kinetochore proteins. The other primary determinant is Cse4 (CENP-A homologue), a histone H3 variant, that forms part of a specific centromeric nucleosome (Smith, 2002).

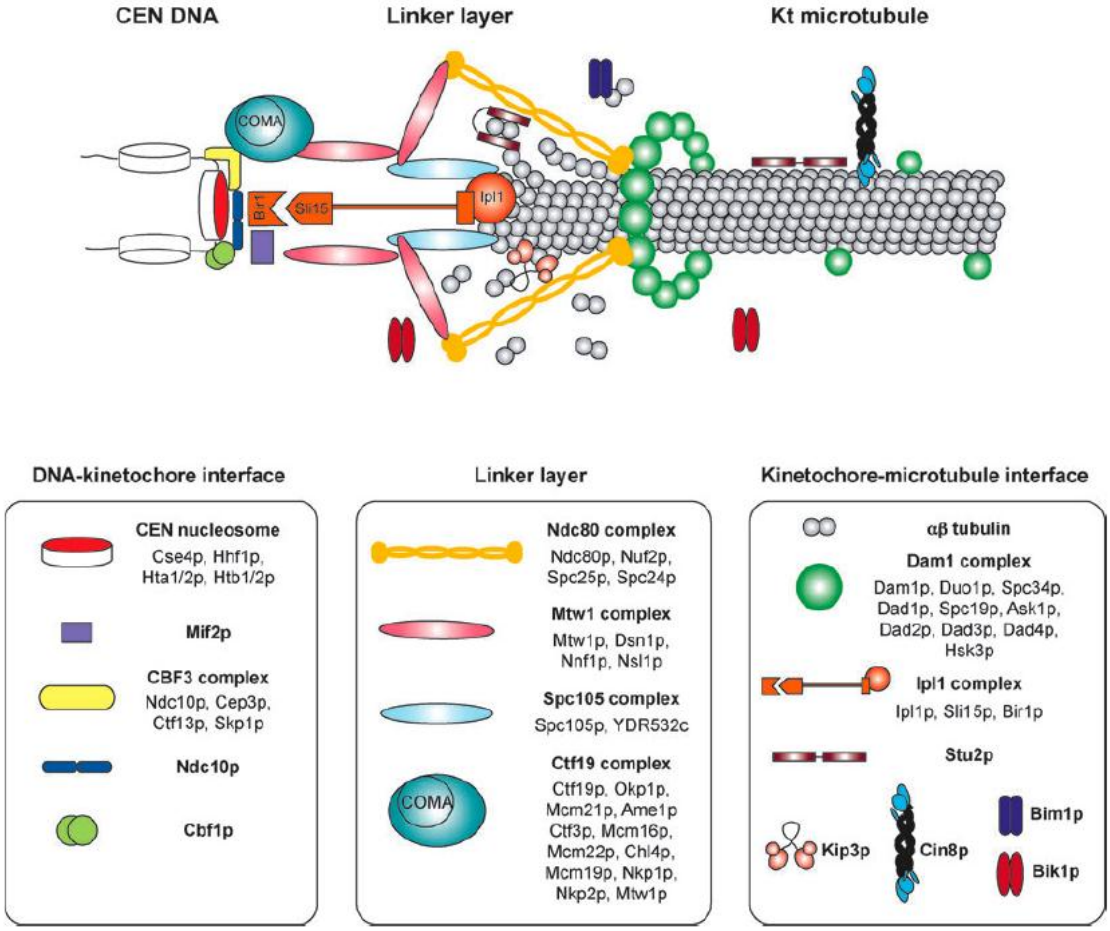

Figure 4.1 The budding yeast kinetochore
An overview of the budding yeast kinetochore. This picture illustrates the three groups of kinetochore proteins and their positions in the overall kinetochore architecture. This picture was taken from (Westermann et al., 2007).

Mif2 (CENP-C homolougue) was found to be associated with Cse4 nucleosomes and the MIND (Mtw1, Nsl1, Nnf1 and Dsn1) complex, suggesting that it functions as a linker between the inner kinetochore complex and the central kinetochore complex (Westermann et al., 2003). The central kinetochore proteins include the MIND complex, the Ndc80 complex (Ndc80, Nuf2, Spc25 and Spc24), the Spc105 complex (Spc105 and YDR532c), the COMA complex (Ctf19, Okp1, Mcm21 and Ame1) and the other members of the Ctf19 complex (Westermann et al., 2007). The function of central kinetochore proteins is to connect microtubule-binding proteins with inner kinetochore proteins. Furthermore, the Ndc80 complex and Spc105 have reported microtubule binding activity (Cheeseman et al., 2006, Wei et al., 2007). Therefore,

defects in central kinetochore proteins usually give common phenotypes such as chromosome missegregation. Recent advances in fluorescence microscopy have allowed the generation of a map of budding yeast kinetochore proteins and their relative positions on the DNA-microtubule axis (Joglekar et al., 2009). This study together with early localisation studies suggest the COMA complex is closely associated with the Cse4 containing nucleosome complex and the MIND complex sits between the Spc25/Spc24 end of the Ndc80 complex and the COMA complex. Spc105 closely associates with Dsn1 of the MIND complex and the Spc25/Spc24 subcomplex whereas the N-terminus of Ndc80 is the furthest away from the centromere (Figure 4.2).

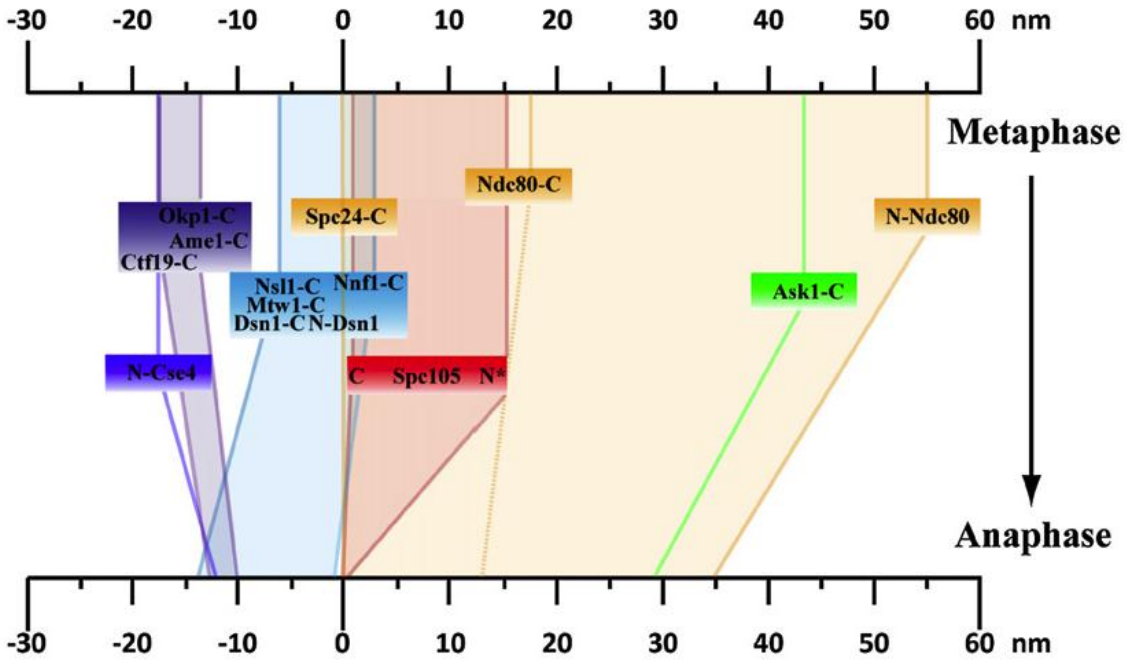

Figure 4.2 The relative locations of kinetochore proteins along the axis of kinetochore-microtubule
Two-colour *in vivo* fluorescence microscopy was applied to measure the relative positions between the C-terminus of the Spc24 and other kinetochore proteins in metaphase and anaphase. The relative positions of MIND complex, COMA complex, Cse4 nucleosome, Spc105 complex and the Dam1 complex were determined. This figure was taken from (Joglekar et al., 2009).

At the microtubule-binding interface, there are many microtubule-associated proteins such as Stu2, the Ipl1 complex (Ipl1, Sli15 and Bir1) and the Dam1 complex. Stu2 has functions in stabilising the attachment of the microtubule to the kinetochore and promoting microtubule depolymerisation (Tanaka et al., 2005, He et al., 2001). The Ipl1 (Aurora B homologue) in complex with Sli15 has important roles in the quality control of kinetochore microtubule attachment. The complex detects improperly attached kinetochores and detaches them to activate the spindle checkpoint (Pinsky et al., 2006). The Dam1 complex consists of ten different proteins identified by two-hybrid analysis and biochemical purification. The complex localises to the kinetochore and binds microtubules with proposed function as a force coupler, which translates mechanical energy into directed movement (Westermann et al., 2006)

4.1.2.2 The Ndc80 complex

Ndc80 was first identified by Kilmartin and coworkers through mass spectrometry analysis of highly enriched yeast spindle pole bodies (Wigge et al., 1998). It was later shown that Ndc80 forms a complex with Nuf2, Spc25 and Spc24 (Janke et al., 2001, Wigge and Kilmartin, 2001). This four-protein complex is essential for cell viability. Initial observation of temperature-sensitive *ndc80* alleles showed a complete detachment of chromosomes from mitotic spindles under non-permissive conditions (Wigge et al., 1998). Other temperature-sensitive alleles of *spc24* and *spc25* also exhibit defects in chromosome segregation (Janke et al., 2001, Wigge and Kilmartin, 2001). The Ndc80/Nuf2 subcomplex was later found to have direct microtubule-binding activity (Cheeseman et al., 2006, DeLuca et al., 2006, Wei et al., 2007). The interaction between Ndc80/Nuf2 and the microtubule can be greatly enhanced by addition of Spc105 (Knl-1 homologue) and the MIND complex by means of forming a so-called KMN (Knl-1, Mtw1 complex and Ndc80 complex) network (Cheeseman et al., 2006). Yeast *spc24* or *spc25* temperature-sensitive alleles also show loss of the spindle checkpoint response (Janke et al., 2001), and similar observation was made in Xenopus as well (McCleland et al., 2003). These results suggest a direct or indirect connection between the recruitment of spindle checkpoint machinery and the Ndc80 complex. One

of the possibilities is that the Spc24/Spc25 subcomplex might function as a docking site for spindle checkpoint proteins on the kinetochore. Indeed, an interaction between Spc25 and spindle checkpoint protein Mad1 has been detected in yeast two-hybrid based interaction assay (Newman et al., 2000), but further investigation is required to explore this attractive idea.

The Ndc80 complex is highly conserved among all eukaryotes. The human homologue of *NDC80* was first identified as *HEC1*, a gene highly expressed in cancer cells. Disruption of the Ndc80 complex in higher eukaryotes results in similar defects as observed in budding yeast, including chromosome missegregation and impaired spindle checkpoint. The electron-microscopy structure of the yeast Ndc80 complex and a crystal structure of the partial yeast Spc24/Spc25 subcomplex have nicely illustrated the three-dimensional arrangement of the complex (Wei et al., 2005, Wei et al., 2006). Overall, the Ndc80 complex exhibits a dumbbell shape with a long coiled-coil region in the middle, which is formed by the C-terminus of Ndc80/Nuf2 and the N-terminus of Spc25/Spc24, and globular domains on either side (Figure 4.3A). A similar structural appearance was seen in the "bonsai" version of human Ndc80 complex, in which Ndc80 is fused with Spc25, and Nuf2 is fused with Spc24 with shortened central coil-coiled regions on both fusions (Figure 4.3B)(Ciferri et al., 2008). The globular domain formed of Ndc80 and Nuf2 interacts with microtubules, whereas the globular domain formed of Spc24 and Spc25 is oriented towards the centromere, interacting with other central kinetochore proteins, such as the MIND complex and Spc105 (Cheeseman et al., 2006, Wei et al., 2007). The partial crystal structure of Spc24/Spc25 illustrates that the C-terminal globular domains cover amino acids 133-221 of Spc25 and amino acids 154-213 of Spc24. The heterodimeric complex also forms a centromere-oriented groove with highly conserved residues, which may provide an interaction platform for other kinetochore proteins (Figure 4.3C). Interestingly, the structure of the C-terminal domains of Spc24/Spc25 also shows disordered segments between the globular domains and the N-terminal coiled-coil regions. Due to the limited length coverage by this partial crystal structure, it is not clear how long this unstructured region is, and it is not clear if it is physiologically important (Wei et al., 2006).

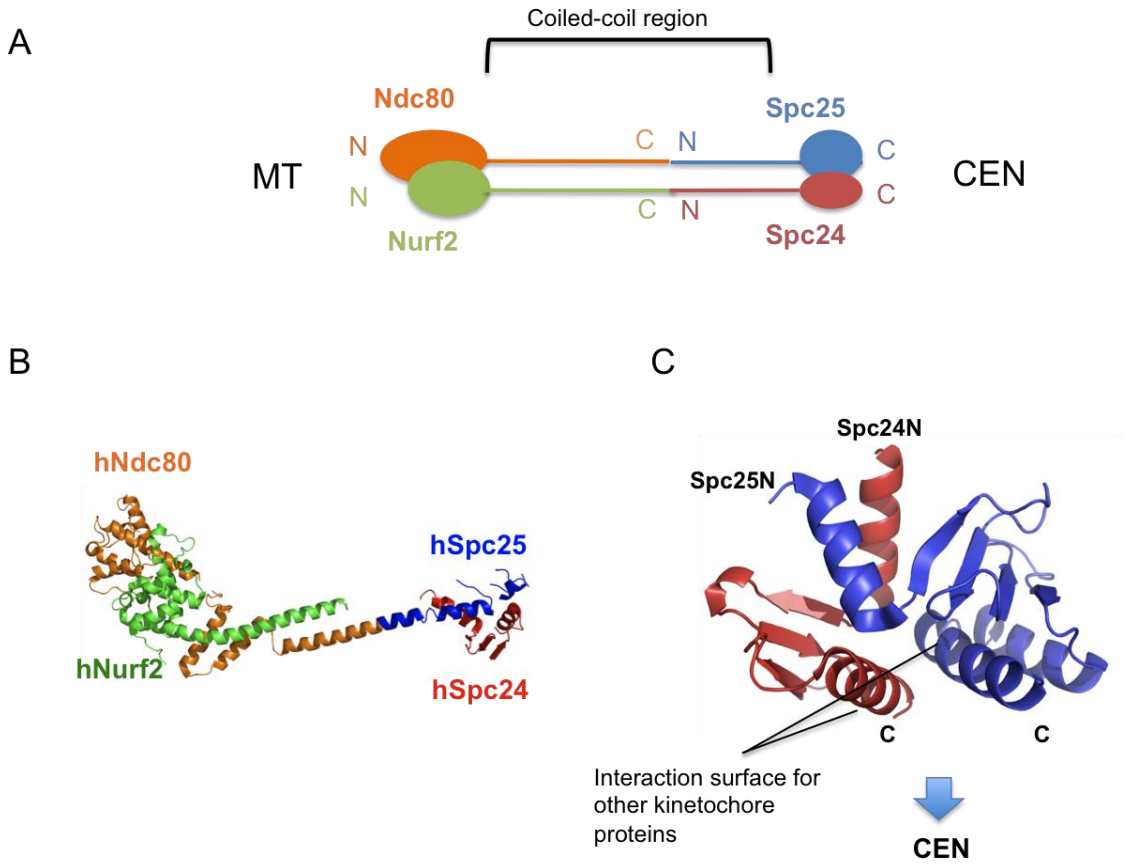

Figure 4.3 Structures of budding yeast and human Ndc80 complex
(A) A schematic diagram of the Ndc80 complex. MT: microtubule, CEN: centromere. Ndc80 (orange), Nuf2 (green), Spc25 (blue) and Spc24 (red) form an overall rod-like structure with a long coiled-coil region in the middle and globular domains at either end of the complex. (B) Crystal structure of human Ndc80$^{\Delta N\text{-bonsai}}$ complex, PDB code: 2VE7. In this structure, hNdc80 (orange) and hNuf2 (green) have shortened C-termini, whereas hSpc25 (blue) and hSpc24 (red) have shortened N-termini. hNdc80 is fused with hSpc25 and hNuf2 is fused with hSpc24. (C) Crystal structure of budding yeast Spc24 (155-211)/Spc25 (136-221) globular domain subcomplex, PDB code: 2FTX. The indicated surface facing the centromere provides a binding platform for other kinetochore proteins. Figure 4.3B and C were generated by PyMol.

4.1.2.3 Posttranslational Modifications in the Kinetochore

Posttranslational modification has been reported to play regulatory roles in the kinetochore in a couple of instances. Firstly, within the Ndc80 complex, the microtubule binding activity of Ndc80 is regulated by Aurora B-mediated phosphorylation. *In vitro* experiments showed that phosphorylation of Ndc80 by Aurora B, which acts as a quality control process to counteract improper kinetochore-

microtubule attachment, reduces its affinity for the microtubule (Cheeseman et al., 2006). This is achieved by altering the positive charges of the calponin homology (CH) domain and the N-terminal tail of Ndc80 and therefore affects their interaction with the negatively charged tubulin C-terminal tails (Ciferri et al., 2008). *In vivo*, Ndc80 is not the only target of Aurora B to regulate microtubule association of the kinetochore. In fact, Aurora B phosphorylates the KMN network, and it is the combinational effect of phosphorylation on a number of proteins within the KMN network that modulates the overall microtubule binding activity, with the fully phosphorylated state severely compromising microtubule binding. The spatial distribution of the targets along the DNA-microtubule axis can lead to differential phosphorylation in response to changes to tension and the attachment state (Welburn et al., 2010, Akiyoshi et al., 2009). The small ubiquitin-like modifier SUMO also acts to regulate kinetochore functions. Matunis and coworkers reported that SUMO2/3 conjugates are present in the centromere and kinetochore, suggesting SUMO-modified proteins are localised at these places. Inhibition of SUMOylation blocks the microtubule motor protein CENP-E association with kinetochores, activates the spindle checkpoint and causes cell cycle arrest. Further investigation showed that CENP-E binds to polymeric SUMO2/3 chains via its SUMO-interacting motif (SIM) and found this feature to be required for the kinetochore localisation of CENP-E (Zhang et al., 2008). In that study, the exact substrate, which is modified by SUMO and responsible for CENP-E recruitment, are not clear. Nevertheless, it illustrated that SUMOylation occurs in kinetochore and plays an important regulatory role in the recruitment of certain kinetochore proteins. Other biologically relevant posttranslational modifications of kinetochore proteins remain to be identified. For instance, a two-hybrid system based interaction map for mitotic spindle has revealed interactions between Spc25 and Ubc4, Spc25 and Slx5, Ndc80 and Ufd1, Ctf19 and Slx5, plus connections between APC/C subunits and multiple kinetochore proteins. These interactions between ubiquitylation machinery and kinetochore proteins suggest a potential involvement of ubiquitin signalling in regulating kinetochore functions (Wong et al., 2007).

In this chapter, I reported that Spc25 is identified as a ubiquitin-binding protein. Its ubiquitin-binding property is characterised by several different methods. Further investigation was performed to study the biological function of the ubiquitin-binding domain in Spc25. This work for the first time suggests a function of ubiquitin signalling in maintaining the stability of the kinetochore complex.

4.2 Identification of Novel Ubiquitin-binding Factors by Yeast Two-hybrid Screening

The molecular mechanism downstream of polyubiquitylated PCNA is largely unknown. It has been proposed that an error-free pathway, which may involve a template switch mechanism, could use genetic information from the undamaged sister chromatid to bypass the lesion. However, factors involved in this process have not been identified yet. I was interested in using fusion constructs Ub^*_n-$PCNA^*$ (as described in Figure 3.3) to identify their interaction partners, which may have a role in the *RAD6* pathway downstream of PCNA polyubiquitylation, by a genome-wide yeast two-hybrid screen. Meanwhile, such a screen would also reveal many ubiquitin-binding factors, possibly even previously unidentified ubiquitin-binding factors. For this purpose, $Ub^*_{(3-4)}$ (L)-$PCNA^*$ and Ub^*_4-$PCNA^*$ were cloned into a pGBT9 vector to generate bait constructs, where the inserts were N-terminally in frame with a DNA-binding domain derived from Gal4 transcription factor (Figure 4.4). Factors bound to these bait constructs should then interact with polyubiquitylated PCNA *in vivo*. $PCNA^*$ alone and ubiquitin chains alone [$Ub^*_{(3-4)}$ and Ub^*_4] were also included in the screen as bait constructs (Figure 4.4). $PCNA^*$ (K127R, K164R) worked as control for factors bound to the unmodified PCNA and mutations at K127/K164 exclusively eliminated the possibility of further modification of the construct *in vivo*. $Ub^*_{(3-4)}$(L) and Ub^*_4 chains described in Figure 3.3 were also sub-cloned into pGBT9 vectors. The various ubiquitin chain constructs not only served as controls to exclude factors generally bound to ubiquitin chains, but were also used to actively search for novel ubiquitin-binding factors. Ideally, a factor that specifically recognises PCNA polyubiquitylation in the *RAD6* pathway would bind to Ub^*_n-$PCNA^*$ fusion and possibly also bind to $PCNA^*$ alone because the ubiquitylation may only enhance the interaction between such a factor and PCNA.

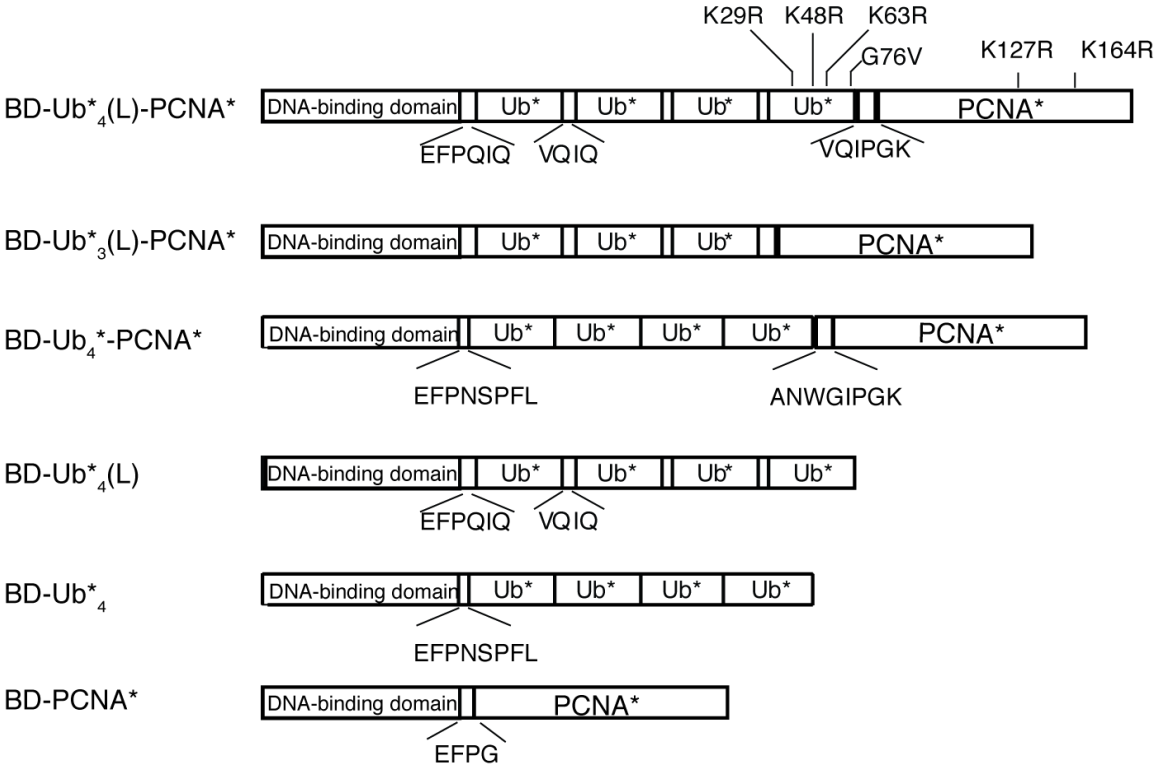

Figure 4.4 Bait constructs used in the yeast two-hybrid screens
Schematic view of the bait constructs used in the genome-wide yeast two-hybrid screens. The DNA-binding domain is derived from the Gal4 transcription factor. Mutations in the open reading frames of ubiquitin (K29/K48/K63, G76V) and PCNA (K127R, K164R) are indicated only once; the mutation versions are designated as Ub* and PCNA*. Amino acid sequences of linker peptides are shown below the constructs.

A good yeast genomic library is crucial for a successful screen. The yeast genomic library used in the screen was described in (James et al., 1996). It was made from putting fragmented yeast genomic DNA sequences into pGAD424 series vectors in frame with a transcription-activation domain from Gal4 transcription factor in all three open reading frames (James et al., 1996). The yeast genomic libraries were then transformed into a yeast two-hybrid reporter strain Y187 (Clontech) (Albers et al., 2005). In order to maximise the chance of covering the entire yeast genome, approximately 2 million transformants were collected from each transformation. Colonies were washed off from selective plates with YPD medium and slowly frozen down to -80 ℃ to ensure a high recovery rate. The resulting transformants together with the bait constructs were sent to a company for the actual screen as described in (Albers et al., 2005), where the bait constructs were transformed into a yeast strain with an

opposite mating type and those transformants were mated with the collection of transformants containing the yeast genomic library. A physical interaction between the bait protein and an unknown factor X expressed from the genomic library would activate transcription at the *LacZ* reporter gene. The entire screen was performed fully automated on microtiter plates with pipetting robots. Therefore this approach was not biased on restreaks or retransformations, which are typically involved in a traditional manual screen. In addition, the readout system was based on quantitative analysis of reporter signals and used statistics to identify the hits (Albers et al., 2005). In the end, colonies representing positive interactions were then amplified and subjected to sequencing to determine the identity of the inserts.

Based on this approach, a few factors were found to interact with Ub^{*}_{n}-$PCNA^{*}$ in the screen (Table 4.1). However, most of those factors, like Bob1, were cytoplasmic proteins, which were less likely to be involved in the *RAD6* pathway. Moreover, factors such as End3, Vps9, Lsb5, Sla1, Spc25 and Etp1 were also found to interact with one or both of the ubiquitin chain constructs (Table 4.1), suggesting that all of them are general ubiquitin-binding factors rather than factors specifically bound to polyubiquitylated PCNA. This result was rather disappointing since none of the factors fit our criteria. However, the control screen using $PCNA^{*}$ alone as bait only identified Srs2 as an interactor among the over twenty known PCNA-binding proteins, suggesting that the two-hybrid system may be not suitable to study protein-protein interaction for PCNA. This could be due to the fact that PCNA needs to be trimerised and loaded onto DNA for its biological function. A fusion of the DNA-binding domain with PCNA may not be able to bind other PCNA-interacting protein properly. To rule out the possibility that the DNA-binding domain in two-hybrid vector specifically blocked the access of other proteins to PCNA, a large-scale pull-down experiment was performed using purified $^{GST}Ub^{*}_{4}$-$PCNA^{*}$ to search for binding factors in total yeast extracts (Figure 4.5A). GST and $^{GST}PCNA^{*}$ were used as background control in parallel experiments. The bound materials were eluted from the glutathione column and analysed by mass spectrometry, which was performed in Dr. Mark Skehel's Mass Spectrometry Lab in Cancer Research UK Clare Hall Laboratories. Through this approach, some more but not all PCNA-

interacting factors were found in the pull-down experiment with $^{GST}PCNA^{*}$, such as Msh2, Pol32, etc (Figure 4.5B). Factors bound to $^{GST}Ub^{*}_{4}$-$PCNA^{*}$ included those PCNA-binding proteins and many other factors involved in the general ubiquitin pathway (Figure 4.5B). Unfortunately, no factor involved in genome stability was found in the $^{GST}Ub^{*}_{4}$-$PCNA^{*}$ pull-down exclusively. Therefore, two different approaches of using Ub^{*}_{n}-$PCNA^{*}$ fusions to identify factors that specifically recognise polyubiquitylated PCNA were not successful.

Bait	Hits	Number of times each clone was identified	Minimal region covered by repetitive clones (amino acids)
$PCNA^{*}$	*SRS2*	2	782-1039
Ub^{*}_{3}(L)-$PCNA^{*}$	*BOB1*	1	141-392
	SLA1	1	94-345
	ETP1	1	415-586
Ub^{*}_{4}(L)-$PCNA^{*}$	*END3*	6	388-638
	LSB5	9	161-355
	VPS9	1	382-573
	SLA1	5	1086-1139
	ETP1	13	459-573
	SPC25	3	107-222
Ub^{*}_{4}-$PCNA^{*}$	*END3*	6	389-619
	VPS9	1	383-573
	SLA1	2	1086-1307
	ETP1	54	415-586
Ub^{*}_{4}	*END3*	1	342-602
	PAN1	1	218-445
	VPS9	4	446-573
	ETP1	17	415-586
Ub^{*}_{4}(L)	*END3*	18	392-638
	LSB5	3	161-355
	VPS9	10	443-572
	SLA1	2	259-381
	RSC6	1	94-211
	SPC25	9	107-222
	DDI1	2	188-441
	ETP1	11	415-586

Table 4-1: Potential ubiquitin-binding proteins obtained from a genome-wide yeast two-hybrid screen

This table lists the names of the genes that were found to bind Ub^{*}_{4} or Ub^{*}_{4}(L) in a genome-wide yeast two-hybrid screen. Other information includes the number of times each clone was identified and the minimal range of amino acids covered by repetitive clones.

A

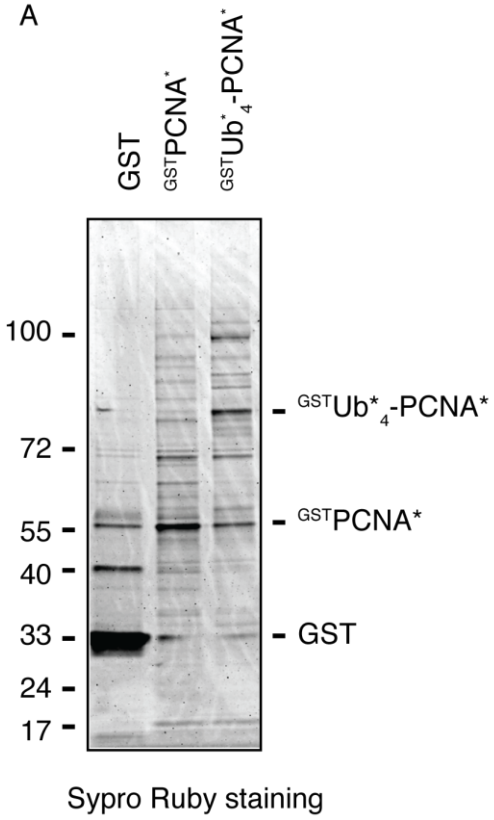

B

	GSTPCNA*		GSTUb*4-PCNA*
Hits Identified by Mass Spectrometry	Specific interactors	Common interactors	Specific interactors
	EF3A, EF2, PAM1, ELG1, EF1A, CLA4, PTK2, HSP82, HSP7F, HSP60, MGS1, DED1, KES1, BMH1, BMH2	UBP2, MSH6, POL3, PCNA, POL32, RIM1, DNL1	YBE7, SLA2, SYP1, MSH2, VPS27, RUP1, ENT2, ATG20, ENT1, HSE1, RFA3

Figure 4.5 Identification of PCNA* and Ub*4-PCNA* binding factors by pull-down/mass spectrometry
Pull-down experiments were performed in total cell extracts with purified GST, GSTPCNA* and GSTUb*4-PCNA*. GST fusion proteins were first immobilised on glutathione sepharose beads and yeast cell extracts were incubated with the charged beads at 4℃ for 2 h. After washing with the binding buffer for five times, the bound proteins were eluted from the beads and separated on a 4-12% gradient gel, stained with Sypro Ruby. (B) Three lanes in (A) were sliced and sent to mass spectrometry for protein identification. This table lists all candidate proteins found in the gel. At least 3 peptides were identified for each of the proteins listed.

Despite the failure in identifying factors bound to polyubiquitylated PCNA, a number of general ubiquitin-binding proteins were identified via the two-hybrid screen (Table 4.1). Among those hits, there were some known ubiquitin-binding factors. For instance, Vps9 was identified as a ubiquitin-binding factor from both bait constructs and it contains an UBA-like domain, which binds to ubiquitin, suggesting the two-hybrid screen was working. A few previously unknown potential ubiquitin-binding factors caught our attention. First of all, Spc25, which is a subunit of an evolutionarily conserved kinetochore complex, the Ndc80 complex (Janke et al., 2001, Wigge and Kilmartin,

2001), was found to interact with Ub^*_4(L) and Ub^*_4 (L)-PCNA*. Sequence analysis of Spc25 did not find any known ubiquitin-binding domain within the protein, suggesting that it may contain a new class of ubiquitin-binding domain. Most interestingly, there is no previous record about a function of ubiquitin-binding factors in the kinetochore complex. Secondly, a factor called Etp1 was identified as an interactor for both Ub^*_4 and Ub^*_4(L). In fact, Etp1 has a ZnF-UBP domain that is known to interact with ubiquitin (Seigneurin-Berny et al., 2001); however, the identified fragment of Etp1 in the two-hybrid screen contains its C-terminal region (amino acids 458-586), which excluded the ZnF-UBP domain. Sequence analysis of Etp1 did not reveal any known UBDs in its C-terminal region, and I therefore predicted that Etp1 might also contain a novel ubiquitin-binding domain. It would be interesting to find out why Etp1 has two distinct types of UBDs and how these UBDs contribute to the function of Etp1. Last but not least, a component of a chromatin remodelling factor, Rsc6, was identified in the screen against Ub^*_4 (L). Again, there were no known UBDs within the Rsc6 sequence. Some other factors such as Pan1, Lsb5, End3 and Sla1 were involved in the endocytosis pathway, which is widely known to involve several types of ubiquitin-binding factors (Raiborg et al., 2003) and made an involvement in genome stability unlikely. I therefore did not pursue these any further, but decided to concentrate any further analysis on Spc25, Etp1 and Rsc6.

As a first step, it was important to confirm the interaction between these factors and ubiquitin. The fragment of Spc25 found to interact with ubiquitin in the screen covered a C-terminal region of the protein (amino acids 107-221), the fragment of Etp1 also covered a C-terminal region (amino acids 458-586) and the fragment of Rsc6 covered a central part of the protein (amino acids 94-211). To verify these interactions, I generated yeast two-hybrid constructs expressing either full-length protein or the fragments that were found to bind ubiquitin as fusions to both the DNA-binding and the activation domain of Gal4 (Figure 4.6). The constructs were then analysed in a different reporter strain, PJ69-4A, which allows an estimation of interaction strengths by means of specific reporter genes. In the PJ69-4A strain, a *HIS3* reporter gene selects relatively weak interactions, whereas an *ADE2* reporter gene was used to identify strong

interactions (James et al., 1996). The results showed that the full-length Etp1 protein interacted with both Ub^*_4 and Ub^*_4(L) quite strongly, as a positive signal was detected from both *HIS3* and *ADE2* reporters. The C-terminal portion of Etp1 (amino acids 458-586) also exhibited similar interaction patterns, with an additional interaction observed even with monoubiquitin (Figure 4.6). Full-length Spc25 in this experiment was found to interact with Ub^*_4(L) strongly because a positive signal was observed with the *ADE2* reporter gene. This was consistent with that fact that Spc25 was only identified to interact with Ub^*_4(L) in the screen. The C-terminal fragment of Spc25 (amino acids 107-221) exhibited a slightly reduced but significant interaction with Ub^*_4(L) (Figure 4.6). Unfortunately, I was not able to confirm the interaction between Rsc6 and ubiquitin because this interaction was negative in one direction of the two-hybrid experiment when Rsc6 was fused to the activation domain, and auto-activation of the *HIS3* reporter was observed when Rsc6 was fused to the DNA-binding domain (Figure 4.6). To summarise, Spc25 and Etp1 were confirmed to be potential novel ubiquitin-binding factors based on this two-hybrid experiment. Since Spc25 has been studied for its function in the kinetochore, my following study would focus on the role of ubiquitin-binding of Spc25 in maintaining genome stability.

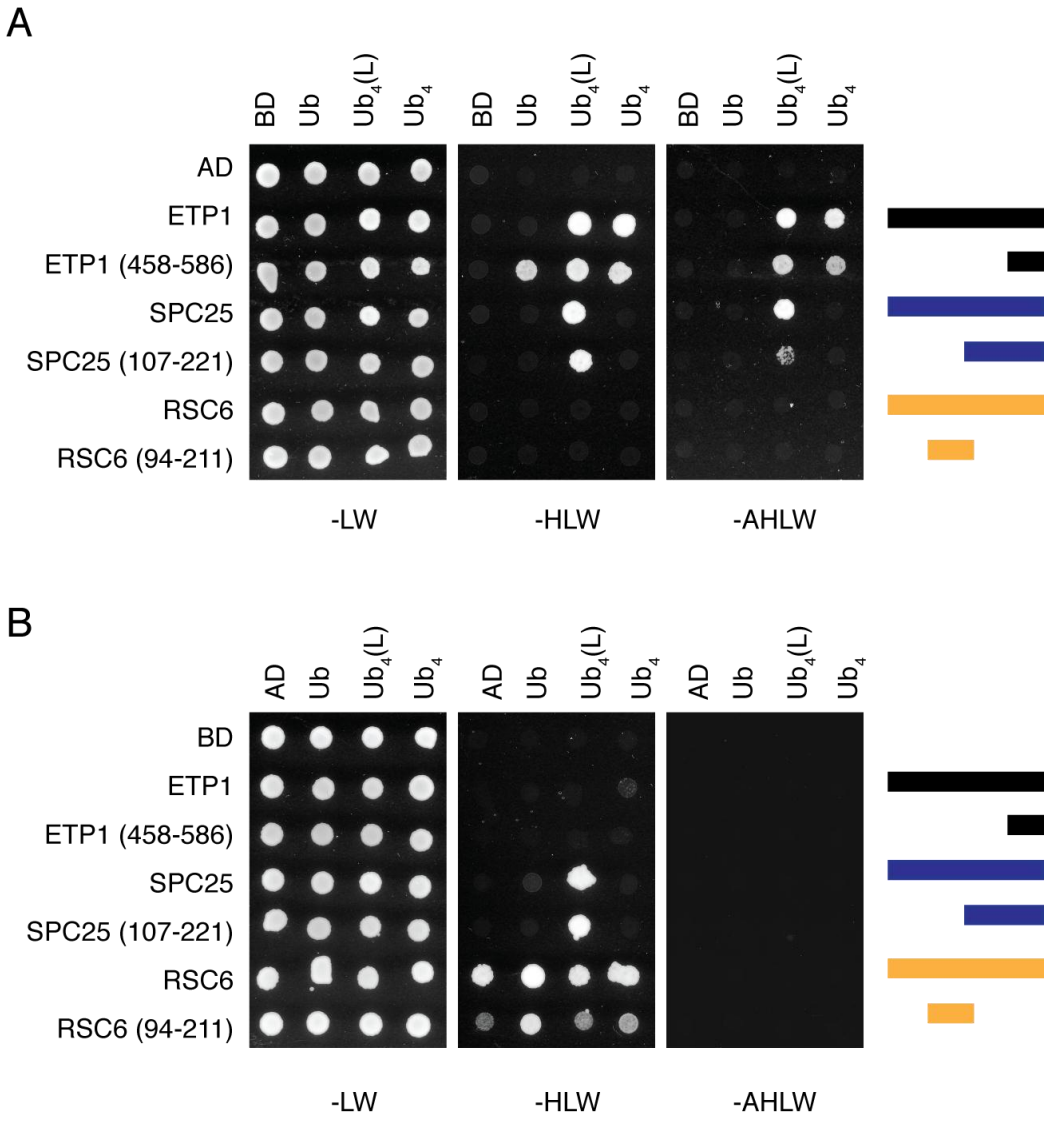

Figure 4.6 Protein-protein interaction analysis of Etp1, Spc25 and Rsc6 with ubiquitin in the yeast two-hybrid system
The open reading frames of the indicated proteins were expressed as fusions to Gal4 activation (AD) or DNA-binding (BD) domains. The presence of the expression vectors in the cells was controlled by growth on plates with selective medium (–LW). Positive interactions were shown as growth on plates without histidine (-HLW), which represents weakly selective conditions, and on plates without adenine and histidine (-AHLW), which represents relatively strongly selective conditions. The coloured bars schematically represent the constructs of the different proteins used in this two-hybrid interaction assay. (A) The BD domain was fused to ubiquitin and the AD domain was fused to the candidate proteins. This orientation is the same as in the original screen, but using different reporter genes and a different strain background. (B) The AD domain was fused to ubiquitin and the BD domain was fused to the candidate proteins. This orientation was not covered by the original screens.

4.3 Identification of the Minimum Region in Spc25 Required for Ubiquitin Binding

Spc25 is a subunit of the Ndc80 complex, which is an important complex providing a connection between microtubules and inner kinetochore complexes, since Ndc80-Nuf2 binds microtubules directly (Cheeseman et al., 2006, DeLuca et al., 2006). A number of posttranslational modifications have roles in regulating kinetochore function. Phosphorylation of Ndc80 by Aurora B kinase has been shown to regulate microtubule attachment (DeLuca et al., 2006). A SUMO-interacting motif has been found in kinetochore protein CENP-E and is absolutely required for localization of CENP-E to the kinetochore, potentially via interacting with other SUMOylated kinetochore factors (Zhang et al., 2008). So far, there have been no reports of ubiquitin-binding domains in the context of the kinetochore. Having identified Spc25, a kinetochore protein, as a potential novel ubiquitin-binding factor, I decided to characterise further the biological function of ubiquitin binding in Spc25.

The first step was trying to identify a minimum region required for ubiquitin interaction. Sequence analysis of the SPC25 open reading frame did not reveal any known ubiquitin-binding domains. Therefore, a series of truncations were made to represent different parts of Spc25 (Figure 4.7A). The N-terminal part of Spc25 (amino acids 16-77) is a coiled-coil region and the C-terminal part (amino acids 133-221) of the protein folds into a tight globular domain together with its dimerisation partner Spc24. A flexible and disordered segment (amino acids 117-132) connects the two parts (Wei et al., 2006). The globular domain consists of two alpha-helical regions (amino acids 133-146 and 187-221) and a beta sheet region (amino acids 147-186). Since NMR and X-ray crystal structures of the globular domain from yeast Spc25 are available (Wei et al., 2006), truncations within the globular domain were designed based on this secondary structure information. Truncation fragments were again cloned into the two-hybrid vectors and analysed for interactions with ubiquitin. It turned out that only the full-length protein and the C-terminal fragment (amino acids 107-221) showed positive interactions (Figure 4.7B). All truncations within the globular domain lost the interaction with ubiquitin completely (Figure 4.7B). This result suggested that the

globular domain (amino acids 133-221) and a flexible extension from the N-terminus of the globular domain were both required for interaction with ubiquitin.

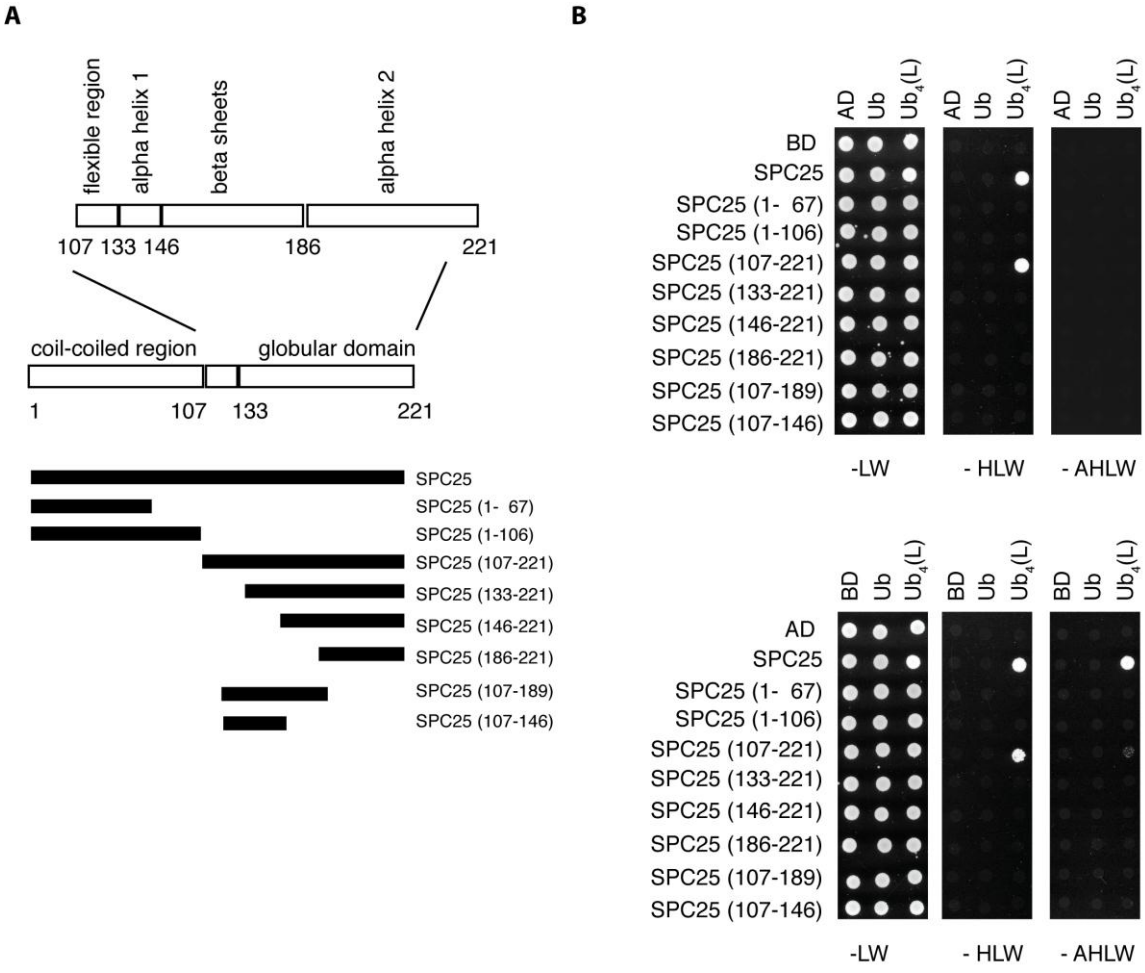

Figure 4.7 Identification of a minimal ubiquitin-binding region in Spc25
(A) A schematic view of Spc25 domains. Names of each region and information about secondary structure are given above the scheme, and the numbers of amino acids at the domain boundaries are labelled below the scheme. A series of black bars represent the lengths of the truncation constructs used in panel B. (B) Yeast two-hybrid analysis for protein-protein interaction between the series of truncations of Spc25 described in panel A and Ub^{*}_{4} (L). The experiment was performed in both orientations as described in Figure 4.6.

Although my truncations were designed based on secondary structure information to minimise any negative impact on the overall structure of the protein, this did not rule out the possibility that truncations might cause problems in protein folding and therefore abolish ubiquitin-binding. To address this question, Spc24 was introduced as an internal control for protein folding. Spc24 forms a heterodimer with Spc25 *in vivo* as part of the Ndc80 complex, and the globular domain of Spc25 tightly associates with Spc24 even in the absence of the long N-terminal coiled-coil regions of both proteins. Therefore, any truncation constructs that interacted with Spc24 should have maintained correct folding. The interaction between Spc24 and all the truncation constructs were tested in a yeast two-hybrid experiment. I found that the globular domain alone (amino acids 133-221) and a larger C-terminal fragment (amino acids 107-221) both interacted with Spc24 (Figure 4.8A), but only the latter construct was able to bind $Ub^{*}_{4}(L)$, confirming that a complete, well-folded globular domain plus a flexible extension from its N-terminus towards the coiled-coil region were required for ubiquitin interaction. All truncations within the globular domain lost the ability to bind Spc24.

Because Spc25 forms a stable heterodimer with Spc24 *in vivo*, it was formally possible that Spc24 mediates the interaction between Spc25 and ubiquitin. To address this question, I tested whether Spc24 interacts with ubiquitin. In yeast two-hybrid experiments no evidence was found to support an interaction between Spc24 and any of my ubiquitin constructs, whereas the positive control Spc25 showed an interaction with Spc24 (Figure 4.8B). This suggested that Spc24 is unlikely to be directly involved in the interaction between Spc25 and ubiquitin.

Taken together, these yeast two-hybrid based interaction data suggest that Spc25 interacts with ubiquitin, but its dimerisation partner Spc24 does not. The C-terminal fragment (amino acids 107-221), which contains the entire globular domain together with a flexible extension from the N-terminus of the globular domain towards the coiled-coil region, is necessary for ubiquitin binding.

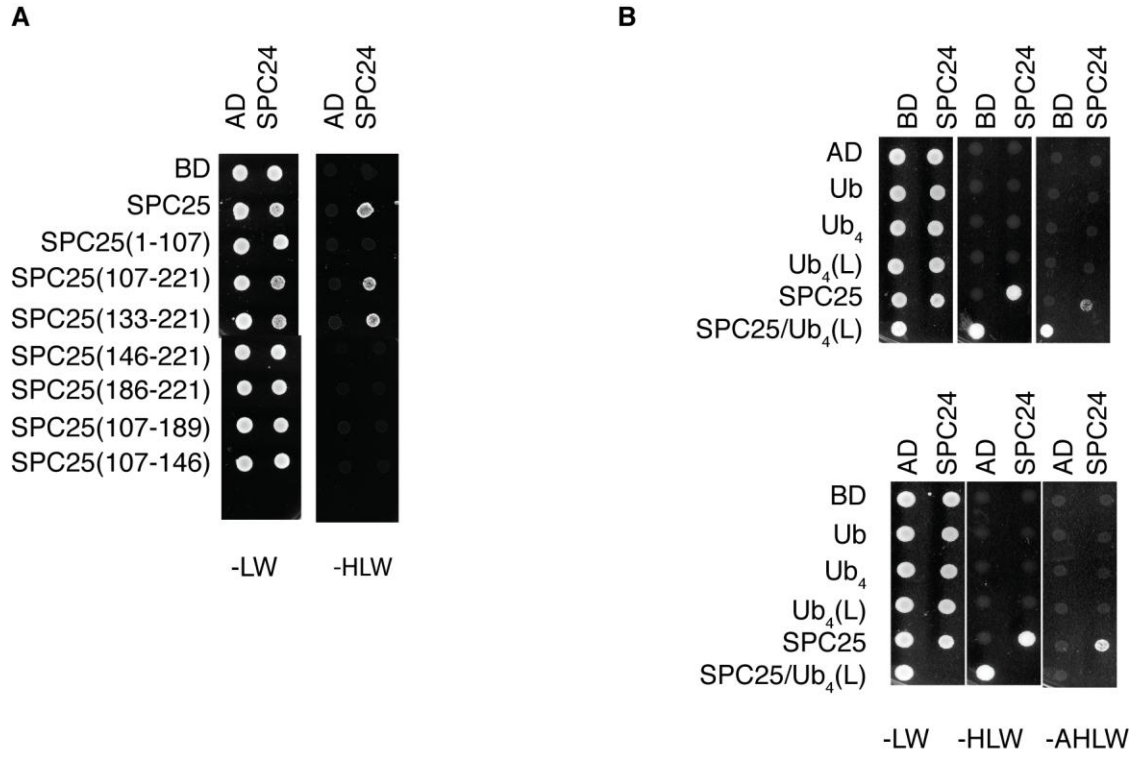

Figure 4.8 Yeast two-hybrid analysis of interactions between Spc25, ubiquitin and Spc24
(A) Two-hybrid analysis of interactions between a series of truncations of Spc25 and full length Spc24. (B) Two-hybrid analysis of interactions between Spc24 and ubiquitin. Interaction between Spc24 and Spc25, Spc25 and $Ub^{*}_{4}(L)$ served as positive controls. The experiment was performed as described in Figure 4.6.

4.4 The Spc25-Spc24 Complex Binds Ubiquitin Directly

The yeast two-hybrid analysis indicated an interaction between Spc25 and ubiquitin. However, one of the problems with this kind of approach is that the interaction might be indirect. In this case, Spc25 is a subunit of the Ndc80 complex, which interacts with several other protein complexes in the kinetochore. It is therefore possible that the interaction between Spc25 and ubiquitin was mediated by other kinetochore proteins that tightly associate with Spc25. To address this question, an *in vitro* pull-down experiment with purified protein components was performed.

The first approach was to purify Spc25 (amino acids 107-221) as GST fusion protein. The purification was quite successful, however the subsequent pull-down experiment did not succeed. Considering that many kinetochore proteins only become soluble when they are coexpressed with their binding partners as a complex, indeed Wei and co-workers obtained a stable sub-complex by coexpressing Spc25 with Spc24 (Wei et al., 2005). It was most likely that the GST moiety helps to solubilise Spc25, but the fragment itself might not fold correctly. I therefore decided to purify the C-terminal fragment of Spc25 (amino acids 107-221) and the globular domain of Spc24 (amino acids 154-213) together as a complex and perform a pull-down experiment with ubiquitin-conjugated Sepharose beads to analyse the interaction. These two constructs were named as Spc25(C) and Spc24(G) respectively. The Spc25(C) fragment was expressed as an N-terminal GST fusion protein and the Spc24(G) fragment was expressed as a fusion protein with an N-terminal 6His-tag in *E.coli*. Separate purification processes were initially attempted; however, ^{6His}Spc24(G) precipitated in the elution buffer shortly after the purification. Although ^{GST}Spc25(C) did remain soluble after elution, it was possibly that the GST moiety helped to maintain a folded structure. This suggested that Spc24(G) and Spc25(C) might have to be purified together to form a correctly folded heterodimer. I therefore expressed both proteins separately in *E.coli* and mixed the lysates during the purification step. After a single step of glutathione affinity chromatography, ^{6His}Spc24(G) was co-purified with ^{GST}Spc25(C) with a stoichiometric ratio around 1:1 as shown on a Coomassie-stained gel (Figure 4.9A). Using the purified preparation, a pull-down experiment was performed with ubiquitin-conjugated Sepharose beads to detect if the ^{GST}Spc25(C)-^{6His}Spc24(G) complex could bind ubiquitin. Indeed, the ^{GST}Spc25(C)- ^{6His}Spc24(G) complex was bound to the ubiquitin-conjugated Sepharose beads specifically, whereas only a barely-detectable amount of the complex was bound to protein G-conjugated beads in a parallel control experiment, and the GST protein alone did not bind to the ubiquitin-conjugated Sepharose beads either (Figure 4.9B). This result indicated that the Spc25-Spc24 complex was able to interact with ubiquitin directly *in vitro*.

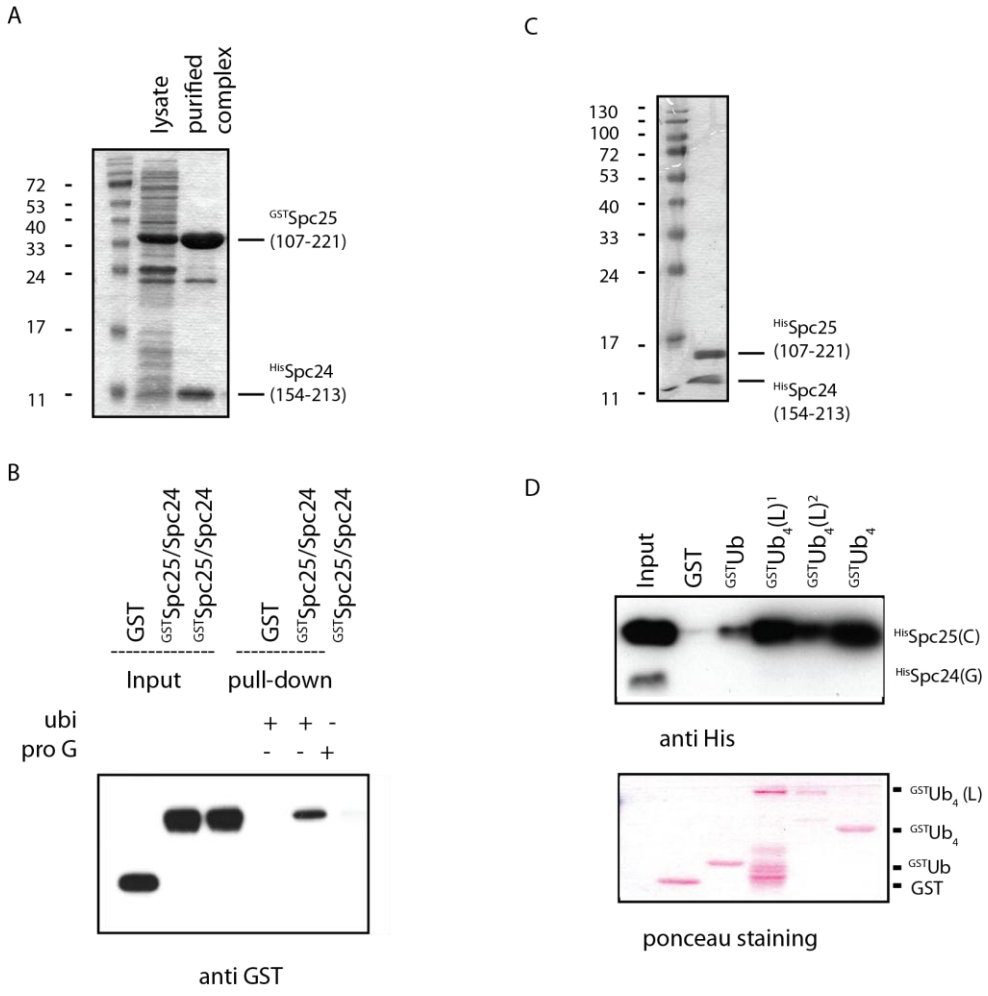

Figure 4.9 *In vitro* analysis of ubiquitin binding by the Spc25-Spc24 complex
(A) A Coomassie-stained gel shows co-purified ^{GST}Spc25 (107-221)-^{His}Spc24 (154-213) complex with a stoichiometric subunit ratio around 1:1. After mixing the cell lysates, derived from *E.coli* cultures expressing ^{GST}Spc25 (107-221) and ^{His}Spc24 (154-213) respectively, a single step glutathione affinity chromatography was applied to the lysate and the complex was eluted from the column using reduced glutathione. (B) An *in vitro* pull-down experiment shows an interaction between Spc25-Spc24 and ubiquitin. Ubiquitin sepharose beads were used to pull down either GST or ^{GST}Spc25(C)-^{His}Spc24(G) complex. Protein G-conjugated beads were used as another control for non-specific binding of the complex to the beads. The bound materials were detected by anti-GST Western blots. 5% of the input and 12.5% of the total bound materials were loaded on this gel. (C) A Coomassie-stained gel shows purified ^{His}Spc25 (107-221)-^{His}Spc24 (154-213) complex with a stoichiometric subunit ratio around 1:1. ^{His}Spc25 (107-221) and ^{His}Spc24 (154-213) were coexpressed in *E.coli* and purified by Ni-NTA affinity chromatography. The eluted proteins were then applied to a gel filtration column, and fractions corresponding in size to the heterodimeric complex were collected. (D) An *in vitro* pull-down experiment shows interactions between Spc25-Spc24 and monoubiquitin as well as tetraubiquitin chains. ^{GST}Ub$_4$(L) and ^{GST}Ub$_4$ were expressed in *E.coli* and purified by glutathione affinity chromatography. GST, ^{GST}Ub$_4$(L) and ^{GST}Ub$_4$ were immobilised on glutathione beads. Two different preparations of ^{GST}Ub$_4$(L) were tested in this pull-down experiment labelled 1 and 2. Bound proteins were detected by anti-His Western blots and Ponceau staining of the membrane.

The arrangement of ubiquitin molecules on the surface of ubiquitin-conjugated Sepharose beads is poorly defined. It is therefore difficult to determine if the ^{GST}Spc25(C)-^{6His}Spc24(G) complex interacts with monoubiquitin or polyubiquitin chains. For this reason, a pull-down experiment was performed with ^{GST}Ub or ^{GST}Ub$_4$ immobilized on the glutathione Sepharose instead of ubiquitin-conjugated Sepharose. As ^{GST}Spc25(C) was not suitable for this kind of experiment, a new expression construct was generated to purify Spc25(C) as an N-terminally 6His-tagged protein. The ^{6His}Spc25(C)-^{6His}Spc24(G) complex was coexpressed in the same *E.coli* strain and the complex was purified by Ni-NTA affinity chromatography. Because both proteins have a 6His-tag, the eluted protein complex from the Ni-NTA column was not obtained with a 1:1 stoichiometry, and some precipitation was observed after the purification, suggesting that one of the two proteins was in excess and then precipitated from the solution. Therefore, the eluted proteins were applied to a gel filtration column and the fractions representing a dimeric complex of ^{6His}Spc25(C)-^{6His}Spc24(G) were collected and analysed by SDS-PAGE. In the end, a purified dimeric complex of ^{6His}Spc25(C)-^{6His}Spc24(G) with a stoichiometric ratio around 1:1 was obtained (Figure 4.9C). In a pull-down experiment, a small but detectable amount of this protein complex was bound to ^{GST}Ub, and the amount of bound material greatly increased when ^{GST}Ub$_4$(L) was used (Figure 4.9D). A similar interaction was observed with ^{GST}Ub$_4$. These data confirmed the results from the previous pull-down experiment and showed that the Spc25(C)-Spc24(G) complex is able to interact with monoubiquitin as well as linear tetraubiquitin chains. Further experiments were attempted to determine if Spc25(C)-Spc24(G) binds to K63- or K48-linked polyubiquitin chains. Unfortunately, the protein complex did not show significant binding to either of them. I therefore favoured the idea that the Spc25-Spc24 complex interacts mainly with monoubiquitin. The observed interaction with linear tetraubiquitin chains could be simply explained by the increase in the number of ubiquitin units available for binding. In such case, an enhanced interaction would be observed, but would not be an indication of genuine polyubiquitin binding.

I was interested to quantify the binding affinity of Spc25-Spc24 to monoubiquitin via a biophysical approach. The surface plasmon resonance-based BIACORE® technology was used to determine the dissociation constant for this interaction. A CM5 chip was chemically coupled with anti-GST antibody to immobilize either GST or ^{GST}Ub onto its surface, and the Spc25(C)-Spc24(G) complex was then injected at varying concentrations. The SPR signals detected in the GST sample were considered as background and were subtracted from signals obtained with ^{GST}Ub. A series of concentrations of the Spc25(C)-Spc24(G) complex from 1 μM to 40 μM was used, and SPR signals at each concentration were recorded for 300 sec (Figure 4.10A). Because Spc25-Spc24 binding to monoubiquitin exhibited fast association and dissociation rates, a dissociation constant of 14.2 μM was calculated from the SPR signals at the equilibrium state of each sample concentration (Figure 4.10B). Considering that many UBDs bind monoubiquitin quite weakly, the observed binding affinity was among the relatively strong interactions (Hurley et al., 2006). Finally, yeast two-hybrid showed that Spc25 selectively bind Ub^*_4 (L), but *in vitro* pull-down experiments showed that Spc25 bind both Ub^*_4 (L) and Ub^*_4. I therefore analysed the interaction between Spc25 and both types of tetraubiquitin chains by the BIACORE system. Equimolar amounts of GST, ^{GST}Ub, $^{GST}Ub^*_4$ (L) and $^{GST}Ub^*_4$ were captured on the surface of a CM5 chip, which had been divided into four parallel flow cells and chemically coupled with anti-GST antibody. The Spc25(C)-Spc24(G) complex was injected at 10 μM and the sensorgrams were recorded. $^{GST}Ub^*_4$ (L) was seen to bind the complex best, whereas $^{GST}Ub^*_4$ showed a weaker binding compared with $^{GST}Ub^*_4$ (L) (Figure 4.10C). Again, this experiment confirmed a positive interaction between Spc25 and both types of tetraubiquitin chains, and a stronger interaction with Ub^*_4 (L).

In summary, the purified Spc25(C)-Spc24(G) complex was able to bind monoubiquitin directly with relatively strong binding affinity. Whether or not it binds to polyubiquitin chains of defined geometries remains unclear.

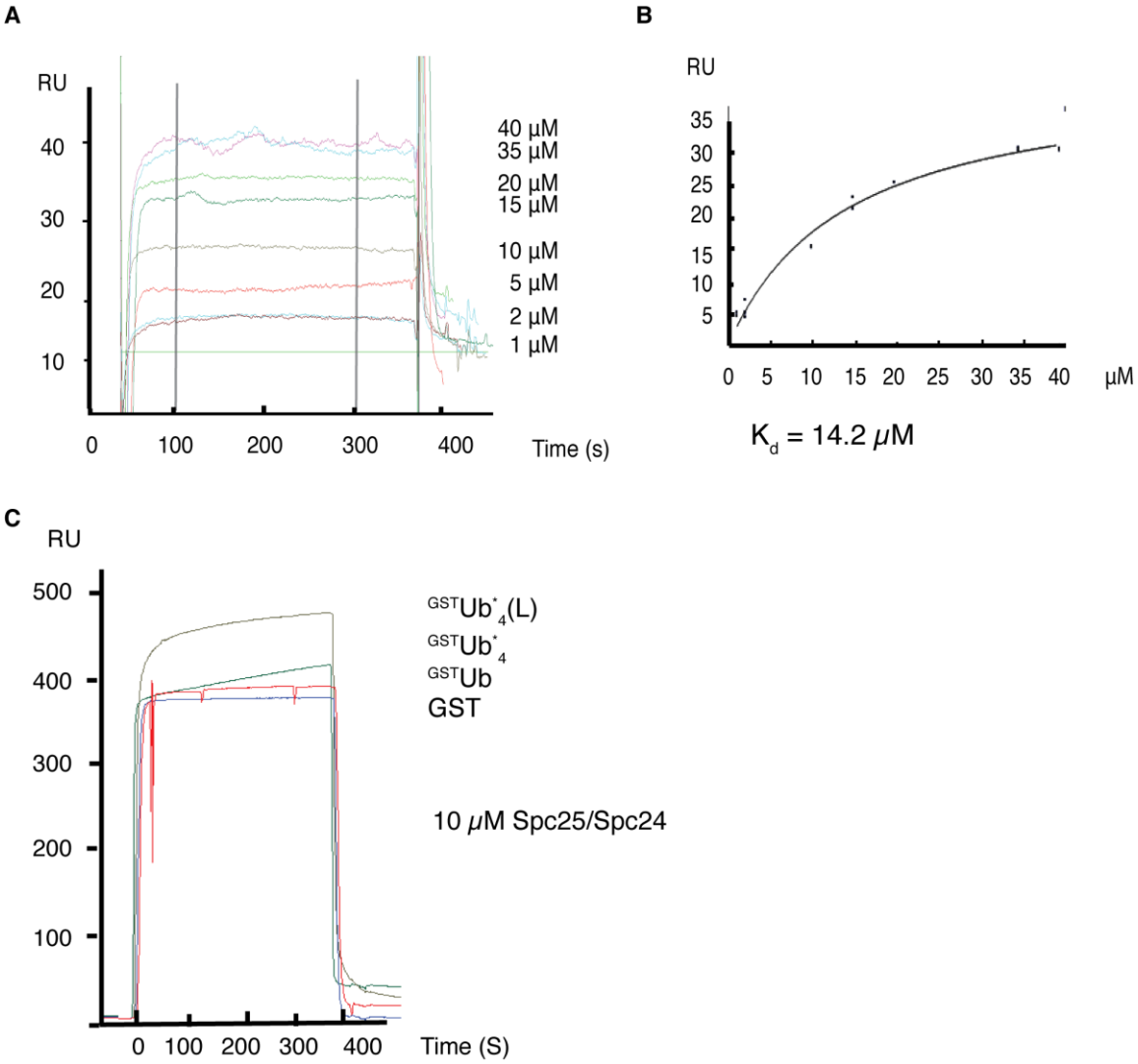

Figure 4.10 Surface plasmon resonance analysis of Spc25(C)-Spc24(G) binding to monoubiquitin and tetraubiquitin

(A) A Biacore sensor chip (CM5) was conjugated with 5000 resonance units (RU) of anti-GST antibody, and equimolar amounts of GST or ^{GST}Ub were captured on the surface of the chip (500 and 673 RU, respectively). ^{His}Spc25 (107-221)-^{His}Spc24 (154-213) complex was injected across the sensor chip at the indicated protein concentrations. Background signals from the GST sample were subtracted from the signals obtained with ^{GST}Ub. The experiments were performed in duplicate at each concentration, and only one sensorgram per concentration is shown. Signals between the two vertical lines were averaged for each protein concentration and used to calculate the dissociation constant. (B) Response units were plotted against the protein concentrations for calculation of the dissociation constant (K_d) for the interaction between Spc25-Spc24 and ubiquitin. (C) GST, ^{GST}Ub, $^{GST}Ub^{*}_{4}$ (L) and $^{GST}Ub^{*}_{4}$ (585, 706, 1004, and 933 RU respectively) were captured on the surface of a CM5 chip, and 10 µM Spc25(C)-Spc24(G) complex was injected and the sensorgrams were recorded.

4.5 Characterisation of the Interaction Between Spc25 and Ubiquitin

The evidence of a direct physical interaction between Spc25-Spc24 and ubiquitin encouraged me to further characterise residues that are important for this interaction, ideally even to determine the contact surfaces on both proteins. Most UBDs bind to a hydrophobic patch on the β-sheet of ubiquitin around I44, although there are some exceptions that UBDs bind to ubiquitin independent of this hydrophobic patch (Beal et al., 1998, Hurley et al., 2006). In the case of Spc25-Spc24, bioinformatic analysis did not identify any similarities to known UBDs (personal communication with Kay Hofmann). I therefore tested if Spc25-Spc24 binding to ubiquitin requires the canonical hydrophobic patch. A pull-down experiment with ^{GST}Ub and ^{GST}Ub (I44A) was performed to analyse the interaction with Spc25(C)-Spc24(G) as described previously. The experiment showed that ^{GST}Ub was able to bind the Spc25(C)-Spc24(G) complex, and this interaction was abolished by the I44A mutation in ^{GST}Ub (Figure 4.11). This result suggested that the Spc25-Spc24 complex interacts with ubiquitin through the canonical hydrophobic patch.

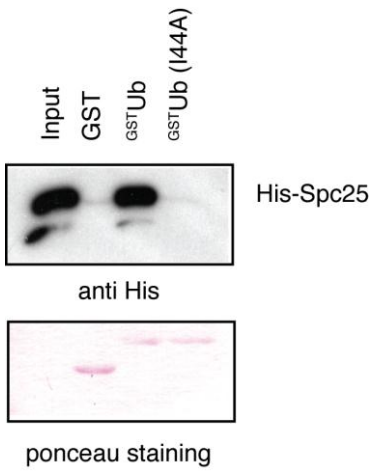

Figure 4.11 *In vitro* analysis of I44A mutant ubiquitin binding by the Spc25-Spc24 complex
Pull-down experiment shows that an interaction between Spc25-Spc24 and ubiquitin is abolished by an I44A mutation of ubiquitin. ^{GST}Ub and ^{GST}Ub (I44A) were expressed and purified from *E.coli* using glutathione affinity chromatography. In the pull-down experiment, proteins bound to the beads were finally detected by an anti-His Western blot and Ponceau staining of the membrane.

Identification of residues on Spc25 that are important for ubiquitin interaction was achieved by searching for mutations that abolish ubiquitin binding. From the work described in section 4.4, it was known that ubiquitin binding requires the entire globular domain and the N-terminal flexible extension. Most importantly, the globular domain (amino acids 133-221) of Spc25 alone does not interact with ubiquitin, suggesting there must be important residues within the region of the flexible extension (amino acids 107-133) responsible for contacting ubiquitin. To find out the identity of those residues, a sequence alignment was performed for Spc25 from different organisms to search for evolutionarily conserved residues, particularly within the fragment spanning amino acids 107-133. Given that this region of interest represents a flexible linker, I argued that any conserved residues in this sequence might be functionally significant. Three well-conserved residues were found within that region: L109, L113 and R116 (Figure 4.12A).

To test whether any of these three residues may contribute to the interaction with ubiquitin, the following constructs were generated: Spc25 (3A), in which L109, L113 and R116 were mutated to alanine, Spc25 (107-133) representing the flexible region only, Spc25 (1-133) representing the flexible region plus the N-terminal coiled-coil region and Spc25 (117-221) which excludes the conserved residues. Figure 4.12B gives a schematic view of all the constructs. If any of these three conserved residues were important for ubiquitin-binding, a similar result would be expected from the triple-mutation construct Spc25 (3A) and the truncation construct Spc25 (amino acids 117-221). In addition to that, the constructs Spc25 (amino acids 107-133) and Spc25 (amino acids 1-133) would help me to answer the question if the N-terminal part of Spc25 would have something to do with ubiquitin binding since all previous experiments were focused on the C-terminal part of the protein. All the constructs were analysed in the yeast two-hybrid system for ubiquitin binding along with some previously analysed constructs as positive controls. The result showed that the Spc25 (3A) mutant lost ubiquitin-binding in both orientations. This was consistent with results from the truncation construct Spc25 (117-221), which lacks the relevant region completely (Figure 4.12B). Importantly, both the mutant and the truncated forms of Spc25 were

able to interact with Spc24, suggesting that both proteins folded properly (Figure 4.12B). Furthermore, construct Spc25 (1-133) interacted with Spc24, presumably due to the dimerisation of the coiled-coil region. However, Spc25 (1-133) did not interact with ubiquitin (Figure 4.12B). These experiments showed that at least one residue among L109, L113, and R116 must be important for ubiquitin-binding of Spc25. The fact that neither the flexible region alone (amino acids 107-133) nor this region plus the N-terminal coiled-coil domain (amino acids 1-133) were able to interact with ubiquitin suggests a second potential contacting surface, most likely within the globular domain of Spc25.

Finally, individual mutations of L109A, L113A and R116A were made to separate their contributions to the ubiquitin binding of Spc25. These individual mutant constructs together with the triple mutant construct were then analysed in the yeast two-hybrid system again. The results showed that the L109A mutation had a dramatic effect: it abolished ubiquitin-binding completely in both orientations. L113A had an intermediate phenotype, in which ubiquitin-binding was partially reduced in one direction of experiment and was not detectable in the other direction of experiment. In contrast, R116A mutation did not have any effect on ubiquitin-binding (Figure 4.13). I therefore concluded that residue L109 was the primary contact site for ubiquitin interaction. L113 could be involved in this interaction as a secondary contact site. R116 is not required for the interaction. Ideally, *in vitro* pull-down and BIACORE experiments would be performed to confirm and quantify the extent to which the L109A mutation abolished the ubiquitin binding of Spc25; such experiments are still waiting to be completed. Nevertheless, this result enabled me to use Spc25 (L109A) as a mutant deficient in ubiquitin binding in the rest of my study to analyse the biological function of ubiquitin binding.

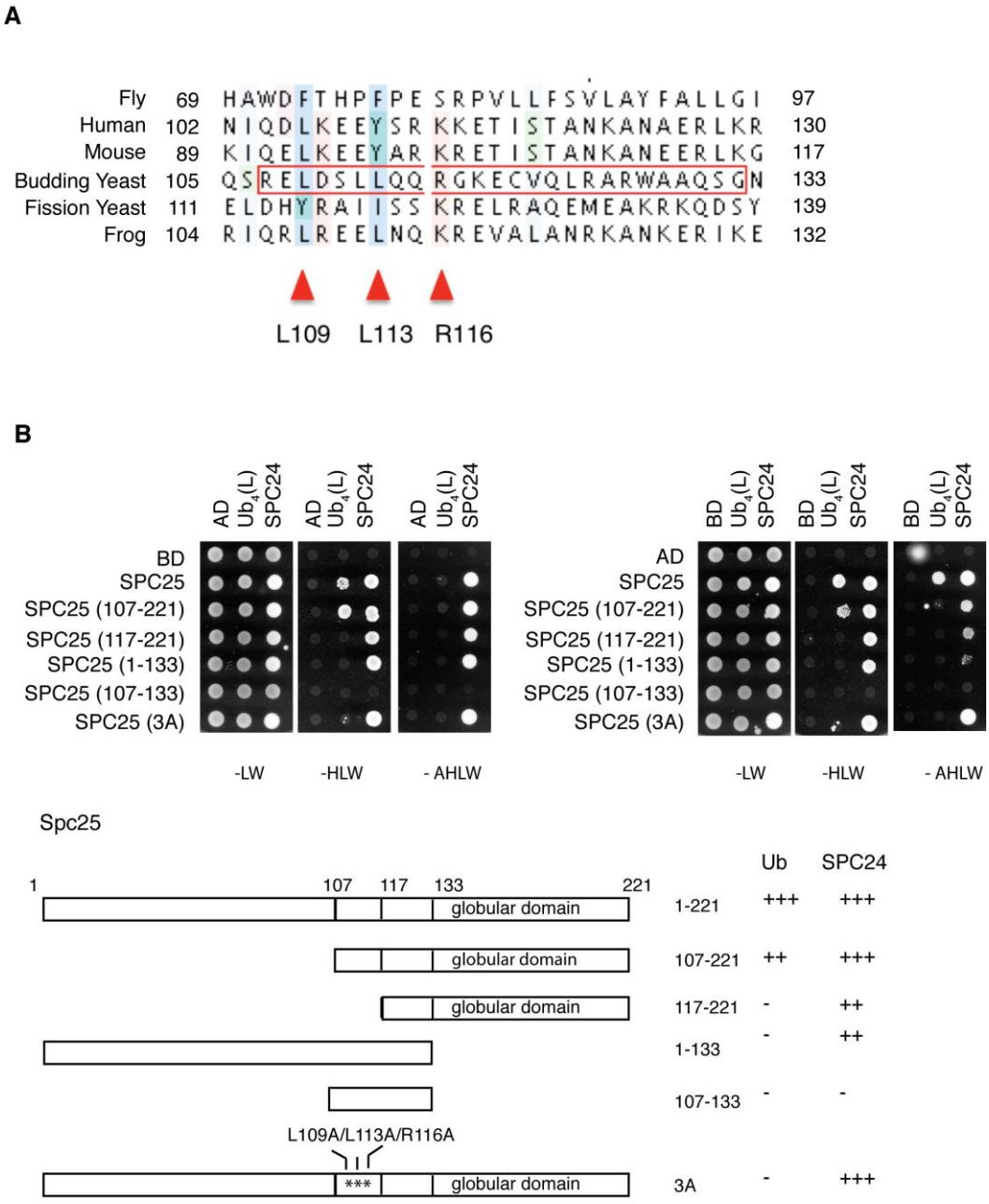

Figure 4.12 Identification of ubiquitin-binding residues on Spc25
(A) A sequence alignment of Spc25 from different organisms including *Drosophila melanogaster, Homo sapiens, Mus musculus, Saccharomyces cerevisiae, Schizosaccharomyces pombe* and *Xenopus laevi*. The alignment was generated by CLUSTALW2 sequence analysis tool available from EBI (European Bioinformatics Institute). The three most conserved residues within the region of interest were indicated by red triangles below the alignment. (B) Two-hybrid analysis of the interaction between Spc25 truncations or mutations and ubiquitin. The scheme at the lower part of the panel summaries the truncations and mutations used in this study. The experiment was performed as described in Figure 4.6.

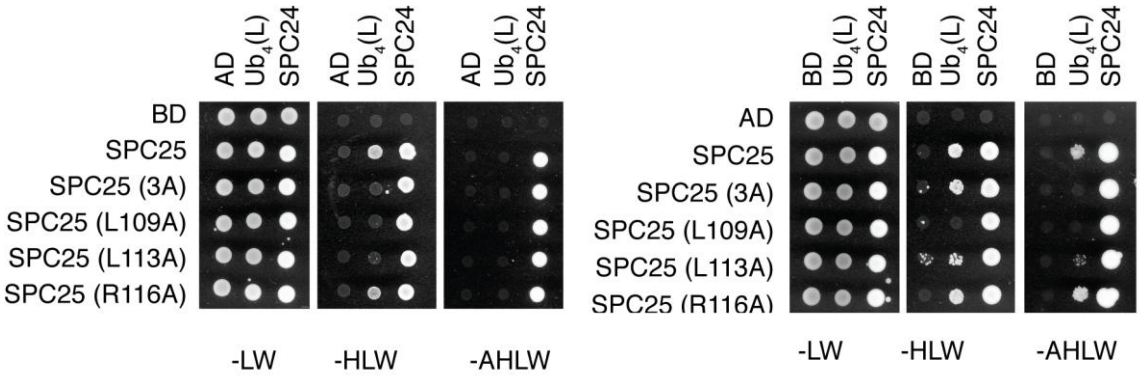

Figure 4.13 The impact of individual mutations on the interaction between Spc25 and ubiquitin
Two-hybrid analysis of the interaction between Spc25 mutants and ubiquitin. Spc24 serves as a control for the folding of the mutant proteins. The experiment was performed as previously described in Figure 4.6.

4.6 *Spc25* Ubiquitin-binding Deficient Mutants Have an Intact Spindle Checkpoint

As introduced earlier in my thesis, Spc25 is a subunit of the Ndc80 complex, which sits on the outer kinetochore and connects the microtubule to the inner kinetochore protein complexes assembled on the centromeric DNA (Janke et al., 2001, Cheeseman et al., 2006). Spc25 is an essential protein, such that deletion mutants of Spc25 are not viable. Based on that information, the first question to ask is if Spc25 ubiquitin-binding deficient mutants are viable. If ubiquitin binding were critical for the proper function of Spc25, complete loss of ubiquitin binding would have a severe defect in the protein function or even cause cell death. In that situation, mutants that have partially reduced ubiquitin binding might still support viability. In order to observe their potential phenotypes, *spc25* mutant alleles were introduced into diploid yeast cells, followed by sporulation. One copy of *SPC25* was deleted by replacing it with a *HIS3* marker in a diploid cell and a copy of the *spc25* mutants *(L109A, L113A and 3A)* was inserted into the yeast genome with the *URA3* marker to generate heterozygous cells, where one copy of Wt *SPC25* would support cell survival. The heterozygotes were then sporulated and the spores separated by tetrad dissection and tested for genetic markers. Figure 4.14A

shows that the *HIS*$^{+}$-*URA*$^{+}$ spores carrying mutations of L109A, L113A or a triple mutation 3A were viable. In addition to that, there were no differences in colony sizes (Figure 4.14A), and mutant cells were not temperature sensitive within 25-37℃ (data not shown). Overall, this suggested that ubiquitin-binding deficient *spc25* mutant cells were viable, and the similar colony sizes derived from the germinating spores indicated similar growth rates.

Because the ubiquitin-binding deficient mutant did not affect cell viability and did not cause any differences in haploid cell growth rate, I was curious to find out the biological function of ubiquitin binding in Spc25. Temperature-sensitive mutants of *SPC25* show defects in chromosome segregation and the spindle checkpoint response (Wigge and Kilmartin, 2001, Janke et al., 2001). In addition to that, an interaction between Spc25 and the spindle checkpoint protein Mad1 had been reported in the two-hybrid system (Newman et al., 2000). It is therefore possible that the ubiquitin-binding function of Spc25 might be involved in spindle checkpoint control. To test this hypothesis, spot assays were performed to analyse the sensitivity towards the spindle poison Benomyl, which destabilises microtubules and causes cell cycle arrest at G2/M phase. Mutants of spindle checkpoint proteins, which are not able to arrest the cell cycle properly in response to mitotic stress, are usually sensitive to these drugs. The result showed that none of the ubiquitin-binding deficient mutants were sensitive to Benomyl, suggesting that these mutants did not have defects in spindle checkpoint function (Figure 4.14B).

The next question was if ubiquitin binding might be involved in chromosome segregation. A plasmid loss experiment was performed to quantitatively analyse the difference in maintaining plasmids between Wt and *spc25 (L109A)*. Two different plasmids were used: one had a native version of an autonomous replication sequence (ARS) and the other contained a shorter ARS, which increases the rate of loss (Henry and Silver, 1996). The mutation *spc25 (L109A)* was introduced into the host strain, and the plasmids were transformed into Wt and mutant strains, respectively. The transformants were grown in selective-medium to saturation and diluted to low density

for another 10 generations of growth in non-selective medium. The final cultures were plated on plasmid-selective plates and colonies were counted for quantitative analysis of the proportion of plasmid loss in both strains. There was no significant difference between Wt and the *spc25 (L109A)* mutant in the rate of plasmid loss, while an increased plasmid loss was observed for the plasmid with a shortened ARS (Figure 4.14C). These data indicated that *spc25 (L109A)* did not have significant defects in plasmid segregation, which was consistent with the observation from a previous experiment that mutant cells were not sensitive to the spindle poison benomyl. Therefore, it is likely that ubiquitin binding is not required for the role of Spc25 in chromosome segregation.

In summary, cells harbouring the ubiquitin-binding deficient *spc25* allele were still able to survive, and the loss of ubiquitin binding did not seem to cause any gross problems in spindle checkpoint control or chromosome segregation.

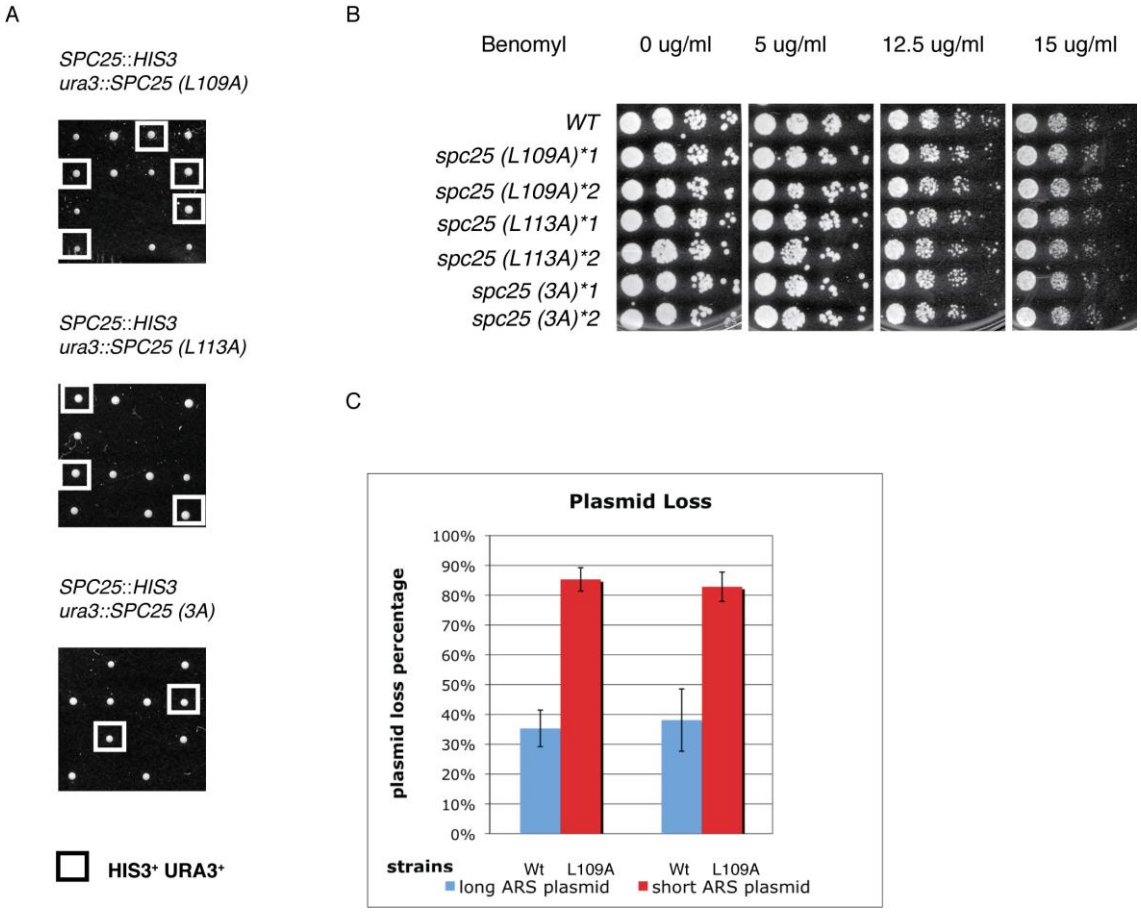

Figure 4.14 *spc25* ubiquitin-binding deficient mutants do not show spindle checkpoint or plasmid segregation defects

(A) Four viable spores resulted from tetrad dissection of *spc25 (L109A)*, *spc25 (L113A)* and *spc25 (3A)* heterozygotes. Mutant *spc25* alleles *(L109A, L113A and 3A)* were integrated into the *URA3* locus in Wt diploid cells after deletion of one copy of *SPC25* by introducing a *HIS3* marker, and the heterozygotes were sporulated at 25℃, followed by tetrad dissection. The distribution of markers for surviving spores was determined by replicating plates onto –His or –Ura selective plates. The desired *spc25* mutant spores were selected as *HIS3*$^{+}$-*URA3*$^{+}$ and labelled in white squares. Mutants were further analysed by sequencing the products from colony PCR of the *SPC25* gene. (B) Sensitivities of indicated strains to benomyl were determined by spot assays. Two different colonies (named *1 and *2) from each strain were analysed here. (C) Plasmid loss experiments were performed by transferring saturated overnight cultures carrying the indicated plasmids from selective medium into YPD medium for 10 generations and plating equivalent numbers of cells on selective and YPD plates. Frequencies of plasmid loss were calculated from the number of colonies on selective plates and YPD plates. The error bars represent standard deviations derived from a set of triplicate experiments.

4.7 Components of the Yeast Kinetochore Complex Are Ubiquitylated

The initial approaches to analyse the function of ubiquitin binding in Spc25 were rather disappointing, as *spc25* ubiquitin-binding deficient mutants had normal growth, a normal spindle checkpoint response and proper chromosome segregation. It was therefore decided to take a systematic approach to look for ubiquitylated potential interactors of Spc25. The ubiquitylated proteins that are recognised by the ubiquitin-binding domain of Spc25 might most likely be found among other kinetochore components that localise in the vicinity of Spc25. A simplified model of yeast kinetochore components is shown in Figure 4.15. A list of candidate proteins that associate with Spc25 was created to look for ubiquitylation among these candidates (Figure 4.15). A number of studies have used different techniques to suggest several potential interaction partners for Spc25. The MIND complex (Mtw1, Nnf1, Dsn1 and Nsl1) and the COMA complex (Ctf19, Okp1, Mcm21 and Ame1) were proposed to be associated with Spc25 from interaction studies based on yeast two-hybrid analysis and approaches involving co-purification and mass spectrometry (Nekrasov et al., 2003, De Wulf et al., 2003). An *in vitro* reconstituted KMN (KNL-1/Spc105, Mis12/MIND complex and Ndc80 complex) network using purified proteins suggested a direct interaction between Spc25-Spc24 and the MIND complex components (Cheeseman et al., 2006). The Ndc80 complex itself, and the MAD proteins were also included in the list of potential interactors of Spc25 because physical association or functional links suggested possible direct interactions between Spc25 and the later (Newman et al., 2000, Ohkuni et al., 2008, Janke et al., 2001). Several recent reports, where authors used fluorescent microscopy to determine the relative positions of many kinetochore proteins in nanometer accuracy (Joglekar et al., 2009, Wan et al., 2009), also helped to further optimise the list of potential interactors of Spc25. Not all kinetochore components shown in Figure 4.15 were included in the list of potential interactors. For instance, the Dam1 complex and the CBF3 complex were not included in the initial list because there was no evidence to indicate a direct association between these complexes and Spc25. Furthermore, some of these complexes were not even included in studies using fluorescent microscopy to map relative positions of kinetochore proteins, suggesting they are less likely to be closely associated with Spc25 (Joglekar et al., 2009,

Wan et al., 2009). The final list of potential interactors of Spc25 contains the components of the MIND complex, the COMA complex, the Ndc80 complex and Mad1-3.

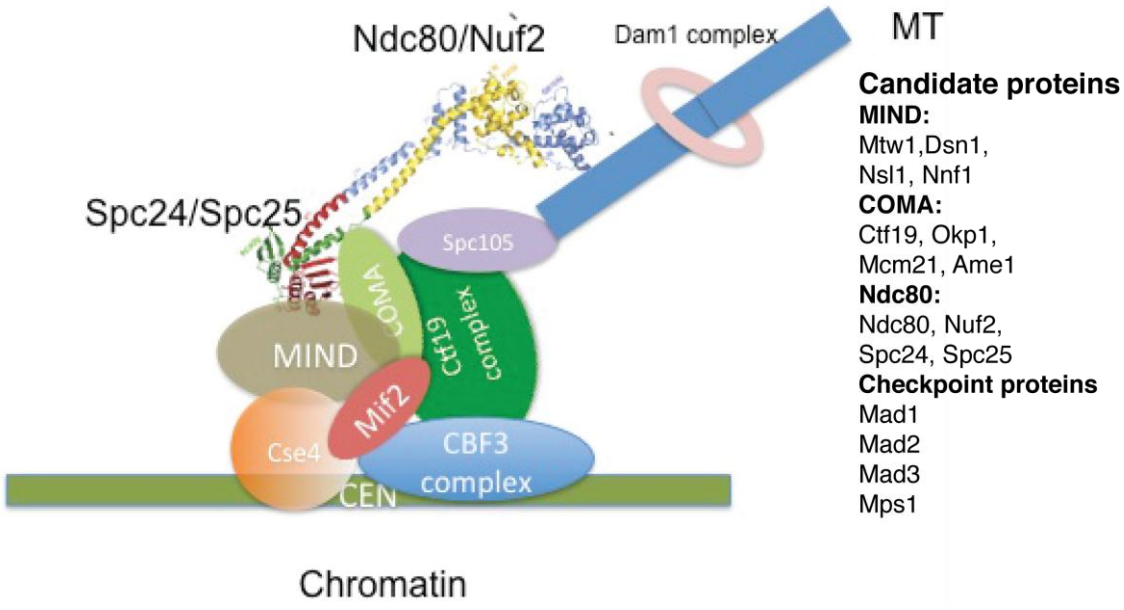

Figure 4.15 The kinetochore of *S. cerevisiae* and a list of potential Spc25 interactors for testing ubiquitylation *in vivo*
A model shows our understanding on the structure and composition of the kinetochore in *S.cerevisiae*. CEN: centromere (green bar), MT: microtubule (blue bar); Spc24/Spc25 subcomplex (green/red crystal structure) is facing towards the centromere and in close contact with other central kinetochore proteins. CBF3 complex is shown as blue oval, Cse4 nucleosome is coloured in orange. Mif2 is in red; the MIND complex is in brown; the COMA complex is in light green; the rest of the Ctf19 complex is in green; the Spc105 complex is in purple and the Dam1 complex is in pink. A list of potential Spc25 interactors includes all candidate proteins tested in subsequent experiments for ubiquitylation *in vivo*.

To find out whether any of these potential Spc25 interactors are ubiquitylated, each single protein within the list was directly analysed for ubiquitylation. Taking advantage of the TAP-tagged yeast strain library, strains harbouring C-terminally TAP-tagged alleles of the respective genes were obtained. An expisomal plasmid expressing His-tagged ubiquitin under control of the copper-inducible *CUP1* promoter was transformed into these strains, and total ubiquitin conjugates were isolated by Ni-NTA beads under denaturing conditions (Ulrich and Davies, 2009). Finally, the pull-down samples were

analysed on western blots with TAP tag-specific antibody. With this approach, the sixteen factors were screened, and among those many proteins were indeed found to be ubiquitylated, but to different extents (Figure 4.16). First of all, MIND complex subunit Dsn1 was found to be strongly ubiquitylated. A band representing the ubiquitylated form of Dsn1 in the lane labelled Dsn1 P (pull-down) migrated more slowly than the unmodified form in the lane Dsn1 I (input). Based on the observed shift in molecular weight, the modified Dsn1 was mainly monoubiquitylated (Figure 4.16A). In contrast, the MIND subunits Mtw1 and Nnf1 were only weakly ubiquitylated with the modified forms barely visible in the lane of pull-down (Figure 4.16A). Mcm21, Okp1 and Ame1, members of the COMA complex, were all polyubiquitylated (Figure 4.16B), but Ctf19 was not ubiquitylated (Figure 4.16C). Within the complex of Ndc80, only very weakly modified species were detected in Spc24, Spc25 and Nuf2 (Figure 4.16C and 4.16D). Spindle checkpoint protein Mad1 was strongly ubiquitylated in this experiment; Mad2 was also ubiquitylated, but not Mad3 (Figure 4.16E). Mps1 was also found to be polyubiquitylated (Figure 4.16D). Noticeably, there were some non-specific bands shown in the control blot for cells without His-tagged ubiquitin (Dsn1, Okp1, Spc25, Ndc80 and Mps1). Similar bands also appeared in the samples from Ni-NTA pull-down (P lanes), but the intensity was not comparable with the ubiquitylated species. Those bands with molecular weights equivalent to the unmodified form of relevant proteins could be results of non-specific stickiness of those TAP-tagged proteins to the beads. To summarise, many kinetochore proteins and spindle checkpoint proteins were modified by ubiquitin to different levels.

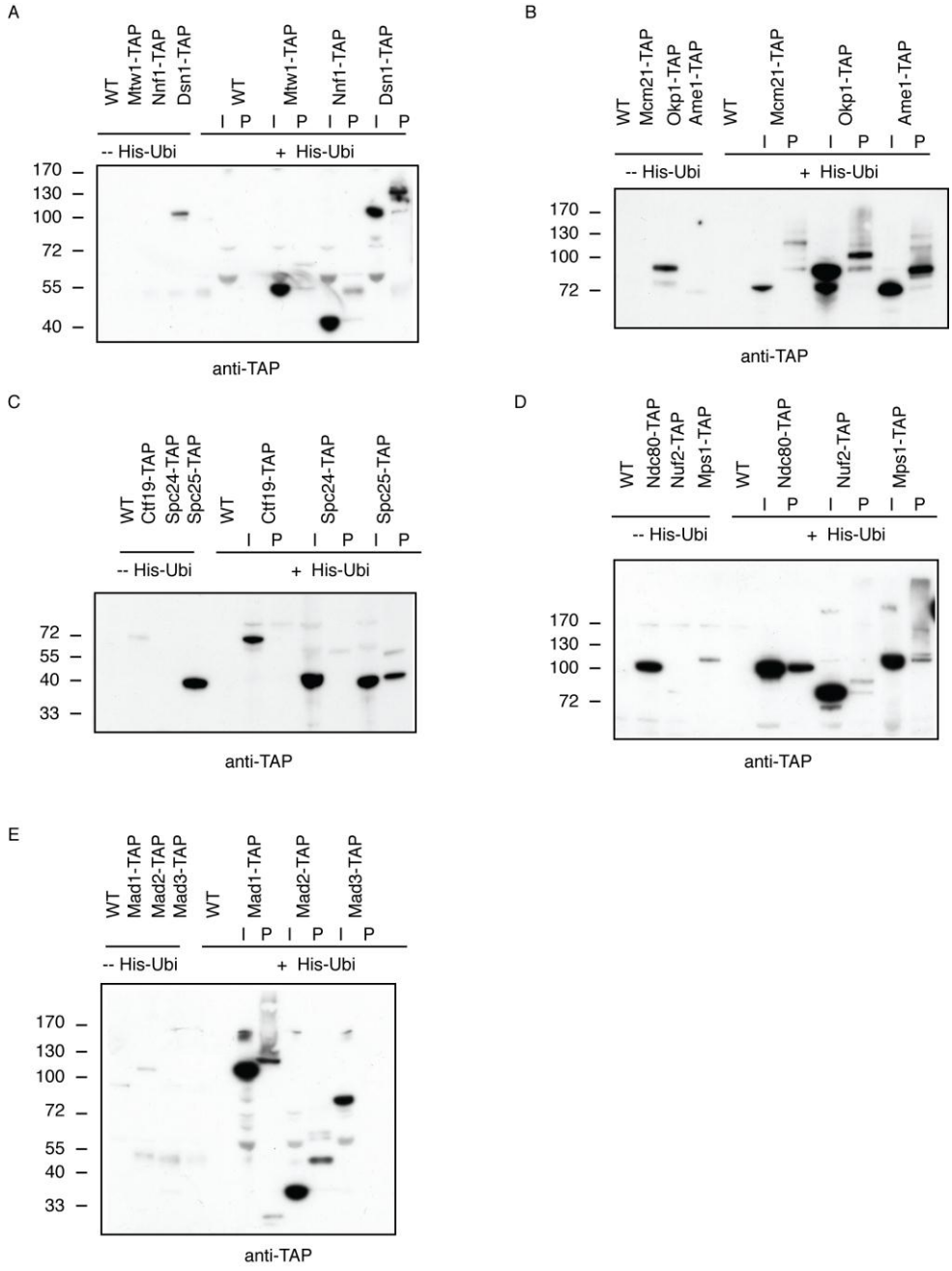

Figure 4.16 *In vivo* ubiquitylation of kinetochore components
Cells harbouring TAP-tagged alleles of the indicated genes were transformed with either a plasmid expressing His-tagged ubiquitin or an empty plasmid. The expression of His-tagged ubiquitin was under control of the copper inducible *CUP1* promoter, and His-tagged ubiquitin was overepxressed by addition of copper to the growth medium in those cells. Total ubiquitin conjugates were isolated by Ni-NTA pull-down under denaturing conditions, and samples were analysed by Western blot with an anti-TAP antibody. Pull-down samples (P) were loaded next to the total cell extract (I) and a shift of molecular weight in (P) compared with (I) indicated ubiquitylated forms of target proteins. (A)-(E) Western blot analysis for samples from denaturing pull-down of the MIND complex, the COMA complex, the Ndc80 complex, Mps1 and MAD1-3.

However, these experiments were performed in yeast cells overexpressing His-tagged ubiquitin. While these elevated ubiquitylation signals made detection easier, it might also introduce some false positive results. The weak modification signals from some candidate proteins could be due to these artefacts. Therefore, similar experiments were performed to confirm some of the most promising ubiquitylation events in cells with an ubiquitin level close to the endogenous level. Dsn1, Mcm21 and Mad1 were first analysed because they were strongly ubiquitylated in the initial screen and had the most promising physical or genetic interaction data supporting a link with Spc25. For this purpose, the *CUP1* promoter was not induced, with the result that the basal expression of His-tagged ubiquitin in the absence of copper was enough to isolate ubiquitylated species via Ni-NTA pull-down, while maintaining an ubiquitin level comparable to the endogenous situation (Figure 4.17A). This assay confirmed the monoubiquitylation of Dsn1, the polyubiquitylation of Mcm21, but not much modification for Mad1 (Figure 4.17B). Although there was non-specific binding of unmodified Dsn1 on the beads in the pull-down sample, a similar band migrating at the same molecular weight was seen in the parallel control experiment, where cells did not contain the plasmid expressing His-tagged ubiquitin. However, enrichment of the ubiquitylated form compared with the non-specifically binding species indicated that Dsn1 was really monoubiquitylated.

Overall, by this approach, I found that many proteins within the kinetochore complex or close to the kinetochore appeared to be ubiquitylated *in vivo*. I focused on three potential targets, Mcm21, Mad1 and Dsn1, whose modification appeared strongest in the initial experiments, and further confirmed the observed modifications for Mcm21 and Dsn1 with a ubiquitin level close to the endogenous one. Because Dsn1 was monoubiquitylated and Mcm21 was polyubiquitylated, an overall non-specific ubiquitylation as a general modification among the kinetochore components is unlikely. Instead, it appears more probable that the modifications are specific regulatory events for the respective target proteins. Preliminary immunoprecipitation assays have confirmed the association of Mcm21 and Dsn1 with Spc25 (data not shown), and previous studies have reported very similar outcomes (Wan et al., 2009, Nekrasov et al.,

2003, De Wulf et al., 2003). All of those put forth Mcm21 and Dsn1 as very attractive candidates with a possible relevance for the function of ubiquitin binding in Spc25.

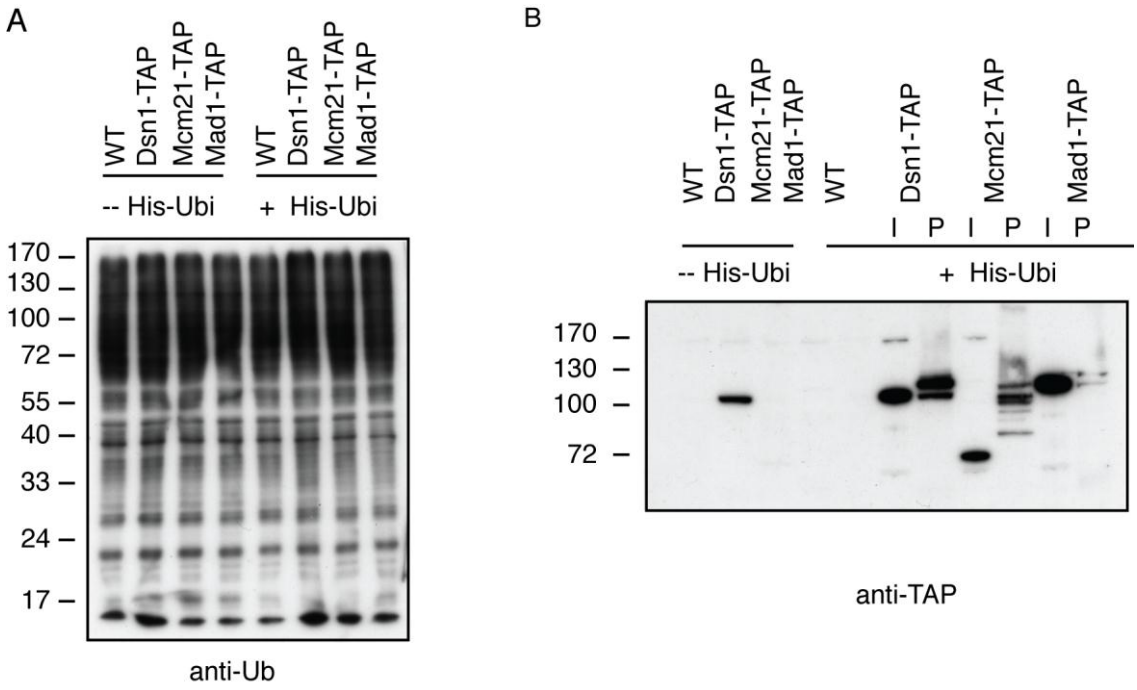

Figure 4.17 *In vivo* ubiquitylation of Dsn1 and Mcm21 at native ubiquitin levels
(A) Cells harbouring TAP-tagged alleles of the indicated genes were transformed with either an empty plasmid or a plasmid expressing His-tagged ubiquitin, and grown in the absence of copper. The basal activity of the *CUP1* promoter results in residual amounts of His-tagged ubiquitin useful for pull-down assays. The total cellular ubiquitin conjugates, detected by Western blots with an anti-ubiquitin antibody, indicate no significant increase in total ubiquitin levels in the absence of the His-tagged construct. (B) Ni-NTA denaturing pull-down as described in Figure 4.16. TAP-tagged proteins were detected by Western blots with an anti-TAP antibody.

4.8 *SPC25 (L109A)* Is Sensitized to Kinetochore Destabilisation

As Mcm21 was found to be polyubiquitylated in the previous pull-down experiment looking for ubiquitylated species, its potential link with the ubiquitin-binding function of Spc25 was further investigated. Mcm21 is a subunit of the COMA complex, which consists of Ctf19, Okp1, Ame1 and Mcm21 (Ortiz et al., 1999). The COMA complex was shown to co-purify with the Ndc80 complex (De Wulf et al., 2003). In an initial attempt to confirm an association of Mcm21 with Spc25 *in vivo* by co-

immunoprecipitation, it was noticed that a combination of *spc25 (L109A)* with *MCM21-GFP* (Mcm21 tagged with GFP at its C-terminus) caused slow growth of the cells. Based on these interesting initial observations, an experiment was performed to monitor the growth of strains including Wt, *spc25 (L109A)*, *MCM21-GFP* and *spc25 (L109A) MCM21-GFP* in parallel. After an overnight incubation of all strains, cultures were diluted and the cell density was then monitored spectrophotometrically at OD_{600}. In this experiment, *spc25 (L109A)* or *MCM21-GFP* alone showed a growth rate almost identical to Wt cells. In contrast, introducing the *spc25 (L109A)* mutation into the *MCM21-GFP* strain significantly reduced the growth rate (Figure 4.18A). This result demonstrated that the ubiquitin-binding deficient *spc25* allele caused a growth defect in a situation where the kinetochore complex was sensitised to destabilisation by a big epitope tag such as GFP on a protein within the complex. This result was also consistent with an earlier observation that a different *SPC25* allele, *spc25-7,* showed increased temperature sensitivity in combination with *mcm21Δ* (Janke et al., 2001).

Mutants in *DSN1,* encoding the second ubiquitylation target within the kinetochore complex, had already been shown to share some phenotypes with *spc25* mutants such as the failure of chromosomes to attach one pole and the activation of the spindle checkpoint (Nekrasov et al., 2003). Therefore, a potential genetic relationship between *dsn1* mutants and the *spc25 (L109A)* allele was examined. Two temperature-sensitive alleles, *dsn1-7* and *dsn1-8* (Nekrasov et al., 2003), were crossed with *spc25 (L109A)*, and growth of the resulting double mutants was monitored at different temperatures.

While *spc25 (L109A)* did not show any temperature sensitivity, the *dsn1-7* mutant started to show temperature sensitivity at 30 ℃ and completely ceased to grow at 33 ℃. The double mutant of *dsn1-7 spc25 (L109A)* had a slightly increased temperature sensitivity with severe growth inhibition already at 30 ℃ (Figure 4.18B). For the *dsn1-8* mutant, a more dramatic effect was observed. While *dsn1-8* alone did not show much sensitivity below 35 ℃, the double mutant *dsn1-8 spc25 (L109A)* showed impaired growth at 31 ℃ (Figure 4.18B). Both results were consistent and together suggested a

genetic interaction between *DSN1* and the ubiquitin-binding function of *SPC25*. In this case, again *dsn1* temperature sensitive mutants represented a destabilized kinetochore complex, and under this condition the *spc25 (L109A)* mutation further sensitised the cells. Together with the synthetic growth defect observed with *MCM21-GFP* previously, these data indicate that *spc25 (L109A)* sensitises a pre-destabilised kinetochore complex, suggesting that ubiquitin binding of the Spc25 might positively contribute to the stability of kinetochore.

It is formally possible that the L109A mutation might result in destabilisation of the protein, which in turn contributes to the observed phenotype that I proposed to be a result of ubiquitin-binding defects. To address this concern, the protein levels of Spc25 (L109A) and Spc25 Wt were analysed. A 9myc-tag was introduced to the C-terminus of SPC25 at the genomic locus to detect the protein and Spc25 (L109A)-9myc showed a protein level very similar to the tagged Wt protein (Figure 4.18C). Together with the fact that Spc25 (L109A) interacts with Spc24, I considered the idea that L109A mutation destabilises Spc25 less likely.

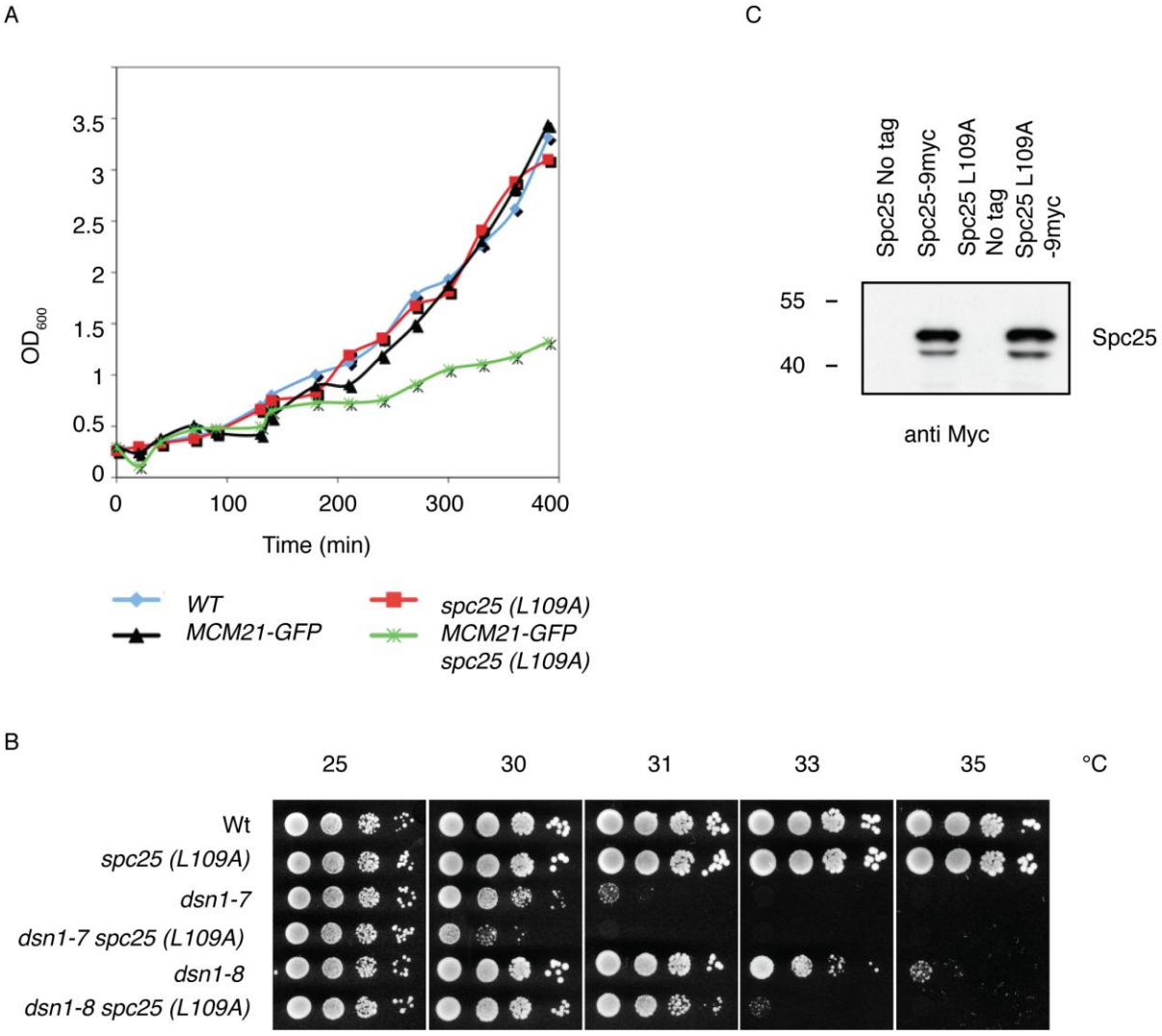

Figure 4.18 *Spc25 (L109A)* is sensitised to kinetochore destabilisation
(A) Growth of the indicated strains was monitored by spectrophotometrically measuring cell density at 600 nm. Overnight cultures, grown at 30 ℃, were diluted to OD_{600}=0.2, and growth of the cultures was measured by means of the OD_{600} plotted against the time. (B) Temperature sensitivities of the indicated strains were determined by spotting serial dilutions onto YPD plates and incubation for 3 days at different temperatures. (C) Protein levels of Spc25 Wt and the L109A mutant were analysed by Western blot with an anti-myc antibody. A 9myc-tag was introduced to the C-terminus of SPC25 at its genomic locus.

4.9 Discussion

A yeast two-hybrid screen was performed to identify potential interactors of polyubiquitylated PCNA and other ubiquitin-binding factors. This screen did not identify any proteins specifically associated with polyubiquitylated PCNA, but identified Spc25 as a novel ubiquitin-binding factor. The ubiquitin-binding properties of Spc25 were further characterised, and a C-terminal region (amino acids 107-221), which consists of the entire globular domain preceeded by a flexible extension from the N-terminus of the domain, was identified as the minimal region required for interacting with ubiquitin. I also found a mutation, L109A, that abolishes ubiquitin binding by Spc25. Most interestingly, cells containing the *spc25 (L109A)* allele were sensitised to kinetochore destabilisation. While these observations provided evidences that ubiquitin-mediated signalling could play a role in the kinetochore, more questions were raised in the course of my study and remain to be answered.

4.9.1 The two-hybrid screens did not identify factors specifically associated with polyubiquitylated PCNA

A yeast two-hybrid screen was performed using $Ub^{*}_{(3-4)}$ (L)-$PCNA^{*}$ and Ub^{*}_{4} -$PCNA^{*}$ to identify factors specially associated with polyubiquitylated PCNA. The result was rather disappointing, and there are several possible reasons for the failure. First of all, PCNA is trimerised and loaded onto DNA *in vivo* for its proper function during replication and post-replicative repair process. For example, PCNA loading onto DNA stimulates the SUMOylation reaction of PCNA *in vitro* and *in vivo* (Parker et al., 2008), suggesting that loaded PCNA presents a conformation different from the unloaded one. There are more than twenty known PCNA interaction partners (Moldovan et al., 2007), and only Srs2 was found in the parallel control screen, suggesting the screen was not effective for identifying PCNA interactors. It is likely that many PCNA interactors do not bind PCNA in its monomeric form, which would be localised to DNA through its fusion to the DNA-binding domain of Gal4 transcription factor. A second approach using $^{GST}Ub^{*}_{4}$ -$PCNA^{*}$ to pull down interactors in total yeast extract was not very successful either. More known PCNA-binding proteins were found this time. However,

the majority of the known PCNA interactors were still missing. In this case, $^{GST}Ub^{*}_{4}$-PCNA* were densely presented on the surface of glutathione beads and it is unknown how well the protein would form trimers under these conditions. Secondly, it is also formally possible that the constructs do not fully resemble polyubiquitylated PCNA. This could be due to the combination of an imperfect chain mimic with an imperfect modification site. Although K63-linked polyubiquitin chains are able to support DNA damage bypass at the N-terminus of PCNA, this modification site is not physiological. Once this imperfect modification site combined with linear ubiquitin chain, an imperfect mimic of K63-linked chain, factors normally bind to K63-polyubiquitylated PCNA are less likely to bind the fusion constructs. Indeed my genetic analysis in Figure 3.5 has shown that $Ub^{*}_{(3-4)}$(L)-PCNA* and Ub^{*}_{4}-PCNA* are not functional in the error-free branch of the *RAD6* pathway. Therefore, factors specifically bound to the polyubiquitylated PCNA do not recognise the constructs. However, at the time we performed the two-hybrid screen, the genetic data from the rescue experiment were not available, which would otherwise influence our decision on conducting this screen using such imperfect mimics. Nevertheless, $Ub^{*}_{(3-4)}$ (L)-PCNA* did function in translesion synthesis, yet failed to isolate even factors involved in translesion synthesis, suggesting that an inappropriate mimic may not be the only reason for the failure of the screen. Theoretically, the best approach would be immunoprecipitating PCNA from cells with or without UV irradiation. Co-purified proteins could then be determined by mass spectrometry. However, this approach may not be suitable for PCNA because the polyubiquitin chains on PCNA are quickly trimmed by deubiquitinases in the cell extract during the experiment. Ub^{K63*}-PCNA* has been shown to rescue the UV sensitivity of *rad18* strain by both branches of DNA damage bypass. Isolating Ub^{K63*}-PCNA* in UV treated cells in comparison with Ub^{*}-PCNA* may identify some co-purified factors specific for polyubiquitylated PCNA. The deubiquitylation enzyme targeting K63-polyubiquitylated PCNA may not work effectively on polyubiquitylated Ub^{K63*}-PCNA* and there is high chance to preserve the modification. Alternatively, a genetic screen to identify factors that suppress the TLS-independent rescue effect would be helpful. Additionally, a recent study showing a split ^{Ubi}PCNA with an N-terminal fragment (amino acids 1-163) and a ubiquitin moiety fused C-terminal fragment (ubiquitin + amino acids 164-258) can self-assemble and function as monoubiquitylated

PCNA to support cell viability and translesion synthesis (Freudenthal et al.). This is a very attractive tool and it is definitely worth investigating whether a split PCNA with a polyubiquitin chain attached to its K164 would support the error-free branch of DNA damage tolerance. If that is the case, these constructs would be a great tool to isolate factors specifically bound to polyubiquitylated PCNA.

4.9.2 The interaction between Spc25 and ubiquitin

Spc25 did not detectably interact with monoubiquitin in a two-hybrid experiment (Figure 4.6 and 4.7B), but the purified Spc25 C-terminal region (amino acids 107-221) together with the globular domain of Spc24 could bind to monoubiquitin *in vitro* (Figure 4.9D and 4.10). This observed discrepancy between two-hybrid based data and *in vitro* data could be due to intrinsic limitations of the experimental methods. The yeast two-hybrid system is sometimes not sensitive enough to detect weak interactions. The dissociation constant for Spc25 binding to monoubiquitin was determined to be around 14.2 μM, which was relatively strong compared to various other UBDs, but should still be considered as a weak protein-protein interaction. Furthermore, ubiquitin is mainly present as a monomer in yeast cells (Xu et al., 2009) and the concentration of free ubiquitin in the cell is also within the micromolar range (2-20 μM) (Ikeda and Dikic, 2008), which makes *in vivo* detection of monoubiquitin binding quite difficult. In contrast to the *in vivo* situation, the concentration of ^{GST}Ub in an *in vitro* pull-down experiment was around 300 μM, which makes the interaction between Spc25 and monoubiquitin much easier to detect. Under these conditions a positive interaction was indeed detected between tetraubiquitin and Spc25 by two-hybrid analysis because the overall apparent affinity towards Spc25 was high. In this case, multiple binding sites close to each other on tetraubiquitin may result in an "avidity" effect rather than an increase in the individual affinity constants.

Spc25 was initially identified to interact with Ub^*_4(L), but not Ub^*_4 in the yeast two-hybrid screen and subsequent assays (Table 4.1, Figure 4.6). However, it was capable of

interacting with both types of linear tetraubiquitin chains in an *in vitro* pull-down experiment (Figure 4.9D) and an SPR experiment (Figure 4.10C). Furthermore, I was not able to detect an interaction between Spc25 and K48- or K63-linked polyubiquitin chains in pull-down experiments (data not shown). These observations raised the question if Spc25 was able to bind polyubiquitin chains *in vivo*. In the yeast two-hybrid system, Spc25 showed a selective binding to Ub^*_4(L) but not Ub^*_4, which could be due to an interaction with Ub^*_4 below the detection limit. Although pull-down experiments showed a similar picture for Ub^*_4(L) and Ub^*_4, the BIACORE experiment did reveal a stronger binding to Ub^*_4(L) (Figure 4.10C). Therefore, Spc25 interacts with Ub^*_4(L) better. The most straightforward explanation is that the linker version of tetraubiquitin can be more regarded as a loose collection of four individual monoubiquitin units, and the binding of Spc25 to this arrangement is therefore a lot better than to monoubiquitin. The linker-less version is more densely packed, and ubiquitin moieties within the chain may not be easily accessible by Spc25. In this case, the distal ubiquitin resembles a free accessible monoubiquitin, and therefore it can still bind to Spc25. The pull-down experiment with K48-/K63-linked chains was performed with ^{GST}Spc25/^{6His}Spc24 immobilised on glutathione beads and specifically linked $ubiquitin_{(2-7)}$ chains free in binding solution. This condition was different from the way tetraubiquitin/Spc25 interaction studies were performed. In such a condition, an experiment testing the interaction between Spc25 and monoubiquitin has not been performed either. These preliminary data from separate experiments performed in different ways were not enough to draw a conclusion. Currently, there is no direct evidence showing that Spc25 can interact with natural polyubiquitin chains. Therefore, I favour the idea that Spc25 is a monoubiquitin-binding protein.

4.9.3 A binding model for Spc25 interacting with ubiquitin

The ubiquitin-binding region (amino acids 107-221) of Spc25 consists of a complete globular domain and a flexible region extended from the N-terminus of the globular domain. From two-hybrid based truncation analysis it is clear that the globular domain alone (amino acids 133-221) was not enough for ubiquitin binding (Figure 4.8A) and

the N-terminus of the protein (amino acids 1-133) excluding the globular domain was not sufficient either (Figure 4.12B). Mutations within the flexible region L109A and L113A either completely or partially abolished ubiquitin binding, suggesting that this region made a direct contact with ubiquitin. Removal of the globular domain of Spc25 also abolished the ubiquitin-binding but did not interrupt its N-terminal coiled-coil region forming a heterodimer with Spc24 (Figure 4.12B), suggesting another yet unidentified ubiquitin-contacting surface within the globular domain. Based on that information, Spc25 might interact with ubiquitin in a way as shown in Figure 4.19.

Spc24 also appears in the model and its role in ubiquitin binding of Spc25 is likely rather indirect. First of all, Spc24 does not bind to ubiquitin in the yeast two-hybrid experiment (Figure 4.8), suggesting a direct interaction between these two is less likely. During the purification of ^{6His}Spc25(C), the protein was not stable in solution without Spc24. Therefore it is more likely that Spc24 is required to form a stable heterodimer with Spc25 *in vitro*. However, it is difficult to fully exclude the possibility that Spc24 may contribute to the ubiquitin binding. A structural study of Spc24/Spc25 in complex with ubiquitin could provide further information on if there is any ubiquitin-contacting site on Spc24.

The identification of L109 as a crucial residue for ubiquitin binding of Spc25 is quite important for further characterisation of the biological function. The initial clue was from a sequence alignment analysis of the flexible linker region (amino acids 107-133) from different organisms (Figure 4.12A). L109 was one of the most conserved residues within that flexible region and the L109A mutation abolished ubiquitin binding of Spc25 completely in a yeast two-hybrid experiment (Figure 4.12B). This approach is based on the fact that Spc25 is an evolutionarily conserved protein and assumes that the ubiquitin binding of Spc25 is also conserved among different species. Therefore, it will be important to provide such evidence. hSpc25 (human Spc25) has been cloned and tested for ubiquitin binding in yeast two-hybrid analysis, but a positive interaction was not detected. Since Spc24 is required to form a stable heterodimer with Spc25, hSpc25

alone may not fold properly. In fact, hSpc25 does not interact with yeast Spc24 in a yeast two-hybrid experiment suggesting yeast Spc24 could not form a heterodimer with hSpc25. To address this problem, hSpc24 needs to be expressed in the same yeast strain together with hSpc25 to test for an interaction with ubiquitin.

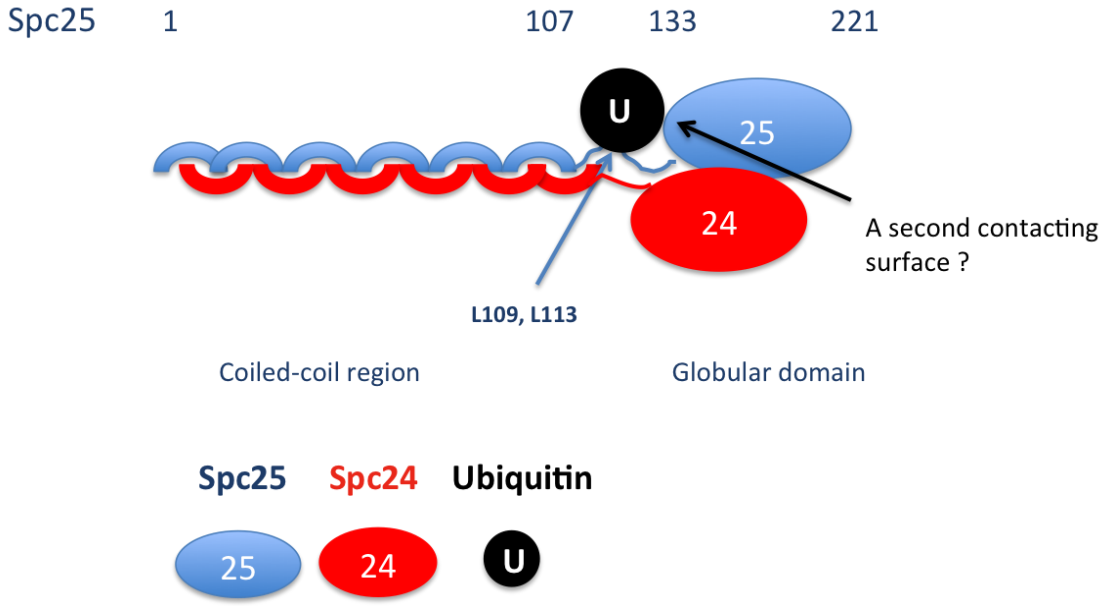

Figure 4.19 A model for Spc25 interacting with ubiquitin
Spc25 (blue) forms a heterodimer with Spc24 (red). Ubiquitin (black filled circle) binds to Spc25 through two contacting surfaces indicated with blue and black arrows. The first contact site indicated with the blue arrow includes residues L109 and L113.

Many UBDs have been identified so far, and they normally have certain structural features that are known to bind ubiquitin, such as α-helical structure, zinc-fingers, the ubiquitin-conjugating domains, pleckstrin homology folds, etc (Hurley et al., 2006, Dikic et al., 2009). Interestingly, Spc25 is an intriguing example for a flexible unstructured region that – together with a compact globular domain – forms an interaction site for ubiquitin. The exact nature of the second contact surface within the globular domain remains unknown, but the globular domain of Spc25 has several α-helices and β-sheets, which are known structural features for ubiquitin binding. It is

therefore not surprising if any of these contribute to ubiquitin binding within the globular domain. It will be interesting to find the second ubiquitin-binding surface within the globular domain of Spc25. Because Spc25 is highly conserved among different organisms, mutagenesis of conserved residues would not be a smart approach. Wei and colleagues determined the NMR structure of the Spc25 globular domain (Wei et al., 2006); it should therefore be feasible to determine the ubiquitin-binding surface of Spc25 by NMR. Additional information from NMR studies should reveal whether the first contact site, which is an unstructured region, would undergo a conformational change or become conformationally constrained once ubiquitin is bound to Spc25.

4.9.4 Ubiquitin-binding and ubiquitylation in the kinetochore complex

Many components of the kinetochore were found to be ubiquitylated to different extents in the candidate-based screen aiming to identify ubiquitylated binding partners of Spc25. Although the initial pull-down experiments were performed with cells overexpressing His-tagged ubiquitin, which may cause some artefacts, not all the proteins in the screen were ubiquitylated and the ubiquitylation signals varied from monoubiquitin to polyubiquitin chains. For example, three proteins (Mcm21, Okp1 and Ame1) within the COMA complex were all ubiquitylated to a similar extent (Figure 4.16B), but Ctf19 within the same complex was not ubiquitylated (Figure 4.16C). Dsn1 was monoubiquitylated whereas Mcm21 was polyubiquitylated (Figure 4.16A and 4.17B). These observations indicated that ubiquitylation might commonly, but specifically occur on kinetochore proteins, not just as an isolated event. In fact there was an early indication that ubiquitylation machinery may have a role in kinetochore structure or function because Ubc4 was found to interact with Spc25 in a two-hybrid analysis (Wong et al., 2007). But the function of the modification remains an open question. Because those modified kinetochore proteins were not analysed further, both proteolytic and non-proteolytic functions for these observed modifications are conceivable. In the case of a proteolytic function, it might be involved in regulating the stability of those relevant kinetochore proteins. Since the kinetochore is assembled on the centromeric region after DNA replication (Santaguida and Musacchio, 2009), the

dynamics of kinetochore proteins may require proteasome-ubiquitin signalling as a regulating mechanism. Analysis of the cell cycle dependence of these ubiquitylation events or the stability of ubiquitylated kinetochore proteins would help us to explore this possibility further. The ubiquitylation events could be occurring preferentially in response to certain stress conditions. The kinetochore complex is involved in microtubule attachment; spindle checkpoint control and many details of these processes are not yet fully understood. Ubiquitylation events could play a role in regulating these events in response to kinetochore stress or spindle poisons. For this hypothesis, identification of the conditions that trigger ubiquitylation would be the first step. On the other hand, ubiquitylation might have a non-degradative role. In this case, other components of the kinetochore or proteins associated with the kinetochore would have ubiquitin-binding domains that specifically bind to the ubiquitylated kinetochore proteins. My observation that Spc25 was able to bind ubiquitin supports this scenario, and there might be other unidentified kinetochore proteins that also have UBDs since ubiquitylation commonly occurs within the kinetochore. A similar observation has been reported for SUMO, as SUMOylation and SUMO-interacting motifs play important roles in recruiting the SUMOylated motor protein CENP-E to the kinetochore in mammalian cells (Zhang et al., 2008). Identification of other ubiquitin-binding factors among the kinetochore proteins would help to reveal in much more detail the mechanism how ubiquitin binding is involved in kinetochore function.

Although many ubiquitylation targets were observed in the kinetochore complex, not all of them may be relevant to the ubiquitin-binding function of Spc25. Further characterisation of those targets is essential. The first approach is to identify and mutate the sites of ubiquitylation on those targets. Mass spectrometry analysis of purified target proteins could help to identify potential ubiquitylation sites. Relevant mutants could then be analysed for phenotypes related to the loss of ubiquitylation, and in such a case fusing ubiquitin at the N- or C-terminus of the mutant protein may be able to rescue that phenotype. In comparison with the phenotypes shown in ubiquitin-binding deficient alleles of *spc25*, a matched phenotype would suggest a link between a target protein and the function of ubiquitin binding in Spc25. An epistatic relationship would be expected

from a ubiquitylation deficient mutant of target gene and the ubiquitin-binding deficient alleles of *spc25*. Through this approach, it might be possible to find the most relevant ubiquitylated protein, which will reveal the function of the ubiquitin-binding domain of Spc25.

In the process of characterising the function of the ubiquitin-binding domain in Spc25, I did not find any phenotype associated with the *spc25 (L109A)* single mutant. However, the plasmid loss assay is not enough to fully exclude the possibility that *spc25 (L109A)* has defects in chromosome segregation. There are different methods that can measure small defects in chromosome segregation. For example, a colony colour assay uses an ochre-suppressing form of a tRNA gene, *SUP11*, as a marker on natural chromosomes (Hieter et al., 1985). In diploid homozygous *ade2* strains, cells carrying no copy of the *SUP11* gene are red, those carrying one copy are pink, and those carrying two or more copies are white. The *SUP11* gene can be integrated into a specific chromosome and the loss frequency of that specific chromosome can be determined based on the colour of sectored colonies. The rate of chromosome loss events per cell division can be calculated. A similar colony colour based assay was also described to monitor mitotic stability of minichromosomes (Koshland et al., 1985). Furthermore, Spc25 (L109A) has not been sufficiently characterised. Although yeast two-hybrid experiments have shown an abolishment of ubiquitin binding for this mutant, the dissociation constant for the interaction between Spc25 (L109A) and monoubiquitin has not been measured. It is possible that the Spc25 (L109A) mutant only has a partial reduction in ubiquitin binding, which would give rise to a binding defect in the yeast two-hybrid system, but possibly not in other phenotypic assays. Therefore, a mutant with a stronger defect in ubiquitin binding might have to be used, and a clear phenotype might then be observed in that mutant.

I also found that *spc25 (L109A)*, was sensitised to the destabilisation of the kinetochore (Figure 4.18). Considering the fact that *spc25 (L109A)* alone did not show any defects in cell cycle progression or the spindle checkpoint response (Figure 4.14), an alternative

possibility was that ubiquitin binding might have a function to facilitate a stable association of the kinetochore complex. The Spc25-Spc24 dimer has been shown to associate with the MIND complex (Wan et al., 2009, Cheeseman et al., 2006). In this scenario, ubiquitylated MIND complex components would bind to the ubiquitin-binding protein Spc25, and my data suggested that Dsn1 is monoubiquitylated (Figure 4.17). Consistently, Dsn1 co-purifies with Spc25 as shown by Nekrasov and colleagues (Nekrasov et al., 2003) and my Co-IP experiment (data not shown). More interestingly, the distance between Spc25 and Dsn1 is around 2 nm, which is the shortest among the distances of all the components of MIND complex to Spc25 (Wan et al., 2009). Therefore, a working model for this scenario is that Spc25 binds monoubiquitylated Dsn1 in two ways, including a direct binding of Spc25 to Dsn1, and a direct interaction between Spc25 and the monoubiquitin attached to the Dsn1 (Figure 4.20). The s*pc25 (L109A)* mutation would only have a minor negative effect on this association and therefore would not exhibit any defective phenotype in isolation. A preliminary Co-IP experiment was performed to analyse the association of Dsn1 to either wild type or the L109A mutant of Spc25 and I did not observe any significant changes (data not shown). However, a combination of *dsn1 ts* mutants and *spc25 (L109A)* may have a severe negative effect on the association of Spc25 and Dsn1 and enhanced temperature sensitivity was observed. If this model were true, I would expect to see reduced association between Dsn1 and Spc25 in *dsn1-8 spc25 (L109A)* cells compared with *dsn1-8* or *spc25 (L109A)* single mutant cells. In addition to that, the growth defect observed when an *spc25 (L109A)* mutant was combined with C-terminal GFP-tagged *MCM21* could be a result of accumulation of defects in the kinetochore. This observation was also consistent with a genetic interaction that *spc25-7 mcm21Δ* shows increased temperature sensitivity compared with the *spc25-7* single mutant (Janke et al., 2001). Mcm21 is a subunit of the COMA complex. Although the distance between Mcm21 and Spc25 is not known, the distance between other COMA complex components and Spc25 is around 13-16 nm. The close association of the COMA complex with Spc25 would explain the synthetic growth defect and increased temperature sensitivity.

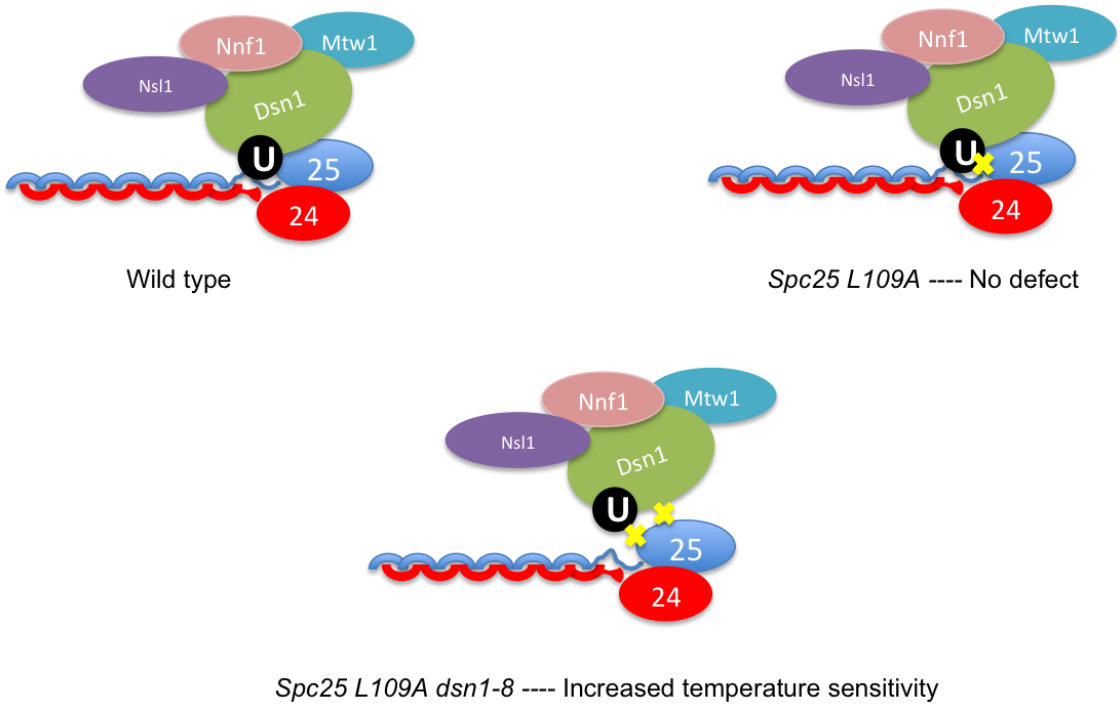

Figure 4.20 A model for Spc25 interacting with monoubiquitylated Dsn1
The Spc25-Spc24 dimer (blue and red) associates with the MIND complex (Nsl1, Nnf1, Mtw1 and Dsn1). Dsn1 is the subunit closest to Spc25 (Wan et al., 2009, Joglekar et al., 2009) and is monoubiquitylated (black filled circle). In addition to the association between Spc25 and Dsn1, ubiquitin may create an extra binding surface for Spc25. In the *spc25 (L109A)* mutant, the interaction between Spc25 and ubiquitin is abolished (yellow cross), but the association between Spc25 and Dsn1 remains stable through a direct contact between Dsn1 and Spc25. In the *spc25 (L109A) dsn1-8* double mutant, in addition to abolished ubiquitin binding, the Spc25-Dsn1 interaction is also reduced (yellow crosses).

There are still alternative scenarios that I cannot rule out. First of all, it is possible that another ubiquitylated kinetochore protein, rather than Dsn1 and Mcm21, can directly bind to Spc25. In this case, an accumulation of general kinetochore stress from loss of ubiquitin binding by Spc25 (L109A) in *dsn1* temperature sensitive mutant strains or cells with *MCM21* GFP-tagged at the C-terminus could also result in the phenotypes described. To address this issue, it would be necessary to make a number of mutants in other kinetochore components in combination with *spc25 (L109A)*. Phenotypic analysis of these mutants would allow us to distinguish whether the observed synthetic defects are specific for *MCM21-GFP* and *dsn1 ts* mutants or more general for anything that destabilises the kinetochore. Secondly, although the interaction of Spc25 (L109A) with

Spc24 in the yeast two-hybrid assay suggested that the mutation did not affect the structure of the protein, I cannot exclude the possibility that this mutation causes a partial instability of Spc25, which in turn contributes to the observed phenotypes related to kinetochore stability. However, Spc25 (L109A) showed a protein level very similar to the Wt Spc25 (Figure 4.18C), suggesting that the mutant protein is unlikely to be destabilised. A useful approach to rule out this possibility would be replacing the flexible linker domain (amino acids 107-133) in Spc25 (L109A) with another UBD and analysing if this could rescue the loss of ubiquitin binding in *spc25 (L109A)* cells. On the other hand, this experiment might not be suitable because Spc25 is an essential protein. Although the globular domain and coiled-coil region remain intact, the geometry of the new linker may also give phenotypes. The best solution would be a biophysical study directly comparing the Wt and L109A mutant forms of Spc24/Spc25 to rule out any structural defects.

4.9.5 Future directions

Overall, there are some remaining questions on the interaction between Spc25/Spc24 and ubiquitin: 1) Where is the second ubiquitin contacting surface on Spc25? 2) Are there conformational changes at the flexible region induced by ubiquitin binding? 3) Are there potential ubiquitin contacting sites on Spc24? 4) Does Spc25 (L109A) have any structural defects? The answers to those questions would come from a structural study of Spc25/Spc24 in complex with ubiquitin. NMR would be a most efficient and effective approach because the NMR structure of Spc25/Spc24 globular domains and ubiquitin are both available. X-ray crystallography is an alternative option, which gives a much more refined picture about the interaction at an atomic level, but might take longer than the NMR approach. The structural information would also allow us to make a mutant of Spc25 completely defective in ubiquitin binding. Subsequent characterisation of phenotypes, which includes all the aspects currently analysed for *spc25 (L109A)*, would help to propose a better model showing the function of the ubiquitin-binding domain in Spc25.

To investigate if ubiquitylation of Mcm21 and Dsn1 is relevant to the ubiquitin-binding function of Spc25, identification of the ubiquitylation sites and the E3 ligase responsible for the modification would be the first step. For a better understanding of the modification, it will be interesting to find out if the ubiquitylation events are constitutive, cell cycle dependent, or induced by certain stress conditions. The regulation of the ubiquitylation is also important for understanding the actual biological function of the modification. Dsn1 is monoubiquitylated and Mcm21 is polyubiquitylated, the linkage of the polyubiquitin chain and the identity of the relevant DUBs are waiting to be discovered. Mutants in other kinetochore proteins, such as other members of the MIND complex or the COMA complex, should also be analysed for a synthetic effect when combined with the *spc25 (L109A)* allele.

Last but not least, it is a very attractive idea that the ubiquitin-binding function of Spc25 would be evolutionarily conserved in different organisms. An analysis to confirm such an interaction in mammalian systems would be the first step. Some preliminary work has been done to generate hSpc24, hSpc25 constructs and an interaction with ubiquitin can be tested in yeast two-hybrid and *in vitro* pull-down experiments. If an interaction can be confirmed, it will be very exciting to identify its function in the context of mammalian cells because despite a high degree of conservation between many core kinetochore complex components, their arrangement differs significantly between higher and lower eukaryotes.

Chapter 5. Discussion

This thesis has addressed several interesting questions related to different aspects of ubiquitin signalling, particularly the recognition of the ubiquitin signal, which includes the site of ubiquitylation, the recognition of highly similar polyubiquitin chains and the recognition of monoubiquitin. The results have expanded our understanding about ubiquitin signalling in two different contexts, the pathway of DNA damage bypass governed by PCNA ubiquitylation and the newly discovered ubiquitin-binding properties of the yeast kinetochore. In this chapter I will separately discuss the importance of this work in advancing our understanding of ubiquitylation sites, polyubiquitin chains and monoubiquitin recognition.

5.1 The Importance of the Ubiquitylation Site

Ubiquitylation, like many other posttranslational modification mechanisms, transfers ubiquitin molecules onto specific lysine residues of a target protein. However, it is an open question whether the same type of ubiquitin signal on different modification sites would generally give the same or different biological consequences.

The function of ubiquitylation needs to be analysed to see whether ubiquitylation at a different site would support a common function. Of the many functions that have been described to ubiquitylation, protein degradation is the most common one. For example, a K48-linked polyubiquitin chain targets substrate proteins for proteasomal degradation, and this does not appear to depend on specific modification sites. An N-end rule substrate Ub-Arg-βGal is heavily ubiquitylated *in vivo* and degraded after cleavage of the N-terminal ubiquitin moiety (Bachmair and Varshavsky, 1989). The ubiquitylation can happen as long as a suitable lysine is available in nearby sequence, within the *lac*I-derived linker (Johnson et al., 1990). Similarly, a UFD pathway substrate, Ub (G76V)-Arg-βGal, a non-cleavable version of the N-end rule substrate, can be heavily ubiquitylated directly on the ubiquitin moiety via the K48-linkage and be degraded

(Johnston et al., 1995). This suggests that the K48-linked chains at different sites can all target the substrate protein for degradation. In fact, ubiquitin shuttling factors like Rad23, Dsk2, bind to multiple polyubiquitylated substrates, where the interaction is mainly through ubiquitin chains and UBDs. It is therefore less important to have a specific modification site. When ubiquitin functions as interaction sites in a situation other than protein degradation, it likely depends on the factor that binds to the ubiquitylated substrate whether ubiquitin attached to a different site on the substrate protein would still have the same function. A mis-attached ubiquitin on the substrate protein would result in different surface alteration and in turn affect the interaction between ubiquitylated substrate and its binding partner. Some factors are not able to tolerant such differences, therefore the interaction would be affected and the outcome of the ubiquitylation would not be the same. Finally, ubiquitylation has the potential not only to facilitate protein interactions, but also allosterically regulate protein functions. For example, ubiquitylation of Josephin deubiquitinase domain in Ataxin-3 activates the enzyme (Todi et al., 2009). This activation is thought to involve a conformational change that exposes the active site of the enzyme (Mao et al., 2005, Nicastro et al., 2005, Nicastro et al., 2009, Komander et al., 2009a). This is a special case in that ubiquitylation at a special location is required to induce a conformational change in an enzyme. Hence, a similar modification on a different site would not have the same function.

Among those different situations, ubiquitin sometimes can perform the same non-proteolytic functions at different sites. A few case reports do exist. Monoubiquitin fused with non-ubiquitylatable FANCD2 (K581A) mutant partially rescues cellular defects in Interstrand crosslinking repair (Matsushita et al., 2005). Parker and colleagues successfully used a linear ubiquitin-PCNA fusion protein (N- or C-terminal fusion) to support translesion synthesis in a yeast *rad18* background where endogenous PCNA cannot be ubiquitylated (Parker et al., 2007). Similar observations of using monoubiquitin-PCNA fusions have meanwhile been made in *S. pombe* and in a different background of *S. cerevisiae* (Pastushok et al., 2010, Ramasubramanyan et al., 2010). These observations suggest that it is sometimes possible to use monoubiquitin

fusions to mimic the function of a naturally monoubiquitylated substrate. I have explored this interesting possibility further and tested if polyubiquitylation of PCNA requires a defined modification site for its function. By expressing Ub^{K63*}-$PCNA^{*}$, where the K63 on ubiquitin is available for Mms2-Ubc13 mediated polyubiquitylation, the UV sensitivity of a *rad18* strain can be rescued via both branches of the DNA damage tolerance pathway (Figure 3.4). Consistent with the *in vitro* observation that Mms2-Ubc13 and Rad5 can polyubiquitylate Ub-PCNA efficiently (Parker and Ulrich, 2009), this result suggests that PCNA polyubiquitylation can occur at the N-terminally fused ubiquitin moiety. Although DNA damage induced polyubiquitylation of Ub^{K63*}-$PCNA^{*}$ *in vivo* was not shown directly, such an experiment could be performed by introducing a 6His-tagged Ub^{K63*}-$PCNA^{*}$ into a *rad18* strain and isolating the fusion protein using Ni-NTA pull-downs as described in Figure 3.12. Nevertheless, the genetic data still allow us to conclude that the K63-linked polyubiquitin chain attached to the N-terminus of PCNA supports the error-free pathway with efficiency comparable to the K63-linked chain conjugated at the natural modification site K164 (Figure 3.4). While this principle may not apply to all cases, this result definitely proves the concept that a polyubiquitin chain can function independent of its modification site on a specific substrate.

Ubiquitylation at different sites leading to the same biological consequence could be explained by the way ubiquitin is attached to the substrate and the specific interaction that ubiquitin mediates. Ubiquitylation can facilitate protein-protein interaction by an interaction between ubiquitin and various UBDs. In this case, the function of the ubiquitin moiety is to provide an extra binding surface on the substrate protein for its binding partner (Ulrich and Walden, 2010). The monoubiquitylation of PCNA is a good example for this. A simulation model based on a crystal structure has proposed a possible conformation of monoubiquitylated PCNA in complex with Polη (Freudenthal et al., 2010), where the UBZ domain, located at the C-terminal tail of Polη, can easily bind the monoubiquitin positioned at the "back" side of the PCNA, the surface opposite to that bound by the polymerases (Figure 5.1A). The C-terminal domain of Polη is long and flexible enough to allow a polymerase switch mechanism that involves displacing

Polδ and moving Polη to the "front" surface of PCNA (Freudenthal et al., 2010). When ubiquitin is attached to the N-terminus of PCNA, the molecule is in principle able to occupy a similar position at the "back" side of the PCNA ring (Figure 5.1B). Although the relative position of the N-terminus is different from K164 (Figure 5.1B), which is located on the other end of the PCNA monomer, the long C-terminal domain of Polη should still be able to bind the ubiquitin at the N-terminus of PCNA. For polyubiquitylated PCNA, the situation is apparently very similar in that K63-linked chains at the N-terminus of PCNA also support the error-free pathway. Since the molecular mechanism by which the error-free pathway can occur remains unclear, a working model cannot be provided. But it is likely that the K63-linked chain at the N-terminus of PCNA would also recruit some unknown factors or displace some PCNA interactors in order to promote the error-free pathway in the same manner that the chain at K164 would act.

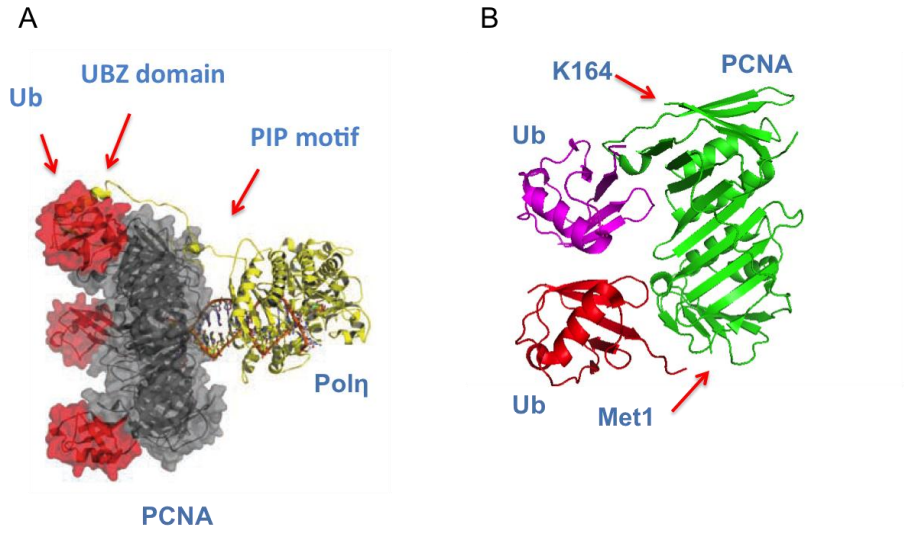

Figure 5.1 Structural models: monoubiquitin attached to K164 or N-terminus of PCNA
(A) Structure of monoubiquitylated PCNA in complex with Polη. This structure was adapted from (Freudenthal et al., 2010). Translesion synthesis polymerase η (yellow) interacts with PCNA (grey) via its PIP motif and interacts with ubiquitin (red) via its UBZ domain at the end of the C-terminus. (B) A structural model of monoubiquitin attached to K164 or the N-terminus of PCNA. Ubiquitin at K164 is presented in magenta and ubiquitin at the N-terminus of PCNA monomer (green) is presented in red. The image was generated by PyMOL with the PDB file of monoubiquitylated PCNA (3LOW) by addition of the N-terminal ubiquitin to the published structure of monoubiquitylated PCNA (Freudenthal et al., 2010).

Understanding the importance of ubiquitylation sites would allow us to create mimics of physiologically ubiquitylated substrate to study the function of these modified proteins *in vitro* and *in vivo*. Many *in vitro* experiments have been limited by the amount of ubiquitylated protein, which has to be purified from *in vitro* ubiquitylation reactions. Functional ubiquitin fusion protein would therefore greatly accelerate the *in vitro* work. Such concept has recently been proved by using a split version of PCNA, which consists of one polypeptide covering a region from the N-terminus to residue 163 and a second polypeptide consisting of ubiquitin fused to residue 165 of the C-terminal portion of PCNA (Freudenthal et al., 2010). It was lucky in this particular case since two separate peptides were able to self-assemble to reconstitute a functional PCNA structure. However, this approach is unlikely to work for every substrate at every position. Like phosphorylation, ubiquitylation is a reversible modification, but unlike phosphorylation, which often allows generating constitutive phospho-mimicking mutants, having a constitutively ubiquitylated form of substrate is not straightforward if modification at the natural site is required. In an ideal situation, a functional ubiquitin fusion allows generating a non-cleavable ubiquitin fusion by making G76V mutation to prevent isopeptidase cleavage. This would allow us to study *in vivo* the consequences of constitutive ubiquitylation, the importance of deubiquitylation, and to identify potential binding partners.

5.2 The Importance of Chain Linkage

Linear and K63-linked polyubiquitin chains have been shown to have an almost identical structure and many UBDs cannot differentiate them (Komander et al., 2009b). Therefore, it was reasonable to speculate that linear ubiquitin chains may substitute K63-linked chains to function in the DNA damage tolerance pathway. K63-linked chains are able to function at the N-terminus of PCNA to support DNA damage tolerance (Figure 3.4). However, two types of linear tetraubiquitin chains did not support error-free damage bypass at exactly the same site (Figure 3.5 and 3.6), suggesting that the damage tolerance pathway in *S. cerevisiae* is able to distinguish these two highly similar types of polyubiquitin signals (Figure 5.2). This result is

consistent with the observation in higher eukaryotes, where the signalling factor NEMO is modified by linear ubiquitin chains as well K63-linked polyubiquitin chains, and both modifications are important for the activation of NF-κB signalling (Iwai and Tokunaga, 2009, Skaug et al., 2009). These two highly similar forms of polyubiquitin chains are conjugated onto a common substrate, and both of them turn out to be functionally important, suggesting that the NF-κB pathway in mammalian cell is able to differentiate these two types of chains as well. Specific UBDs play critical roles in recognising these similar polyubiquitin chains: a UBAN domain in NEMO prefers linear ubiquitin chains over K63-linked chains (Rahighi et al., 2009). However, this differentiation between chain types is not always observed. The UBA domain from cIAP1 binds linear and K63-linked ubiquitin chains equally well, but does not interact with K48-linked chains (Komander et al., 2009b). This observation raises the possibility that linear and K63-linked chains may be interchangeable in some situations when the UBD of the effector protein is not able to differentiate these two modifications.

The potential involvement of the proteasome in the DNA damage tolerance pathway downstream of PCNA polyubiquitylation has also been addressed in this thesis. Since its identification (Hoege et al., 2002), the possibility that K63-polyubiquitylated PCNA may be degraded by the proteasome has never been experimentally addressed, although K63-linked chain is not generally considered as a degradation signal. Figure 3.12 directly illustrates that K63-polyubiquitylated PCNA is not degraded. This result agrees with a non-degradative role for K63-linked chains, and is consistent with the fact that in yeast total K63-linked ubiquitin conjugates do not accumulate upon proteasome inhibition (Xu et al., 2009). Meanwhile, the function of a linear ubiquitin chain as a degradation signal has also been extensively assayed. A linear tetraubiquitin chain has been shown to target its fusion partner PCNA for proteasome dependent degradation in yeast cells (Figure 3.8 and 3.9), and the linear chain alone is sufficient for proteasome targeting *in vitro* (Figure 3.10). Furthermore, linear tetraubiquitin chains can also target another model substrate, βGal, for degradation (Figure 3.15), and the process is mediated by factors involved in the UFD pathway (Figure 3.16 and 3.18). Despite a rather poor efficiency, all experimental systems have so far provided evidence that a

linear ubiquitin chain can function as a degradation signal at least on a range of model substrates. The situation *in vivo* is still unclear as suitable factors may bind linear chains and divert the substrate away from the proteasome degradation pathway. Nevertheless, this study showed two different biological consequences when the highly similar linear and K63-linked polyubiquitin chains are attached to the same site of a model substrate, PCNA (Figure 5.2).

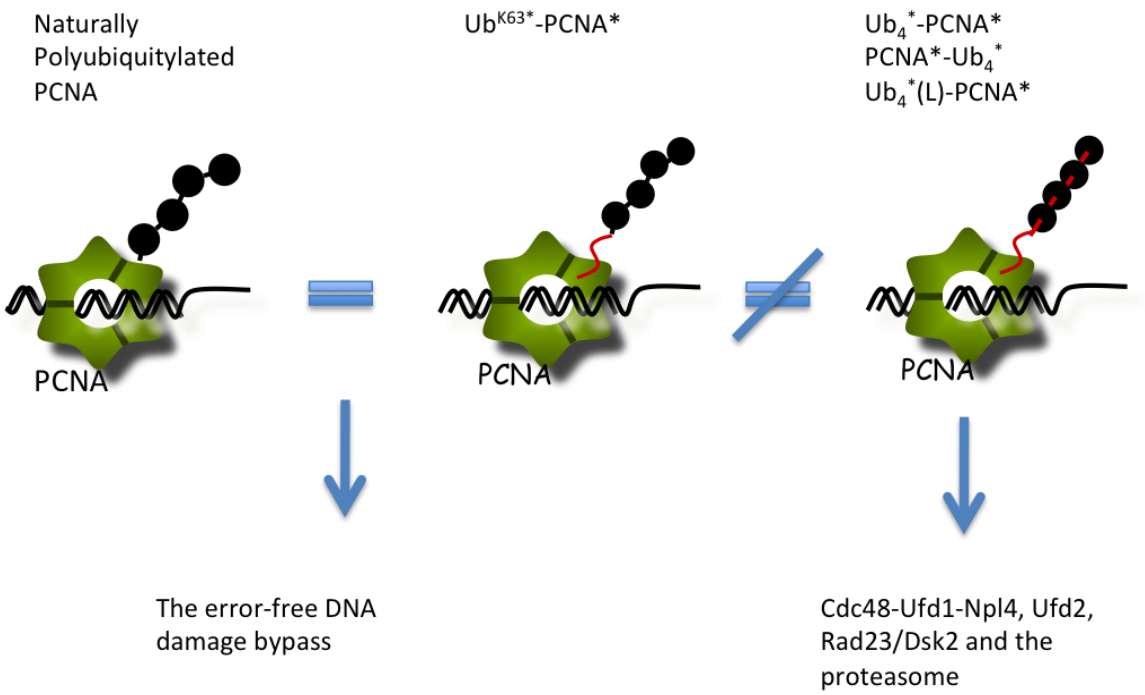

Figure 5.2 Distinct biological consequences of PCNA modification by linear and K63-polyubiquitin chains
Ub^{K63*}-$PCNA^{*}$ (green PCNA modified by a black K63-linked polyubiquitin chain, with red linker between PCNA and ubiquitin chain) can be further ubiquitylated by the PCNA polyubiquitylation machinery and act as a functional mimic of naturally polyubiquitylated PCNA (green PCNA modified by a black K63-linked polyubiquitin chain) to support error-free DNA damage bypass. However, linear fusions of tetraubiquitin chain to PCNA (green PCNA modified by a black linear polyubiquitin chain, with red linker between PCNA and ubiquitin chain) do not support error-free damage bypass. Instead, the linear ubiquitin chain is recognised by the Cdc48 complex, and targeted to the proteasome via Ufd2, Rad23/Dsk2 for degradation.

5.3 Recognition of Monoubiquitin

Currently known UBDs interact with ubiquitin through several distinct structural features. Most UBDs use α-helical structures to bind ubiquitin, and other structural features including zinc fingers (ZnFs), ubiquitin-conjugating enzyme-like (UBC) domains and pleckstrin homology (PH) folds can also interact with ubiquitin (Dikic et al., 2009). UBDs usually recognise monoubiquitin through its hydrophobic patch centred around I44, but alternative contacting surfaces are also observed (Figure 1.4). The interaction between a polyubiquitin chain and a UBD usually involves several contacting surfaces on two ubiquitin moieties as shown in Figure 1.5. UBDs usually bind both mono- and polyubiquitin *in vitro*, but their targets *in vivo* are depending on the ubiquitylation states of a binding partner.

Spc25 was identified as a potential ubiquitin-binding protein in a yeast two-hybrid screen (Table 4.1). The result was confirmed in a separate yeast two-hybrid experiment (Figure 4.6). Further characterisation identified the C-terminal region (amino acids 107-221), which consists of its globular domain and an N-terminal flexible extension, as the minimal region required for ubiquitin binding (Figure 4.7 and 4.8). Surface plasmon resonance-based BIACORE® technology has been used to determine the dissociation constant for the interaction between Spc25-Spc24 and ubiquitin (Figure 4.10). Through sequence alignment of Spc25 homologues from different organisms, highly conserved residues were identified, and by subsequent mutagenesis, the L109A mutation was found to abolish Spc25 ubiquitin binding almost completely in yeast two-hybrid experiments (Figure 4.12). However, the requirement of the globular domain clearly suggests that a second contacting surface exists within the globular domain. Interestingly, Spc25 is able to bind monoubiquitin, tetraubiquitin, but does not bind K48- and K63-linked polyubiquitin chains in tested conditions (Figure 4.9, 4.10 and data not shown). Based on current observations, Spc25 might be a monoubiquitin-binding protein. Although the exact structural features of Spc25 binding to ubiquitin are not clear, the requirement of a globular domain together with a flexible extension has not been observed in any other case. Future work needs to be concentrated on resolving

the structure of the Spc25 C-terminal domain in complex with ubiquitin. Such a structure would bring information about the ubiquitin-contacting surface on Spc25 and residues important for this interaction. With the help of this information, it will be then clear if the ubiquitin-binding feature of Spc25 is indeed different from those known UBDs. As I mention in section 4.9.4, it is possible that *spc25 (L109A)* mutant allele has some residual ubiquitin-binding activity, which causes weak phenotypes. More residues could be tested for their contributions towards ubiquitin binding through mutagenesis analysis and a *spc25* mutant allele completely deficient in ubiquitin binding would be good for further phenotypical analysis.

Since ubiquitin-binding proteins usually act as effectors for ubiquitylated targets, a systematic approach was performed to search for ubiquitylated Spc25 interactors and parallel phenotypic analysis were also focused on those potential candidates. The investigation on *spc25* (*L109A)* allele revealed that it strongly sensitises cells when it is combined with *dsn1 ts* mutants or *MCM21-GFP* (Figure 4.18). Most importantly, Dsn1 and Mcm21 were both detected to be ubiquitylated (Figure 4.16 and 4.17) and associated with Spc25 [(Nekrasov et al., 2003) and (data not shown)]. All of these data suggest a functional link between the ubiquitin-binding domain of Spc25 and the observed ubiquitylation events of Dsn1and Mcm21.

Despite the fact that only an incomplete picture of a novel ubiquitin-binding protein Spc25 is presented in this thesis, it does provide evidence that ubiquitin signalling occurs within the kinetochore. Most importantly, many kinetochore proteins are found to be ubiquitylated in a target-directed screen aiming to identify ubiquitylated Spc25 interactors (Figure 4.16 and 4.17). Because not all tested proteins are ubiquitylated and some proteins are monoubiquitylated while some others are polyubiquitylated (Figure 4.16), they are most likely to be specifically regulated events. Ubiquitylation of kinetochore proteins has not been studied at all. In order to gain further insight into this field, it would therefore be worth systematically analysing all the kinetochore proteins for ubiquitylation. In my initial screen, I mainly focused on outer-kinetochore proteins

in the vicinity of Spc25. It will be interesting to see if inner kinetochore proteins or microtubule-binding factors are also modified by ubiquitin. The fact that many proteins within the kinetochore complex are ubiquitylated is quite reminiscent of the PML-nuclear bodies (PML-NBs) in mammalian cells, which are proteinaceous structures in the nucleus that seem to be interconnected by a network of SUMOylation and non-covalent SUMO interactions (Bernardi and Pandolfi, 2007). Based on our current data, ubiquitin binding of Spc25 appears to positively contribute to the stability of the kinetochore complex. With many ubiquitylated kinetochore components, it is a very attractive speculation that ubiquitylation/ubiquitin-binding domain might play similar roles in the kinetochore as the SUMO interaction network in the PML-NBs.

5.4 Ubiquitin Signalling and Genome Stability

Cells have developed many sophisticated mechanisms to maintain genome stability, and ubiquitin signalling has great influences on those processes. Maintaining genome integrity is mainly achieved at the DNA level, where DNA damage is sensed and properly repaired, and at the chromosome level, where chromosomes are precisely segregated. Overall, genomic instability is an important feature of cancer cells and the ubiquitin signalling pathway is a very attractive target for developing anti-cancer therapy. A better understanding of the function of ubiquitin signalling in maintaining genome stability would therefore likely be helpful for the development of future anti-cancer treatments.

Various pathways operate to repair different types of DNA lesions. In response to double-strand breaks (DSBs), a number of different factors including E3 ligases, E2 enzyme, and ubiquitin-binding proteins are involved in signal amplification and transduction. E3 ligase RNF8, in complex with Ubc13, ubiquitylates H2A and H2AX (Huen et al., 2007, Kolas et al., 2007, Mailand et al., 2007), which is in turn recognised by a second E3 ligase RNF168 via its MIU domain (Stewart et al., 2009, Doil et al., 2009). The ubiquitin conjugates at sites of DSBs were reported to be K63-linked chains

(Stewart et al., 2009, Doil et al., 2009, Sobhian et al., 2007), and the polyubiquitin signals that accumulate at the damage loci finally recruit BRCA1 via RAP80 (Kim et al., 2007, Liu et al., 2007, Sobhian et al., 2007, Wang et al., 2007). To repair interstrand cross-links (ICLs), the mammalian Fanconi anaemia pathway plays a key role. Monoubiquitylation and deubiquitylation of the FANCD2-FANCI complex are absolutely required for the repair of ICLs (Matsushita et al., 2005, Ishiai et al., 2008, Oestergaard et al., 2007, Nijman et al., 2005). When DNA polymerase is stalled at site of lesion, a damage bypass mechanism requires PCNA monoubiquitylation and polyubiquitylation at K164 (Hoege et al., 2002). Monoubiquitylated PCNA recruits error-prone polymerases to perform translesion synthesis to bypass the lesion (Kannouche et al., 2004, Watanabe et al., 2004, Stelter and Ulrich, 2003), whereas polyubiquitylated PCNA initiates a yet not fully understood error-free pathway to allow replication fork progression through the lesion without introducing mutations. The first part of my thesis has provided further insights into this process. K63-polyubiquitylated PCNA is not degraded by the proteasome (Figure 3.12). A K63-linked chain still supports error-free damage bypass even at the N-terminus of PCNA, but a non-cleavable tetraubiquitin chain does not have such a function (Figure 3.4, 3.5 and 3.6). Further efforts were put on identifying interaction partners exclusive for polyubiquitylated PCNA via a yeast two-hybrid screen and pull-down experiments (Table 4.1 and Figure 4.5). All of these have taken us a step forward on the way to fully understand the mechanism of PCNA polyubiquitylation-dependent error-free damage bypass and some of the unsuccessful approaches would also provide valid information that future approaches should take into account.

Chromosome segregation is also tightly regulated during mitosis to ensure that each daughter cell will receive a complete set of the organism's genetic information at the chromosome level. Ubiquitin signalling has been well studied in regulating the timing of chromosome segregation through APC/C mediated ubiquitylation and degradation process. Securin is ubiquitylated by APC/C and degraded in metaphase to release its binding partner, separase, which cleaves the Scc1 cohesion subunit to allow the separation of sister chromatides (Cohen-Fix et al., 1996, Ciosk et al., 1998, Uhlmann et

al., 1999, Uhlmann et al., 2000). The second part of my thesis has provided evidence that ubiquitin signalling may also regulate the stability of the kinetochore complex and thereby positively contribute to genome stability. The Ndc80 complex, an essential protein complex for cell survival, was shown to bind microtubules directly (Cheeseman et al., 2006, DeLuca et al., 2006). Overexpression of Ndc80, also called Hec1 (Highly Expressed in Cancer 1), causes hyperactivation of mitotic checkpoint and formation of tumours with significant levels of aneuploidy (Diaz-Rodriguez et al., 2008). Spc25 as a subunit of Ndc80 complex was shown to bind ubiquitin (Figure 4.6 and 4.9), and an allele deficient in ubiquitin binding sensitises *dsn1 ts* cells (Figure 4.18). These observations suggest that ubiquitin could play a role in maintaining kinetochore stability. More interestingly, many components of the kinetochore complex were identified as substrates for ubiquitylation, which further supports the significance of ubiquitin signalling in the kinetochore. Many questions regarding the details of how ubiquitylation and ubiquitin binding mediate kinetochore stability remain to be answered. Nevertheless, this work definitely improves our knowledge about the involvement of ubiquitin signalling in genome stability.

Reference List

AKIYOSHI, B., NELSON, C. R., RANISH, J. A. & BIGGINS, S. 2009. Analysis of Ipl1-mediated phosphorylation of the Ndc80 kinetochore protein in Saccharomyces cerevisiae. *Genetics,* 183**,** 1591-5.

AL-HAKIM, A. K., ZAGORSKA, A., CHAPMAN, L., DEAK, M., PEGGIE, M. & ALESSI, D. R. 2008. Control of AMPK-related kinases by USP9X and atypical Lys(29)/Lys(33)-linked polyubiquitin chains. *Biochem J,* 411**,** 249-60.

ALBERS, M., KRANZ, H., KOBER, I., KAISER, C., KLINK, M., SUCKOW, J., KERN, R. & KOEGL, M. 2005. Automated yeast two-hybrid screening for nuclear receptor-interacting proteins. *Mol Cell Proteomics,* 4**,** 205-13.

ALEXANDRU, G., GRAUMANN, J., SMITH, G. T., KOLAWA, N. J., FANG, R. & DESHAIES, R. J. 2008. UBXD7 binds multiple ubiquitin ligases and implicates p97 in HIF1alpha turnover. *Cell,* 134**,** 804-16.

ALLSHIRE, R. C. & KARPEN, G. H. 2008. Epigenetic regulation of centromeric chromatin: old dogs, new tricks? *Nat Rev Genet,* 9**,** 923-37.

ARAVIND, L. & KOONIN, E. V. 2000. The U box is a modified RING finger - a common domain in ubiquitination. *Curr Biol,* 10**,** R132-4.

AULD, K. L., HITCHCOCK, A. L., DOHERTY, H. K., FRIETZE, S., HUANG, L. S. & SILVER, P. A. 2006. The conserved ATPase Get3/Arr4 modulates the activity of membrane-associated proteins in Saccharomyces cerevisiae. *Genetics,* 174**,** 215-27.

AVIEL, S., WINBERG, G., MASSUCCI, M. & CIECHANOVER, A. 2000. Degradation of the epstein-barr virus latent membrane protein 1 (LMP1) by the ubiquitin-proteasome pathway. Targeting via ubiquitination of the N-terminal residue. *J Biol Chem,* 275**,** 23491-9.

BACHMAIR, A., FINLEY, D. & VARSHAVSKY, A. 1986. In vivo half-life of a protein is a function of its amino-terminal residue. *Science,* 234**,** 179-86.

BACHMAIR, A. & VARSHAVSKY, A. 1989. The degradation signal in a short-lived protein. *Cell,* 56**,** 1019-32.

BAILLY, V., LAMB, J., SUNG, P., PRAKASH, S. & PRAKASH, L. 1994. Specific complex formation between yeast RAD6 and RAD18 proteins: a potential mechanism for targeting RAD6 ubiquitin-conjugating activity to DNA damage sites. *Genes Dev,* 8**,** 811-20.

BARTEL, B., WUNNING, I. & VARSHAVSKY, A. 1990. The recognition component of the N-end rule pathway. *Embo J,* 9**,** 3179-89.

BEAL, R. E., TOSCANO-CANTAFFA, D., YOUNG, P., RECHSTEINER, M. & PICKART, C. M. 1998. The hydrophobic effect contributes to polyubiquitin chain recognition. *Biochemistry,* 37**,** 2925-34.

BERNARDI, R. & PANDOLFI, P. P. 2007. Structure, dynamics and functions of promyelocytic leukaemia nuclear bodies. *Nat Rev Mol Cell Biol,* 8**,** 1006-16.

BIENKO, M., GREEN, C. M., CROSETTO, N., RUDOLF, F., ZAPART, G., COULL, B., KANNOUCHE, P., WIDER, G., PETER, M., LEHMANN, A. R., HOFMANN, K. & DIKIC, I. 2005. Ubiquitin-binding domains in Y-family polymerases regulate translesion synthesis. *Science,* 310**,** 1821-4.

BREITSCHOPF, K., BENGAL, E., ZIV, T., ADMON, A. & CIECHANOVER, A. 1998. A novel site for ubiquitination: the N-terminal residue, and not internal lysines of MyoD, is essential for conjugation and degradation of the protein. *Embo J,* 17**,** 5964-73.

BREMM, A., FREUND, S. M. & KOMANDER, D. 2010. Lys11-linked ubiquitin chains adopt compact conformations and are preferentially hydrolyzed by the deubiquitinase Cezanne. *Nat Struct Mol Biol*.

BROEMER, M. & MEIER, P. 2009. Ubiquitin-mediated regulation of apoptosis. *Trends Cell Biol,* 19**,** 130-40.

CHASTAGNER, P., ISRAEL, A. & BROU, C. 2006. Itch/AIP4 mediates Deltex degradation through the formation of K29-linked polyubiquitin chains. *EMBO Rep,* 7**,** 1147-53.

CHAU, V., TOBIAS, J. W., BACHMAIR, A., MARRIOTT, D., ECKER, D. J., GONDA, D. K. & VARSHAVSKY, A. 1989. A multiubiquitin chain is confined to specific lysine in a targeted short-lived protein. *Science,* 243**,** 1576-83.

CHEESEMAN, I. M., CHAPPIE, J. S., WILSON-KUBALEK, E. M. & DESAI, A. 2006. The conserved KMN network constitutes the core microtubule-binding site of the kinetochore. *Cell,* 127**,** 983-97.

CHEESEMAN, I. M., DRUBIN, D. G. & BARNES, G. 2002. Simple centromere, complex kinetochore: linking spindle microtubules and centromeric DNA in budding yeast. *J Cell Biol,* 157**,** 199-203.

CIECHANOVER, A., ORIAN, A. & SCHWARTZ, A. L. 2000. Ubiquitin-mediated proteolysis: biological regulation via destruction. *Bioessays,* 22**,** 442-51.

CIFERRI, C., PASQUALATO, S., SCREPANTI, E., VARETTI, G., SANTAGUIDA, S., DOS REIS, G., MAIOLICA, A., POLKA, J., DE LUCA, J. G., DE WULF, P., SALEK, M., RAPPSILBER, J., MOORES, C. A., SALMON, E. D. & MUSACCHIO, A. 2008. Implications for kinetochore-microtubule attachment from the structure of an engineered Ndc80 complex. *Cell,* 133**,** 427-39.

CIOSK, R., ZACHARIAE, W., MICHAELIS, C., SHEVCHENKO, A., MANN, M. & NASMYTH, K. 1998. An ESP1/PDS1 complex regulates loss of sister chromatid cohesion at the metaphase to anaphase transition in yeast. *Cell,* 93**,** 1067-76.

COHEN-FIX, O., PETERS, J. M., KIRSCHNER, M. W. & KOSHLAND, D. 1996. Anaphase initiation in Saccharomyces cerevisiae is controlled by the APC-dependent degradation of the anaphase inhibitor Pds1p. *Genes Dev,* 10**,** 3081-93.

DAIGAKU, Y., DAVIES, A. A. & ULRICH, H. D. 2010. Ubiquitin-dependent DNA damage bypass is separable from genome replication. *Nature,* 465**,** 951-5.

DATTA, A. B., HURA, G. L. & WOLBERGER, C. 2009. The structure and conformation of Lys63-linked tetraubiquitin. *J Mol Biol,* 392**,** 1117-24.

DAVIES, A. A., HUTTNER, D., DAIGAKU, Y., CHEN, S. & ULRICH, H. D. 2008. Activation of ubiquitin-dependent DNA damage bypass is mediated by replication protein a. *Mol Cell,* 29**,** 625-36.

DE WULF, P., MCAINSH, A. D. & SORGER, P. K. 2003. Hierarchical assembly of the budding yeast kinetochore from multiple subcomplexes. *Genes Dev,* 17**,** 2902-21.

DELUCA, J. G., GALL, W. E., CIFERRI, C., CIMINI, D., MUSACCHIO, A. & SALMON, E. D. 2006. Kinetochore microtubule dynamics and attachment stability are regulated by Hec1. *Cell,* 127**,** 969-82.

DENG, L., WANG, C., SPENCER, E., YANG, L., BRAUN, A., YOU, J., SLAUGHTER, C., PICKART, C. & CHEN, Z. J. 2000. Activation of the IkappaB kinase complex by TRAF6 requires a dimeric ubiquitin-conjugating enzyme complex and a unique polyubiquitin chain. *Cell,* 103**,** 351-61.

DIAZ-RODRIGUEZ, E., SOTILLO, R., SCHVARTZMAN, J. M. & BENEZRA, R. 2008. Hec1 overexpression hyperactivates the mitotic checkpoint and induces tumor formation in vivo. *Proc Natl Acad Sci U S A,* 105**,** 16719-24.

DIKIC, I., WAKATSUKI, S. & WALTERS, K. J. 2009. Ubiquitin-binding domains - from structures to functions. *Nat Rev Mol Cell Biol,* 10**,** 659-71.

DITZEL, M., BROEMER, M., TENEV, T., BOLDUC, C., LEE, T. V., RIGBOLT, K. T., ELLIOTT, R., ZVELEBIL, M., BLAGOEV, B., BERGMANN, A. &

MEIER, P. 2008. Inactivation of effector caspases through nondegradative polyubiquitylation. *Mol Cell,* 32**,** 540-53.

DOHMEN, R. J., MADURA, K., BARTEL, B. & VARSHAVSKY, A. 1991. The N-end rule is mediated by the UBC2(RAD6) ubiquitin-conjugating enzyme. *Proc Natl Acad Sci U S A,* 88**,** 7351-5.

DOIL, C., MAILAND, N., BEKKER-JENSEN, S., MENARD, P., LARSEN, D. H., PEPPERKOK, R., ELLENBERG, J., PANIER, S., DUROCHER, D., BARTEK, J., LUKAS, J. & LUKAS, C. 2009. RNF168 binds and amplifies ubiquitin conjugates on damaged chromosomes to allow accumulation of repair proteins. *Cell,* 136**,** 435-46.

DRAG, M., MIKOLAJCZYK, J., BEKES, M., REYES-TURCU, F. E., ELLMAN, J. A., WILKINSON, K. D. & SALVESEN, G. S. 2008. Positional-scanning fluorigenic substrate libraries reveal unexpected specificity determinants of DUBs (deubiquitinating enzymes). *Biochem J,* 415**,** 367-75.

EA, C. K., DENG, L., XIA, Z. P., PINEDA, G. & CHEN, Z. J. 2006. Activation of IKK by TNFalpha requires site-specific ubiquitination of RIP1 and polyubiquitin binding by NEMO. *Mol Cell,* 22**,** 245-57.

EDDINS, M. J., VARADAN, R., FUSHMAN, D., PICKART, C. M. & WOLBERGER, C. 2007. Crystal structure and solution NMR studies of Lys48-linked tetraubiquitin at neutral pH. *J Mol Biol,* 367**,** 204-11.

ELSASSER, S., CHANDLER-MILITELLO, D., MULLER, B., HANNA, J. & FINLEY, D. 2004. Rad23 and Rpn10 serve as alternative ubiquitin receptors for the proteasome. *J Biol Chem,* 279**,** 26817-22.

FINLEY, D. 2009. Recognition and processing of ubiquitin-protein conjugates by the proteasome. *Annu Rev Biochem,* 78**,** 477-513.

FINLEY, D., OZKAYNAK, E. & VARSHAVSKY, A. 1987. The yeast polyubiquitin gene is essential for resistance to high temperatures, starvation, and other stresses. *Cell,* 48**,** 1035-46.

FINLEY, D., SADIS, S., MONIA, B. P., BOUCHER, P., ECKER, D. J., CROOKE, S. T. & CHAU, V. 1994. Inhibition of proteolysis and cell cycle progression in a multiubiquitination-deficient yeast mutant. *Mol Cell Biol,* 14**,** 5501-9.

FLICK, K., OUNI, I., WOHLSCHLEGEL, J. A., CAPATI, C., MCDONALD, W. H., YATES, J. R. & KAISER, P. 2004. Proteolysis-independent regulation of the transcription factor Met4 by a single Lys 48-linked ubiquitin chain. *Nat Cell Biol,* 6**,** 634-41.

FREUDENTHAL, B. D., GAKHAR, L., RAMASWAMY, S. & WASHINGTON, M. T. 2010. Structure of monoubiquitinated PCNA and implications for translesion synthesis and DNA polymerase exchange. *Nat Struct Mol Biol,* 17**,** 479-84.

FUNAKOSHI, M., SASAKI, T., NISHIMOTO, T. & KOBAYASHI, H. 2002. Budding yeast Dsk2p is a polyubiquitin-binding protein that can interact with the proteasome. *Proc Natl Acad Sci U S A,* 99**,** 745-50.

GARCIA-HIGUERA, I., TANIGUCHI, T., GANESAN, S., MEYN, M. S., TIMMERS, C., HEJNA, J., GROMPE, M. & D'ANDREA, A. D. 2001. Interaction of the Fanconi anemia proteins and BRCA1 in a common pathway. *Mol Cell,* 7**,** 249-62.

GARG, P. & BURGERS, P. M. 2005. Ubiquitinated proliferating cell nuclear antigen activates translesion DNA polymerases eta and REV1. *Proc Natl Acad Sci U S A,* 102**,** 18361-6.

GARNETT, M. J., MANSFELD, J., GODWIN, C., MATSUSAKA, T., WU, J., RUSSELL, P., PINES, J. & VENKITARAMAN, A. R. 2009. UBE2S elongates ubiquitin chains on APC/C substrates to promote mitotic exit. *Nat Cell Biol,* 11**,** 1363-9.

GIETZ, R. D. & SUGINO, A. 1988. New yeast-Escherichia coli shuttle vectors constructed with in vitro mutagenized yeast genes lacking six-base pair restriction sites. *Gene,* 74**,** 527-34.

GOLDBERG, A. L. 2003. Protein degradation and protection against misfolded or damaged proteins. *Nature,* 426**,** 895-9.

GOLDKNOPF, I. L. & BUSCH, H. 1977. Isopeptide linkage between nonhistone and histone 2A polypeptides of chromosomal conjugate-protein A24. *Proc Natl Acad Sci U S A,* 74**,** 864-8.

GUO, C., TANG, T. S., BIENKO, M., DIKIC, I. & FRIEDBERG, E. C. 2008. Requirements for the interaction of mouse Polkappa with ubiquitin and its biological significance. *J Biol Chem,* 283**,** 4658-64.

GUO, C., TANG, T. S., BIENKO, M., PARKER, J. L., BIELEN, A. B., SONODA, E., TAKEDA, S., ULRICH, H. D., DIKIC, I., FRIEDBERG, E. C., FRAMPTON, J., IRMISCH, A., GREEN, C. M., NEISS, A., TRICKEY, M., FURUYA, K., WATTS, F. Z., CARR, A. M., LEHMANN, A. R., SARKAR, S., DAVIES, A. A., MCHUGH, P. J., VOGEL, S., CHEN, S., SAGAN, D., PAPOULI, E., HUTTNER, D., KREJCI, L., SUNG, P., BUGNICOURT, A., FROISSARD, M., SERETI, K., HAGUENAUER-TSAPIS, R., GALAN, J. M., SCHURER, K. A., RUDOLPH, C., KRAMER, W., STELTER, P., GILDERSLEEVE, J., JANES, J., ULRICH, H., YANG, P., BARBAS, C. & SCHULTZ, P. G. 2006. Ubiquitin-Binding Motifs in REV1 Protein Are Required For Its Role in the Tolerance of DNA Damage

GYRD-HANSEN, M., DARDING, M., MIASARI, M., SANTORO, M. M., ZENDER, L., XUE, W., TENEV, T., DA FONSECA, P. C., ZVELEBIL, M., BUJNICKI, J. M., LOWE, S., SILKE, J. & MEIER, P. 2008. IAPs contain an evolutionarily conserved ubiquitin-binding domain that regulates NF-kappaB as well as cell survival and oncogenesis. *Nat Cell Biol,* 10**,** 1309-17.

HAAS, A. L., WARMS, J. V., HERSHKO, A. & ROSE, I. A. 1982. Ubiquitin-activating enzyme. Mechanism and role in protein-ubiquitin conjugation. *J Biol Chem,* 257**,** 2543-8.

HE, X., RINES, D. R., ESPELIN, C. W. & SORGER, P. K. 2001. Molecular analysis of kinetochore-microtubule attachment in budding yeast. *Cell,* 106**,** 195-206.

HENRY, M. F. & SILVER, P. A. 1996. A novel methyltransferase (Hmt1p) modifies poly(A)+-RNA-binding proteins. *Mol Cell Biol,* 16**,** 3668-78.

HERSHKO, A. & CIECHANOVER, A. 1998. The ubiquitin system. *Annu Rev Biochem,* 67**,** 425-79.

HICKE, L. 2001. Protein regulation by monoubiquitin. *Nat Rev Mol Cell Biol,* 2**,** 195-201.

HIETER, P., MANN, C., SNYDER, M. & DAVIS, R. W. 1985. Mitotic stability of yeast chromosomes: a colony color assay that measures nondisjunction and chromosome loss. *Cell,* 40**,** 381-92.

HITCHCOCK, A. L., KREBBER, H., FRIETZE, S., LIN, A., LATTERICH, M. & SILVER, P. A. 2001. The conserved npl4 protein complex mediates proteasome-dependent membrane-bound transcription factor activation. *Mol Biol Cell,* 12**,** 3226-41.

HOEGE, C., PFANDER, B., MOLDOVAN, G. L., PYROWOLAKIS, G. & JENTSCH, S. 2002. RAD6-dependent DNA repair is linked to modification of PCNA by ubiquitin and SUMO. *Nature,* 419**,** 135-41.

HOFMANN, K. 2009. Ubiquitin-binding domains and their role in the DNA damage response. *DNA Repair (Amst),* 8**,** 544-56.

HOFMANN, R. M. & PICKART, C. M. 1999. Noncanonical MMS2-encoded ubiquitin-conjugating enzyme functions in assembly of novel polyubiquitin chains for DNA repair. *Cell,* 96**,** 645-53.

HOFMANN, R. M. & PICKART, C. M. 2001. In vitro assembly and recognition of Lys-63 polyubiquitin chains. *J Biol Chem,* 276**,** 27936-43.

HUANG, T. T., NIJMAN, S. M., MIRCHANDANI, K. D., GALARDY, P. J., COHN, M. A., HAAS, W., GYGI, S. P., PLOEGH, H. L., BERNARDS, R. &

D'ANDREA, A. D. 2006. Regulation of monoubiquitinated PCNA by DUB autocleavage. *Nat Cell Biol,* 8**,** 339-47.

HUEN, M. S., GRANT, R., MANKE, I., MINN, K., YU, X., YAFFE, M. B. & CHEN, J. 2007. RNF8 transduces the DNA-damage signal via histone ubiquitylation and checkpoint protein assembly. *Cell,* 131**,** 901-14.

HUIBREGTSE, J. M., SCHEFFNER, M., BEAUDENON, S. & HOWLEY, P. M. 1995. A family of proteins structurally and functionally related to the E6-AP ubiquitin-protein ligase. *Proc Natl Acad Sci U S A,* 92**,** 2563-7.

HURLEY, J. H., LEE, S. & PRAG, G. 2006. Ubiquitin-binding domains. *Biochem J,* 399**,** 361-72.

HUSNJAK, K., ELSASSER, S., ZHANG, N., CHEN, X., RANDLES, L., SHI, Y., HOFMANN, K., WALTERS, K. J., FINLEY, D. & DIKIC, I. 2008. Proteasome subunit Rpn13 is a novel ubiquitin receptor. *Nature,* 453**,** 481-8.

IKEDA, F. & DIKIC, I. 2008. Atypical ubiquitin chains: new molecular signals. 'Protein Modifications: Beyond the Usual Suspects' review series. *EMBO Rep,* 9**,** 536-42.

ISHIAI, M., KITAO, H., SMOGORZEWSKA, A., TOMIDA, J., KINOMURA, A., UCHIDA, E., SABERI, A., KINOSHITA, E., KINOSHITA-KIKUTA, E., KOIKE, T., TASHIRO, S., ELLEDGE, S. J. & TAKATA, M. 2008. FANCI phosphorylation functions as a molecular switch to turn on the Fanconi anemia pathway. *Nat Struct Mol Biol,* 15**,** 1138-46.

IVINS, F. J., MONTGOMERY, M. G., SMITH, S. J., MORRIS-DAVIES, A. C., TAYLOR, I. A. & RITTINGER, K. 2009. NEMO oligomerization and its ubiquitin-binding properties. *Biochem J,* 421**,** 243-51.

IWAI, K. & TOKUNAGA, F. 2009. Linear polyubiquitination: a new regulator of NF-kappaB activation. *EMBO Rep,* 10**,** 706-13.

JACOBSON, A. D., ZHANG, N. Y., XU, P., HAN, K. J., NOONE, S., PENG, J. & LIU, C. W. 2009. The lysine 48 and lysine 63 ubiquitin conjugates are processed differently by the 26 s proteasome. *J Biol Chem,* 284**,** 35485-94.

JAMES, P., HALLADAY, J. & CRAIG, E. A. 1996. Genomic libraries and a host strain designed for highly efficient two-hybrid selection in yeast. *Genetics,* 144**,** 1425-36.

JANKE, C., ORTIZ, J., LECHNER, J., SHEVCHENKO, A., SHEVCHENKO, A., MAGIERA, M. M., SCHRAMM, C. & SCHIEBEL, E. 2001. The budding yeast proteins Spc24p and Spc25p interact with Ndc80p and Nuf2p at the kinetochore and are important for kinetochore clustering and checkpoint control. *Embo J,* 20**,** 777-91.

JENTSCH, S., MCGRATH, J. P. & VARSHAVSKY, A. 1987. The yeast DNA repair gene RAD6 encodes a ubiquitin-conjugating enzyme. *Nature,* 329**,** 131-4.

JIN, L., WILLIAMSON, A., BANERJEE, S., PHILIPP, I. & RAPE, M. 2008. Mechanism of ubiquitin-chain formation by the human anaphase-promoting complex. *Cell,* 133**,** 653-65.

JOGLEKAR, A. P., BLOOM, K. & SALMON, E. D. 2009. In Vivo Protein Architecture of the Eukaryotic Kinetochore with Nanometer Scale Accuracy. *Curr Biol*.

JOHNSON, E. S., BARTEL, B., SEUFERT, W. & VARSHAVSKY, A. 1992. Ubiquitin as a degradation signal. *EMBO J,* 11**,** 497-505.

JOHNSON, E. S., GONDA, D. K. & VARSHAVSKY, A. 1990. cis-trans recognition and subunit-specific degradation of short-lived proteins. *Nature,* 346**,** 287-91.

JOHNSON, E. S., MA, P. C., OTA, I. M. & VARSHAVSKY, A. 1995. A proteolytic pathway that recognizes ubiquitin as a degradation signal. *J Biol Chem,* 270**,** 17442-56.

JOHNSTON, J. A., JOHNSON, E. S., WALLER, P. R. & VARSHAVSKY, A. 1995. Methotrexate inhibits proteolysis of dihydrofolate reductase by the N-end rule pathway. *J Biol Chem,* 270**,** 8172-8.

KANAYAMA, A., SETH, R. B., SUN, L., EA, C. K., HONG, M., SHAITO, A., CHIU, Y. H., DENG, L. & CHEN, Z. J. 2004. TAB2 and TAB3 activate the NF-kappaB pathway through binding to polyubiquitin chains. *Mol Cell,* 15**,** 535-48.

KANNOUCHE, P. L., WING, J. & LEHMANN, A. R. 2004. Interaction of human DNA polymerase eta with monoubiquitinated PCNA: a possible mechanism for the polymerase switch in response to DNA damage. *Mol Cell,* 14**,** 491-500.

KARRAS, G. I. & JENTSCH, S. 2010. The RAD6 DNA damage tolerance pathway operates uncoupled from the replication fork and is functional beyond S phase. *Cell,* 141**,** 255-67.

KIM, H., CHEN, J. & YU, X. 2007. Ubiquitin-binding protein RAP80 mediates BRCA1-dependent DNA damage response. *Science,* 316**,** 1202-5.

KIRISAKO, T., KAMEI, K., MURATA, S., KATO, M., FUKUMOTO, H., KANIE, M., SANO, S., TOKUNAGA, F., TANAKA, K. & IWAI, K. 2006. A ubiquitin ligase complex assembles linear polyubiquitin chains. *Embo J,* 25**,** 4877-87.

KIRKPATRICK, D. S., DENISON, C. & GYGI, S. P. 2005. Weighing in on ubiquitin: the expanding role of mass-spectrometry-based proteomics. *Nat Cell Biol,* 7**,** 750-7.

KIRKPATRICK, D. S., HATHAWAY, N. A., HANNA, J., ELSASSER, S., RUSH, J., FINLEY, D., KING, R. W. & GYGI, S. P. 2006. Quantitative analysis of in vitro ubiquitinated cyclin B1 reveals complex chain topology. *Nat Cell Biol,* 8**,** 700-10.

KNOP, M., SIEGERS, K., PEREIRA, G., ZACHARIAE, W., WINSOR, B., NASMYTH, K. & SCHIEBEL, E. 1999. Epitope tagging of yeast genes using a PCR-based strategy: more tags and improved practical routines. *Yeast,* 15**,** 963-72.

KOEGL, M., HOPPE, T., SCHLENKER, S., ULRICH, H. D., MAYER, T. U. & JENTSCH, S. 1999. A novel ubiquitination factor, E4, is involved in multiubiquitin chain assembly. *Cell,* 96**,** 635-44.

KOEPP, D. M., HARPER, J. W. & ELLEDGE, S. J. 1999. How the cyclin became a cyclin: regulated proteolysis in the cell cycle. *Cell,* 97**,** 431-4.

KOLAS, N. K., CHAPMAN, J. R., NAKADA, S., YLANKO, J., CHAHWAN, R., SWEENEY, F. D., PANIER, S., MENDEZ, M., WILDENHAIN, J., THOMSON, T. M., PELLETIER, L., JACKSON, S. P. & DUROCHER, D. 2007. Orchestration of the DNA-damage response by the RNF8 ubiquitin ligase. *Science,* 318**,** 1637-40.

KOMANDER, D. 2009. The emerging complexity of protein ubiquitination. *Biochem Soc Trans,* 37**,** 937-53.

KOMANDER, D., CLAGUE, M. J. & URBE, S. 2009a. Breaking the chains: structure and function of the deubiquitinases. *Nat Rev Mol Cell Biol,* 10**,** 550-63.

KOMANDER, D., REYES-TURCU, F., LICCHESI, J. D., ODENWAELDER, P., WILKINSON, K. D. & BARFORD, D. 2009b. Molecular discrimination of structurally equivalent Lys 63-linked and linear polyubiquitin chains. *EMBO Rep*.

KOSHLAND, D., KENT, J. C. & HARTWELL, L. H. 1985. Genetic analysis of the mitotic transmission of minichromosomes. *Cell,* 40**,** 393-403.

KULATHU, Y., AKUTSU, M., BREMM, A., HOFMANN, K. & KOMANDER, D. 2009. Two-sided ubiquitin binding explains specificity of the TAB2 NZF domain. *Nat Struct Mol Biol,* 16**,** 1328-30.

LAEMMLI, U. K. 1970. Cleavage of structural proteins during the assembly of the head of bacteriophage T4. *Nature,* 227**,** 680-5.

LAWRENCE, C. 1994. The RAD6 DNA repair pathway in Saccharomyces cerevisiae: what does it do, and how does it do it? *Bioessays,* 16**,** 253-8.

LIU, Z., WU, J. & YU, X. 2007. CCDC98 targets BRCA1 to DNA damage sites. *Nat Struct Mol Biol,* 14**,** 716-20.

LONGTINE, M. S., MCKENZIE, A., 3RD, DEMARINI, D. J., SHAH, N. G., WACH, A., BRACHAT, A., PHILIPPSEN, P. & PRINGLE, J. R. 1998. Additional modules for versatile and economical PCR-based gene deletion and modification in Saccharomyces cerevisiae. *Yeast,* 14**,** 953-61.

MAILAND, N., BEKKER-JENSEN, S., FAUSTRUP, H., MELANDER, F., BARTEK, J., LUKAS, C. & LUKAS, J. 2007. RNF8 ubiquitylates histones at DNA double-strand breaks and promotes assembly of repair proteins. *Cell,* 131**,** 887-900.

MAO, Y., SENIC-MATUGLIA, F., DI FIORE, P. P., POLO, S., HODSDON, M. E. & DE CAMILLI, P. 2005. Deubiquitinating function of ataxin-3: insights from the solution structure of the Josephin domain. *Proc Natl Acad Sci U S A,* 102**,** 12700-5.

MATSUMOTO, M., YADA, M., HATAKEYAMA, S., ISHIMOTO, H., TANIMURA, T., TSUJI, S., KAKIZUKA, A., KITAGAWA, M. & NAKAYAMA, K. I. 2004. Molecular clearance of ataxin-3 is regulated by a mammalian E4. *Embo J,* 23**,** 659-69.

MATSUSHITA, N., KITAO, H., ISHIAI, M., NAGASHIMA, N., HIRANO, S., OKAWA, K., OHTA, T., YU, D. S., MCHUGH, P. J., HICKSON, I. D., VENKITARAMAN, A. R., KURUMIZAKA, H. & TAKATA, M. 2005. A FancD2-monoubiquitin fusion reveals hidden functions of Fanconi anemia core complex in DNA repair. *Mol Cell,* 19**,** 841-7.

MCAINSH, A. D., TYTELL, J. D. & SORGER, P. K. 2003. Structure, function, and regulation of budding yeast kinetochores. *Annu Rev Cell Dev Biol,* 19**,** 519-39.

MCCLELAND, M. L., GARDNER, R. D., KALLIO, M. J., DAUM, J. R., GORBSKY, G. J., BURKE, D. J. & STUKENBERG, P. T. 2003. The highly conserved Ndc80 complex is required for kinetochore assembly, chromosome congression, and spindle checkpoint activity. *Genes Dev,* 17**,** 101-14.

MCINTYRE, J., PODLASKA, A., SKONECZNA, A., HALAS, A. & SLEDZIEWSKA-GOJSKA, E. 2006. Analysis of the spontaneous mutator phenotype associated with 20S proteasome deficiency in S. cerevisiae. *Mutat Res,* 593**,** 153-63.

MEISTER, S., SCHUBERT, U., NEUBERT, K., HERRMANN, K., BURGER, R., GRAMATZKI, M., HAHN, S., SCHREIBER, S., WILHELM, S., HERRMANN, M., JACK, H. M. & VOLL, R. E. 2007. Extensive immunoglobulin production sensitizes myeloma cells for proteasome inhibition. *Cancer Res,* 67**,** 1783-92.

MEYER, H. H., SHORTER, J. G., SEEMANN, J., PAPPIN, D. & WARREN, G. 2000. A complex of mammalian ufd1 and npl4 links the AAA-ATPase, p97, to ubiquitin and nuclear transport pathways. *Embo J,* 19**,** 2181-92.

MOIR, D., STEWART, S. E., OSMOND, B. C. & BOTSTEIN, D. 1982. Cold-sensitive cell-division-cycle mutants of yeast: isolation, properties, and pseudoreversion studies. *Genetics,* 100**,** 547-63.

MOLDOVAN, G. L., PFANDER, B. & JENTSCH, S. 2007. PCNA, the maestro of the replication fork. *Cell,* 129**,** 665-79.

MORIZANE, Y., HONDA, R., FUKAMI, K. & YASUDA, H. 2005. X-linked inhibitor of apoptosis functions as ubiquitin ligase toward mature caspase-9 and cytosolic Smac/DIABLO. *J Biochem,* 137**,** 125-32.

MOTEGI, A., LIAW, H. J., LEE, K. Y., ROEST, H. P., MAAS, A., WU, X., MOINOVA, H., MARKOWITZ, S. D., DING, H., HOEIJMAKERS, J. H. & MYUNG, K. 2008. Polyubiquitination of proliferating cell nuclear antigen by HLTF and SHPRH prevents genomic instability from stalled replication forks. *Proc Natl Acad Sci U S A,* 105**,** 12411-6.

MOTEGI, A., SOOD, R., MOINOVA, H., MARKOWITZ, S. D., LIU, P. P. & MYUNG, K. 2006. Human SHPRH suppresses genomic instability through proliferating cell nuclear antigen polyubiquitination. *J Cell Biol,* 175**,** 703-8.

NEKRASOV, V. S., SMITH, M. A., PEAK-CHEW, S. & KILMARTIN, J. V. 2003. Interactions between centromere complexes in Saccharomyces cerevisiae. *Mol Biol Cell,* 14**,** 4931-46.

NEWMAN, J. R., WOLF, E. & KIM, P. S. 2000. A computationally directed screen identifying interacting coiled coils from Saccharomyces cerevisiae. *Proc Natl Acad Sci U S A,* 97**,** 13203-8.

NICASTRO, G., MASINO, L., ESPOSITO, V., MENON, R. P., DE SIMONE, A., FRATERNALI, F. & PASTORE, A. 2009. Josephin domain of ataxin-3 contains two distinct ubiquitin-binding sites. *Biopolymers,* 91**,** 1203-14.

NICASTRO, G., MENON, R. P., MASINO, L., KNOWLES, P. P., MCDONALD, N. Q. & PASTORE, A. 2005. The solution structure of the Josephin domain of ataxin-3: structural determinants for molecular recognition. *Proc Natl Acad Sci U S A,* 102**,** 10493-8.

NIJMAN, S. M., HUANG, T. T., DIRAC, A. M., BRUMMELKAMP, T. R., KERKHOVEN, R. M., D'ANDREA, A. D. & BERNARDS, R. 2005. The deubiquitinating enzyme USP1 regulates the Fanconi anemia pathway. *Mol Cell,* 17**,** 331-9.

NISHIKAWA, H., OOKA, S., SATO, K., ARIMA, K., OKAMOTO, J., KLEVIT, R. E., FUKUDA, M. & OHTA, T. 2004. Mass spectrometric and mutational analyses reveal Lys-6-linked polyubiquitin chains catalyzed by BRCA1-BARD1 ubiquitin ligase. *J Biol Chem,* 279**,** 3916-24.

OESTERGAARD, V. H., LANGEVIN, F., KUIKEN, H. J., PACE, P., NIEDZWIEDZ, W., SIMPSON, L. J., OHZEKI, M., TAKATA, M., SALE, J. E. & PATEL, K. J. 2007. Deubiquitination of FANCD2 is required for DNA crosslink repair. *Mol Cell,* 28**,** 798-809.

OHKUNI, K., ABDULLE, R., TONG, A. H., BOONE, C. & KITAGAWA, K. 2008. Ybp2 associates with the central kinetochore of Saccharomyces cerevisiae and mediates proper mitotic progression. *PLoS One,* 3**,** e1617.

OHMORI, H., FRIEDBERG, E. C., FUCHS, R. P., GOODMAN, M. F., HANAOKA, F., HINKLE, D., KUNKEL, T. A., LAWRENCE, C. W., LIVNEH, Z., NOHMI, T., PRAKASH, L., PRAKASH, S., TODO, T., WALKER, G. C., WANG, Z. & WOODGATE, R. 2001. The Y-family of DNA polymerases. *Mol Cell,* 8**,** 7-8.

ORTIZ, J., STEMMANN, O., RANK, S. & LECHNER, J. 1999. A putative protein complex consisting of Ctf19, Mcm21, and Okp1 represents a missing link in the budding yeast kinetochore. *Genes Dev,* 13**,** 1140-55.

OZKAYNAK, E., FINLEY, D. & VARSHAVSKY, A. 1984. The yeast ubiquitin gene: head-to-tail repeats encoding a polyubiquitin precursor protein. *Nature,* 312**,** 663-6.

PAPOULI, E., CHEN, S., DAVIES, A. A., HUTTNER, D., KREJCI, L., SUNG, P. & ULRICH, H. D. 2005. Crosstalk between SUMO and ubiquitin on PCNA is mediated by recruitment of the helicase Srs2p. *Mol Cell,* 19**,** 123-33.

PARKER, J. L., BIELEN, A. B., DIKIC, I. & ULRICH, H. D. 2007. Contributions of ubiquitin- and PCNA-binding domains to the activity of Polymerase eta in Saccharomyces cerevisiae. *Nucleic Acids Res,* 35**,** 881-9.

PARKER, J. L., BUCCERI, A., DAVIES, A. A., HEIDRICH, K., WINDECKER, H. & ULRICH, H. D. 2008. SUMO modification of PCNA is controlled by DNA. *Embo J,* 27**,** 2422-31.

PARKER, J. L. & ULRICH, H. D. 2009. Mechanistic analysis of PCNA poly-ubiquitylation by the ubiquitin protein ligases Rad18 and Rad5. *Embo J,* 28**,** 3657-66.

PASTUSHOK, L., HANNA, M. & XIAO, W. 2010. Constitutive fusion of ubiquitin to PCNA provides DNA damage tolerance independent of translesion polymerase activities. *Nucleic Acids Res*.

PENG, J., SCHWARTZ, D., ELIAS, J. E., THOREEN, C. C., CHENG, D., MARSISCHKY, G., ROELOFS, J., FINLEY, D. & GYGI, S. P. 2003. A proteomics approach to understanding protein ubiquitination. *Nat Biotechnol,* 21**,** 921-6.

PETROSKI, M. D. & DESHAIES, R. J. 2005. Function and regulation of cullin-RING ubiquitin ligases. *Nat Rev Mol Cell Biol,* 6**,** 9-20.

PFANDER, B., MOLDOVAN, G. L., SACHER, M., HOEGE, C. & JENTSCH, S. 2005. SUMO-modified PCNA recruits Srs2 to prevent recombination during S phase. *Nature,* 436**,** 428-33.

PICKART, C. M. 2001. Mechanisms underlying ubiquitination. *Annu Rev Biochem,* 70**,** 503-33.

PICKART, C. M. & FUSHMAN, D. 2004. Polyubiquitin chains: polymeric protein signals. *Curr Opin Chem Biol,* 8**,** 610-6.

PINSKY, B. A., KUNG, C., SHOKAT, K. M. & BIGGINS, S. 2006. The Ipl1-Aurora protein kinase activates the spindle checkpoint by creating unattached kinetochores. *Nat Cell Biol,* 8**,** 78-83.

PLOSKY, B. S., VIDAL, A. E., FERNANDEZ DE HENESTROSA, A. R., MCLENIGAN, M. P., MCDONALD, J. P., MEAD, S. & WOODGATE, R. 2006. Controlling the subcellular localization of DNA polymerases iota and eta via interactions with ubiquitin. *Embo J,* 25**,** 2847-55.

PODLASKA, A., MCINTYRE, J., SKONECZNA, A. & SLEDZIEWSKA-GOJSKA, E. 2003. The link between 20S proteasome activity and post-replication DNA repair in Saccharomyces cerevisiae. *Mol Microbiol,* 49**,** 1321-32.

PRAKASH, S., INOBE, T., HATCH, A. J. & MATOUSCHEK, A. 2008. Substrate selection by the proteasome during degradation of protein complexes. *Nat Chem Biol*.

PRAKASH, S., JOHNSON, R. E. & PRAKASH, L. 2005. Eukaryotic translesion synthesis DNA polymerases: specificity of structure and function. *Annu Rev Biochem,* 74**,** 317-53.

RAASI, S., VARADAN, R., FUSHMAN, D. & PICKART, C. M. 2005. Diverse polyubiquitin interaction properties of ubiquitin-associated domains. *Nat Struct Mol Biol,* 12**,** 708-14.

RAHIGHI, S., IKEDA, F., KAWASAKI, M., AKUTSU, M., SUZUKI, N., KATO, R., KENSCHE, T., UEJIMA, T., BLOOR, S., KOMANDER, D., RANDOW, F., WAKATSUKI, S. & DIKIC, I. 2009. Specific recognition of linear ubiquitin chains by NEMO is important for NF-kappaB activation. *Cell,* 136**,** 1098-109.

RAIBORG, C., RUSTEN, T. E. & STENMARK, H. 2003. Protein sorting into multivesicular endosomes. *Curr Opin Cell Biol,* 15**,** 446-55.

RAMASUBRAMANYAN, S., COULON, S., FUCHS, R. P., LEHMANN, A. R. & GREEN, C. M. 2010. Ubiquitin-PCNA fusion as a mimic for mono-ubiquitinated PCNA in Schizosaccharomyces pombe. *DNA Repair (Amst).*

RAPE, M., HOPPE, T., GORR, I., KALOCAY, M., RICHLY, H. & JENTSCH, S. 2001. Mobilization of processed, membrane-tethered SPT23 transcription factor by CDC48(UFD1/NPL4), a ubiquitin-selective chaperone. *Cell,* 107**,** 667-77.

REYES-TURCU, F. E., VENTII, K. H. & WILKINSON, K. D. 2009. Regulation and cellular roles of ubiquitin-specific deubiquitinating enzymes. *Annu Rev Biochem,* 78**,** 363-97.

RICHLY, H., RAPE, M., BRAUN, S., RUMPF, S., HOEGE, C. & JENTSCH, S. 2005. A series of ubiquitin binding factors connects CDC48/p97 to substrate multiubiquitylation and proteasomal targeting. *Cell,* 120**,** 73-84.

ROBZYK, K., RECHT, J. & OSLEY, M. A. 2000. Rad6-dependent ubiquitination of histone H2B in yeast. *Science,* 287**,** 501-4.

ROTH, A. F. & DAVIS, N. G. 2000. Ubiquitination of the PEST-like endocytosis signal of the yeast a-factor receptor. *J Biol Chem,* 275**,** 8143-53.

SAEKI, Y., E. ISONO, AND A. TOH-E 2005. preparation of ubiquitinated substrates by the PY motif-insertion method for monitoring 26S proteasome activity. *Methods In Enzymology,* 399**,** 215-227.

SAEKI, Y., ISONO, E., OGUCHI, T., SHIMADA, M., SONE, T., KAWAHARA, H., YOKOSAWA, H. & TOH-E, A. 2004a. Intracellularly inducible, ubiquitin hydrolase-insensitive tandem ubiquitins inhibit the 26S proteasome activity and cell division. *Genes Genet Syst,* 79**,** 77-86.

SAEKI, Y., KUDO, T., SONE, T., KIKUCHI, Y., YOKOSAWA, H., TOH, E. A. & TANAKA, K. 2009. Lysine 63-linked polyubiquitin chain may serve as a targeting signal for the 26S proteasome. *EMBO J.*

SAEKI, Y., TAYAMA, Y., TOH-E, A. & YOKOSAWA, H. 2004b. Definitive evidence for Ufd2-catalyzed elongation of the ubiquitin chain through Lys48 linkage. *Biochem Biophys Res Commun,* 320**,** 840-5.

SAMBROOK, J., FRITSCH, E. F. AND MANIATIS, T. 1989. *Molecular cloning: A laboratory manual,* Cold Spring Harbor, New York, Cold Spring Harbor Laboratory Press.

SANTAGUIDA, S. & MUSACCHIO, A. 2009. The life and miracles of kinetochores. *Embo J,* 28**,** 2511-31.

SATO, Y., YOSHIKAWA, A., YAMAGATA, A., MIMURA, H., YAMASHITA, M., OOKATA, K., NUREKI, O., IWAI, K., KOMADA, M. & FUKAI, S. 2008. Structural basis for specific cleavage of Lys 63-linked polyubiquitin chains. *Nature,* 455**,** 358-62.

SEIGNEURIN-BERNY, D., VERDEL, A., CURTET, S., LEMERCIER, C., GARIN, J., ROUSSEAUX, S. & KHOCHBIN, S. 2001. Identification of components of the murine histone deacetylase 6 complex: link between acetylation and ubiquitination signaling pathways. *Mol Cell Biol,* 21**,** 8035-44.

SEUFERT, W. & JENTSCH, S. 1992. In vivo function of the proteasome in the ubiquitin pathway. *Embo J,* 11**,** 3077-80.

SHIH, S. C., SLOPER-MOULD, K. E. & HICKE, L. 2000. Monoubiquitin carries a novel internalization signal that is appended to activated receptors. *Embo J,* 19**,** 187-98.

SKAUG, B., JIANG, X. & CHEN, Z. J. 2009. The role of ubiquitin in NF-kappaB regulatory pathways. *Annu Rev Biochem,* 78**,** 769-96.

SMITH, M. M. 2002. Centromeres and variant histones: what, where, when and why? *Curr Opin Cell Biol,* 14**,** 279-85.

SMOGORZEWSKA, A., MATSUOKA, S., VINCIGUERRA, P., MCDONALD, E. R., 3RD, HUROV, K. E., LUO, J., BALLIF, B. A., GYGI, S. P., HOFMANN, K., D'ANDREA, A. D. & ELLEDGE, S. J. 2007. Identification of the FANCI protein, a monoubiquitinated FANCD2 paralog required for DNA repair. *Cell,* 129**,** 289-301.

SOBHIAN, B., SHAO, G., LILLI, D. R., CULHANE, A. C., MOREAU, L. A., XIA, B., LIVINGSTON, D. M. & GREENBERG, R. A. 2007. RAP80 targets BRCA1 to specific ubiquitin structures at DNA damage sites. *Science,* 316**,** 1198-202.

SPENCE, J., SADIS, S., HAAS, A. L. & FINLEY, D. 1995. A ubiquitin mutant with specific defects in DNA repair and multiubiquitination. *Mol Cell Biol,* 15**,** 1265-73.

STACK, J. H., WHITNEY, M., RODEMS, S. M. & POLLOK, B. A. 2000. A ubiquitin-based tagging system for controlled modulation of protein stability. *Nat Biotechnol,* 18**,** 1298-302.

STELTER, P. & ULRICH, H. D. 2003. Control of spontaneous and damage-induced mutagenesis by SUMO and ubiquitin conjugation. *Nature,* 425**,** 188-91.

STEWART, G. S., PANIER, S., TOWNSEND, K., AL-HAKIM, A. K., KOLAS, N. K., MILLER, E. S., NAKADA, S., YLANKO, J., OLIVARIUS, S., MENDEZ, M., OLDREIVE, C., WILDENHAIN, J., TAGLIAFERRO, A., PELLETIER, L., TAUBENHEIM, N., DURANDY, A., BYRD, P. J., STANKOVIC, T.,

TAYLOR, A. M. & DUROCHER, D. 2009. The RIDDLE syndrome protein mediates a ubiquitin-dependent signaling cascade at sites of DNA damage. *Cell,* 136**,** 420-34.

STRASSER, K., MASUDA, S., MASON, P., PFANNSTIEL, J., OPPIZZI, M., RODRIGUEZ-NAVARRO, S., RONDON, A. G., AGUILERA, A., STRUHL, K., REED, R. & HURT, E. 2002. TREX is a conserved complex coupling transcription with messenger RNA export. *Nature,* 417**,** 304-8.

SUZUKI, Y., NAKABAYASHI, Y. & TAKAHASHI, R. 2001. Ubiquitin-protein ligase activity of X-linked inhibitor of apoptosis protein promotes proteasomal degradation of caspase-3 and enhances its anti-apoptotic effect in Fas-induced cell death. *Proc Natl Acad Sci U S A,* 98**,** 8662-7.

TANAKA, K., MUKAE, N., DEWAR, H., VAN BREUGEL, M., JAMES, E. K., PRESCOTT, A. R., ANTONY, C. & TANAKA, T. U. 2005. Molecular mechanisms of kinetochore capture by spindle microtubules. *Nature,* 434**,** 987-94.

TENNO, T., FUJIWARA, K., TOCHIO, H., IWAI, K., MORITA, E. H., HAYASHI, H., MURATA, S., HIROAKI, H., SATO, M., TANAKA, K. & SHIRAKAWA, M. 2004. Structural basis for distinct roles of Lys63- and Lys48-linked polyubiquitin chains. *Genes Cells,* 9**,** 865-75.

THROWER, J. S., HOFFMAN, L., RECHSTEINER, M. & PICKART, C. M. 2000. Recognition of the polyubiquitin proteolytic signal. *Embo J,* 19**,** 94-102.

TODI, S. V., WINBORN, B. J., SCAGLIONE, K. M., BLOUNT, J. R., TRAVIS, S. M. & PAULSON, H. L. 2009. Ubiquitination directly enhances activity of the deubiquitinating enzyme ataxin-3. *Embo J,* 28**,** 372-82.

TOKUNAGA, F., SAKATA, S. I., SAEKI, Y., SATOMI, Y., KIRISAKO, T., KAMEI, K., NAKAGAWA, T., KATO, M., MURATA, S., YAMAOKA, S., YAMAMOTO, M., AKIRA, S., TAKAO, T., TANAKA, K. & IWAI, K. 2009. Involvement of linear polyubiquitylation of NEMO in NF-kappaB activation. *Nat Cell Biol*.

TREIER, M., STASZEWSKI, L. M. & BOHMANN, D. 1994. Ubiquitin-dependent c-Jun degradation in vivo is mediated by the delta domain. *Cell,* 78**,** 787-98.

TU, D., LI, W., YE, Y. & BRUNGER, A. T. 2007. Inaugural Article: Structure and function of the yeast U-box-containing ubiquitin ligase Ufd2p. *Proc Natl Acad Sci U S A,* 104**,** 15599-606.

TURNER, G. C. & VARSHAVSKY, A. 2000. Detecting and measuring cotranslational protein degradation in vivo. *Science,* 289**,** 2117-20.

UHLMANN, F., LOTTSPEICH, F. & NASMYTH, K. 1999. Sister-chromatid separation at anaphase onset is promoted by cleavage of the cohesin subunit Scc1. *Nature,* 400**,** 37-42.

UHLMANN, F., WERNIC, D., POUPART, M. A., KOONIN, E. V. & NASMYTH, K. 2000. Cleavage of cohesin by the CD clan protease separin triggers anaphase in yeast. *Cell,* 103**,** 375-86.

ULRICH, H. D. 2009. Regulating post-translational modifications of the eukaryotic replication clamp PCNA. *DNA Repair (Amst),* 8**,** 461-9.

ULRICH, H. D. & DAVIES, A. A. 2009. In vivo detection and characterization of sumoylation targets in Saccharomyces cerevisiae. *Methods Mol Biol,* 497**,** 81-103.

ULRICH, H. D. & JENTSCH, S. 2000. Two RING finger proteins mediate cooperation between ubiquitin-conjugating enzymes in DNA repair. *Embo J,* 19**,** 3388-97.

ULRICH, H. D. & WALDEN, H. 2010. Ubiquitin signalling in DNA replication and repair. *Nat Rev Mol Cell Biol,* 11**,** 479-89.

UNK, I., HAJDU, I., FATYOL, K., HURWITZ, J., YOON, J. H., PRAKASH, L., PRAKASH, S. & HARACSKA, L. 2008. Human HLTF functions as a ubiquitin ligase for proliferating cell nuclear antigen polyubiquitination. *Proc Natl Acad Sci U S A,* 105**,** 3768-73.

UNK, I., HAJDU, I., FATYOL, K., SZAKAL, B., BLASTYAK, A., BERMUDEZ, V., HURWITZ, J., PRAKASH, L., PRAKASH, S. & HARACSKA, L. 2006. Human SHPRH is a ubiquitin ligase for Mms2-Ubc13-dependent polyubiquitylation of proliferating cell nuclear antigen. *Proc Natl Acad Sci U S A,* 103**,** 18107-12.

VARADAN, R., ASSFALG, M., HARIRINIA, A., RAASI, S., PICKART, C. & FUSHMAN, D. 2004. Solution conformation of Lys63-linked di-ubiquitin chain provides clues to functional diversity of polyubiquitin signaling. *J Biol Chem,* 279**,** 7055-63.

VARADAN, R., ASSFALG, M., RAASI, S., PICKART, C. & FUSHMAN, D. 2005. Structural determinants for selective recognition of a Lys48-linked polyubiquitin chain by a UBA domain. *Mol Cell,* 18**,** 687-98.

VARADAN, R., WALKER, O., PICKART, C. & FUSHMAN, D. 2002. Structural properties of polyubiquitin chains in solution. *J Mol Biol,* 324**,** 637-47.

VARSHAVSKY, A. 1996. The N-end rule: functions, mysteries, uses. *Proc Natl Acad Sci U S A,* 93**,** 12142-9.

VERMA, R., ARAVIND, L., OANIA, R., MCDONALD, W. H., YATES, J. R., 3RD, KOONIN, E. V. & DESHAIES, R. J. 2002. Role of Rpn11 metalloprotease in deubiquitination and degradation by the 26S proteasome. *Science,* 298**,** 611-5.

VERMA, R., OANIA, R., GRAUMANN, J. & DESHAIES, R. J. 2004. Multiubiquitin chain receptors define a layer of substrate selectivity in the ubiquitin-proteasome system. *Cell,* 118**,** 99-110.

VISSERS, J. H., NICASSIO, F., VAN LOHUIZEN, M., DI FIORE, P. P. & CITTERIO, E. 2008. The many faces of ubiquitinated histone H2A: insights from the DUBs. *Cell Div,* 3**,** 8.

WAN, X., O'QUINN, R. P., PIERCE, H. L., JOGLEKAR, A. P., GALL, W. E., DELUCA, J. G., CARROLL, C. W., LIU, S. T., YEN, T. J., MCEWEN, B. F., STUKENBERG, P. T., DESAI, A. & SALMON, E. D. 2009. Protein architecture of the human kinetochore microtubule attachment site. *Cell,* 137**,** 672-84.

WANG, B., MATSUOKA, S., BALLIF, B. A., ZHANG, D., SMOGORZEWSKA, A., GYGI, S. P. & ELLEDGE, S. J. 2007. Abraxas and RAP80 form a BRCA1 protein complex required for the DNA damage response. *Science,* 316**,** 1194-8.

WATANABE, K., TATEISHI, S., KAWASUJI, M., TSURIMOTO, T., INOUE, H. & YAMAIZUMI, M. 2004. Rad18 guides poleta to replication stalling sites through physical interaction and PCNA monoubiquitination. *Embo J,* 23**,** 3886-96.

WEI, R. R., AL-BASSAM, J. & HARRISON, S. C. 2007. The Ndc80/HEC1 complex is a contact point for kinetochore-microtubule attachment. *Nat Struct Mol Biol,* 14**,** 54-9.

WEI, R. R., SCHNELL, J. R., LARSEN, N. A., SORGER, P. K., CHOU, J. J. & HARRISON, S. C. 2006. Structure of a central component of the yeast kinetochore: the Spc24p/Spc25p globular domain. *Structure,* 14**,** 1003-9.

WEI, R. R., SORGER, P. K. & HARRISON, S. C. 2005. Molecular organization of the Ndc80 complex, an essential kinetochore component. *Proc Natl Acad Sci U S A,* 102**,** 5363-7.

WELBURN, J. P., VLEUGEL, M., LIU, D., YATES, J. R., 3RD, LAMPSON, M. A., FUKAGAWA, T. & CHEESEMAN, I. M. 2010. Aurora B phosphorylates spatially distinct targets to differentially regulate the kinetochore-microtubule interface. *Mol Cell,* 38**,** 383-92.

WESTERMANN, S., CHEESEMAN, I. M., ANDERSON, S., YATES, J. R., 3RD, DRUBIN, D. G. & BARNES, G. 2003. Architecture of the budding yeast kinetochore reveals a conserved molecular core. *J Cell Biol,* 163**,** 215-22.

WESTERMANN, S., DRUBIN, D. G. & BARNES, G. 2007. Structures and functions of yeast kinetochore complexes. *Annu Rev Biochem,* 76**,** 563-91.

WESTERMANN, S., WANG, H. W., AVILA-SAKAR, A., DRUBIN, D. G., NOGALES, E. & BARNES, G. 2006. The Dam1 kinetochore ring complex moves processively on depolymerizing microtubule ends. *Nature,* 440**,** 565-9.

WIGGE, P. A., JENSEN, O. N., HOLMES, S., SOUES, S., MANN, M. & KILMARTIN, J. V. 1998. Analysis of the Saccharomyces spindle pole by matrix-assisted laser desorption/ionization (MALDI) mass spectrometry. *J Cell Biol,* 141**,** 967-77.

WIGGE, P. A. & KILMARTIN, J. V. 2001. The Ndc80p complex from Saccharomyces cerevisiae contains conserved centromere components and has a function in chromosome segregation. *J Cell Biol,* 152**,** 349-60.

WILLIAMS, R. L. & URBE, S. 2007. The emerging shape of the ESCRT machinery. *Nat Rev Mol Cell Biol,* 8**,** 355-68.

WILLIAMSON, A., WICKLIFFE, K. E., MELLONE, B. G., SONG, L., KARPEN, G. H. & RAPE, M. 2009. Identification of a physiological E2 module for the human anaphase-promoting complex. *Proc Natl Acad Sci U S A,* 106**,** 18213-8.

WINDECKER, H. & ULRICH, H. D. 2008. Architecture and assembly of poly-SUMO chains on PCNA in Saccharomyces cerevisiae. *J Mol Biol,* 376**,** 221-31.

WINEY, M., MAMAY, C. L., O'TOOLE, E. T., MASTRONARDE, D. N., GIDDINGS, T. H., JR., MCDONALD, K. L. & MCINTOSH, J. R. 1995. Three-dimensional ultrastructural analysis of the Saccharomyces cerevisiae mitotic spindle. *J Cell Biol,* 129**,** 1601-15.

WONG, J., NAKAJIMA, Y., WESTERMANN, S., SHANG, C., KANG, J. S., GOODNER, C., HOUSHMAND, P., FIELDS, S., CHAN, C. S., DRUBIN, D., BARNES, G. & HAZBUN, T. 2007. A protein interaction map of the mitotic spindle. *Mol Biol Cell,* 18**,** 3800-9.

WU-BAER, F., LAGRAZON, K., YUAN, W. & BAER, R. 2003. The BRCA1/BARD1 heterodimer assembles polyubiquitin chains through an unconventional linkage involving lysine residue K6 of ubiquitin. *J Biol Chem,* 278**,** 34743-6.

WU, C. J., CONZE, D. B., LI, T., SRINIVASULA, S. M. & ASHWELL, J. D. 2006. NEMO is a sensor of Lys 63-linked polyubiquitination and functions in NF-kappaB activation. *Nat Cell Biol,* 8**,** 398-406.

XU, P., DUONG, D. M., SEYFRIED, N. T., CHENG, D., XIE, Y., ROBERT, J., RUSH, J., HOCHSTRASSER, M., FINLEY, D. & PENG, J. 2009. Quantitative proteomics reveals the function of unconventional ubiquitin chains in proteasomal degradation. *Cell,* 137**,** 133-45.

XU, Q., FARAH, M., WEBSTER, J. M. & WOJCIKIEWICZ, R. J. 2004. Bortezomib rapidly suppresses ubiquitin thiolesterification to ubiquitin-conjugating enzymes and inhibits ubiquitination of histones and type I inositol 1,4,5-trisphosphate receptor. *Mol Cancer Ther,* 3**,** 1263-9.

YAO, T. & COHEN, R. E. 2002. A cryptic protease couples deubiquitination and degradation by the proteasome. *Nature,* 419**,** 403-7.

ZHANG, H. & LAWRENCE, C. W. 2005. The error-free component of the RAD6/RAD18 DNA damage tolerance pathway of budding yeast employs sister-strand recombination. *Proc Natl Acad Sci U S A,* 102**,** 15954-9.

ZHANG, X. D., GOERES, J., ZHANG, H., YEN, T. J., PORTER, A. C. & MATUNIS, M. J. 2008. SUMO-2/3 modification and binding regulate the association of CENP-E with kinetochores and progression through mitosis. *Mol Cell,* 29**,** 729-41.

ZHAO, S. & ULRICH, H. D. 2010. Distinct consequences of posttranslational modification by linear versus K63-linked polyubiquitin chains. *Proc Natl Acad Sci U S A,* 107**,** 7704-9.

ZHUANG, Z., JOHNSON, R. E., HARACSKA, L., PRAKASH, L., PRAKASH, S. & BENKOVIC, S. J. 2008. Regulation of polymerase exchange between Poleta and Poldelta by monoubiquitination of PCNA and the movement of DNA polymerase holoenzyme. *Proc Natl Acad Sci U S A,* 105**,** 5361-6.

Appendixes

Appendix 1: Yeast Strains

All yeast strains used in this thesis are listed below in Table 2.1. Relevant genotypes of all yeast strains are included in this table and yeast strains from other sources are acknowledged. Yeast strains generated by myself were subject to standard genetic manipulation as described in section 2.4. YIp128 vectors were integrated into the *LEU2* locus by linearisation with *Bst*EII. YIp211 vectors were integrated into the *URA3* locus by linearisation with *Pst*I.

Strain Number	**Strain Name**	**Genotype**	**Source**
yHU 1	DF5 Diploid	*his1-1, leu2-3,2-112, lys2-801, trp1-1, ura3-52*	(Finley et al., 1987)
yHU 2	DF5 Mat alpha	*his1-1, leu2-3,2-112, lys2-801, trp1-1, ura3-52*	(Finley et al., 1987)
yHU 3	DF5 Mat a	*his1-1, leu2-3,2-112, lys2-801, trp1-1, ura3-52*	(Finley et al., 1987)
yHU 1745	Y187	*ura3-52, his3-200, ade2-101, trp1-901, leu2-3,112, gal4Δ, met⁻, gal80Δ, URA3::GAL1$_{UAS}$GAL1$_{TATA}$-lacZ, MEL1*	Clontech
yHU 195	PJ69-4A	*trp1-901, leu2-3,112, ura3-52, his3-200, gal4Δ, gal80Δ, LYS2::GAL1-HIS3, GAL2-ADE2, met2::GAL7-lacZ*	(James et al., 1996)
yHU 142	*rad18*	DF5 *rad18::TRP*	(Parker et al., 2007)
yHU 1878	*rad18 ΔTLS*	DF5 *rad18::TRP rad30::HIS3 rev1::URA3 rev3::KanMX*	(Parker et al., 2007)
yHU 5	*PRE1*	DF5 *pre1::TRP1 + pSE362-PRE1*	(Seufert and Jentsch, 1992)
yHU 6	*pre1-1*	DF5 *pre1::TRP1 + pSE362-pre1-1*	(Seufert and Jentsch, 1992)
yHU 572	*CIM3*	S288c background	(Seufert and Jentsch, 1992)
yHU 573	*Cim3-1*	S288c background *cim3-1*	(Seufert and Jentsch, 1992)
yHU 2338	^{His}*POL30 PRE1*	*PRE1 Leu2::Yip128-*^{His}*POL30[LEU2]*	This study
yHU 2339	^{His}*POL30 pre1-1*	*Pre1-1 Leu2::Yip128-*^{His}*POL30[LEU2]*	This study
yHU 1097	^{His}*POL30*	DF5 *pol30::URA3 Leu2::Yip128-*	(Papouli et al., 2005)

		^{His}POL30[LEU2]	
yHU 2336	*^{His}POL30 ump1*	DF5 *ump1::klTRP1 pol30::URA3 Leu2::Yip128-^{His}POL30[LEU2]*	This study
yHU 2337	*^{His}POL30 pdr5*	DF5 *pol30::URA3 pdr5::KanMX Leu2::Yip128-^{His}POL30[LEU2]*	This study
yHU 2250	*ufd4*	*DF5 ufd4::KanMX*	This study
yHU 591	*ufd2*	DF5 *ufd2::LEU2*	(Johnson et al., 1995)
yHU 2312	UFD2	DF5 *UFD2-9myc::klTRP1*	This study
yHU 2319	*ufd2(ΔUbox)*	DF5 *ufd2(1-883)-9myc::klTRP1*	This study
yHU 1987	*cdc48-2*	S288c *ura3-52 cdc48-2*	(Moir et al., 1982)
yHU 1988	NPL4	*ura3-52 leu2Δ1 trp1Δ63*	(Auld et al., 2006)
yHU 1989	*npl4-1*	*ura3-52 leu2Δ1 trp1Δ63 npl4-1*	(Auld et al., 2006)
yHU 2249	*rad23 dsk2*	DF5 *rad23::HIS3 dsk2::KanMX*	This study
yHU 2262	*spc25(L109A)*	DF5 *spc25::HIS3 ura3::YIp211-spc25(L109A)*	This study
yHU 2263	*spc25(L113A)*	DF5 *spc25::HIS3 ura3::YIp211-spc25(L113A)*	This study
yHU 2264	*spc25(3A)*	DF5 *spc25::HIS3 ura3::YIp211-spc25(L109A/L113A/R116A)*	This study
yHU 790	BY4741	*leu2Δ0, met15Δ0, ura3Δ0, his3Δ0*	OPEN BIOSYSTEMS
	SPC25^{TAP}	BY4741 + *SPC25-TAP::HIS3*	OPEN BIOSYSTEMS
	SPC24^{TAP}	BY4741 + *SPC24-TAP::HIS3*	OPEN BIOSYSTEMS
	NDC80^{TAP}	BY4741 + *NDC80-TAP::HIS3*	OPEN BIOSYSTEMS
	NUF2^{TAP}	BY4741 + *NUF2-TAP::HIS3*	OPEN BIOSYSTEMS
	MTW1^{TAP}	BY4741 + *MTW1-TAP::HIS3*	OPEN BIOSYSTEMS
	NNF1^{TAP}	BY4741 + *NNF1-TAP::HIS3*	OPEN BIOSYSTEMS
	DSN1^{TAP}	BY4741 + *DSN1-TAP::HIS3*	OPEN BIOSYSTEMS
	NSL1^{TAP}	BY4741 + *NSL1-TAP::HIS3*	OPEN BIOSYSTEMS
	CTF19^{TAP}	BY4741 + *CTF19-TAP::HIS3*	OPEN BIOSYSTEMS
	OKP1^{TAP}	BY4741 + *OKP1-TAP::HIS3*	OPEN BIOSYSTEMS

	MCM21^{TAP}	BY4741 + *MCM21-TAP::HIS3*	OPEN BIOSYSTEMS
	AME1^{TAP}	BY4741 + *AME1-TAP::HIS3*	OPEN BIOSYSTEMS
	MAD1^{TAP}	BY4741 + *MAD1-TAP::HIS3*	OPEN BIOSYSTEMS
	MAD2^{TAP}	BY4741 + *MAD2-TAP::HIS3*	OPEN BIOSYSTEMS
	MAD3^{TAP}	BY4741 + *MAD3-TAP::HIS3*	OPEN BIOSYSTEMS
	MPS1^{TAP}	BY4741 + *MPS1-TAP::HIS3*	OPEN BIOSYSTEMS
	MCM21^{GFP}	BY4741 + *MCM21-eGFP::HIS3*	OPEN BIOSYSTEMS
yHU 2385	*spc25(L109A) MCM21^{GFP}*	DF5 +*spc25::HIS3, ura3::YIp211-spc25(L109A), MCM21-eGFP::KanMX*	This study
yHU 2375	K699	*ade2-1 trp1-1 can1-100 leu2-3,112 his3-11,15 ura3 ssd1*	(Nekrasov et al., 2003)
yHU 2393	*spc25(L109A)*	*ade2-1 trp1-1 can1-100 leu2-3,112 his3-11,15 ura3 ssd1 spc25(L109A)*	This study
yHU 2376	*dsn1-7*	*ade2-1 trp1-1 can1-100 leu2-3,112 his3-11,15 ura3 ssd1 dsn1-7*	(Nekrasov et al., 2003)
yHU 2392	*dsn1-7 spc25(L109A)*	*ade2-1 trp1-1 can1-100 leu2-3,112 his3-11,15 ura3 ssd1 dsn1-7 spc25(L109A)*	This study
yHU 2377	*dsn1-8*	*ade2-1 trp1-1 can1-100 leu2-3,112 his3-11,15 ura3 ssd1 dsn1-8*	(Nekrasov et al., 2003)
yHU 2494	*dsn1-8 spc25(L109A)*	*ade2-1 trp1-1 can1-100 leu2-3,112 his3-11,15 ura3 ssd1 dsn1-8 spc25(L109A)*	This study
yHU 2341	*SPC25^{9myc}*	DF5 *spc25::HIS3, ura3:: klTRP1::YIp211-SPC25^{9myc}*	This study
yHU 2342	*spc25(L109A)^{9myc}*	DF5 *spc25::HIS3, ura3:: klTRP1::YIp211-spc25(L109A)^{9myc}*	This study

Table A- 1 A list of all yeast strains used in this thesis

Appendix 2: *E.coli* Strains

All the *E.coli* strains used in this thesis are listed below.

Name	Source	Genotype	Application
Top10	Invitrogen	F- *mcr*A Δ(*mrr-hsd*RMS-*mcr*BC) Φ80*lac*ZΔM15 Δ*lac*X74 *rec*A1 *ara*Δ139 Δ(*ara-leu*)7697 *gal*U *gal*K *rps*L (Str$_R$) *end*A1 *nup*G	Molecular cloning
BL21 Codon $^{2+}$	Novagen	E. *coli* B F *ompT hsdS*(r_B^- m_B^-) *dcm*$^+$ Tet^r *gal endA* Hte	Protein purification

Table A- 2 A list of *E.coli* strains used in this thesis

Appendix 3: Plasmids

All plasmids used in this thesis are listed in these two tables. Plasmids from other sources are acknowledged. Details about the plasmids generated by myself can be found in the construction column of the table and in section 2.2.2 and 2.2.3.

Plasmid number	Plasmid name	Source
pHU 66	YIplac128	(Gietz and Sugino, 1988)
pHU 710	YIp128-P30-PCNA*	(Parker et al., 2007)
pHU 1176	YIp128-P30-Ub*-PCNA*	(Parker et al., 2007)
pHU 732	YIp128-P30-His-PCNA	(Davies et al., 2008)
pHU 1533	pGEX- Ub$^{*}_{4}$	Irene Saugar
pHU 1672	pGEX-UBAN (NEMO)	(Komander et al., 2009b)
pHU 477	Ub-ßGal	(Johnson et al., 1995)
pHU 1036	pGBT9-Ub*	Ulrich lab strain collection
pHU 1035	pGAD424-Ub*	Ulrich lab strain collection
pHU 1623	pGEX-Ub (I44A) (human)	Roy Anindya (Svejstrup Lab)
pHU 669	pHK110/ pRS426-ADE3	(Henry and Silver, 1996)
pHU 794	pHT4467Δ	(Strasser et al., 2002)
pHU 308	YEplac181	Ulrich lab strain collection (Gietz and Sugino, 1988)
pHU 821	YEp181-CUP1-His-Ub	Ulrich lab strain collection

Table A- 3 A list of plasmids that were constructed by others

Plasmid number	Plasmid name	Construction	Source
pHU 1647	YIp128-P30-Ub$^{*}_{2}$(L)-PCNA*	*BamH*I/*Pst*I fragment from #1441 pGAD-Ub$^{*}_{2}$(L)-POL30(DMO) clone into *BamH*I/*Pst*I digested plasmid #710	This study
pHU 1648	YIp128-P30-Ub$^{*}_{3}$(L)-PCNA*	*BamH*I/*Pst*I fragment from #1440 pGAD-Ub$^{*}_{3}$(L)-POL30(DMO) clone into *BamH*I/*Pst*I digested plasmid #710	This study
pHU 1649	YIp128-P30-Ub$^{*}_{4}$(L)-PCNA*	*BamH*I/*Pst*I fragment from #1439 pGAD-Ub$^{*}_{4}$(L)-POL30(DMO) clone into *BamH*I/*Pst*I digested plasmid #710	This study
pHU 1650	YIp128-P30-Ub$^{*}_{4}$-PCNA*	#1444 pGBT-Ub$^{*}_{4}$-POL30(DMO) *Eco*RI/*Pst*I partial digestion, blunt and clone into *BamH*I/*Pst*I digested/blunted plasmid #710	This study
pHU 1677	YIp128-P30-PCNA*- Ub$^{*}_{4}$	PCR (oHU1524/1525) from plasmid #1529, *Kpn*I/*Pst*I fragment replaces Ub in #1177 YIp128-P30-POL30(DMO)-Ub3R	This study

pHU 1678	YIp128-P30-Ub^{K63*}-PCNA*	PCR (oHU500/501) from plasmid #480, *BamH*I/*Bgl*II fragment clone into *BamH*I site in plasmid #710	This study
pHU 1680	pET28a-His-Ub$^{*}_{4}$-PCNA*	*Eco*RI/*Hind*III and *Eco*RI/*Eco*RI fragments from plasmid #1651 pGAD-Ub$^{*}_{4}$-PCNA*, clone into pET28a *Eco*RI/*Hind*III sites sequentially.	This study
pHU 1653	Ub$^{*}_{4}$-ßGal	PCR (oHU1240/124) from pGAD-Ub$^{*}_{4}$ treat with *Bgl*II/blunt, clone into *Sph*I/blunt #477, plasmid then digested with *BamH*I and religate to remove Ub	This study
pHU 1682	Ub*-ßGal	PCR (oHU500/124) from plasmid #1529 pGAD-Ub$^{*}_{4}$, isolate Ub* from gel, TOPO cloning, *BamH*I/*Bgl*II fragment inserted into *BamH*I site of plasmid #477 gives Ub$_2$-ßgal. *Sph*I/*BamH*I, blunt, religation gives Ub(3R)-ßgal	This study
pHU 1654	ßGal	No.477 Ubi-ßgal digested with *Sph*I/*BamH*I and the vector was first blunted and ligated.	This study
pHU 1655	Ub$^{*}_{8}$-ßGal	PCR (oHU500/1241) from #1529 pGAD-Ub$^{*}_{4}$, *BamH*I/*Bgl*II fragment put into *BamH*I site in #477 to have Ub$_5$-ßgal. (oHU500/501) from #1529 pGAD-Ub$^{*}_{4}$, *BamH*I/*Bgl*II digestion and put into *BamH*I site to have Ub$_9$-ßgal. *Sph*I/*BamH*I, blunt and religate to get Ub$^{*}_{8}$-ßgal	This study
pHU 1531	pGBT9-Ub$^{*}_{4}$(L)	*Sma*I fragment from plasmid # 1442, clone into *Sma*I site of pGBT9 vector, then take out as *BamH*I, put into pGBD-C2 vector	This study
pHU 1532	pGAD424-Ub$^{*}_{4}$(L)	*Sma*I fragment from plasmid #1442, clone into *Sma*I site of pGAD424 vector	This study
pHU 1530	pGBT9-Ub$^{*}_{4}$	*Eco*RI/*BamH*I fragment from plasmid #1529 and clone into *Eco*RI/*Bgl*II of pGBD-C3	This study
pHU 1529	pGAD424-Ub$^{*}_{4}$	PCR (oHU 902/903) from plasmid #14, TOPO cloning, Fragment *Stu*I/*Msc*I ligation & digestion with *Stu*I, *Msc*I isolate ub$_4$ fragment, TOPO blunt cloning, *Eco*RI/blunt into #191 pGAD-C1 *Sma*I.	This study
pHU 1572	pGBT9-ETP1	PCR (oHU1160/1161) from yeast gemonic DNA, *Bgl*II/*Pst*I digestion, clone into *BamH*I/*Pst*I of pGBT9	This study
pHU 1579	pGAD424-ETP1	PCR (oHU1160/1161) from yeast gemonic DNA, *Bgl*II/*Pst*I digestion, clone into *BamH*I/*Pst*I of pGAD424	This study
pHU 1573	pGBT9-ETP1 (459-585)	PCR (oHU1162/1161) amplification from yeast genomic DNA, *Bgl*II/*Pst*I digestion,	This study

		clone into *BamH*I/*Pst*I of pGBT9	
pHU 1580	pGAD424-ETP1 (459-585)	PCR (oHU1162/1161) amplification from yeast genomic DNA, *Bgl*II/*Pst*I digestion, clone into *BamH*I/*Pst*I of pGAD424	This study
pHU 1684	pGBT9-SPC25	PCR (oHU1163/1164) from yeast genomic DNA, *BamH*I digestion and clone into *BamH*I site of pGBT9 vector.	This study
pHU 1700	pGAD424-SPC25	PCR (oHU1163/1164) from yeast genomic DNA, *BamH*I digestion and clone into *BamH*I site of pGAD424 vector.	This study
pHU 1685	pGBT9-SPC25 (107-221)	PCR (oHU1165/1164) amplification from yeast genomic DNA, *BamH*I digestion and clone into *BamH*I site of pGBT9 vector.	This study
pHU 1701	pGAD424-SPC25 (107-221)	PCR (oHU1165/1164) amplification from yeast genomic DNA, *BamH*I digestion and clone into *BamH*I site of pGAD424 vector.	This study
pHU 2079	pGBT9-RSC6	PCR (oHU1166/1167) amplification from yeast genomic DNA, *BamH*I digestion and clone into *BamH*I site of pGBT9 vector.	This study
pHU 2080	pGAD424-RSC6	PCR (oHU1166/1167) amplification from yeast genomic DNA, *BamH*I digestion and clone into *BamH*I site of pGAD424 vector.	This study
pHU 2081	pGBT9-RSC6 (94-211)	PCR (oHU1168/1169) amplification from yeast genomic DNA, *BamH*I/*Pst*I digestion and clone into *BamH*I/*Pst*I site of pGB9 vector.	This study
pHU 2082	pGAD424-RSC6 (94-211)	PCR (oHU1168/1169) amplification from yeast genomic DNA, *BamH*I/*Pst*I digestion and clone into *BamH*I/*Pst*I site of pGAD424 vector.	This study
pHU 1686	pGBT9-SPC25 (1-67)	PCR (oHU1211/1163) amplification from plasmid #1700, *BamH*I/*Pst*I digestion, clone 210bp band into *BamH*I/*Pst*I site of pGBT9 vector.	This study
pHU 1702	pGAD424-SPC25 (1-67)	*BamH*I/*Pst*I digestion from plamsid #1686 and clone into *BamH*I/*Pst*I site of pGAD424 vector.	This study
pHU 1687	pGBT9-SPC25 (1-106)	PCR (oHU1211/1163) amplification from plasmid #1700. *BamH*I/*Pst*I digestion, clone both products into *BamH*I/*Pst*I site of pGBT9 vector.	This study
pHU 1703	pGAD424-SPC25 (1-106)	*BamH*I/*Pst*I digestion from plamsid #1687 and clone into *BamH*I/*Pst*I site of pGAD424 vector.	This study
pHU 1688	pGBT9-SPC25 (133-221)	PCR (oHU1205/1206) amplification from plasmid #1700. *BamH*I/*Pst*I digestion, clone into *BamH*I/*Pst*I site of pGBT9 vector.	This study

pHU 1704	pGAD424-SPC25 (133-221)	*BamH*I/*Pst*I digestion from plamsid #1688 and clone into *BamH*I/*Pst*I site of pGAD424 vector.	This study
pHU 1689	pGBT9-SPC25 (146-221)	PCR (oHU1208/1206) amplification from plasmid #1700, *BamH*I/*Pst*I digestion and clone into *BamH*I/*Pst*I site of pGBT9 vector.	This study
pHU 1705	pGAD424-SPC25 (146-221)	*BamH*I/*Pst*I digestion from plamsid #1689 and clone into *BamH*I/*Pst*I site of pGAD424 vector.	This study
pHU 1690	pGBT9-SPC25 (186-221)	PCR (oHU1207/1206) amplification from plasmid #1700, *BamH*I/*Pst*I digestion and clone into *BamH*I/*Pst*I site of pGBT9 vector.	This study
pHU 1706	pGAD424-SPC25 (186-221)	*BamH*I/*Pst*I digestion from plamsid #1690 and clone into *BamH*I/*Pst*I site of pGAD424 vector.	This study
pHU 1691	pGBT9-SPC25 (107-189)	PCR (oHU1209/1165) amplification from plasmid #1700, *BamH*I/*Pst*I digestion and clone into *BamH*I/*Pst*I site of pGBT9 vector.	This study
pHU 1707	pGAD424-SPC25 (107-189)	*BamH*I/*Pst*I digestion from plamsid #1691 and clone into *BamH*I/*Pst*I site of pGAD424 vector.	This study
pHU 1692	pGBT9-SPC25 (107-146)	PCR (oHU1210/1165) amplification from plasmid #1700, *BamH*I/*Pst*I digestion and clone into *BamH*I/*Pst*I site of pGBT9 vector.	This study
pHU 1708	pGAD424-SPC25 (107-146)	*BamH*I/*Pst*I digestion from plamsid #1692 and clone into *BamH*I/*Pst*I site of pGAD424 vector.	This study
pHU 1693	pGBT9-SPC25 (117-221)	PCR (oHU1321/1206) amplification from plasmid #1700, *EcoR*I/*Pst*I digestion and clone into *EcoR*I/*Pst*I site of pGBT9 vector.	This study
pHU 1709	pGAD424-SPC25 (117-221)	*EcoR*I/*Pst*I digestion from plamsid #1693 and clone into *EcoR*I/*Pst*I site of pGAD424 vector.	This study
pHU 1694	pGBT9-SPC25 (1-133)	PCR (oHU1163/1320) amplification from plasmid #1700, *BamH*I/*Pst*I digestion and clone into *BamH*I/*Pst*I site of pGBT9 vector.	This study
pHU 1710	pGAD424-SPC25 (1-133)	*BamH*I/*Pst*I digestion from plamsid #1694 and clone into *BamH*I/*Pst*I site of pGAD424 vector.	This study
pHU 1695	pGBT9-SPC25 (107-133)	PCR (oHU1165/1320) amplification from plasmid #1700, *BamH*I/*Pst*I digestion and clone into *BamH*I/*Pst*I site of pGBT9	This study

		vector.	
pHU 1711	pGAD424-SPC25 (107-133)	*BamH*I/*Pst*I digestion from plamsid #1695 and clone into *BamH*I/*Pst*I site of pGAD424 vector.	This study
pHU 1696	pGBT9-SPC25 (3A)	PCR mutagenesis with oHU1322/1323 to introduce mutation L109A, L113A, R116A and amplify with oHU1163/ 1206, *BamH*I/*Pst*I clone into pGBT9 vector.	This study
pHU 1712	pGAD424-SPC25 (3A)	*BamH*I/*Pst*I digestion from plamsid #1696 and clone into *BamH*I/*Pst*I site of pGAD424 vector.	This study
pHU 1697	pGBT9-SPC25 (L109A)	PCR mutagenesis with oHU 1426/1427 to introduce mutation L109A and amplify with oHU1163/ 1206, *BamH*I/*Pst*I clone into pGBT9 vector.	This study
pHU 1713	pGAD424-SPC25 (L109A)	*BamH*I/*Pst*I digestion from plamsid #1697 and clone into *BamH*I/*Pst*I site of pGAD424 vector.	This study
pHU 1698	pGBT9-SPC25 (L113A)	PCR mutagenesis with oHU1428/1429 to introduce mutation L113A and amplify with oHU1163/ 1206, *BamH*I/*Pst*I clone into pGBT9 vector.	This study
pHU 1714	pGAD424-SPC25 (L113A)	*BamH*I/*Pst*I digestion from plamsid #1698 and clone into *BamH*I/*Pst*I site of pGAD424 vector.	This study
pHU 1699	pGBT9-SPC25 (R116A)	PCR mutagenesis with oHU 1430/1431 to introduce mutation R116A and amplify with oHU1163/ 1206, *BamH*I/*Pst*I clone into pGBT9 vector.	This study
pHU 1715	pGAD424-SPC25 (R116A)	*BamH*I/*Pst*I digestion from plamsid #1699 and clone into *BamH*I/*Pst*I site of pGAD424 vector.	This study
pHU 1718	pGBT9-SPC24	PCR (oHU1228/1266) from yeast genomic DNA, *BamH*I/*EcoR*I digestion and clone into pGBT9 vector.	This study
pHU 1719	pGAD424-SPC24	*BamH*I/*EcoR*I digestion from plasmid #1718 pGBT-SPC24 and clone into pGAD424 vector.	This study
pHU 1716	pGEX-SPC25 (107-221)	*Sma*I/*Sal*I fragment from plasmid # 1701 pGAD-Spc25 (107-221) and clone into pGEX4T1 vector	This study
pHU 1717	pET28a-SPC25 (107-221)	*Sma*I/*Sal*I fragment from plasmid # 1701 pGAD-Spc25 (107-221) and clone into pGEX4T1 vector	This study
pHU 1720	pET15b-SPC24 (154-213)	PCR (oHU1228/1227) from yeast genomic DNA, *BamH*I/*Xho*I digestion and clone into pET15b vector.	This study
pHU 1724	YIp211-SPC25	PCR amplify SPC25 ORF and	This study

	(L109A)	promoter/terminator with oHU1432/1433 and mutagenesis with oHU 1426/1427 to introduce mutation L109A, *Eco*RI/*Hind*III digestion and clone into vector YIp211.	
pHU 1725	YIp211-SPC25 (L113A)	PCR amplify SPC25 ORF and promoter/terminator with oHU1432/1433 and mutagenesis with oHU 1429/1428 to introduce mutation L113A, *Eco*RI/*Hind*III digestion and clone into vector YIp211.	This study
pHU 1727	YIp211-SPC25 (3A)	PCR amplify SPC25 ORF and promoter/terminator with oHU1432/1433 and mutagenesis with oHU 1422/1423 to introduce mutation L113A, *Eco*RI/*Hind*III digestion and clone into vector YIp211.	This study

Table A- 4 A list of plasmids that were constructed by myself

Appendix 4: Oligonucleotides

DNA oligonucleotides used in this thesis to generate plasmids and yeast strains are listed below. All of them were purchased from SIGMA.

Number	Name	Sequence	Application
oHU 1011	UMP1 KO up	TCTTTTCAATGGTTTACGTGACAGATGTATAAAGAAATTGAGAGCAATTTATCGATGAATTCGAGCTCG	Deletion of *UMP1*
oHU 1012	UMP1 KO down	AGGGAATGAGTATTAAATAGACAAGACCAGAAACAGCCTGCATACCAACTCGTACGCTGCAGGTCGAC	Deletion of *UMP1*
oHU 1013	UMP1 KO test	CATGTTAGCATATAATGGCCAC	*UMP1* knock-out test
oHU 1147	PDR5 3' up	CATGTTAGCATATAATGGCCAC	Amplification of *pdr5::KanMX* from deletion collection
oHU 1148	PDR5 5' down	TGATTCCGTGGAAAGGTCAG	Amplification of *pdr5::KanMX* from deletion collection
oHU 1149	PDR5 KO test	GTGCCACAACATTTTCAGATT	*PDR5* knock-out test
oHU 1551	UFD2 tagging up	GCCTTATTTGATTAGGGTCAATTTTGCAATTTATTCTATCACTTATTCATATCGATGAATTCGAGCTCG	PCR-based tagging of *UFD2*
oHU 1552	UFD2 tagging down	TTTGTTTCAAAAAACAAAAAAAGGAAGAAGCAAAACATAAAGCAAGCGAGCGTACGCTGCAGGTCGAC	PCR-based tagging of *UFD2*
oHU 1569	UFD2 (1-883) tagging down	AAAGAAAGGCTGATGAAGAGGAAGATCTTGAGTATGGTGATGTTCCTGACCGTACGCTGCAGGTCGAC	PCR-based tagging of *UFD2* (1-883)
oHU 1555	UFD2 tagging test	TAACAGACAATTCCCCCGG	*UFD2* tagging test
oHU 1420	RAD23 KO down	AACTCCACCTTTAAATCACAGATCACACAAAGACAACATACAATAGAAAACGTACGCTGCAGGTCGAC	Deletion of *RAD23*
oHU 1421	RAD23 KO up	TGAGATTGTAGTAATGTTATGGCTTGAAGTATCTTCACTTATTCTCGACAATCGATGAATTCG	Deletion of *RAD23*

		AGCTCG	
oHU 1422	RAD23 KO test	CTAGGCAAGAAATAGCGACA	*RAD23* knock-out test
oHU 1423	DSK2 KO down	CGAGAGGCAAATAAGACGGA TCAAAGACACCGAATCATTCT AGCACGATACGTACGCTGCA GGTCGAC	Deletion of *DSK2*
oHU 1424	DSK2 KO up	GCCGATAGAGTAGGGTAAAA GTATATAGGTTGCGGCATCTA GACGTTTATATCGATGAATTC GAGCTCG	Deletion of *DSK2*
oHU 1425	DSK2 KO test	GCCATTTAGCGTACGATATA	*DSK2* knock-out test
oHU 1576	MCM21 tagging down	TGGATGATTTGGAATTAAAAT TAAACCATTCTTTCGCGACAA TATTCAAGCGTACGCTGCAGG TCGAC	PCR-based tagging of *MCM21*
oHU 1577	MCM21 tagging up	AGAGAAAATTAGCTCTATCCT CTTTCTATAAAGTATATTTTTG TTAACATATCGATGAATTCGA GCTCG	PCR-based tagging of *MCM21*
oHU 1578	MCM21 tagging test	CTCATGATGACGCCTATT	*MCM21* tagging test
oHU 500	UB down *BamH*I	CTGGGATCCAAATGCAGATTT TCGTCAAGAC	Construction of Ub^*_n(L)
oHU 501	UB up *Bgl*II	CCGAGATCTGAACGACACCTC TTAGCCTTAGC	Construction of Ub^*_n(L)
oHU 902	UB down *Stu*I	GAAGGCCTCATGCAGATTTTC GTCAAGACTTTGAC	Construction of Ub^*_4
oHU 903	UB down *Msc*I	GCCGTGTGGCCACGTAGCCTT AGCACAAGATGTA	Construction of Ub^*_4
oHU 1524	UB down *Sac*II	GGGGTACCGCGGAGATCCAA ATGCAGATTTTCG	Construction of $PCNA^*$- Ub^*_4
oHU 1525	UB (ΔGG) up *Pst*I	TAAGCTTGGCTGCAGATCCTC ATCTTAGCCTTAGCAC	Construction of $PCNA^*$- Ub^*_4
oHU 1240	Ub^*_4 down	GGGAATTCCATATGTAGCCCT TCCTCATGCA	Construction of Ub^*_4-βGAL
oHU 1241	Ub^*_4 up	GGAAGATCTGTGCGCCCTTCC ACGTAGC	Construction of Ub^*_4-βGAL
oHU 1160	YHL010C down	GGAAGATCTCTATGGATCAAT TTGAGTATAT	Amplification of *ETP1* (ORF)
oHU 1161	YHL010C up	TGCACTGCAGTCATTTCCCTG CTTTTTTATTT	Amplification of *ETP1* (ORF)
oHU 1162	YHL010C 459 down	GGAAGATCTCGAATGTTGAA AGTTTGAAGAA	Amplification of *ETP1* (459-585)
oHU 1163	SPC25 down	CGCGGATCCGAATGGCCAGC ATAGACGCATT	Amplification of *SPC25* (ORF)

oHU 1164	SPC25 up	CGCGGATCCTTATAAAGATGC CAGAAGCATA	Amplification of *SPC25* (ORF)
oHU 1165	SPC25 107 down	CGCGGATCCCGCGCGAGCTG GACTCGCTGCT	Amplification of *SPC25* (107-221)
oHU 1166	RSC6 down	CGCGGATCCAAATGGTAACA CAGACCAATCC	Amplification of *RSC6* (ORF)
oHU 1167	RSC6 up	CGCGGATCCTTATAGTCTTCC TTGGGAGTAC	Amplification of *RSC6* (ORF)
oHU 1168	RSC6 94 down	CGCGGATCCCAGCGGACTCA GGCAAGACTA	Amplification of *RSC6* (94-211)
oHU 1169	RSC6 211 up	TGCACTGCAGTTATCTCTTGA TGTCGATACCATCA	Amplification of *RSC6* (94-211)
oHU 1211	SPC25 106 up	TGCACTGCAGTTACGATTGGG CTGCTAAGGTCGA	Amplification of *SPC25* (1-106)
oHU 1205	SPC25 133 down	CGCGGATCCCGAACGATGCC GCAGAGGTCGCA	Amplification of *SPC25* (133-221)
oHU 1208	SPC25 146 down	CGCGGATCCCGCAGCTTCGTG TACTACCCGGA	Amplification of *SPC25* (146-221)
oHU 1207	SPC25 186 down	CGCGGATCCCGCCGGCGCTGG ACCCCAAGAGT	Amplification of *SPC25* (186-221)
oHU 1209	SPC25 189 up	TGCACTGCAGTTAGTCCAGCG CCGGGTGAGAGTT	Amplification of *SPC25* (107-189)
oHU 1210	SPC25 146 up	TGCACTGCAGTTACTGCAACA GCCGTTCGTACAG	Amplification of *SPC25* (107-146)
oHU 1321	SPC25 117 down	CGGAATTCGGTAAAGAGTGT GTCCAA	Amplification of *SPC25* (117-221)
oHU 1320	SPC25 133 up	TGCACTGCAGTTAGTTACCCG ACTGCGCAGC	Amplification of *SPC25* (1-133)
oHU 1322	SPC25 L109A L113A R116A down	CGCGCGAGGCCGACTCGCTG GCCCAACAGGCTGGTAAAGA GTGTGTCCAATTACGC	Mutagenesis of *SPC25* (L109A, L113A, R116A)
oHU 1323	SPC25 L109A L113A R116A up	TCTTTACCAGCCTGTTGGGCC AGCGAGTCGGCCTCGCGCGAT TGGGCTGCTAAGGTCGA	Mutagenesis of *SPC25* (L109A, L113A, R116A)
oHU 1426	SPC25 L109A down	CGCGCGAGGCCGACTCGCTGC TGCAACAGCGTGGT	Mutagenesis of *SPC25* (L109A)
oHU 1427	SPC25 L109A up	AGCGAGTCGGCCTCGCGCGAT TGGGCTGCTAAGGT	Mutagenesis of *SPC25* (L109A)
oHU 1428	SPC25 L113A down	ACTCGCTGGCCCAACAGCGTG GTAAAGAGTGTGTC	Mutagenesis of *SPC25* (L113A)
oHU 1429	SPC25 L113A up	CGCTGTTGGGCCAGCGAGTCC AGCTCGCGCGATTG	Mutagenesis of *SPC25* (L113A)
oHU 1430	SPC25 R116A down	TGCAACAGGCCGGTAAAGAG TGTGTCCAATTACGC	Mutagenesis of *SPC25* (R116A)
oHU 1431	SPC25	TCTTTACCGGCCTGTTGCAGC	Mutagenesis of

	R116A up	AGCGAGTCCAGCTC	*SPC25* (R116A)
oHU 1266	SPC24 down	CGGAATTCATGTCACAAAAG GATAACCT	Amplification of *SPC24* (ORF)
oHU 1228	SPC24 up	CGGGATCCTCACTTTCCTAAT CTTTCCC	Amplification of *SPC24* (ORF)
oHU 1227	SPC24 154 down	CCGCTCGAGGAAGCAAACGA AAATATTCT	Amplification of *SPC24* (154-213)
oHU 1432	SPC25 promoter down	CGGAATTCCGATCTGCTTTTT TTCCCTTTT	Amplification of *SPC25* (ORF) with promoter
oHU 1433	SPC25 terminator up	CCCAAGCTTGGGTGGATGATG CCTTTATTTGA	Amplification of *SPC25* (ORF) with terminator
oHU 1476	SPC25 KO down	GATTCAATTAAAACCGCTCAT ACGTATACAACACATACACAC ATACAAGACGTACGCTGCAG GTCGAC	Deletion of *SPC25*
oHU 1477	SPC25 KO up	TCATCTAAATCATAGGCCCAG AATAAACTGAACAGATGCGT ATAAAGGCGATCGATGAATTC GAGCTCG	Deletion of *SPC25*
oHU 1580	SPC25 tagging up	TCATCTAAATCATAGGCCCAG AATAAACTGAACAGATGCGT ATAAAGGCGATCGATGAATTC GAGCTCG	PCR-based tagging of *SPC25*
oHU 412	POL30 K127R down	GATTTCTTAAGAATTGAAGAA TTACAGTACGACT	Northern blot *POL30* probe
oHU 79	POL30 up	CCGGATCCTGCAGTTATTCTT CGTCATTAAATTTAG	Northern blot *POL30* probe
oHU 640	LacZ a	ACTGGGTGGATCAGTCGCTG	Northern blot *LacZ* probe
oHU 641	LacZ b	CGCCAGACGCCACTGCTGCC	Northern blot *LacZ* probe

Table A- 5 A list of all DNA oligonucleotides used in this thesis.

Appendix 5: Antibodies

Primary Antibodies

Name	Source	Type, Working Dilution
Anti-ubiquitin (P4D1)	Cell Signaling Technology	Monoclonal, 1:5000
Anti- (yeast) 3-phosphoglycerate kinase (PGK) (22C5)	Molecular Probes	Monoclonal, 1:5000
Anti-His (clone His-1)	Sigma	Monoclonal, 1:5000
Anti-GST (B-14)	Santa Cruz Biotechnology	Monoclonal, 1:5000
Anti-Myc (9E10)	Cancer Research UK	Monoclonal, 1:5000
Anti-Myc	Santa Cruz Biotechnology	Polyclonal, 1:5000
Anti-GFP (mixture of clone7.1 and clone 13.1	Roche	Monoclonal,1:5000
Anti-PCNA (5E6, 3B9, 4E10)	Cancer Research UK	Monoclonal, 1:3000
Anti-PCNA	Ulrich Lab	Polyclonal, 1:5000
Anti-βGal	Promega	Monoclonal, 1:5000
Anti-TAP	Cambio	Polyclonal, 1:5000

Table A- 6 A list of primary antibodies used in this thesis. Monoclonal antibodies are all derived from mice, and polyclonal antibodies are from rabbit.

Secondary Antibodies

Name	Source	Working Dilution
HRP-conjugated goat polyclonal anti-mouse	Dako	1:5000
HRP conjugated swine polyclonal anti-rabbit	Dako	1:5000

Table A- 7 A list of secondary antibodies used in this thesis

Appendix 6: Publication

Distinct consequences of posttranslational modification by linear versus K63-linked polyubiquitin chains

Shengkai Zhao and Helle D. Ulrich[1]

Cancer Research UK London Research Institute, Clare Hall Laboratories, Blanche Lane, South Mimms, EN6 3LD, United Kingdom

Edited by Aaron J. Ciechanover, Technion Israel Institute of Technology, Bat Galim, Haifa, Israel, and approved December 22, 2009 (received for review August 4, 2009)

Polyubiquitin chains mediate a variety of biological processes, ranging from proteasomal targeting to inflammatory signaling and DNA repair. Their functional diversity is in part due to their ability to adopt distinct conformations, depending on how the ubiquitin moieties within the chain are linked. We have used the eukaryotic replication clamp PCNA, a natural target of lysine (K)63-linked polyubiquitylation, as a model substrate to directly compare the consequences of modification by different types of polyubiquitin chains. We show here that K63-polyubiquitylated PCNA is not subject to proteasomal degradation. In contrast, linear, noncleavable ubiquitin chains do not promote DNA damage tolerance, but function as general degradation signals. We find that a linear tetraubiquitin chain is sufficient to afford proteasomal targeting through the Cdc48-Npl4-Ufd1 complex without further modification. Although a minimum chain length of four is required for degradation, a longer chain does not further reduce the half-life of the respective substrate protein. Our results suggest that the cellular machinery responsible for recognition of ubiquitylated substrates can make subtle distinctions between highly similar forms of the polyubiquitin signal.

DNA damage bypass | polyubiquitin chain linkage | proteasome | protein degradation | UFD pathway

Ubiquitin belongs to a family of posttranslational modifiers that alter the properties of their targets in various ways, usually by affecting their interactions, localization, or stability. Although best known for its role in regulated protein degradation (1), ubiquitin mediates a variety of nonproteolytic functions (2). By means of an enzymatic cascade involving an activating enzyme (E1), a conjugating enzyme (E2), and a ligase (E3) that determines substrate selectivity, ubiquitin is generally attached to its targets through an isopeptide linkage between the modifier's carboxy (C) terminus and the ϵ-amino group of a lysine (K) residue within the target (1). Its versatility as a signaling molecule is at least in part due to its ability to form polymeric chains. These can adopt a number of different geometries, depending on which of the seven lysines of ubiquitin is used as an acceptor for chain formation (3). Downstream effector proteins that selectively recognize a particular type of chain are believed to mediate the outcome of the modification.

A polyubiquitin chain whose monomers are linked through K48 acts as a signal for degradation by the 26S proteasome (4). K29-linked polyubiquitin chains also mediate degradation, as shown for the ubiquitin fusion degradation (UFD) pathway in yeast, which recognizes a single, noncleavable ubiquitin moiety at the N terminus of a target protein as a substrate for further modification (5). However, the short K29-linked chains assembled by the UFD-specific E3 Ufd4 are relatively inefficient in proteasomal targeting and are therefore extended via K48-linkage by a dedicated enzyme, Ufd2, also called E4 (6, 7). Downstream factors responsible for the recognition of the polyubiquitin chain and the targeting of the modified substrate to the proteasome include the escort factors Cdc48, Npl4, and Ufd1 and ubiquitin adaptors such as Rad23 and/or Dsk2 (8).

K63-linked polyubiquitin chains assembled by the heterodimeric E2 complex of Ubc13 and the E2-like Uev1/Mms2 feature prominently in the NFκB-dependent inflammatory response (9) and also in a system of DNA damage bypass known as the *RAD6* pathway (10). Here, the relevant modification target is the eukaryotic sliding clamp PCNA, a processivity factor for replicative DNA polymerases (11). Damage-induced monoubiquitylation promotes the recruitment of damage-tolerant DNA polymerases for a process named translesion synthesis (TLS) (12, 13). In contrast, modification by a K63-linked polyubiquitin chain activates an alternative pathway of damage avoidance that allows cells to overcome replication-blocking lesions in the template strand in an error-free manner, possibly involving a template switch (11, 14). The mechanism by which the K63-linked ubiquitin chains act remains unknown. In the context of NFκB activation, K63-polyubiquitylation is unrelated to proteolysis, as the chains appear to act as scaffolds for the assembly of a signaling complex, but a proteolytic function has not been excluded for the damage tolerance pathway. When linked to a model substrate in vitro, K63-linked polyubiquitin chains in fact trigger proteasomal degradation (15), and recent evidence suggests that they may also function as a degradation signal in vivo (16).

The picture of ubiquitin chain linkage is further complicated by the recent discovery of an E3 in higher eukaryotes, LUBAC, which catalyzes the assembly of linear chains where the ubiquitin moieties are linked in a tandem arrangement via ubiquitin's amino (N) terminus (17). As the latter is spacially very close to K63, linear chains adopt a conformation almost identical to that of K63-linked chains (18). Yet, although LUBAC was found to be important for NFκB signaling as well (19), the function of the linear chains does not coincide with that of the K63-linked chains, consistent with subtle differences in their recognition by the ubiquitin-binding (UBAN) domain of the Iκ kinase subunit NEMO (18, 20). Moreover, LUBAC can promote the degradation of a model substrate in vivo, indicating a possible function of linear chains in proteasomal targeting (17).

These observations raise the general questions as to what extent linear and K63-linked polyubiquitin chains are interchangeable in their functions, and whether or not they act as degradation signals. PCNA as a natural target of K63-linked polyubiquitylation has provided us with the unique opportunity of directly comparing the effects of linear versus K63-linked

Author contributions: S.Z. and H.D.U. designed research; S.Z. performed research; S.Z. and H.D.U. analyzed data; and H.D.U. wrote the paper.

The authors declare no conflict of interest.

This article is a PNAS Direct Submission.

Freely available online through the PNAS open access option.

[1]To whom correspondence should be addressed. E-mail: helle.ulrich@cancer.org.uk.

This article contains supporting information online at www.pnas.org/lookup/suppl/doi:10.1073/pnas.0908764107/-/DCSupplemental.

polyubiquitylation of a common substrate. Our results indicate that—similar to the NFκB pathway—the system of DNA damage bypass is able to differentiate between linear and K63-linked polyubiquitin chains.

Results

Linear Polyubiquitin Chains Do Not Promote DNA Damage Tolerance. In order to directly compare the effects of linear versus K63-linked chains on a common substrate, we designed linear fusions of polyubiquitin arrays to the N or C terminus of PCNA (Fig. 1*A*). We had previously shown that a single ubiquitin fused to PCNA successfully complements a defect in monoubiquitylation at the native site, K164, indicating that the position of ubiquitin on PCNA is not critical for function in TLS (21). In order to allow for some conformational flexibility we designed a series of constructs containing two to four ubiquitin repeats separated by a short linker (Ub^*_n(L)-PCNA*), and two constructs in which four ubiquitin moieties were joined precisely in a head-to-tail arrangement (Ub^*_4-PCNA* and PCNA*-Ub^*_4). In order to prevent further modification, the major acceptor sites for ubiquitin and/or the small ubiquitin-related modifier (SUMO) on PCNA (K164 and K127) and ubiquitin (K29, K48, and K63) were mutated to arginine (indicated by an asterisk in our notation), and disassembly of the chains was prevented by mutation of the C-terminal glycine of each ubiquitin to valine.

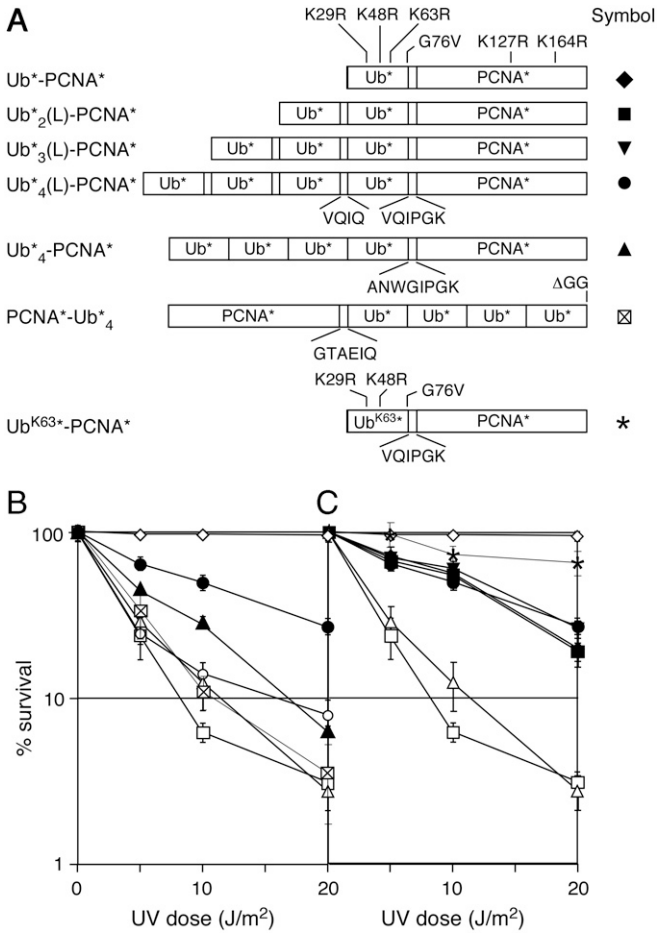

Fig. 1. Linear noncleavable polyubiquitin chains on PCNA cannot substitute for the K63-linked modification in DNA damage bypass. (*A*) Schematic view of the linear ubiquitin-PCNA fusion constructs used in this study. Mutations in the open reading frames of ubiquitin and PCNA are indicated only once; the mutant versions are represented as Ub* and PCNA*, respectively. Sequences of linker peptides are shown below the constructs, and symbols correspond to those used in *B* and *C*. (*B*) Linear tetraubiquitin fusions to PCNA rescue the UV sensitivity of *rad18* cells to different extents. UV sensitivities were determined for *rad18* cells bearing the indicated constructs. (*C*) The number of ubiquitin units fused to PCNA* does not affect the extent of rescue. UV survival assays were carried out as in (*B*). diamond shape: WT; square shape: *rad18*; triangle shape: *rad18*+*vector*; circle shape: *rad18*+PCNA*; square with an "x"inside: *rad18*+PCNA*-Ub^*_4; solid black triangle: *rad18*+Ub*-PCNA*; solid black circle: *rad18*+Ub^*_4(L)-PCNA*; solid black diamond: *rad18*+Ub*-PCNA*; solid black square: *rad18*+Ub^*_2(L)-PCNA*; upside down solid black triangle: *rad18*+Ub^*_3(L)-PCNA*; *: *rad18*+Ub^{K63*}-PCNA*.

The constructs were expressed from the *POL30* promoter in a *rad18* strain, which is unable to ubiquitylate endogenous PCNA, and the resulting strains were tested for sensitivity to UV radiation and the alkylating agent methyl methanesulfonate (MMS). Ub^*_4(L)-PCNA* suppressed the damage sensitivity of *rad18* cells to some degree (Fig. 1*B* and Fig. S1*A*). In contrast, the linkerless versions, Ub^*_4-PCNA* and PCNA*-Ub^*_4, did not afford significant rescue beyond the effect of PCNA* alone (Fig. 1*B* and Fig. S1*B*). Interestingly, all of the linker-bearing fusions, Ub^*_2(L)-PCNA*, Ub^*_3(L)-PCNA* and Ub^*_4(L)-PCNA*, conferred damage sensitivities identical to that of the "monoubiquitylated" version, Ub*-PCNA* (Fig. 1*C* and Fig. S1*A*). Moreover, rescue of viability by these constructs was completely dependent on the presence of the TLS polymerases, as none of them had any effect on the sensitivity of a *rad18 ΔTLS* strain, carrying deletions of the genes encoding the budding yeast damage-tolerant polymerases (Fig. S1*A*). We therefore conclude that the rescue observed with Ub^*_n(L)-PCNA*—as with the monoubiquitin fusion—was due to TLS rather than error-free damage bypass. The failure of the linkerless constructs to support TLS is intriguing, as it might indicate a steric obstruction of the interaction site for the damage-tolerant polymerases on the PCNA-proximal ubiquitin moiety by the head-to-tail linkage.

In order to exclude the possibility that a nonphysiological location of the ubiquitin chain prevented its function in damage bypass, we generated a variant of Ub*-PCNA*, named Ub^{K63*}-PCNA* (Fig. 1*A*). In vitro, this arrangement permits polyubiquitin chain formation on K63 of the ubiquitin moiety (22). In a *rad18* strain, we observed a suppression of the damage sensitivity that was largely independent of TLS and exceeded the effect of Ub*-PCNA* considerably (Fig. 1*C* and Fig. S1*C*), indicating that polyubiquitin-dependent damage bypass was functional, even though the chains were attached to the N terminus of PCNA. Given that none of the linear constructs was able to support error-free damage bypass, these data suggest that linear and K63-linked polyubiquitin chains are functionally distinct.

Linear Polyubiquitin Chains Target PCNA for Proteasomal Degradation. On Western blots we noticed a dramatic reduction in the abundance of all fusion proteins bearing tetraubiquitin chains when compared with the shorter versions or endogenous PCNA (Fig. 2*A* and Fig. S2*A*). The effect was not due to reduced mRNA levels of the corresponding constructs (Fig. S2*B*). Given the notion that the mimimum length of a K48-polyubiquitin chain for efficient recognition by the 26S proteasome is four ubiquitin moieties (23), we hypothesized that the linear tetrameric chains might act as proteasomal degradation signals. In support of this model, recombinant Ub^*_4-PCNA*, but not native PCNA*, was degraded by purified 26S proteasome in vitro (Fig. S3*A*). In vivo we observed increased steady-state levels of the tetraubiquitin fusions in *pre1-1* proteasome mutants (Fig. 2*B*). Moreover, chase experiments with the translation inhibitor cycloheximide indicated that they were degraded in WT cells, but stabilized in the *pre1-1* mutant (Fig. 2*C*). As purified Ub^*_4-PCNA* readily formed trimers (Fig. S3*B*), misfolding was unlikely to be the cause of instability. Hence, these findings suggest that linear polyubiquitin chains of sufficient length on PCNA act as proteasomal degradation signals. Intriguingly, however, the rates of proteolysis varied considerably between the three constructs and were hardly comparable to those of some short-lived endogenous proteins or model substrates (1, 5).

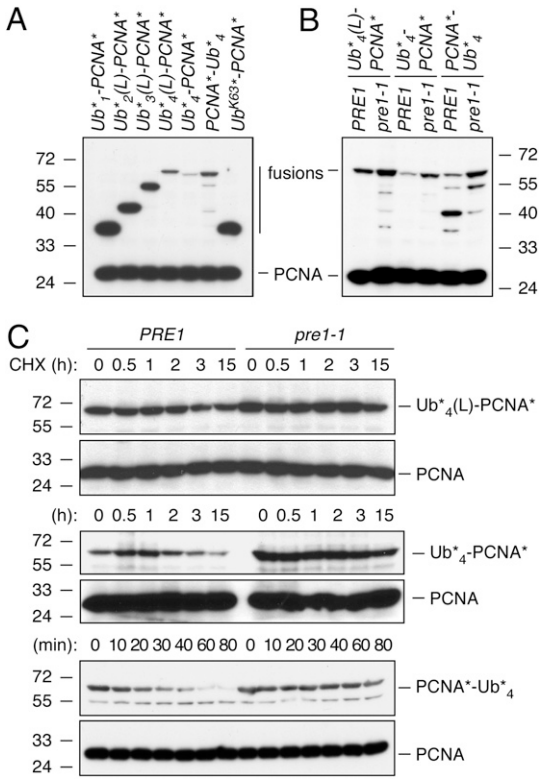

Fig. 2. Linear noncleavable tetraubiquitin chains target PCNA for degradation by the 26S proteasome. Protein levels of the ubiquitin-PCNA fusion constructs and endogenous PCNA were compared by Western blot with an anti-PCNA antibody. (*A*) Linear tetraubiquitin chains destabilize the respective fusion proteins. (*B*) Steady-state protein levels of tetraubiquitin fusions to PCNA are increased in a proteasome mutant. (*C*) Cycloheximide chase experiments show the degradation of the tetraubiquitin fusion proteins in *PRE1* cells and their stabilization in *pre1-1*. Exponential cultures were treated with 100 μg/mL cycloheximide to inhibit de novo protein synthesis, and samples corresponding to equal culture volumes were processed for Western blot analysis at the indicated time points.

K63-Polyubiquitylation Does Not Target PCNA for Degradation. Polyubiquitylation of PCNA by K63-linked chains, triggered by conditions of DNA damage, does not result in an obvious decrease in total cellular levels of PCNA (11). However, as the fraction of PCNA ubiquitylated at any given time is exceedingly small, this does not necessarily indicate a nondegradative function of the modification. In fact, proteasome mutants were previously reported to cause DNA damage sensitivity and exhibit an epistatic relationship with mutants in the *RAD6* pathway, thus possibly linking proteasome activity to PCNA modification (24). We were therefore interested to directly assess the fate of K63-polyubiquitylated PCNA. As expected, we observed an accumulation of total ubiquitin conjugates in cell extracts of cultures treated with the proteasome inhibitor MG132 or mutated in the genes encoding the proteasome maturation factor Ump1 or the catalytic subunit Pre1 (Fig. 3 *A* and *B*). In contrast, the levels of polyubiquitylated PCNA, observable after treatment with the DNA-damaging agent MMS, were not increased, but rather reduced upon attenuation of proteasome activity, and no high molecular weight species accumulated that could have indicated a conversion to longer chains (Fig. 3 *C* and *D*). Therefore, it appears that polyubiquitylated PCNA is not normally a substrate of the proteasome. Instead, the reduction in the amount of ubiquitylated PCNA in the presence of MG132 and in the proteasome mutants is likely due to the depletion of free ubiquitin that results from a lack of recycling (25).

A Linear Polyubiquitin Chain Acts as a General Degradation Signal. In order to generalize our results and exclude potential PCNA-specific effects on the turnover rate elicited by linear ubiquitin chains, we constructed an analogous fusion of the head-to-tail tetraubiquitin chain to the N terminus of β-galactosidase (Ub^*_4-βGal, Fig. 4*A*), a model proteasome substrate whose degradation pattern has been studied in detail (26, 5). Whereas the protein by itself (βGal) is stable in yeast cells, fusion of a single, noncleavable ubiquitin moiety to its N terminus (Ub-βGal, Fig. 4*A*) renders it extremely short-lived (26). Hence, comparing the stability of Ub^*_4-βGal with Ub-βGal and βGal should allow an estimation of the efficiency of the linear tetraubiquitin chain as a

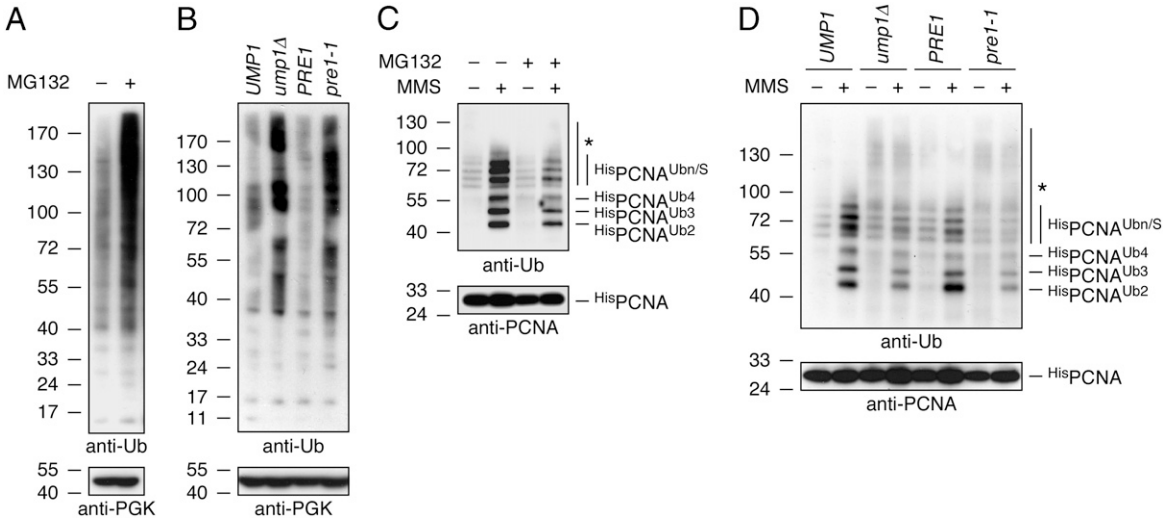

Fig. 3. K63-polyubiquitylated PCNA is not a target of proteasomal degradation. (*A*) Inhibition of the proteasome by the chemical inhibitor MG132 causes an accumulation of total ubiquitin conjugates. Exponential cultures of *HISPOL30 pdr5* cells were treated with 50 μM MG132 for 2 h where indicated, and ubiquitylated species were detected in total extracts by Western blots with an anti-ubiquitin antibody. Detection of phosphoglycerate kinase served as loading control. (*B*) Mutants with attenuated proteasome activity accumulate total ubiquitin conjugates. Extracts were prepared from the indicated strains and probed as in (*A*). (*C*) Damage-induced ubiquitylation of PCNA is reduced upon chemical inhibition of the proteasome. HisPCNA was isolated by denaturing Ni-NTA pull-down from extracts of *HISPOL30 pdr5* cells treated with 50 μM MG132 for 2 h and 0.02% MMS for 90 min where indicated, and Western blots were developed with anti-PCNA and anti-ubiquitin antibodies. (*D*) Damage-induced ubiquitylation of PCNA is reduced in mutants affecting proteasome activity. HisPCNA and its ubiquitylated forms were isolated from the indicated strains and detected as in (*C*). The high-molecular weight signals in (*C*) and (*D*) marked with an asterisk are due to nonspecific isolation of ubiquitin conjugates; they are neither PCNA-reactive nor damage-dependent.

general degradation signal. Northern blots indicated that the expression levels of all three constructs were comparable (Fig. 4*B*). However, cycloheximide chase experiments revealed remarkable differences in protein stability (Fig. 4*C*). Whereas Ub-βGal was degraded within minutes, the levels of Ub^*_4-βGal dropped appreciably over the course of several hours, comparable to the degradation kinetics of the analogous Ub^*_4-PCNA*. Unmodified βGal remained stable over the course of the entire experiment, and mutation of K29, K48, and K63 in the ubiquitin moiety of Ub-βGal also afforded complete stabilization (Fig. S4). As expected, both Ub-βGal and Ub^*_4-βGal were stabilized in a *cim3* mutant, indicating that their degradation is mediated by the proteasome (Fig. 4*C*). Thus, the linear noncleavable tetraubiquitin chain serves as a general, but relatively inefficient proteasomal degradation signal.

Substrates Marked by Linear Polyubiquitin Chains Are Targeted to the Proteasome by Components of the UFD Pathway. Given the similarity between the Ub^*_4-βGal construct and a polyubiquitylated UFD substrate, we asked whether degradation of the former would require factors of the UFD pathway. Ufd4, the E3 responsible for the initial modification of Ub-βGal, was found to be dispensable for Ub^*_4-βGal degradation (Fig. S5*A*), consistent with the absence of higher modified forms of the fusion protein in WT cells or proteasome mutants (Fig. 4*C* and Fig. S5). Interestingly, the construct was stabilized in *ufd2Δ* cells (Fig. S5*B*). However, a C terminally truncated allele lacking the catalytic U box restored degradation (Fig. S5*C*), indicating that the requirement for Ufd2 was not due to its E4 activity, but rather to its function in stabilizing the association of the Cdc48-Ufd1-Npl4 complex with the ubiquitin adaptors Rad23 and/or Dsk2 (8). Accumulation of Ub^*_4-βGal in *cdc48-2*, *npl4-1*, and a *rad23 dsk2* double mutant indeed suggested that the linear chains are recognized in a manner very similar to K48-linked polyubiquitin chains (Fig. S5 *D–F*). In summary, it appears that the pathway by which the Ub^*_4-βGal construct is targeted to the proteasome largely overlaps with the UFD pathway, with the notable exception of the initial polyubiquitin chain assembly by E3 and E4. Stabilization of the analogous Ub^*_4-PCNA* in the *npl4-1* mutant indicated processing by the same pathway (Fig. S6).

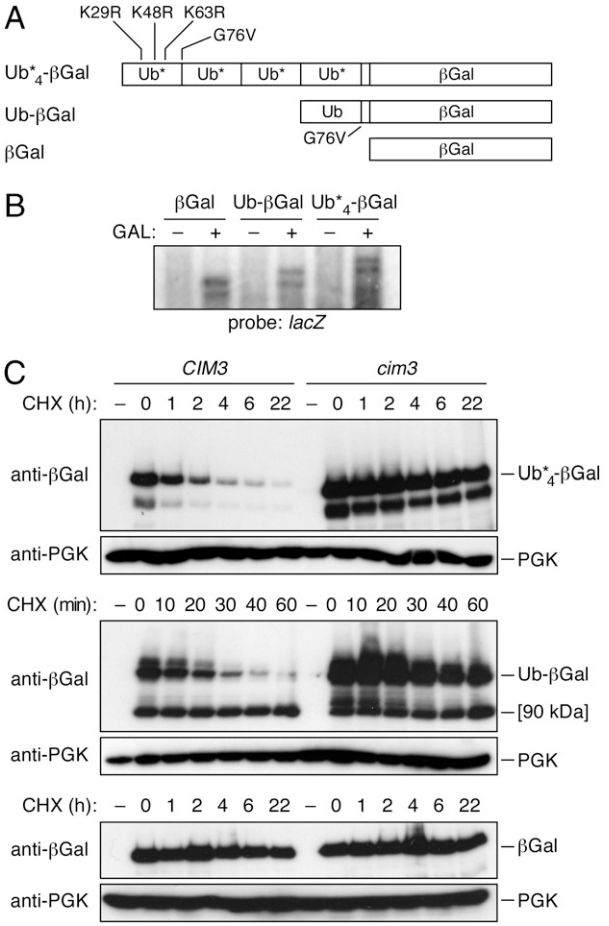

Fig. 4. A linear noncleavable tetraubiquitin chain acts as a general, but inefficient degradation signal. (*A*) Schematic view of the βGal constructs used in this study. The asterisk denotes the ubiquitin mutant (K29/48/63R, G76V). Ub-βGal was originally described as Ub^{V76}-V-$e^{\Delta K}$-βgal (41). (*B*) Northern blot analysis indicates similar expression levels of all three βGal constructs upon induction with galactose (GAL). (*C*) Ub^*_4-βGal and Ub-βGal are degraded by the 26S proteasome with distinct kinetics. After growth in galactose medium for 2 h, a promoter shut-off (by shift to glucose) was combined with a cycloheximide chase (100 μg/mL) to inhibit de novo protein synthesis in the indicated strains, and samples were processed as in Fig. 2*C*. The βGal construct served as a stable control protein. Lanes labeled "-" represent samples from cultures grown in glucose medium. Note that degradation of Ub-βGal produces a stable fragment of ca. 90 kDa (26).

Linear Polyubiquitin Chain Length Is Not a Limiting Factor for Degradation. Our data raised the possibility that the relatively low rate of degradation of our fusion proteins was due to an inefficient recognition of the linear tetraubiquitin chain by the proteasome or its targeting factors. Considering that a K48-linked chain of four ubiquitin units was found to function as the minimal recognition signal for efficient proteasomal degradation (23), we therefore asked whether an increase in chain length could compensate for a poor recognition and thus accelerate the degradation of the model substrate βGal. We duplicated the Ub^*_4 module at the N terminus of the protein to generate Ub^*_8-βGal (Fig. 5*A*). Degradation of this construct, however, was comparable to that of Ub^*_4-βGal (Fig. 5*B*), indicating that chain length is not a limiting factor for degradation in our system.

Discussion

Why do Linear Chains Not Function in Damage Bypass? A linear arrangement of ubiquitin molecules adopts an extended conformation identical to that of a K63-linked chain, and many ubiquitin-binding domains make no distinction between linear and K63-linked chains (18). Nevertheless, our fusions of linear tetraubiquitin to PCNA did not rescue a PCNA polyubiquitylation defect in vivo, despite the notion that a K63-chain attached to PCNA's N terminus is functional. We can envision several reasons for the failure of these constructs to promote damage tolerance. First, it is formally possible that the instability of the fusion proteins prevents efficient error-free damage bypass, although we consider this unlikely because the Ub^*_4(L)-PCNA* construct is active in TLS, and the levels of physiologically K63-modified PCNA are

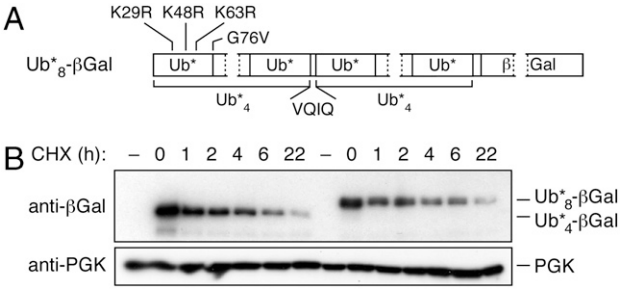

Fig. 5. Ubiquitin chain length is not a limiting factor in the degradation of linear ubiquitin fusions. (*A*) Schematic view of a Ub^*_8-βGal construct. Note that each of the Ub^*_4 modules used to create the octaubiquitin chain is identical to that used in Ub^*_4-βGal. (*B*) Ub^*_8-βGal is degraded at a rate comparable to that of Ub^*_4-βGal. Promoter shut-off/cycloheximide chase experiments were performed with the two constructs in a WT strain as described in Fig. 4*C*.

naturally very low. Second, we cannot exclude that the noncleavable nature of the chain interferes with correct function. This may apply if the deubiquitylation step is physiologically relevant for error-free damage bypass—even though removal of monoubiquitin from PCNA is not required for TLS (21). Finally, the linear chains might not be recognized by a K63-selective downstream effector protein that mediates the error-free bypass pathway. On one hand, although the Ub_4^* array was bound by the UBAN domain of NEMO (Fig. S7), which is highly selective for linear chains (18, 20), the G76V mutation might interfere with the recognition by a PCNA-specific ubiquitin receptor. On the other hand, there are ubiquitin-binding domains that bind exclusively to K63-linked chains, such as the C-terminal NZF domain of TAB2 (18, 27). At present it is difficult to distinguish between these possibilities, as replacement of our chains with a cleavable version would result in its processing to monoubiquitylated or unmodified PCNA, and characterization of a downstream effector will have to await its identification.

Why Is K63-Polyubiquitylated PCNA Not Degraded? Genetic data linking DNA damage bypass to proteasome activity have been indirect and ambiguous. While Hofmann and Pickart (15) used a lack of synergism between *pre1-1 pre2-2* and *rev3* mutants with respect to UV sensitivity as an argument against proteolytic function in error-free damage tolerance, others postulated a role of the proteasome in limiting the mutagenic activity of TLS, based on epistasis and mutation rate analysis (24, 28). We have finally directly assessed the response of polyubiquitylated PCNA to variations in proteasome activity and find no evidence for a degradation of the modified clamp. Our findings instead reflect the global behavior of K63-linked chains, which do not accumulate upon inhibition of the proteasome (29). Hence, the recent finding that proteasome-dependent processing of the transcription factor Mga2 occurs after K63-ubiquitylation by the E3 Rsp5 remains an isolated incident of K63-mediated proteolysis (16). In that study, contributions of K48-linked chains or chain editing by means of Rsp5-associated deubiquitylating activity were not rigorously excluded. Yet, K63-linked chains bind the proteasome with similar efficiency as K48-linked chains (15, 30), and little selectivity was observed in their affinities for the ubiquitin adaptors Rad23 and Dsk2 (31). The most straightforward explanation for the inefficiency of K63-linked chains as a degradation signal on PCNA may therefore be an insufficient chain length. Whereas the minimal number of ubiquitin moieties in a K48-linked chain required for efficient recognition by the proteasome was shown to be four (23), PCNA modifications exceeding the tetraubiquitylated state are undetectable in vivo, and even the latter is much less abundant than the mono- and diubiquitylated forms (32). It remains to be determined how chain length is limited in vivo, but the use of deubiquitylating enzymes such as the mammalian Usp1 (33) may represent an effective strategy for the evasion of degradation.

Linear Polyubiquitin Chains as Degradation Signals. In vitro, the 26S proteasome is not particularly selective in the recognition of ubiquitylated proteins (15, 34). It is therefore not surprising that linear ubiquitin chains competitively inhibit degradation of K48-polyubiquitylated substrates (23), and a linear noncleavable tetraubiquitin chain fused to a model protein can elicit the degradation of its fusion partner (35). However, little is known about the suitability of linear chains as degradation signals in vivo. Noncleavable tandem arrays of 2–8 ubiquitin units were shown to confer half-lives of less than 10 min to their fusion partners in reticulocyte lysates and cell culture (35, 36). When overexpressed in yeast, they effectively inhibit the proteasomal degradation of short-lived proteins (37). However, extensive modification by further ubiquitylation was noted in these cases, suggesting that the arrays mainly serve as efficient ubiquitin acceptors. In our system, further modification of the ubiquitin moieties, for example via K11, is unlikely, as this should also affect the shorter chains to at least some degree. Yet, instability was observed only for those constructs bearing at least four ubiquitin moieties, and previous reports had demonstrated chain extension via K29 and K48 for UFD substrates (5–7). Thus, a linear tetraubiquitin chain appears to be sufficient to induce proteasomal degradation in vivo.

LUBAC, an E3 that catalyzes linear polyubiquitylation, destabilizes a fusion of ubiquitin to the green fluorescent protein (GFP) in mammalian cell culture when overexpressed (17). At the same time, however, linear chains attached by LUBAC to K285 and/or K309 of NEMO apparently do not promote degradation (19), suggesting that the positioning of the chain on the target may affect its efficiency as a degradation signal. Similarly, we found that turnover rates varied significantly between Ub_4^*-PCNA* and PCNA*-Ub_4^*, and degradation of Ub_4^*-βGal was quite inefficient compared to an analogous UFD substrate. These observations initially suggested that inefficient recognition of the short linear chains by the proteasome might be responsible for the slow turnover. However, extension of the ubiquitin module to eight units did not accelerate degradation, and although linear chains are somewhat less effective at competing for proteasome binding than K48-linked chains (23), association of linear noncleavable tetraubiquitin with the proteasome had been observed in vivo (37). Taken together, these data therefore imply that inefficient processing rather than targeting is responsible for the slow degradation. This scenario is supported by the notion that the proteasome-associated isopeptidase Rpn11 positively contributes to proteolysis in vivo, presumably by removing polyubiquitin chains *en bloc* from substrates as they enter the channel into the proteasome (38, 39). In our system, the noncleavable tandem ubiquitin array needs to be unfolded and degraded along with the substrate. Considering the tightly folded structure of ubiquitin, this may present a barrier for proteolysis, in particular as substrate unfolding is known to affect degradation rates in vitro (23, 40). Alternatively, prolonged association of the tetraubiquitin module with ubiquitin receptors at the proteasome lid might delay entry of the substrate moiety into the catalytic cavity. In either case, variation of the ubiquitin attachment site might change the way in which the substrate is presented to the proteolytic core, thus ultimately affecting degradation rates.

Whether linear polyubiquitin chains naturally act as degradation signals remains an open question. In higher eukaryotes, dedicated ubiquitin binding domains specific for linear chains might shield these from recognition by proteasomal targeting factors, but as linear chains have not been detected in budding yeast (29), this organism might lack relevant receptors, thus resulting in proteasomal targeting through a lack of suitable downstream effectors.

Outlook. The distinct fates of PCNA modified by linear versus K63-linked polyubiquitin chains highlight the complexity of ubiquitin signaling that has emerged from numerous recent studies. Taken together, they indicate that not only the linkage of a polyubiquitin chain, but also its length, its position on the substrate and the capability to be edited and processed may determine the outcome of the modification. It is likely that the relevant downstream effector proteins responsible for the recognition of a particular chain in the context of its substrate will exhibit distinct interaction properties and will have to be considered individually in order to explain the choice of biological pathway dictated by polyubiquitylation.

Materials and Methods

Yeast Strains and Plasmids. Standard procedures were followed for the growth and manipulation of *Saccharomyces cerevisiae*. A list of strains is given in the *Supplemental Information* (Table S1). Experiments involving the proteasome inhibitor MG132 were carried out in a *pdr5* deletion. Temperature-sensitive mutants were pregrown at 25 °C, but experiments

addressing protein stability were performed at 30 °C. Plasmids encoding linear fusions of ubiquitin to the *pol30(K127/164R)* open reading frame were derived from constructs described previously (21), and fusions to βGal from a galactose-inducible construct originally called Ub^{V76}-V-$e^{\Delta K}$-βgal, obtained from E. Johnson (41). Details about their construction are given in the *Supplemental Information*. Fusion proteins were detected by Western blot with a polyclonal anti-PCNA (42) or a monoclonal anti-βGal antibody (Promega), respectively.

Detection of Ubiquitin Conjugates. Total ubiquitin conjugates in denatured cell extracts, prepared as described (43), were detected by Western blots using a monoclonal ubiquitin-specific antibody, P4D1 (Cell Signaling Technologies). Damage-induced ubiquitylation of PCNA was detected by denaturing Ni-NTA affinity chromatography and Western blot analysis as described previously, using PCNA- and ubiquitin-specific antibodies (44). Cells were treated with 0.02% MMS for 90 min to induce the modification. For inhibition of the proteasome, MG132 (50 μM) was added 2 h before inducing DNA damage.

Determination of UV Sensitivities. UV sensitivities were determined by plating defined numbers of cells from exponential cultures onto YPD medium, irradiation at 254 nm in a UV crosslinker (Stratalinker 2400, Stratagene), incubation in the dark for 3 days, and colony counting. Graphs represent averages and standard deviations of triplicate experiments.

Northern Blot Analysis. Total RNA was extracted from yeast cultures using an RNeasy mini kit (Qiagen). RNA samples were separated on agarose gels in a buffer containing 30 mM Bis-Tris, 10 mM Pipes, 1 mM EDTA, pH ~ 6.7, after denaturation by glyoxal. Blots were hybridized with a 464 bp βGal-specific probe generated from a polymerase chain reaction (PCR) product by labeling with Ready-To-Go DNA labeling beads (GE Healthcare). Hybridization was performed in ExpressHyb solution (Clontech) at 68 °C for 1 h.

Determination of Protein Stability by Cycloheximide Chase. Yeast strains expressing the relevant PCNA* constructs were grown in YPD medium at 30 °C to exponential phase and treated with 100 μg/mL cycloheximide to inhibit global protein synthesis. Aliquots were taken at the indicated time points, cell lysates were prepared from equal culture volumes as described (43) and the fusion protein was detected by Western blot with a polyclonal anti-PCNA antibody, along with native PCNA as a loading control. For analysis of the βGal constructs, yeast cultures were grown overnight in uracil-free synthetic complete medium containing 2% lactate as a carbon source, and expression of the constructs was induced by addition of 2% galactose for 2 h. Cells were then shifted to glucose medium containing 100 μg/mL cycloheximide. Aliquots of equal volume were taken at the indicated time points, and the βGal constructs were detected in total extracts by Western blot with a monoclonal anti-βGal antibody (Promega). Detection of phosphoglycerate kinase with a monoclonal antibody (Molecular Probes) served as a loading control.

ACKNOWLEDGMENTS. We thank P. Silver for the *npl4-1* and *cdc48-2* mutants, E. Johnson for Ub-βGal, D. Komander for the UBAN construct, J. Uhler for help with Northern blots and members of the lab for reagents, helpful discussions and critical reading of the manuscript. This work was funded by Cancer Research UK.

1. Ciechanover A, Orian A, Schwartz AL (2000) Ubiquitin-mediated proteolysis: Biological regulation via destruction. *Bioessays* 22:442–451.
2. Chen ZJ, Sun LJ (2009) Nonproteolytic functions of ubiquitin in cell signaling. *Mol Cell* 33:275–286.
3. Ikeda F, Dikic I (2008) Atypical ubiquitin chains: New molecular signals 'Protein Modifications: Beyond the Usual Suspects' review series. *EMBO Rep* 9:536–542.
4. Chau V, et al. (1989) A multiubiquitin chain is confined to specific lysine in a targeted short-lived protein. *Science* 243:1576–1583.
5. Johnson ES, Ma PC, Ota IM, Varshavsky A (1995) A proteolytic pathway that recognizes ubiquitin as a degradation signal. *J Biol Chem* 270:17442–17456.
6. Koegl M, et al. (1999) A novel ubiquitination factor, E4, is involved in multiubiquitin chain assembly. *Cell* 96:635–644.
7. Saeki Y, Tayama Y, Toh-e A, Yokosawa H (2004) Definitive evidence for Ufd2-catalyzed elongation of the ubiquitin chain through Lys48 linkage. *Biochem Biophys Res Commun* 320:840–845.
8. Richly H, et al. (2005) A series of ubiquitin binding factors connects CDC48/p97 to substrate multiubiquitylation and proteasomal targeting. *Cell* 120:73–84.
9. Deng L, et al. (2000) Activation of the IκB kinase complex by TRAF6 requires a dimeric ubiquitin-conjugating enzyme complex and a unique polyubiquitin chain. *Cell* 103:351–361.
10. Ulrich HD (2009) Regulating post-translational modifications of the eukaryotic replication clamp PCNA. *DNA Repair* 8:461–469.
11. Hoege C, Pfander B, Moldovan GL, Pyrowolakis G, Jentsch S (2002) *RAD6*-dependent DNA repair is linked to modification of PCNA by ubiquitin and SUMO. *Nature* 419:135–141.
12. Stelter P, Ulrich HD (2003) Control of spontaneous and damage-induced mutagenesis by SUMO and ubiquitin conjugation. *Nature* 425:188–191.
13. Kannouche PL, Wing J, Lehmann AR (2004) Interaction of human DNA polymerase η with monoubiquitinated PCNA: A possible mechanism for the polymerase switch in response to DNA damage. *Mol Cell* 14:491–500.
14. Zhang H, Lawrence CW (2005) The error-free component of the *RAD6/RAD18* DNA damage tolerance pathway of budding yeast employs sister-strand recombination. *Proc Natl Acad Sci USA* 102:15954–15959.
15. Hofmann RM, Pickart CM (2001) In vitro assembly and recognition of Lys-63 polyubiquitin chains. *J Biol Chem* 276:27936–27943.
16. Saeki Y, et al. (2009) Lysine 63-linked polyubiquitin chain may serve as a targeting signal for the 26S proteasome. *EMBO J* 28:359–371.
17. Kirisako T, et al. (2006) A ubiquitin ligase complex assembles linear polyubiquitin chains. *EMBO J* 25:4877–4887.
18. Komander D, et al. (2009) Molecular discrimination of structurally equivalent Lys 63-linked and linear polyubiquitin chains. *EMBO Rep* 10:466–473.
19. Tokunaga F, et al. (2009) Involvement of linear polyubiquitylation of NEMO in NF-κB activation. *Nat Cell Biol* 11:123–132.
20. Rahighi S, et al. (2009) Specific recognition of linear ubiquitin chains by NEMO is important for NF-κB activation. *Cell* 136:1098–1109.
21. Parker JL, Bielen AB, Dikic I, Ulrich HD (2007) Contributions of ubiquitin- and PCNA-binding domains to the activity of Polymerase η in *Saccharomyces cerevisiae*. *Nucleic Acids Res* 35:881–889.
22. Parker JL, Ulrich HD (2009) Mechanistic analysis of PCNA poly-ubiquitylation by the ubiquitin protein ligases Rad18 and Rad5. *EMBO J* 28:3657–3666.
23. Thrower JS, Hoffman L, Rechsteiner M, Pickart CM (2000) Recognition of the polyubiquitin proteolytic signal. *EMBO J* 19:94–102.
24. Podlaska A, McIntyre J, Skoneczna A, Sledziewska-Gojska E (2003) The link between 20S proteasome activity and post-replication DNA repair in *Saccharomyces cerevisiae*. *Mol Microbiol* 49:1321–1332.
25. Xu Q, Farah M, Webster JM, Wojcikiewicz RJ (2004) Bortezomib rapidly suppresses ubiquitin thiolesterification to ubiquitin-conjugating enzymes and inhibits ubiquitination of histones and type I inositol 1,4,5-trisphosphate receptor. *Mol Cancer Ther* 3:1263–1269.
26. Bachmair A, Finley D, Varshavsky A (1986) In vivo half-life of a protein is a function of its amino-terminal residue. *Science* 234:179–186.
27. Kulathu Y, Akutsu M, Bremm A, Hofmann K, Komander D (2009) Two-sided ubiquitin binding explains specificity of the TAB2 NZF domain. *Nat Struct Mol Biol* 16:1328–1330.
28. McIntyre J, Podlaska A, Skoneczna A, Halas A, Sledziewska-Gojska E (2006) Analysis of the spontaneous mutator phenotype associated with 20S proteasome deficiency in *S. cerevisiae*. *Mutat Res* 593:153–163.
29. Xu P, et al. (2009) Quantitative proteomics reveals the function of unconventional ubiquitin chains in proteasomal degradation. *Cell* 137:133–145.
30. Haririnia A, D'Onofrio M, Fushman D (2007) Mapping the interactions between Lys48 and Lys63-linked di-ubiquitins and a ubiquitin-interacting motif of S5a. *J Mol Biol* 368:753–766.
31. Raasi S, Varadan R, Fushman D, Pickart CM (2005) Diverse polyubiquitin interaction properties of ubiquitin-associated domains. *Nat Struct Mol Biol* 12:708–714.
32. Windecker H, Ulrich HD (2008) Architecture and assembly of poly-SUMO chains on PCNA in *Saccharomyces cerevisiae*. *J Mol Biol* 376:221–231.
33. Huang TT, et al. (2006) Regulation of monoubiquitinated PCNA by DUB autocleavage. *Nat Cell Biol* 8:339–347.
34. Kirkpatrick DS, et al. (2006) Quantitative analysis of in vitro ubiquitinated cyclin B1 reveals complex chain topology. *Nat Cell Biol* 8:700–710.
35. Prakash S, Inobe T, Hatch AJ, Matouschek A (2009) Substrate selection by the proteasome during degradation of protein complexes. *Nat Chem Biol* 5:29–36.
36. Stack JH, Whitney M, Rodems SM, Pollok BA (2000) A ubiquitin-based tagging system for controlled modulation of protein stability. *Nat Biotechnol* 18:1298–1302.
37. Saeki Y, et al. (2004) Intracellularly inducible, ubiquitin hydrolase-insensitive tandem ubiquitins inhibit the 26S proteasome activity and cell division. *Genes Genet Syst* 79:77–86.
38. Verma R, et al. (2002) Role of Rpn11 metalloprotease in deubiquitination and degradation by the 26S proteasome. *Science* 298:611–615.
39. Yao T, Cohen RE (2002) A cryptic protease couples deubiquitination and degradation by the proteasome. *Nature* 419:403–407.
40. Johnston JA, Johnson ES, Waller PR, Varshavsky A (1995) Methotrexate inhibits proteolysis of dihydrofolate reductase by the N-end rule pathway. *J Biol Chem* 270:8172–8178.
41. Johnson ES, Bartel B, Seufert W, Varshavsky A (1992) Ubiquitin as a degradation signal. *EMBO J* 11:497–505.
42. Papouli E, et al. (2005) Crosstalk between SUMO and ubiquitin on PCNA is mediated by recruitment of the helicase Srs2p. *Mol Cell* 19:123–133.
43. Silver PA, Chiang A, Sadler I (1988) Mutations that alter both localization and production of a yeast nuclear protein. *Genes Dev* 2:707–717.
44. Davies AA, Huttner D, Daigaku Y, Chen S, Ulrich HD (2008) Activation of ubiquitin-dependent DNA damage bypass is mediated by Replication Protein A. *Mol Cell* 29:625–636.